AD _____



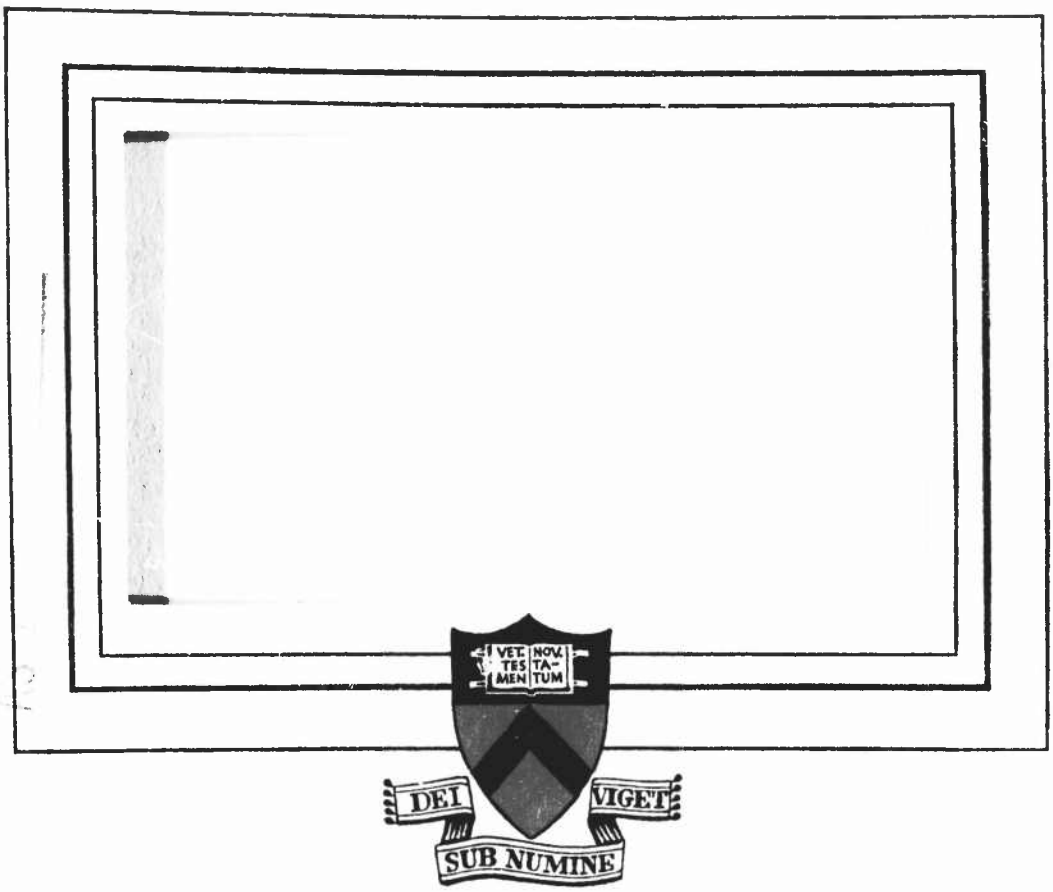


# PRINCETON UNIVERSITY

## DEPARTMENT OF AERONAUTICAL ENGINEERING

Office of Naval Research

Project NONR-1858(40)

# HYDROFOIL INSTABILITY AT LOW MASS DENSITY RATIOS

R. L. Caporali and E. J. Brunelle

Aerospace and Mechanical Sciences Report #670

March 1964

## ACKNOWLEDGEMENTS

The authors wish to express their deepest appreciation to Dr. B. Silverstein, Office of Naval Research, and Mr. A. Giddings, Bureau of Ships, whose joint efforts made it possible for this research to be conducted under Contract No. NONR-1858(40). Their enthusiasm for our preliminary studies was a strengthening influence throughout the course of our investigations.

Many thanks must be offered to the Princeton University Computation Center for the unfettered use of their IBM 7090 facility which is supported in part by National Science Foundation Grant NSF-GP579.

Finally, this acknowledgement would not be complete without commenting on the competent and cheerful manner with which Mrs. Grace Arnesen typed our manuscript.

## TABLE OF CONTENTS


| | Page No. |
|---|---|
| ACKNOWLEDGEMENTS | i |
| LIST OF SYMBOLS | iv |
| LIST OF FIGURES | viii |
| ABSTRACT | 1 |
| GENERAL INTRODUCTION | 2 |
| DISCUSSION AND RESULTS | 6 |
| PART I - THE TWO-DIMENSIONAL, TWO-DEGREE-OF-FREEDOM TYPICAL SECTION | 6 |
| I-A Background | 6 |
| I-B Preliminary Evaluation | 9 |
| I-C The Zero Mass-Density Ratio Analysis | 12 |
| Solutions for the Limiting Zero Mass-Density Ratio Case | 12 |
| Solution Gradients as the Mass-Density Ratio Becomes Finite | 22 |
| I-D The Non-Zero Mass-Density Ratio Analysis | 26 |
| The Fundamental Approach | 26 |
| Development of the Equations Used for the Non-Zero Mass-Density Ratio Analyses | 30 |
| Possible Types of Low Mass-Density Ratio Flutter Boundaries | 39 |
| Constraints on the Flutter Boundary of a Section Which are Imposed by the Character of the Asymptotic Flutter Speed Solutions | 43 |
| Constraints on the Flutter Boundary of a Section Which are Imposed by the Character of the Zero Flutter Speed Solutions | 60 |
| Results Obtained by Utilizing the "Exact" Two-Dimensional Unsteady Hydrodynamic Theory | 76 |
| On the Apparent Contradictory Aspects of the Flutter Behavior of a Typical Section as the Low Mass-Density Ratio Region is Approached | 78 |

## TABLE OF CONTENTS (continued)


| | | Page No. |
|---|---|---|
| I-E | Conclusions Resulting from Part I | 81 |
| PART II - | THE LOW MASS-DENSITY RATIO HYDROELASTIC BEHAVIOR OF A UNIFORM CANTILEVERED LIST-ING SURFACE | 85 |
| II-A | Background | 85 |
| II-B | The Axis-Normal and Streamwise Formulations | 88 |
| II-C | The Salient Features of the Streamwise Approach Applied to the Uniform Cantilevered Lifting Surface | 91 |
| II-D | Simplification of the Flutter Determinant | 95 |
| II-E | Some Typical Results Based Upon the Simplified Theory | 100 |
| II-F | Investigation of the Sensitivity of Solutions to the Assumed Flutter Modes | 106 |
| II-G | The Zero Mass-Density Ratio Analysis | 108 |
| II-H | A Physical Interpretation of the Low Mass-Density Ratio Flutter Mechanism | 118 |
| II-J | Conclusions Resulting from Part II | 121 |
| GENERAL CONCLUSIONS AND RECOMMENDATIONS | | 124 |
| APPENDIX A | | 126 |
| APPENDIX B | | 130 |
| | Additional Symbols Used in Appendix B | 138 |
| REFERENCES | | 139 |
| FIGURES | | 142 |

## LIST OF SYMBOLS

| | |
|---|---|
| a | Non-dimensional distance between elastic axis and midchord. Positive for elastic axis aft of midchord. (Written as (a) when discussed in the text) |
| A.R. | Aspect ratio |
| b | Semichord of section or unswept foil |
| $b_\Lambda$ | Streamwise semichord of swept foil |
| C(k) | Theodorsen function |
| $\frac{d^n}{dt^n}$ | $n^{th}$ time derivative |
| F | Real part of the complex Theodorsen function |
| G | Imaginary part of the complex Theodorsen function |
| h | Plunge of elastic axis (bending coordinate) |
| $I_\alpha$ | Mass moment of inertia per unit span about the elastic axis |
| j | $\sqrt{-1}$ |
| k | Reduced frequency = $\frac{b\omega}{U}$ (Used interchangeably with $k_f = \frac{b\omega_f}{U_f}$ |
| $k_h$ and $k_\alpha$ | Plunging and pitching spring constants, respectively |
| $\ell$ | Length from cantilever support to tip of unswept strut. Length of elastic axis |
| $L_h$ | Unsteady two-dimensional lift derivative with respect to h |

## LIST OF SYMBOLS (continued)

| | |
|---|---|
| $L_\alpha$ | Unsteady two-dimensional lift derivative with respect to $\alpha$ |
| $M_h$ | Unsteady two-dimensional moment derivative with respect to h |
| $M_\alpha$ | Unsteady two-dimensional moment derivative with respect to $\alpha$ |
| m | Mass per unit span |
| $r_\alpha^2$ | Non-dimensional radius of gyration about the elastic axis squared = $I_\alpha/mb^2$ |
| $r_c^2$ | Non-dimensional radius of gyration about the center of gravity squared = $r_\alpha^2 - x_\alpha^2$ |
| s | Non-dimensional time = $Ut/b$ |
| $s^n$ | $n^{th}$ non-dimensional time derivative = $(b/U)^n(d^n/dt^n)$ |
| $S_\alpha$ | Static unbalance per unit span |
| U | Free stream velocity |
| $U_f$ | Flutter speed |
| $U_f/b\omega_\alpha$ and $\frac{U_f}{b\omega_\alpha^*}$ | Flutter speed coefficients (Non-dimensional) |
| $x_\alpha$ | Non-dimensional distance between elastic axis and center of gravity = $S_\alpha/mb$. Positive for center of gravity aft of elastic axis |
| $x_m$ | Non-dimensional distance between midchord and center of gravity = $x_\alpha + a$. Positive for center of gravity aft of midchord |

## LIST OF SYMBOLS (continued)

| | |
|---|---|
| $\alpha$ | Pitch about elastic axis (torsional coordinate) |
| $\xi$ | Non-dimensional plunging displacement = h/b |
| $\varkappa$ | The sweep parameter of a uniform cantilevered strut = $\frac{2 \tan \Lambda}{l/b}$ |
| $\Lambda$ | Sweep angle. Measured as the angle between the elastic axis and the normal to the streamwise velocity vector. Positive for sweepback |
| $\mu$ | Mass-density ratio |
| $\mu_a$ | Critical mass-density ratio - defined from two-degree-of-freedom section theory as the value of $\mu$ for which the flutter speed becomes infinite. (Unprimed symbol indicates that the quasi-steady hydrodynamics associated with a reduced frequency of zero (C(k) = 1) were used in the derivation; the primed symbol indicates use of the quasi-unsteady hydrodynamics associated with a reduced frequency of infinity, (C(k) = $\frac{1}{2}$) |
| $\mu_o$ | Defined from two-degree-of-freedom section theory as the value of $\mu$ for which the flutter speed becomes zero. (Determined using the quasi-unsteady hydrodynamics associated with a reduced frequency of infinity, (C(k) = $\frac{1}{2}$) |
| $\Pi^2$ | "In vacuum" frequency ratio squared = $(\omega_h/\omega_\alpha)^2$. In the text, this and the next symbol are often simply referred to as the frequency ratio. No confusion should result as the frequencies always enter the equations in squared form |
| $\Pi^2_*$ | "In fluid" frequency ratio squared = $(\omega^*_h/\omega^*_\alpha)^2$ |
| $\rho$ | Fluid mass-density |
| $\omega_f$ | Flutter frequency |

LIST OF SYMBOLS (continued)

| | |
|---|---|
| $\omega_h$ and $\omega_\alpha$ | Artificially uncoupled vacuum frequencies in plunging and pitching, respectively |
| $\omega_h^*$ and $\omega_\alpha^*$ | Artificially uncoupled "in fluid" frequencies in plunging and pitching, respectively |
| $\frac{\omega_\alpha}{\omega_f}$ and $\frac{\omega_\alpha^*}{\omega_f}$ | Flutter frequency coefficients (Non-dimensional) |

Additional symbols are defined when introduced

## LIST OF FIGURES


| | Figure No. |
|---|---|
| A Typical Section Flutter Boundary | 1 |
| Coordinate Systems Employed | 2 |
| Parametric Combinations Which Yield a Zero Flutter Speed Solution for a Zero Mass-Density Ratio (Typical Section Analysis) | 3 |
| Axis System Used to Portray the Results of the Zero Mass-Density Ratio Analysis of the Typical Section | 4 |
| Possible "Boundaries" Terminating in Zero-Zero Solutions | 5a & 5b |
| Comparison of Elastic Axis and Axis of Zero Static Coupling | 6 |
| Typical Flutter Boundary and its Accompanying "Region of Interest" | 7 |
| Possible Flutter Boundaries Confined to Mass-Density Ratios Less than the "Critical" Value | 8a - 8d |
| Possible "New" Boundaries Not Entirely Confined to Mass-Density Ratio Region Below the "Critical" Value | 9 |
| Possible Double Valued Flutter Boundary | 10 |
| Variation of the "Critical" Mass-Density Ratio as a Function of the Structural Non-Dimensional Parameters | 11a - 11g |
| A Comparison of the "Critical" Mass-Density Ratio as a Function of the Location of the Center of Gravity for the Frequency Ratio Extremes | 12 |
| Parametric Combinations Which Will Yield a Positive "Critical" Mass-Density Ratio | 13a - 13i |
| Predicted Regions of Real Solutions for the Zero Frequency Ratio Case (Quasi-Steady Theory) | 14 |
| (Quasi-Unsteady Theory) | 15 |
| "Critical" and "Zero" Mass-Density Ratios as Determined by the Quasi-Steady and Unsteady Theories | 16a - 16o |

LIST OF FIGURES (continued)


| | Figure No. |
|---|---|
| Qualitative Dependence of a Section Flutter Boundary Upon the Section "Zero" and "Critical" Mass-Density Ratios | 17a - 17e |
| Relative Sensitivity of Various Flutter Boundaries to Changes in the Non-Dimensional System Parameters | 18a - 18h |
| A Comparison of the Quasi-Unsteady and "Exact" Flutter Boundaries | 19 |
| A Typical Comparison of Section Flutter Boundaries | 20 |
| A Qualitative Portrayal of Finite Span Effects | 21 |
| Unswept Reference Strut and its Swept Counterpart | 22 |
| The Sweep Parameter as a Function of the Unswept Cantilevered Length to Semi-Chord Ratio for Various Angles of Sweep | 23 |
| A Comparison of a Flutter Boundary Predicted by the Simplified Analysis with a Boundary Predicted by Herr, (Unswept) | 24 |
| (Fifteen Degrees of Sweep) | 25 |
| A Comparison of a Flutter Boundary Predicted by the Simplified Analysis with Boundaries Predicted by Baird and Squires | 26 |
| Flutter Speed Coefficient as a Function of the Mass-Density Ratio for Various Values of the Sweep Parameter | 27 |
| Low Mass-Density Ratio Flutter Boundaries for Various Values of the Sweep Parameter | 28 |
| The Inverse of the Flutter Frequency Coefficient as a Function of the Mass-Density Ratio for Various Values of the Sweep Parameter | 29 |
| The Inverse of the Flutter Frequency Coefficient as a Function of the Mass-Density Ratio for Various Values of the Sweep Parameter - Low $\mu$ Region | 30 |
| The Inverse of the Flutter Frequency Coefficient as a Function of the Sweep Parameter | 31 |

LIST OF FIGURES (continued)


| | Figure No. |
|---|---|
| Flutter Speed Coefficient as a Function of the Sweep Parameter | 32 |
| A Comparison of Flutter Boundaries Predicted by the "Exact" and the Approximate Quasi-Steady Theories (Unswept) | 33 |
| A Comparison of the Inverse of the Flutter Frequency Coefficients Predicted by the "Exact" and the Approximate Quasi-Steady Theories (Unswept) | 34 |
| A Comparison of Flutter Boundaries Predicted by the "Exact" and the Approximate Quasi-Steady Theories (Swept) | 35 |
| A Comparison of the Inverse of the Flutter Frequency Coefficients Predicted by the "Exact" and the Approximate Quasi-Steady Theories (Swept) | 36 |
| Flutter Boundaries Computed by Using an Off-Diagonal Coupling Constant of One | 37 |
| A Comparison of the Flutter Boundaries Obtained with Varying Amounts of Off-Diagonal Coupling | 38 |
| The Inverse of the Flutter Frequency Coefficient as a Function of the Sweep Parameter (Zero Mass-Density Ratio) | 39 |
| Flutter Speed Coefficient as a Function of the Sweep Parameter (Zero Mass-Density Ratio) | 40 |
| The "Critical" Sweep Parameter Value as a Function of the System Parameters for a Zero Mass-Density Ratio (Quartic Solution) | 41 |
| The Inverse of the Flutter Frequency Coefficient as a Function of the Sweep Parameter for a Configuration Possessing a Low Mass-Density Ratio Flutter Boundary | 42 |
| Flutter Speed Coefficient as a Function of the Sweep Parameter for a Configuration Possessing a Low Mass-Density Ratio Flutter Boundary | 43 |
| Flutter Speed Coefficient as a Function of the Elastic Axis Location with $\mathcal{K} = \mathcal{K}_{crit}$ (Zero Mass-Density Ratio) | 44 |

LIST OF FIGURES (continued)


| | Figure No. |
|---|---|
| Flutter Speed Coefficient as a Function of the Elastic Axis Location with $\mathcal{K} = \mathcal{K}_{crit}$ (Non-zero Mass Density Ratio) | 45 |
| The "Critical" Sweep Parameter Value as a Function of the System Parameters for a Zero Mass-Density Ratio (Quadratic Solution) | 46 |
| A Plot of the Flutter Speed and Flutter Frequency as a Function of the Angle of Sweepback for Squires' Model | 47 |

## ABSTRACT

This study deals with the low mass-density ratio hydroelastic behavior of fully wetted lifting surfaces of sufficiently high aspect ratio to justify the fundamental assumptions of two-dimensional, unsteady hydrodynamic fluid forces and the concept of a rigid streamwise section. Hence, this study is particularly applicable to lifting surfaces in marine usage. In particular, the strut supports of hydrofoil boats which operate at sub-cavitating speeds may be regarded as typical of the hydroelastic systems toward which this investigation is directed.

Part I of this investigation is specifically concerned with the low mass-density ratio flutter behavior of the two-degree-of-freedom "typical section." Part I shows that there exists a "critical" mass-density ratio ($\mu_a$) below which the classic "typical section" analysis will predict no dynamic instabilities. However, some extremely sensitive cause and effect relationships are noted and discussed in Part I.

Part II of this investigation deals with the low mass-density ratio hydroelastic behavior of fully wetted, uniform, cantilevered struts or other lifting surfaces, both with and without an angle of sweepback. As a result of this study, it has been ascertained that the low mass-density ratio ($\mu < \mu_a$) flutter behavior of such structures can only be properly predicted if the spanwise character of the strut is explicitly included in the mathematical model used in the analysis. Further, it is shown in Part II that a positive non-zero sweep angle is essential for low mass-density ratio bending-torsion flutter of uniform cantilevered struts to occur. In addition, Part II shows what structural parametric combinations may be expected to have a low mass-density ratio flutter problem. Finally, a physical explanation of the phenomenon is offered.

Viewed as a whole, this study shows that the low mass-density ratio region is one of extreme sensitivity where small parametric variations can result in large changes in the hydroelastic behavior pattern of a lifting surface.

## GENERAL INTRODUCTION

Recent interest in hydrofoils has quite naturally resulted in numerous investigations of the engineering problems associated with the design of such craft. Because of the obvious similarities between hydrofoils and airfoils, it had been assumed that many of the problems encountered in aircraft design could well be expected to arise with hydrofoils. However, several investigations conducted during the last decade seemed to indicate that the problem list might well have one important exception. In particular, these investigations (Refs. 2, 3, 4, 5) indicated that flutter, a problem of considerable magnitude in aircraft design, might not occur with hydrofoils. The fact that the lifting surfaces of some marine craft had long been subjected to dynamic pressures higher than those attained by the fastest aircraft and had not encountered flutter strengthened the notion.

Specifically, the investigators referenced above demonstrated, by simplified analytical arguments based upon a simplified representation of the problem, that when the ratio of the mass of a foil section of unit span to the mass of a cylinder of surrounding fluid ($\mu$) fell below some "critical" value, classical flutter was unlikely. Further, a limited amount of experimental evidence seemed to confirm what the theoretical analyses indicated. Accordingly, by 1960, the majority of the literature available on the subject of low mass-density ratio flutter concluded that the occurrence of the phenomena was highly unlikely. However, in spite of this pleasant outlook, several reports purported to document actual observed cases of hydrofoil or other very low mass-density ratio flutter, (e.g., Ref. 7). These reports were not numerous and the flutter occurrences usually not well documented. Nevertheless, the possible consequences of ignoring these reports necessitated a thorough investigation of the subject. To complicate matters even further, Herr (5) had obtained

unstable flutter solutions for certain discrete swept foils in spite of the fact that his own simplified, "typical section" theory had indicated that such solutions should be non-existent.

Obviously, the contradictory evidence outlined above necessitated that other more exhaustive investigations be undertaken. One of these investigations was the one undertaken by Baird, Squires, and Caporali, (Ref. 10). In the course of that investigation, it was demonstrated both analytically and experimentally that coupled bending-torsion flutter could, in general, occur regardless of the mass-density ratio. There were, however, several disquieting aspects, particularly with regard to the theoretical portion of the study.

First, the analytical method which successfully predicted the existence of a flutter boundary was the standard "production" modal analysis technique in which the flutter mode was assumed to be a linear combination of a finite number of the natural modes of the structure. The disturbing aspect of these analyses was that a preliminary check based upon the method outlined in Ref. (5) (derived from the "typical section" analysis) showed the mass-density ratio below which no flutter should occur to be well above the mass-density ratio associated with the test struts. Quite naturally, the first thought was that the section analysis was an over-simplification and that the modal analysis succeeded because the character of the structure was more accurately represented by the inclusion of more modes. This theory, however, was shown to be less than entirely correct when it was demonstrated that flutter could be predicted by the modal technique when as few as two modes were used. Admittedly, the predictions were not accurate. Nevertheless, the discrepancies were obviously a matter of degree and not the result of fundamental errors in principle. Thus, it became apparent that the difference between the two methods of analysis was much more subtle. This was indeed unfortunate as the modal technique, although well suited to production type work, involved a degree

of numerical complexity that made a true physical understanding of the phenomena difficult to obtain. Inasmuch as the possibility of classical flutter had been established, the extrapolation of the results for use as a design"tool" required precisely this physical understanding. Historically, this type of understanding had always been obtained from the more simple but well proven two-degree-of-freedom "typical section" analysis, such as outlined in Ref. (1). Since conclusions based upon results obtained from the typical section analysis had been proven wrong, two possibilities existed. Either the erroneous conclusions had been the result of mis-interpretations of the simplified analysis, or the fundamental analytical technique had been inadequate. The study of the two possibilities and the conclusions resulting therefrom is precisely the subject matter contained herein.

It would seem that the possibility of a mis-interpretation should have been easy to discard. However, preliminary work by Brunelle (Refs. 6 and 8) and Squires (Ref. 12) showed the possibility definitely existed that all of the pertinent information had not been extracted from the simplified analysis. Essentially, this preliminary work implied that it might be possible to show that the "critical" mass-density ratio did not in fact establish a true limit.

The second possibility was also quickly confirmed. The author and others (Ref. 10) noted that the unstable flutter solutions obtained by the modal technique were always obtained for swept, cantilevered lifting surfaces. Thus, the angle of sweep, and possibly the cantilevered mounting, could be singled out as the possible differences between the two methods inasmuch as the analysis based upon the two-degree-of-freedom section had not explicitly included sweep or the spanwise characteristics of the cantilevered structures as distinct parameters.

Thus, this investigation was undertaken in an effort to explain low mass-density ratio classical flutter. This investigation can be described as consisting of two related parts.

1) A comprehensive investigation of the two-degree-of-freedom section analysis using both the simplified quasi-steady hydrodynamics and the full unsteady hydrodynamics; the purpose of this phase being to determine whether finite-valued flutter boundaries could exist at very low mass-density ratios for unswept, fully wetted sections. (i.e., values of $\mu$ below the "critical" $\mu$ of a given section.)
2) A comprehensive investigation of the characteristics peculiar to a swept, cantilevered lifting surface to determine the effects of such characteristics upon the low mass-density ratio flutter boundaries of such structures.

Principally, this documentation of the investigation outlined above shows that:

1. For any given structure assumed to be represented by a "typical section" there exists a mass-density ratio below which, for all practical purposes, no dynamic hydroelastic instabilities can be predicted. (i.e., for $\mu < \mu_a$.)
2. The low mass-density ratio flutter behavior of a swept, cantilevered lifting surface is directly a function of the structural characteristics peculiar to such a structure; namely the spanwise variation in the local pitch to bending ratio and the sweep of the elastic axis.

In addition, related items of interest uncovered in the course of determining the above are included herein.

## DISCUSSION AND RESULTS

### PART I - THE TWO-DIMENSIONAL, TWO-DEGREE-OF-FREEDOM TYPICAL SECTION

#### I-A - Background

Flutter analysts in the aircraft field have long used the technique of examining the behavior of a representative two-degree-of-freedom, two-dimensional section of a structure to qualitatively determine the flutter characteristics of the entire structure. Since even this simplified analysis leads one to two transcendental equations which must be simultaneously satisfied when the complete unsteady hydrodynamic theory is used, the usual practice, at least when only qualitative results have been desired, has been to use quasi-steady hydrodynamic coefficients obtained by setting the ordinarily complex Theodorsen function, C(k), equal to either 1 or $\frac{1}{2}$. (See Ref. (1) or Ref. (13) for a complete explanation of the Theodorsen function.) Briefly, these two values of C(k) are the limiting values obtained by letting the reduced frequency $k \to 0$ and $k \to \infty$ respectively. Appendix A shows a plot of the dependence of the Theodorsen function upon k. (In order to differentiate between the coefficients, the set obtained with $C(k) = \frac{1}{2}$ will be referred to as the quasi-unsteady set).

Essentially, the conclusion that hydrofoil or other low mass-density ratio flutter was unlikely to occur was largely the result of extending the simplified techniques discussed above to the low mass-density ratio regime. Several investigators (e.g., Ref. 5) demonstrated that the flutter boundary of some physically plausible two-degree-of-freedom, two-dimensional sections could be expressed, as a function of the mass density ratio, as shown in Fig. 1.

The normal procedure followed was to show that under the quasi-steady assumption the flutter speed coefficient $(\frac{U_f}{b\omega_\alpha})$ could be expressed as the ratio of two polynomials in $\mu$. By setting the denominator of the

polynomial equal to zero, it was possible to demonstrate that for some "critical" value of the mass-density ratio, the flutter speed would be infinite. This value has been termed $\mu$ - asymptote ($\mu_a$). The equation from which $\mu_a$ has been determined is reproduced here to reveal its general character. This equation is discussed in considerable detail elsewhere in this report.

$$\mu_a = \frac{\frac{1}{2} + \left(\frac{\omega_h}{\omega_\alpha}\right)^2 \frac{1}{r_\alpha^2}\left(\frac{a^2}{2} - \frac{a}{8} + \frac{1}{16}\right)}{\frac{1}{2} + a + x_\alpha - \left(\frac{\omega_h}{\omega_\alpha}\right)^2 \frac{1}{r_\alpha^2}\left[x_\alpha\left(a^2 + a - \frac{1}{4}\right) + r_\alpha^2\left(\frac{1}{2} + a\right)\right]} \qquad \text{(I-1)}$$

It was, of course, well known that finite flutter speeds existed for mass-density ratios larger than $\mu_a$. However, the notion that no finite flutter boundaries existed for mass-density ratios less than the ratio which yielded an infinite flutter speed was extrapolated from the fact that no boundaries were ever found for the particular combinations of system parameters used in the calculations. Thus, the rather widely accepted idea of a minimum mass-density ratio below which no unstable solutions existed was really an assumption taken to be valid until (and if) some negating calculations could be shown. To express the issue somewhat more precisely, it had not been established, even for the simplified quasi-steady and quasi-unsteady cases, that no physically plausible combination of parameters existed which could result in a re-appearance of real solutions for some mass-density ratio below the so-called "critical" value. Mathematically stated, it had not been demonstrated that the ratio of polynomials in $\mu$ could not undergo a second sign reversal for some positive mass-density ratio less than $\mu_a$. Therefore, a careful re-examination of the simplified analyses described above became the starting point of investigations attempting to determine why the two-degree-of-freedom section analysis had apparently led to erroneous

conclusions. The results of several of these re-examinations have been documented in Refs. 6, 8, and 12. In addition, the author has also studied the problem and certain aspects of the results are discussed herein. To summarize, these investigations indicated that, under special circumstances, certain unswept, fully wetted lifting surfaces apparently had finite valued flutter boundaries for mass-density ratios well below the "critical" value. However, the results were not conclusive.

Using the quasi-steady hydrodynamic theory associated with a reduced frequency (k) of zero, it was established that at least some physically plausible configurations had finite valued flutter boundaries at very low mass-density ratios. For the special case of an "in vacuum" uncoupled plunging to uncoupled pitching frequency ratio of zero, Squires (Ref. 12) established that the existence of solutions for $\mu < \mu_a$ was entirely a function of the center of gravity location ($x_m$). Brunelle also included several examples in Refs. 6 and 8. However, Brunelle also noted that the reduced frequencies calculated for points on the flutter boundaries ($\mu < \mu_a$) which were obtained from the quasi-steady hydrodynamics tended to invalidate the fundamental quasi-steady assumption of a low reduced frequency. Attempts to obtain finite-valued flutter boundaries for $\mu < \mu_a$ using the quasi-unsteady hydrodynamic theory associated with a reduced frequency of infinity, for the very same configurations, were completely unsuccessful. Thus, the unfortunate and unexpected strong dependence of the low mass-density ratio solutions on the reduced frequency limit assumed was discovered. The term unexpected is used because at the mass-density ratios normally encountered in aircraft flutter analyses, the flutter boundary is normally only weakly dependent upon the reduced frequency. The discovery is termed unfortunate because it implied that the determination of the validity of the two-degree-of-freedom section analysis for low mass-density ratios would require the inclusion of the complete complex value of the Theodorsen function, C(k), in the analysis. This step would

have increased the complexity of the problem by at least an order of magnitude. The transcendental nature of the resulting equations would have required that a lengthy numerical technique be used to obtain solutions with the result that general statements regarding classes of configurations would have been virtually impossible to make without a prohibitive amount of computational effort. Accordingly, a systematic method for evaluating the two-degree-of-freedom section analysis was devised. The method and the conclusions resulting from its application are the subject treated in Part I. In effect, Part I of this report might be regarded as "an analysis of an analysis."

I-B - Preliminary Evaluation

The difficulties and inconsistencies encountered when attempting to study numerically the flutter behavior of a two-degree-of-freedom typical section while incorporating only the approximate quasi-steady or quasi-unsteady hydrodynamic theories have been discussed. Clearly, these inconsistencies imply that the full two-dimensional, incompressible, unsteady theory must be employed to assure the validity of any conclusions.

The development of the complex "flutter determinant" by using the "exact" complex Theodorsen function, C(k), is a classical derivation. Virtually any text on the subject of flutter (e.g., Refs. 13, 14, 15) will contain the development in some form. For completeness, an abbreviated development is included herein as Appendix A. However, for purposes of this discussion, it is convenient to show several of the steps here.

By using Lagrange's equation, the equations of motion for the typical section of Figure 2 may be written as:

$$\begin{aligned} m\ddot{h} + S_\alpha \ddot{\alpha} + m\omega_h^2 h &= -L \\ S_\alpha \ddot{h} + I_\alpha \ddot{\alpha} + I_\alpha \omega_\alpha^2 \alpha &= M \end{aligned} \qquad \text{(I-2)}$$

where L is the lift per unit span and M the moment about the elastic axis per unit span. The assumption of simple harmonic motion at the inception of the flutter condition changes equations (I-2) into:

$$\begin{aligned} -\omega_f^2 mh - \omega_f^2 S_\alpha \alpha + \omega_h^2 mh &= -L_{har} \\ -\omega_f^2 S_\alpha h - \omega_f^2 I_\alpha \alpha + \omega_\alpha^2 I_\alpha \alpha &= M_{har} \end{aligned} \qquad \text{(I-3)}$$

The terms L and M are dependent upon the Mach-number range considered. Since this study is fundamentally concerned with the behavior of foils in water, the expressions used to replace L and M are obtained from incompressible theory. This allows L and M to be put into the notation of Ref. 16. The resultant homogeneous equations constitute an algebraic eigenvalue problem with meaningful solutions occurring at those combinations of speed and frequency for which the characteristic determinant vanishes. This is called the flutter determinant and may be written as:

$$\begin{vmatrix} \{\mu[1 - \frac{\omega_h^2}{\omega_\alpha^2}\frac{\omega_\alpha^2}{\omega_f^2}] + L_h\} & \{\mu x_\alpha + [L_\alpha - L_h(\tfrac{1}{2}+a)]\} \\ \{\mu x_\alpha + M_h - L_h(\tfrac{1}{2}+a)\} & \{\mu r_\alpha^2[1 - \frac{\omega_\alpha^2}{\omega_f^2}] + M_\alpha \\ & -(L_\alpha + M_h)(\tfrac{1}{2}+a) + L_h(\tfrac{1}{2}+a)^2\} \end{vmatrix} = 0 \qquad \text{(I-4)}$$

where the $L_h$, $L_\alpha$, and $M_\alpha$ are functions of the reduced frequency (k) only and $M_h$ is equal to $\frac{1}{2}$ for the incompressible case, (see Appendix A). Examination of the determinant reveals that the flutter frequency ratio $\omega_f/\omega_\alpha$ and the reduced frequency (k) are dependent upon the values of five dimensionless parameters. These parameters, which are listed in the table of symbols are:

$a$ - the elastic axis location

$\omega_h/\omega_\alpha$ - the plunging-pitching frequency ratio

$x_\alpha$ - the nondimensional static unbalance

$r_\alpha$ - the nondimensional radius of gyration

$\mu$ - the mass-density ratio.

It is thus apparent that a reasonably comprehensive parameter study is not a trivial undertaking. This fact is made even more apparent when one briefly considers the actual details of solving Eq. (I-4). The complex form of the aerodynamic coefficients causes the determinant to expand into real and imaginary equations. Because of the nature of the hydrodynamic terms, both equations include complicated functions of k. Thus to solve for the flutter frequency ratio and the reduced frequency with the above physical properties known requires a lengthy trial and error process. Hence, it may be concluded that a comprehensive study of the behavior of the two-degree-of-freedom analysis as a function of the above noted system parameters presents practical computational and data processing difficulties of such a magnitude that the time required for completion would be prohibitive; even with the use of high speed digital equipment (IBM 7090) and the range of interest for each individual parameter confined by practical considerations. Furthermore, past experience (Refs. 5, 10) has indicated that the low mass-density ratio regime may be characterized by an extreme sensitivity to small changes in the values of the system parameters - thus implying that unusually small step changes might be required in order to correctly ascertain trends over all ranges of interest.

In view of the anticipated computational difficulties, it is apparent that some scheme which serves to reduce the dimensional size of the problem is highly desirable - at least for the start of the investigation. A scheme outlined by Brunelle in Ref. 6 is promising as it offers the possibility of ignoring two of the system parameters. Fundamentally, the analysis involves a study of the special case of a zero mass-density ratio.

## I-C - The Zero Mass-Density Ratio Analysis

### Solutions for the Limiting Zero Mass-Density Ratio Case

An analysis based upon a zero mass-density ratio has several attractive features. One is concerned with the fact that two of the system parameters do not have to be considered. In particular, the non-dimensional mass unbalance and the non-dimensional radius of gyration do not appear independently in the flutter equations. Physically this could be interpreted as the result of the inertial effects of the structure becoming negligible when compared to the virtual or apparent inertial effects of the surrounding fluid. A second attractive feature is that the zero mass-density ratio case is a logical limiting case for the low mass-density ratio regime. Thus, one might intuitively expect that any peculiarities resulting from a low mass-density ratio would be most pronounced for the limiting condition. Unfortunately, a study of the zero mass-density ratio case cannot be undertaken without introducing a different set of non-dimensional system parameters.

It may be seen from equations (I-2) and (I-3) that although the equations describe a two-degree-of-freedom spring-mass system, the spring constants $k_h$ and $k_\alpha$ do not appear explicitly. Rather, the spring constants have been replaced by functions involving the uncoupled natural frequencies in plunging and in pitching through use of the relations $k_h = m\omega_h^2$ and $k_\alpha = I_\alpha \omega_\alpha^2$. As was pointed out by Brunelle (Ref. 6), regarding the spring constants as being fixed requires that during the limiting process of $m \sim \mu \to 0$, $\omega_h^2$ and $\omega_\alpha^2$ both approach infinity in such a fashion as to keep

$k_h$ and $k_\alpha$ at their predetermined values. It was further noted by Brunelle that as $\omega_\alpha^2$ approaches infinity, the flutter speed coefficient $(U_f/b\omega_\alpha)$ has to approach zero even though the flutter speed might in reality have a finite non-zero value. Hence, it is apparent that the substitutions for $k_h$ and $k_\alpha$ noted above are poorly suited for investigating the case of the mass, and subsequently the mass-density ratio, approaching zero, since all flutter points collapse onto the origin. It is then obvious that the study of the zero mass-density case requires that $k_h$ and $k_\alpha$ be expressed in terms of generalized masses and frequencies that do not become zero or infinite as the mass-density ratio approaches zero. Following Ref. (6), it is possible to obtain a more useful set of generalized masses and frequencies by writing the equations for a "typical section" (Fig. 2) which is submerged in a stationary fluid. If all the coupling terms are suppressed, the equations may be written:

$$[m + \pi\rho b^2]\ddot{h} + k_h h = 0$$

and (I-5)

$$[I_\alpha + \pi\rho b^4(\frac{1}{8} + a^2)]\ddot{\alpha} + k_\alpha \alpha = 0$$

Thus, the artificially uncoupled "in fluid" frequencies become:

$$\omega_h^{*2} = \frac{k_h}{m + \pi\rho b^2} \quad \text{and} \quad \omega_\alpha^{*2} = \frac{k_\alpha}{I_\alpha + \pi\rho b^4(\frac{1}{8} + a^2)} \tag{I-6}$$

If the zero mass-density ratio is taken to be the limit reached as the mass is made to approach zero, rather than the limit achieved as the fluid density is made to approach infinity, the artificially uncoupled water frequencies are seen to approach $\omega_h^{*2} = k_h/\pi\rho b^2$ and $\omega_\alpha^{*2} = k_\alpha/\pi\rho b^4(\frac{1}{8}+a^2)$. Clearly this implies that the generalized mass and the generalized moment of inertia - for the zero mass-density ratio case - are determined by the density of the fluid.

As one would expect, the "in fluid" and the "in vacuum" frequencies are directly related, the exact relationships being a function of the mass-density ratio. For purposes of comparison the following equations are given:

$$\omega_h^{*2} = \frac{\mu}{1+\mu}\,\omega_h^2 \qquad \omega_\alpha^{*2} = \frac{\mu r_\alpha^2}{(\frac{1}{8}+a^2)+\mu r_\alpha^2}$$

and (I-7)

$$\Pi_*^2 = \frac{(\frac{1}{8}+a^2+\mu r_\alpha^2)\,\Pi^2}{(1+\mu)\,r_\alpha^2}$$

If the above relations are used in conjunction with the unsteady, two dimensional, incompressible hydrodynamic theory exemplified by an arbitrary C(k), the equations of harmonic motion of the typical section are given by:

$$(1+\mu)\ddot{\xi} + 2C(k)\dot{\xi} + (\mu+1)(b\omega_\alpha^*/U)^2\Pi_*^2\,\xi + (\mu x_\alpha - a)\ddot{\alpha}$$

$$+ 2[\tfrac{1}{2} + C(k)(\tfrac{1}{2} - a)]\dot{\alpha} + 2C(k)\alpha = 0$$

(I-8)

$$(\mu x_\alpha - a)\ddot{\xi} - 2(a+\tfrac{1}{2})C(k)\dot{\xi} + [\mu r_\alpha^2 + (\tfrac{1}{8}+a^2)]\ddot{\alpha}$$

$$+ (\tfrac{1}{2}-a)[1 - 2C(k)(\tfrac{1}{2}+a)]\dot{\alpha} + \{[\mu r_\alpha^2 + (\tfrac{1}{8}+a^2)](b\omega_\alpha^*/U)^2$$

$$- 2(a+\tfrac{1}{2})C(k)\}\alpha = 0$$

For purposes of suitably non-dimensionalizing the above, the differentiations indicated are with respect to a non-dimensional time. That is $(\cdot\cdot)$ indicates $\frac{d^2}{ds^2} = (\frac{b}{U})^2 \frac{d^2}{dt^2}$, etc., as is indicated in the list of symbols.

At this point, Brunelle solved the equations of motion for the limiting case of a zero mass-density ratio using both the approximate hydrodynamics associated with a reduced frequency of zero and of infinity. This solution was based upon the customary harmonic substitution $d^n/ds^n \equiv (j\tilde{\omega})^n e^{i\tilde{\omega}s}$ and further noting that $\tilde{\omega} = (\omega_f/\omega_\alpha^*)\Big/(U_f/b\omega_\alpha^*)$. The results are presented below:

For $\mu = 0$ and $k = 0$

$$\frac{U_f}{b\omega_\alpha^*} = \frac{1}{2\sqrt{2}} \sqrt{\frac{q^2 + (1 + 8a^2)[\Pi_*^2(1 - q) - q]}{q + (2a + 1)\Pi_*^2}} \tag{I-9a}$$

$$\frac{\omega_f}{\omega_\alpha^*} = \sqrt{q} \quad \text{where } q = 4a(2a - 1)\Pi_*^2 + (1 + 8a^2) \tag{I-9b}$$

For $\mu = 0$ and $k = \infty$

$$\frac{U_f}{b\omega_\alpha^*} = \tfrac{1}{2} \sqrt{\frac{q^2 + (1 + 8a^2)[\Pi_*^2(1 - q) - q]}{q + (2a + 1)\Pi_*^2}} \tag{I-10a}$$

$$\frac{\omega_f}{\omega_\alpha^*} = \sqrt{q} \quad \text{where } q = \frac{1}{3}[2(2a - 1)^2\Pi_*^2 + (1 + 8a^2)] \tag{I-10b}$$

These results are seen to be quite simple and allow for a direct calculation of the frequency and flutter speed coefficient as a function of $\Pi_*^2$ and (a). Unfortunately, the results obtained by using the above equations suffered from the inconsistencies described in the previous section. Namely, when equations (I-9) were used, many practical combinations of $\Pi_*^2$ and (a) were found which yielded real, positive values for $U_f/b\omega_\alpha{}^*$ and $\omega_f/\omega_\alpha{}^*$. However, the resultant reduced frequency obtained by combining the frequency and flutter speed coefficients was invariably much too large to justify the choice of the quasi-steady hydrodynamic theory. Rather, the values of reduced frequency which were obtained indicated that equations (I-10) should be used. However, the use of equations (I-10) failed to yield any real, positive values for $U_f/b\omega_\alpha{}^*$ and $\omega_f/\omega_\alpha{}^*$ for any of the $\Pi_*^2$ and (a) combinations checked. Thus the use of the "exact" theory is implied.

To obtain the equations associated with the "exact" unsteady hydrodynamic theory and a mass-density ratio of zero requires that the equations of motion, Eqs. (I-8), be solved for the zero-mass-density ratio case with the complex form of the Theodorsen function, $(C(k) = F + jg)$, employed. Again the solution is based upon the customary harmonic substitution and follows closely the development shown in Appendix A. By making the appropriate substitutions, and after a considerable amount of algebraic manipulation, one form of the resultant flutter equations may be written as shown on the following page as Eq. (I-11).

The symbols used in Eq. (I-11) are all included in the list of symbols.

$$\left(\frac{U_f}{b\omega_\alpha}_*\right)^2 = \frac{\Pi_*^2(1 + 8a^2)}{k^2(1 + 8a^2)(1 + \Pi_*^2) + 2Gk(1 + 8a^2 - 2\Pi_*^2 + 8a^2\Pi_*^2) + 8\Pi_*^2 F(1 + 2a)}$$

$$+ \frac{[k(\frac{F}{4} - \frac{1}{2}) - G][\Pi_*^2(1 + 8a^2)]}{\{k[2F(\frac{1}{8}+a^2)+(\frac{1}{2}-\frac{F}{2}-a+2a^2F)\Pi_*^2] - \Pi_*^2 G(1+2a)\}\{k^2 - 2Gk - 8F\}}$$

(I-11a)

$$\frac{\omega_\alpha^*}{\omega_f} = \frac{U_f}{b\omega_\alpha^*} \cdot \frac{Gk - k^2(\frac{F}{4} - \frac{1}{2})}{k[2F(\frac{1}{8}+a^2)+(\frac{1}{2}-\frac{F}{2} - a + 2a^2F)\Pi_*^2] - \Pi_*^2 G(1 + 2a)}$$

(I-11b)

To solve Eqs. (I-11), a trial and error process must be used.

Briefly, this involves assuming a value of the reduced frequency k, which in turn prescribes the F and G values, solving for the flutter speed and flutter frequency coefficients, and then combining the coefficients so as to obtain a computed value for the reduced frequency. A valid solution is obtained when the calculated value of the reduced frequency is the same as the assumed value.

An examination of Eq. (I-11) shows that the non-dimensional static unbalance, $x_\alpha$, and the non-dimensional radius of gyration, $r_\alpha$, do not appear. The exclusion of these two non-dimensional system parameters, coupled with the mass-density ratio being fixed at zero, allowed a rather extensive parameter study to be undertaken. Even though the computational process remained lengthy, it was possible, by using high speed digital

equipment, to check literally hundreds of combinations of $\Pi_*^2$ and (a) over a range of reduced frequencies which effectively covered the entire unsteady region.

Practical considerations dictated that limits be placed upon the values of $\Pi_*^2$ and (a) to be investigated. Clearly, only values of $\Pi_*^2 \geq 0$ have any physical meaning; accordingly only positive values were studied. With regard to the elastic axis location, (a), one might conclude that only values of (a) between plus and minus one need be considered. However, for reasons which will be explained later, the limits chosen were $-4 \leq a \leq 3$. Actually, no lengthy discussion of parametric combinations is necessary at this time - it being sufficient to remark that none of the combinations investigated yielded real finite flutter points. However, it was noted that certain of the combinations of $\Pi_*^2$ and (a) did appear to be approaching flutter solutions as the reduced frequency was increased; the trend continuing even for extremely large values, (on the order of $10^3$). For any practical physical system, b and $\omega_\alpha$ must be real, finite, and non zero. Hence, the above noted behavior implied that certain of the combinations appeared to have a zero flutter speed. Since a zero flutter speed is associated with a reduced frequency of infinity, it was concluded that the combinations yielding a zero flutter speed could be deduced from the equations resulting from the use of the approximate quasi-unsteady aerodynamics; Eq. (I-10).

Examination of Eq. (I-10a) reveals that a zero flutter speed results if:

$$q^2 + (1 + 8a^2)\,[\Pi_*^2 (1 - q) - q] = 0$$

$$\text{where } q = \frac{1}{3}\,[2\,(2a - 1)^2\,\Pi_*^2 + (1 + 8a^2)] \qquad (I\text{-}12)$$

Substituting for q and re-arranging leads to an expression which can be identified as a quadratic in $\Pi_*^2$. The resultant expression may be written as:

$$(2a - 1)^2 [4(2a - 1)^2 - 6 (1 + 8a^2)]\Pi_*^4$$

$$+ (1 + 8a^2)[9 - 3 (1 + 8a^2) - 2 (2a - 1)^2\Pi_*^2 - 2 (1 + 8a^2)^2 = 0 \qquad \text{(I-13)}$$

The solution to Eq. (I-13) is obtained by applying the quadratic formula and is found to be quite simple, largely because the radical term is identically zero. Hence Eq. (I-13) is a perfect square of the form:

$$[\Pi_*^2 - f(a)]^2 = 0 \qquad \text{(I-14)}$$

In particular, the solution of Eq. (I-13) may be written as:

$$\Pi_*^2 = \frac{8a^2 + 1}{(1 - 2a)(1 + 4a)} \qquad \text{(I-15)}$$

Obviously only positive values of the frequency ratio $\Pi_*^2$ are of practical interest; hence, it may be seen that positive values of $\Pi_*^2$ will only result for $-\frac{1}{4} < a < \frac{1}{2}$. Thus, for any elastic axis location between the three-eighth and the three-quarter chord positions, there exists a frequency ratio $\Pi_*^2$ which will result in a zero flutter speed solution at a mass-density ratio of zero. Figure 3 is a plot of all such combinations. As a check, it was verified that the combinations obtained by using Eq. (I-15) included those that were indicated by the numerical analyses using the "exact" unsteady hydrodynamics. In effect, the "exact" analysis showed that the flutter points obtained by using the quasi-steady theory associated with a reduced frequency of zero could not be accepted as valid while the quasi-unsteady theory ($k \to \infty$) had indeed been correct in not predicting any finite, real, non-zero solutions. Some insight as to why the quasi-unsteady theory should prove more reliable than the quasi-steady ($k \to 0$) theory may be gained by examining Eq. (I-11).

A glance at Eq. (I-11) reveals that the expressions for both the flutter speed coefficient and the flutter frequency coefficient include the reduced frequency (k). It may be further noted that the highest power of k to be found in each expression is never combined with the term G; G being the imaginary portion of the Theodorsen function.

The behavior of the Theodorsen function as a function of the reduced frequency is well known; a simple plot being included in Appendix A. Briefly, for the quasi-steady case of $k \rightarrow 0$, $F = 1$ and $G = 0$. As k is increased, F tends toward a value of $\frac{1}{2}$ while G approaches its largest (absolute) value of approximately -.2 for a k of approximately .2. Further increases in k cause G to again rapidly approach zero in such a fashion that for a k of 6.0, the value of G is approximately -.02.

Returning again to Eq. (I-11), it is clear that for large values of the reduced frequency (k), the terms including the higher powers of k will be dominant. Since these higher powers are never combined with the terms containing G, neglecting the already small values of G by setting G equal to zero could logically be expected to have little effect upon the character of the resultant solutions. On the other hand, for very small values of the reduced frequency, the higher powers of k tend to become insignificant. Thus the inclusion of the correct value of G, however small, might be expected to have a correspondingly greater effect. Hence one would expect to find the results based upon the quasi-steady theory unreliable for even small departures from zero k values; while the quasi-unsteady results would be expected to remain valid over a much larger range of reduced frequencies.

The results discussed so far may be summarized on an extremely simple plot. On Figure 4, the $\mu = 0$ case appears as the ordinate of the set of axes.

By an extensive numerical search it has been established that no reasonable or practical combination of $\Pi_*^2$ and (a) exists which will yield a finite, positive, non-zero $U_f/b\omega_\alpha^*$. Hence no flutter points exist along

the ordinate between zero and infinity. Similarly, the numerical search coupled with a study of the quasi-unsteady flutter equations have shown that certain combinations do yield a $U_f/b\omega_\alpha^*$ of zero. Thus solutions exist at the origin. To complete the study requires only that the possibility of a $U_f/b\omega_\alpha^*$ of infinity be considered; that is, the possibility of the zero mass-density ratio ordinate being an asymptote. This possibility can be investigated by examining Eqs. (I-9), which are derived from the quasi-steady approximation, inasmuch as these equations become exact as the flutter speed coefficient approaches infinity.

It may be seen from Eq. (I-9a) that a flutter speed coefficient of infinity requires that:

$$g + (2a + 1)\Pi_*^2 = 0 \qquad \text{(I-16a)}$$

where: $g = 4a(2a - 1)\Pi_*^2 + (1 + 8a^2)$

Substituting and collecting terms yields a quadratic in (a) of the form:

$$a^2(1 + \Pi_*^2)8 - 2a\Pi_*^2 + (1 + \Pi_*^2) = 0 \qquad \text{(I-16b)}$$

No real values of (a) will satisfy Eq. (I-16b) if $\Pi_*^2$ is restricted to positive values. Thus no physically possible combination of $\Pi_*^2$ and (a) can be expected to asymptotically approach a flutter solution along the $\mu = 0$ ordinate.

Expressed in the terms of Figure 4, the only valid flutter solutions found for the zero mass-density case have been found to be at the origin of the axes, and these have required certain carefully prescribed combinations of $\Pi_*^2$ and (a).

Solution Gradients as the Mass-Density Ratio Becomes Finite

Clearly, to be of any practical significance, the zero flutter speed solutions discussed in the previous section would have to be the terminal points of valid flutter boundaries. To express the situation graphically, consider Figures 5a and 5b. Note that to avoid imaginary terms, the ordinate has been designated the square of the flutter speed coefficient.

If the zero flutter speed solutions are associated with flutter boundaries of the types depicted by Fig. 5a, they are of practical interest. Conversely, boundaries of the type depicted by Fig. 5b are of little significance. To determine whether any of the configurations depicted by Fig. 3 are associated with the types of boundaries shown in Fig. 5a requires that at least a representative sample of the $\Pi_*^2$ and (a) combinations be investigated at mass-density ratios other than zero.

Unfortunately, investigations conducted for non-zero mass-density ratios require that all of the non-dimensional system parameters be included. Thus the computational problem would once again appear to be a major obstacle. However, since the anticipated boundaries should depart from the zero flutter speed point, it is reasonable to expect that for at least a limited range of mass-density ratios the quasi-unsteady equations associated with a k of infinity will satisfactorily predict the trend of the solutions. In addition, for very low mass-density ratios, the effects of the structural mass and inertial parameters will be minimal. Thus the initial departure of the solutions from the origin of the axes should be only slightly dependent upon the values of $x_\alpha$ and $r_\alpha$, so long as the numerical values are physically reasonable. Clearly then, the intended method of investigation requires that the flutter equations based upon first the quasi-unsteady and then the "exact" unsteady hydrodynamics be developed. Both can be easily obtained from Eqs. (I-8), the fundamental equations of motion.

By replacing the C(k) terms in Eq. (I-8) by $\frac{1}{2}$ and then solving the associated flutter determinant, the quasi-unsteady flutter equations take the following form:

$$\frac{\omega_\alpha^{*2}}{\omega_f^2} = \frac{3 + 2\mu(1 - 4a + 4a^2 + 8a\,x_\alpha - 4x_\alpha + 4r_\alpha^2)}{1 + 8a^2 + 2\Pi_*^2(1 - 4a + 4a^2)(1 + \mu) + \mu 8 r_\alpha^2} \tag{I-17}$$

$$(1 + \mu)(1 + 8a^2 + \mu 8 r_\alpha^2)[\Pi_*^2 - \frac{\omega_f^2}{\omega_\alpha^{*2}}(1 + \Pi_*^2)]$$

$$\left(\frac{U_f}{b\omega_\alpha}_*\right)^2 = \frac{+\left(\frac{\omega_f}{\omega_\alpha}\right)^4 \{1 + \mu[1 + 8a^2 + 16ax_\alpha - \mu 8x_\alpha^2 + 8r_\alpha^2(1 + \mu)]\}}{4\Pi_*^2(1 + \mu)(1 + 2a) + 4\frac{\omega_f^2}{\omega_\alpha^{*2}}[1 - \mu(1 + 2a + 2x_\alpha)]}$$

In a similar fashion, the flutter equations incorporating the "exact" unsteady theory may be obtained by substituting the complex Theodorsen function (F + jG) into Eq. (I-8). These results may be written as shown on the following page, (Eqs. I-18).

$$\left(\frac{\omega_\alpha^*}{\omega_f}\right)^2 = \frac{k[2 - F + 2\mu(1 - F - 2a + 4a^2 F x_\alpha + 8aFx_\alpha - 2x_\alpha + 4Fr_\alpha^2)] + 4G[1 - \mu(1 + 2a + 2x_\alpha)]}{k[F(1 + 8a^2) + \Pi_*^2(2 - 2F - 4a + 8a^2 F)(1 + \mu) + \mu 8r_\alpha^2 F] - 4\Pi_*^2 G(1 + 2a)(1 + \mu)}$$

$$\left(\frac{U}{b\omega_\alpha^*}\right)^2 = \frac{\Pi_*^2(1 + \mu)(1 + 8a^2 + \mu 8r_\alpha^2)}{k^2\{(1 + \mu)(1 + \Pi_*^2)(1 + 8a^2 + \mu 8r_\alpha^2)\} + k\{(1 + 8a^2)2G + 4\Pi_*^2 G(4a^2 - 1)(1 + \mu)}$$

$$+ \mu 16r_\alpha^2 G\} + 8\Pi_*^2 F(1 + 2a)(1 + \mu) - \left(\frac{\omega_f}{\omega_\alpha^*}\right)^2 \{k^2 - 2Gk - 8F$$

$$+ \mu k^2 [1 + 8a^2 + 16ax_\alpha - \mu 8x_\alpha^2 + 8r_\alpha^2 (1 + \mu)]$$

$$+ \mu 4Gk[4a(a + 2x_\alpha) + 4r_\alpha^2 - 1] + \mu 8F(1 + 2a + 2x_\alpha)\}$$

Eqs. (I-18a) and (I-18b)

If Eqs. (I-17 and 18) are compared with their respective counterparts for the zero mass-density ratio case, Eqs. (I-10 and 11), the increase in complexity is seen to be considerable. However, the remarks made for the $\mu = 0$ case, Eq. (I-11), regarding the grouping of the k and G terms are seen to remain valid for the more general case represented by Eq. (I-18). Thus the conclusions reached regarding the reliability of the solutions obtained from Eq. (I-10) still apply to Eq. (I-17).

Having obtained the necessary relationships, the investigative procedure consisted of taking a number of the combinations depicted by Figure 3 (chosen so as to cover the complete range of possible elastic axis locations), substituting these values into Eqs. (I-17), and noting the resultant flutter frequency and flutter speed coefficients. Values of $x_\alpha$ and $r_\alpha$ were chosen so as to more than cover the range normally encountered, in spite of the fact that the expected effect of these parameters at very low mass-density ratios was expected to be slight; while the range of $\mu$ values investigated went from zero to one in such a fashion that very small step sizes were taken near zero with the step sizes increasing as $\mu$ increased. Obviously, the computational effort involved was considerable even though high speed digital equipment was used. Again no detailed discussion of the results is required as no valid flutter speed solutions were found. In general, the flutter frequency coefficients were positive and on the order of unity. However, the resultant squares of the flutter speed coefficients were all negative - indicative of imaginary flutter speeds. Graphically the results could be portrayed by a plot similar to Figure 5b.

It might be of academic interest to mention that the configuration consisting of $\Pi_*^2 = 1$ and $x_\alpha = a = 0$ was found to yield a zero flutter speed solution for all $\mu$.

Having obtained the results based upon the quasi-unsteady theory, a number of the configurations were checked by the "exact" theory as depicted by Eqs. (I-18). Because of the increased complexity of the

calculations, the number of configurations checked was restricted. Further, because of the transcendental nature of the equations, imaginary solutions could not be assumed and thus the "flutter boundaries" obtained from the approximate theory could not be duplicated. However, it is noteworthy that no positive finite flutter points were obtained.

To summarize, the non-zero mass-density ratio investigations described in this section may be regarded as the final portion of the work undertaken in an effort to ascertain what type of flutter behavior is to be expected near a zero mass-density ratio. The work described in this section, in conjunction with that described in the previous section effectively shows that for a two-dimensional, fully wetted, unswept lifting surface, no flutter points of practical significance may be expected for a mass-density ratio of zero. Further, it has been shown that the zero flutter speed solutions obtained for the limiting case are not the terminal points of real, finite flutter boundaries; but rather are associated with a family of imaginary solutions and, hence, of only academic interest.

## I-D - The Non-Zero Mass-Density Ratio Analysis

### The Fundamental Approach

The fact that the two-degree-of-freedom typical section analysis for the limiting condition of a zero mass-density ratio will not yield any flutter points of practical interest may be regarded as a valuable portion of the complete low mass-density ratio investigation as it allows the conclusion that no finite flutter speed boundaries, plotted as a function of the mass-density ratio $\mu$, may either approach or intersect the $\mu = 0$ ordinate of Figure 1. This simplifies considerably the remaining investigation.

Obviously, the absence of a finite flutter speed at $\mu = 0$ for physically plausible configurations does not preclude the existence of a flutter boundary for small but non-zero values of the mass-density

ratio. Unfortunately, a parametric study for finite values of the mass-density ratio is considerably more involved than for the $\mu = 0$ case simply because the mass and inertial properties of the structure must be considered. This meant that every effort had to be made to decrease the computational requirements without sacrificing the general applicability of any conclusions resulting from the study. Accordingly, it was decided to follow a program designed to keep the computational work to a minimum by changing what were to be regarded as the fundamental non-dimensional system parameters and also by obtaining as much information as possible from the simplified quasi-steady and quasi-unsteady flutter equations. The several changes in the system of non-dimensional parameters will be discussed first.

Historically, the flutter speed coefficient ($U_f/b\omega_\alpha$) and flutter frequency coefficient ($\omega_\alpha/\omega_f$) are considered to be functions of the five system parameters u, $\Pi^2$, a, $x_\alpha$, and $r_\alpha$. For the non-zero mass density ratio portion of this investigation, the non-dimensional parameters chosen are:

$\mu$ and $\Pi^2$ - the mass-density ratio and frequency ratio squared respectively; same definitions as previously given.

a - the non-dimensional elastic axis location for a "typical section"; more generally the location of the axis of zero static coupling. Positive for axis aft of midchord.

$x_m$ - the non-dimensional distance between the midchord and the center of gravity = $x_\alpha + a$. Positive for c.g. aft of midchord.

$r_c$ - non-dimensional radius of gyration about the center of gravity = $(r_\alpha^2 - x_\alpha^2)^{\frac{1}{2}}$ or $\frac{I_{c.g.}}{mb^2}$

The use of the mass-density ratio $\mu$ requires no discussion. However, the very fact that it is desired to keep the effects of the mass-density ratio entirely separate leads to the choice of the "in vacuum" frequency ratio squared, $\Pi^2$, and subsequently to the use of the "in vacuum" pitching frequency ($\omega_\alpha$) in the expressions defining the flutter speed and flutter frequency coefficients.

It may be recalled that the analysis performed for the zero mass-density ratio required that the frequencies be computed for the structure submerged in the surrounding fluid, ($\Pi^2_*$, $\omega_\alpha{}^*$, and $\omega_h^*$). No disadvantage was encountered by the inclusion of the mass-density ratio in the frequency parameters as the entire investigation was conducted for one specific value of $\mu$. Conversely, it may be noted that requiring that the "in fluid" frequency ratio remain constant over a range of mass-density ratios would be to imply a change in the structure itself; the change being a function of the mass-density ratio change involved. Thus, although any results of such an investigation would certainly be mathematically correct, a physical interpretation might be somewhat difficult to obtain. On the other hand, by using the "in vacuum" frequencies, and thereby keeping the mass-density ratio entirely separate, it is a simple matter to trace the flutter behavior of any reasonable physical configuration through any range of values of the mass-density ratio; the simple physical interpretation being that of a given structure submerged in fluids of varying density. The two approaches are, of course, entirely equivalent everywhere except at $\mu = 0$. Thus, although it must be admitted that the "in fluid" frequencies are probably more representative of the fluid-structure system taken as a whole, the desirability of completely isolating any effects due to changes in the mass-density ratio requires the use of parameters which are not explicitly dependent upon the mass-density ratio in any way.

The remaining three dimensionless parameters are completely determined by the configuration of the structure which the section is assumed to represent. The parameter (a) is the classical non-dimensional

location of the axis of zero static coupling, as denoted in Figure 2, and is only discussed because this axis does not necessarily coincide with the elastic axis of the section itself. Historically, the typical section has been assumed to be a section located at some specified spanwise station of a straight wing which could be analyzed and would give results valid for the entire wing. Clearly, the correct location of the axis of zero static coupling for such a representation is indeed the elastic axis of the section. However, there are several important classes of structures for which the elastic axis of the section may not be regarded as the axis of zero static coupling. For example, it is not difficult to visualize certain completely movable control surfaces for which the axis of zero static coupling might be more closely related to the pivot point than to the elastic axis of a similar section. Further, and of even more importance insofar as this investigation is concerned, one of the effects of sweeping a cantilever, when $\alpha$ is taken in a streamwise plane, is to locate the axis of zero static coupling at other than the section elastic axis; the exact location being a function of the spanwise location of the representative section. Figure 6 shows this comparison. Hence, it is logical to expect that part of the static mechanical effects of sweeping a structure can be inserted into the basic section analysis by the proper choice of an (a) value. This is precisely why the range of (a) values investigated was much larger than that required to cover the section proper. (i.e., range for numerical work was $-4 \leq a \leq 3$.) It was felt that the investigation of the swept cantilever effects (Part II) could be simplified and the results clarified by the resultant separation of the causes and effects. In what follows, the term "elastic axis" means the axis of zero static coupling and not the section elastic axis, unless it is so specified.

The decision to regard the elastic axis location (a) as essentially independent of the shape of the section makes it desirable to separate the inertial characteristics from the elastic axis location. Accordingly, the last two non-dimensional parameters adopted are $x_m$ and $r_c$

rather than their classical counterparts, $x_\alpha$ and $r_\alpha$, since the latter set explicitly includes the location of the elastic axis (a). Conversely, the location of the center of gravity with respect to the midchord ($x_m$) and the value of the radius of gyration about the center of gravity ($r_c$) are obviously independent of any artificially contrived axis of zero static coupling. Again, it must be realized that either system could be used; the choice being strictly a matter of convenience. However, a clear understanding of the physical changes in the system implied by the various parametric variations is not ea sily obtained if the parameters are inter-related.

From a numerical standpoint, the value of $r_c^2$ may be regarded as a constant for most reasonable section shapes, a value of .25 being representative. (For physically sensible section shapes, $r_c^2$ varies between approximately .20 and .33 depending on the exact shape of the section.) Since previous investigations have shown the flutter behavior of a section to be comparatively insensitive to small changes in the radius of gyration, it is apparent that the numerical work using, in general, the single value of $r_c^2$ may be regarded as representative, thus reducing the computational effort. However, certain qualitative effects of varying $r_c^2$ are discussed later in some detail.

Contrary to what has been said regarding $r_c^2$, the location of the center of gravity ($x_m$) is a strong function of the shape of the section. Hence the choice of a particular value for $x_m$, (c.g. confined to section proper or $-1 \leq x \leq 1$), qualitatively determines the actual shape of the structure being investigated.

Development of the Equations Used for the Non-Zero

Mass-Density Ratio Analyses

As previously noted, much information may be obtained from the approximate quasi-steady and quasi-unsteady results. In order to show how the approximate theories may be useful in determining areas where

finite flutter boundaries exist, the flutter equations resulting from both the approximate and the "exact" unsteady theories must be presented.

The derivation of the "exact" flutter equations follows naturally from the expansion of the flutter determinant (Eq. I-4) as illustrated in Appendix A. The approximate flutter equations can be obtained from the "exact" results or directly from Eq. I-4 by using the suitable unsteady hydrodynamic derivatives. These derivatives are listed below.

| For $C(k) = \frac{1}{2}$ | For $C(k) = 1$ |
|---|---|
| $L_h = 1 - j\,\frac{U_f}{b\omega_f}$ | $L_h = 1 - j\,2\,\frac{U_f}{b\omega_f}$ |
| $L_\alpha = \frac{1}{2} - j\,2\,\frac{U_f}{b\omega_f} - \left(\frac{U_f}{b\omega_f}\right)^2$ | $L_\alpha = \frac{1}{2} - j\,3\,\frac{U_f}{b\omega_f} - 2\left(\frac{U_f}{b\omega_f}\right)^2$ |
| $M_h = \frac{1}{2}$ | $M_h = \frac{1}{2}$ |
| $M_\alpha = \frac{3}{8} - j\,\frac{U_f}{b\omega_f}$ | $M_\alpha = \frac{3}{8} - j\,\frac{U_f}{b\omega_f}$ |

Regardless of the method, the equations to be presented can be obtained without any conceptual difficulty, although the algebraic effort required is considerable.

Case 1. $C(k) = \frac{1}{2}$

$$\frac{\omega_\alpha^2}{\omega_f^2} = \Omega^2 = \frac{\mu(a^2 - a + \frac{1}{4} + r_\alpha^2 + 2ax_\alpha - x_\alpha) + \frac{3}{8}}{\mu r_\alpha^2 + \mu\Pi^2(a^2 - a + \frac{1}{4})}$$

(I-19)

$$\Omega^2\mu(r_\alpha^2 + \mu r_\alpha^2 + \mu r_\alpha^2\Pi^2 + \frac{\Pi^2}{8} + a^2\Pi^2) - \Omega^4\mu^2\Pi^2 r_\alpha^2$$

$$(\frac{U_f}{b\omega_\alpha})^2 = X^2 = \frac{-\mu(r_\alpha^2 + \mu r_\alpha^2 - \mu x_\alpha^2 + 2ax_\alpha = a^2 + \frac{1}{8}) - \frac{1}{8}}{\Omega^2[\mu a(1 - \Omega^2\Pi^2) + \frac{\mu}{2}(1 - \Omega^2\Pi^2) + \mu x_\alpha - \frac{1}{2}]}$$

To incorporate the system parameters chosen for this investigation, the following substitutions are made:

$$x_\alpha = x_m - a$$

$$r_\alpha^2 = r_c^2 + (x_m - a)^2$$

This results in Eqs. (I-19) taking the form:

$$\Omega^2 = \frac{\mu[r_c^2 + (x_m - \frac{1}{2})^2] + \frac{3}{8}}{\mu[r_c^2 + (x_m - a)^2 + \Pi^2(a - \frac{1}{2})^2]} \qquad \text{(I-20a)}$$

$$\Omega^2\mu\left[(r_c^2 + [x_m - a]^2)(1 + \mu + \mu\Pi^2) + \Pi^2\left(\frac{1}{8} + a\right)\right]$$

$$- \Omega^4\mu^2\Pi^2\left[r_c^2 - (x_m - a)^2 - \mu\left\{\left[r_c^2 + (x_m - a)^2\right][1 + \mu\right]\right.$$

$$X^2 = \frac{\left. - \mu(x_m - a)^2 + 2ax_m - a^2 + \frac{1}{8}\right\} - \frac{1}{8}}{\Omega^2\left[\mu a(1 - \Omega^2\Pi^2) + \frac{\mu}{2}(1 - \Omega^2\Pi^2) + \mu x_m - \mu a - \frac{1}{2}\right]} \qquad \text{(I-20b)}$$

Since $X^2$ does not appear in Eq. (I-20a) it follows that substitution of Eq. (I-20a) into Eq. (I-20b) will result in an explicit expression for the flutter speed coefficient. For present purposes, it is only necessary to remark that the resultant expression may be written as a ratio of polynomials in $\mu$ of the general form:

$$X^2 = \frac{\sum_o^i \mu^\eta [f_\eta(r_c^2,\ x_m,\ a,\ \Pi^2)]}{\sum_o^i \mu^p [g_p(r_c^2,\ x_m,\ a,\ \Pi^2)]} \qquad \text{(I-21)}$$

where, for any given typical section, the coefficients of the $\mu^{p,\eta}$ may be regarded as constants.

Case 2. C(k) = 1

Proceeding as in Case 1, the following quasi-steady flutter equations may be obtained.

$$\Omega^2 = \frac{r_\alpha^2 - a(\tfrac{1}{2} - a) - x_\alpha(\tfrac{1}{2} - 2a) + \frac{1}{8}\mu}{r_\alpha^2 - a(\tfrac{1}{2} - a)\Pi^2}$$

(I-22)

$$\Omega^4\mu^2 r_\alpha^2\Pi^2 + (\mu r_\alpha^2 + \frac{1}{8} + a^2)(\mu + 1 - \Omega^2\mu\Pi^2)$$

$$X^2 = \frac{-\Omega^2\mu r_\alpha^2(\mu + 1) - (\mu x_\alpha - a)^2}{2\Omega^4\mu\Pi^2(\tfrac{1}{2}+a) - 2\Omega^2[-\tfrac{1}{2} + \mu(\tfrac{1}{2} + a + x_\alpha)]}$$

By replacing $r_\alpha^2$ and $x_\alpha$ with $r_c^2$ and $x_m$, Eqs. (I-22) may be re-written in the form:

$$\Omega^2 = \frac{\mu[r_c^2 + x_m(x_m - \tfrac{1}{2}) + \frac{1}{8}}{\mu[r_c^2 + (x_m - a)^2 + a\Pi^2(a - \tfrac{1}{2})]} \qquad \text{(I-23a)}$$

$$\Omega^4\mu^2\Pi^2[r_c^2 + (x_m - a)^2] +$$

$$[\mu + 1 - \Omega^2\mu\Pi^2]\{\mu[r_c^2 + (x_m - a)^2] + a^2 + \frac{1}{8}\}$$

$$X^2 = \frac{-\Omega^2\mu(\mu + 1)[r_c^2 + (x_m - a)^2] - [\mu(x_m - a) - a]^2}{2\Omega^4\mu\Pi^2(\tfrac{1}{2}+a) - 2\Omega^2[\mu(x_m + \tfrac{1}{2}) - \tfrac{1}{2}]} \qquad \text{(I-23b)}$$

As in the previous case, substitution of Eq. (I-23a) into Eq. (I-23b) results in an explicit expression for the flutter speed coefficient which may be regarded as a ratio of polynomials in $\mu$ (Eq. I-21). Thus the flutter equations obtained from the approximate quasi-steady and quasi-unsteady hydrodynamics are seen to be similar in form.

Case 3. $C(k) = F(k) + jG(k)$

For the case where the "exact" unsteady theory is used, the flutter equations may be written as shown below, (Eqs. I-24). Once again, $r_\alpha^2$ and $x_\alpha$ may be replaced by $r_c^2 + (x_m - a)^2$ and $(x_m - a)$, respectively, to yield Eqs. (I-25), as shown on page 36.

$$\Omega^2 = \frac{\{\frac{1}{8}+a^2+\mu r_\alpha^2\}\{k[2-F+\mu 2(1-F-2a+4a^2F+8aFx_\alpha-2x_\alpha+4Fr_\alpha^2)] + 4G[1-\mu(1+2a+2x_\alpha)]\}}{\mu k[F(1+8a^2)r_\alpha^2+\Pi^2(\frac{1}{8}+a^2+\mu r_\alpha^2)(2-2F-4a+8a^2F)+\mu 8r_\alpha^4F] - \mu 4\Pi^2G(\frac{1}{8}+a^2+\mu r_\alpha^2)(1+2a)}$$

$$X^2 = \frac{\mu 8\Pi^2 r_\alpha^2}{\mu 8k^2\{\{(1+\mu)r_\alpha^2+\Pi^2(\frac{1}{8}+a^2+\mu r_\alpha^2)\}+\mu 8k\{2Gr_\alpha^2+G\Pi^2(2a^2-\frac{1}{2})\} + \mu 8\Pi^2F(1+2a)-\frac{1}{\Omega^2}\{k^2-2Gk-8F+\mu k^2[1+8a^2+16ax_\alpha-\mu 8x_\alpha^2 + 8r_\alpha^2(1+\mu)]+\mu 4Gk[4a(a+2x_\alpha)+4r_\alpha^2-1]+\mu 8F(1+2a+2x_\alpha)\}}$$

Eqs. (I-24a) and (I-24b)

$$\Omega^2 = \frac{\left\{\frac{1}{8}+a^2+\mu\left(r_c^2+[x_m-a]^2\right)\right\}\left\{k[2-F+\mu 2(1-2x_m+F[4x_m^2+4r_c^2-1])]\right.}{\left.+\,4G[1-\mu(1+2x_m)]\right\}}$$

$$\mu k\left\{F(1+8a^2)(r_c^2+[x_m-a]^2)+\Pi^2\left(\frac{1}{8}+a^2+\mu\left[r_c^2-(x_m-a)^2\right]\right)(2-2F-4a+8a^2F)\right.$$

$$\left.+\,\mu 8F(r_c^2+[x_m-a]^2)^2\right\}-\mu 4\Pi^2G(1+2a)\left(\frac{1}{8}+a^2+\mu[r_c^2+(x_m-a)^2]\right)$$

$$X^2 = \frac{\mu 8\Pi^2\left[r_c^2+(x_m-a)^2\right]}{\mu 8k^2\left\{(1+\mu)\left[r_c^2+(x_m-a)^2\right]+\Pi^2\left(\frac{1}{8}+a^2+\mu\left[r_c^2+(x_m-a)^2\right]\right)\right\}}$$

$$+\,\mu 8k\left\{2G\left[r_c^2+(x_m-a)^2\right]+G\Pi^2\left(2a^2-\tfrac{1}{2}\right)\right\}+\mu 8\Pi^2F(1+2a)$$

$$-\frac{1}{\Omega^2}\left\{k^2-2Gk-8F+\mu k^2\left[1+8x_m^2+8(1+\mu)r_c^2\right]\right.$$

$$\left.+\,\mu 4Gk\left[4r_c^2+4x_m^2-1\right]+\mu 8F(1+2x_m)\right\}$$

Eqs. (I-25a) and (I-25b)

As with the approximate equations, it may be seen that $X^2$ does not appear in Eq. (I-25a). Thus, in principle, Eq. (I-25a) may be substituted into Eq. (I-25b) to obtain an expression for the flutter speed coefficient as a function of the five system parameters, ($\Pi^2$, a, $\mu$, $x_m$, $r_c^2$), the reduced frequency k, and the real and complex parts of the Theodorsen function, (F and G respectively), which are themselves functions of k. Obviously, such an expression may only be regarded as valid for those combinations of the system parameters and the reduced frequency for which the solutions to Eq. I-25a and I-25b can be combined to yield $\Omega^2 X^2 = \frac{1}{k^2}$. With this restriction in mind, it may be noted that the resultant expression for the flutter speed coefficient may be written as a ratio of polynomials in $\mu$ of the general form:

$$X^2 = \frac{\sum_0^i \mu^\eta [f_\eta (r_c^2,\ x_m,\ a,\ \Pi^2,\ k,\ F(k),\ G(k))]}{\sum_0^j \mu^p [g_p (r_c^2,\ x_m,\ a,\ \Pi^2,\ k,\ (F(k),\ G(k))]} \qquad \text{(I-26)}$$

Now, unlike the equations resulting from the approximate theories, the coefficients of the $\mu^{\eta, p}$ cannot be regarded as constants for any given typical section since, in general, the value of the reduced frequency k obtained from solving Eqs. I-25a and I-25b changes as the mass density ratio is changed. Further, it is possible for more than one value of k to satisfy Eqs. I-25a and I-25b for certain sets of system parameters. Thus a given typical section operating at some fixed mass-density ratio could mathematically have more than one flutter speed coefficient. The implications of this last possibility will be discussed in greater detail later.

All of the equations presented in this section are useful in determining the general character of the flutter solutions in the low mass-density ratio region and will be discussed when their specific contributions are considered. For present purposes it is sufficient to discuss the general forms of the expressions for the flutter speed coefficient

squared in order to justify the reasoning used in limiting the types of flutter boundaries which might possibly occur in the low mass-ratio region. The reasoning only requires that for real, finite values of the system parameters, the square of the flutter speed coefficient be a continuous function of $\mu$ everywhere except that at certain discrete values of $\mu$ the denominator may vanish.

For the approximate unsteady hydrodynamic theories, the flutter speed coefficient squared has been shown to be expressible as a ratio of polynominals in $\mu$, (Eq. I-21); where for any given typical section the coefficients of the polynomials may be regarded as constants. Accordingly, one may expect the expression for $X^2$ as a function of $\mu$ to be smooth and well behaved everywhere except at those points for which the denominator vanishes. Hence, a plot of $X^2$ versus $\mu$ may be expected to be smooth and continuous with the possible exception of certain discrete values of $\mu$ for which $X^2$ may be infinite. Clearly only positive values of $X^2$ have any practical physical significance, but the smooth behavior of the expression may be expected regardless of the practical significance of the result.

For the "exact" theory, the square of the flutter speed coefficient has also been shown to be expressible as a ratio of polynomials in $\mu$, (Eq. I-26). However, the coefficients of the $\mu$ terms may not be regarded as constant for fixed values of $\Pi^2$, a, $x_m$, and $r_c^2$; but rather are also dependent upon the reduced frequency k. Nevertheless, considering the fact that F and G are continuous functions of k and considering the form of the expression, it is not unreasonable to expect a plot of $X^2$ versus $\mu$ to be smooth; again excepting those points for which the denominator vanishes. There are reasons other than the form of the expression for expecting a smooth behavior. First, it is well known that the results for moderate values of the mass-density ratio have always exhibited a smooth dependence of X upon $\mu$, as depicted in Figure 1. Second, as has been shown, the results obtainable from the quasi-steady and

quasi-unsteady theories must, in general, be smooth and well behaved. These approximate theories are the opposite extremes of the "exact" theory. It is mentioned again, however, that it is possible, for certain combinations of the system parameters, for more than one value of the reduced frequency to satisfy the "exact" flutter equations. This implies that for certain values of the mass-density ratio, the same typical section may yield more than one flutter speed coefficient. Clearly, from a practical standpoint, only the lower value is of interest. However, the types of flutter boundaries which might result because of these multiple values have been considered and are discussed in later sections.

## Possible Types of Low Mass-Density Ratio Flutter Boundaries

Basically, the arguments of the previous section have been presented to show that real, finite, flutter boundaries of physically plausible structures (e.g., Figure 1) cannot be segments of curves with the terminal points having a finite, non-zero value for either the flutter speed coefficient or the mass-density ratio. Further, the zero mass-density ratio analysis has shown that the flutter boundaries can neither terminate at nor approach asymptotically the line depicting a zero mass-density ratio, (i.e., the ordinate of Figure 1 or Figure 7). It will be shown that the combination of these constraints serves to restrict the form of flutter boundaries that might exist in the low mass-density ratio regime to a relatively small number. Just what forms these boundaries might take can best be illustrated by a few simple plots.

The flutter boundary shown in Figure 7 is representative of the type of boundary known to result from a two-degree-of-freedom analysis of many aircraft wing "typical sections." The line labeled $\mu_a$ represents the value for which the quasi-steady hydrodynamic theory predicts an infinite flutter speed, (Eq.I-1). Other investigators have shown (e.g., Refs. 3, 5), that for so-called "reasonable" sections, the value of $\mu_a$ is

of the order of one. Since the existence of finite flutter boundaries for $\mu > \mu_a$ is an acknowledged fact, generally the region of greatest interest herein is $\mu > \mu_a$; the shaded region of Figure 7. However, one possibility which must be considered is that the boundary depicted in Figure 7 might, for certain as yet uninvestigated configurations, be displaced in such a manner that the flutter free region might be extremely small. In view of the works of previous investigators (Refs. 3, 5), this is deemed unlikely. However, because of the rather extreme section configurations (e.g., center of gravity near trailing edge) sometimes used for hydrofoil struts or lifting surfaces, the dependence of the value of $\mu_a$ upon the other system parameters will be discussed in detail in the next section.

Another possibility for finite low mass-density ratio flutter boundaries is that completely separate and as yet undiscovered boundaries exist for certain reasonable combinations of system parameters. In view of the restrictions previously noted, it may be seen that any "new" boundaries confined to the $\mu < \mu_a$ region would have to have one of the four general forms depicted in Figures 8a-d.

Figures 8a and 8d illustrate the possibility of real solutions reappearing from plus infinity and either tending toward a zero flutter speed or again exhibiting an asymptotic behavior. Figures 8b and 8c show solutions reappearing from zero. These latter boundaries would be the positive extensions of flutter speed coefficient squared $(U_f/b\omega_\alpha)^2$ solutions approaching from minus infinity. Further, the possibility of multiple solutions implies that combinations of the above could exist.

Now it may be noted that since the $\mu = 0$ line has been ruled out as a possible asymptote, the existence of boundaries 8a and 8c would require that the solutions approach infinity for some finite value of the mass-density ratio less than $\mu_a$. In short, for the boundaries 8a and 8c to be possible, it would be necessary to show that for some given set of system parameters, at least a second asymptotic solution (i.e., a second $\mu_a$) could exist for some value of $0 < \mu < \mu_a$. This means that the requisite

information as to whether such boundaries might exist may be obtained by a careful study of the quasi-steady, ($k \to 0$), flutter equations.

On the other hand, the existence of boundaries such as those depicted in Figures 8b and 8d would require that valid solutions exist on the abscissa; i.e., valid zero flutter speed solutions. Hence, these possibilities may be checked by a careful study of the quasi-unsteady, ($k \to \infty$), flutter equations.

Thus, a detailed study of the approximate flutter equations will reveal whether any physically plausible configurations may be expected to yield separate and distinct flutter boundaries in the very low mass-density ratio region - i.e., for some $\mu$ less than the $\mu_a$ predictable for that configuration. Accordingly, the approximate flutter equations have been carefully investigated. These investigations are discussed in detail in the next two sections.

The possibility of the "exact" section analysis predicting several flutter solutions for some range of mass-density ratios has been mentioned. Clearly this suggests several additional types of flutter boundaries that might exist. Two possibilities are depicted in Figure 9, where the "new" boundaries have been superimposed upon what might be termed the typical representation of Figure 7.

In view of the results of the modal analyses discussed in Refs. 10, 11, and 12, the boundary tending toward a flutter speed of zero as the mass-density ratio approaches zero might be viewed as a particularly attractive possibility. Nevertheless, it may be noted that the existence of these "new" boundaries may also be checked by examining the approximate flutter equations as the remarks made for Figures 8 again apply.

The last, and probably least attractive possibility is shown in Figure 10.

This is termed least attractive for several reasons. First, it is noted that previous investigators (e.g., Refs. 3 and 5) have shown

the value of $\mu_a$ to be a good indicator of the limit of the "typical" boundary for all the cases considered, although some valid solutions have been obtained for values of $\mu$ very slightly less than $\mu_a$. Second, it is apparent that the above behavior could only be uncovered by using the "exact" flutter equations for a section. Third, the resultant boundary could not agree with the low mass-density ratio results of the modal solutions performed on actual three dimensional swept structures (e.g., Refs. 10, 11, and 12). Nevertheless, this possibility has been considered and is eventually discussed herein. Essentially, it will be shown that all the evidence indicates that it is extremely unlikely that any boundary such as the one depicted in Figure 10 can exist in the low mass-density ratio region for reasonable two dimensional, unswept configurations.

To summarize, it has been shown that only a limited number of possibilities have to be examined to determine whether very low mass-density ratio flutter may be predicted by a two-degree-of-freedom representative section analysis. Further, it has been noted that most of the possibilities may be either substantiated or discarded by a careful appraisal of the approximate, $(k \to 0; \infty)$, flutter equations. Accordingly, the following is an outline of the work to follow.

1. The approximate flutter equations associated with the quasi-steady hydrodynamic theory $(k \to 0)$ are discussed in detail. This study reveals whether any physically plausible configurations exhibit an asymptotic approach to an infinite flutter speed for more than one value of $\mu$ and hence reveals whether certain of the flutter boundaries discussed above exist. In addition, the dependence of $\mu_a$ upon the various structural system parameters is determined in order to ascertain practical minimum mass-density ratios for which the "typical" flutter boundary of Figure 7 may be expected.
2. The approximate flutter equations associated with the quasi-unsteady hydrodynamic theory, $(k \to \infty)$ are discussed in detail. The purpose of this study is to determine whether (and if so,

under what conditions) zero flutter speed solutions can occur. Thus, the existence of the types of flutter boundaries terminating on the abscissa, Figures 8b, c, d, and 9, is checked.

3. A careful comparison of the asymptotic tendencies of the quasi-steady and quasi-unsteady solutions, ($\mu_a$ and $\mu_a'$), is made - with particular emphasis on the low mass-density ratio region. This comparison indicates whether flutter boundaries of the type shown in Figure 10 can exist. (A flutter boundary of the type being considered logically requires that $\mu_a'$ be appreciably less than $\mu_a$; and further that flutter solutions with a relatively high reduced frequency be expected for some values of $u < \mu_a$.) Some combinations are also checked using the "exact" theory.

The discussions of the above investigations and the conclusions resulting therefrom are treated in the remaining portions of Part I.

Constraints on the Flutter Boundary of a Section Which are Imposed by the Character of the Asymptotic Flutter Speed Solutions

Previous sections have served to show that the typical section analysis will admit to, at most, a limited number of low mass-density ratio flutter boundaries. This section shows how a careful investigation of the dependence of the $\mu_a$ solutions upon the various non-dimensional system parameters further restricts the nature and the number of possible boundaries; the fundamental approach being a study of the quasi-steady flutter equations.

The methods of obtaining the flutter equations associated with a reduced frequency (k) of zero have already been discussed with the resultant expressions presented as Eqs. I-22 and I-23. For convenience,

the numerator and the denominator of Eq. I-23b are divided by $\Omega^2$. This leads to the following set of equations:

$$\Omega^2 = \frac{\mu[r_c^2 + x_m(x_m - \frac{1}{2})] + \frac{1}{8}}{\mu[r_c^2 + (x_m - a)^2 + a\Pi^2(a - \frac{1}{2})]} \tag{I-27a}$$

$$\Omega^2\mu^2\Pi^2[r_c^2 + (x_m - a)^2] +$$

$$[\frac{\mu + 1}{\Omega^2} - \mu\Pi^2]\{\mu[r_c^2 + (x_m - a)^2] + a^2 + \frac{1}{8}\}$$

$$X^2 = \frac{-\mu(\mu + 1)[r_c^2 + (x_m - a)^2] - \frac{1}{\Omega^2}[\mu(x_m - a) - a]^2}{2\Omega^2\mu\Pi^2(\frac{1}{2} + a) - 2[\mu(x_m + \frac{1}{2}) - \frac{1}{2}]} \tag{I-27b}$$

For a physically plausible set of system parameters, the above equations become "exact" as the flutter speed becomes infinite or the flutter frequency zero. Hence, it is possible to obtain from the above equations the value or values of the mass-density ratio, expressed as a function of the other system parameters, for which the flutter speed increases without limit.

Since in any real physical system an infinite flutter speed coefficient implies an infinite flutter speed, it is obvious that an infinite flutter speed results if either the numerator of Eq. (I-27b) is infinite or the denominator zero. Clearly, the former possibility is only of limited interest as it immediately requires that at least one of the system parameters be infinite. To consider any of the system parameters as infinite is, in general, of no practical interest - with the exception of the section

frequency ratio, $\Pi^2$. However, it may be seen that Eq. (I-27b) becomes an indeterminate expression if the frequency ratio is taken to approach infinity. Hence, the flutter speed coefficient becomes, in such a case, a function of the other system parameters and is not, in general, infinite unless the structure is regarded as having no torsional stiffness, ($\omega_\alpha = 0$). For this latter case, the resultant infinite flutter speed coefficient is seen to exist regardless of the values of the other system parameters. This may be regarded as an unfortunate consequence of using the uncoupled torsional frequency as the non-dimensionalizing quantity. Hence it may be concluded that the only infinite flutter speed coefficients of practical interest are those that result from the vanishing of the denominator of Eq. (I-27b).

If Eq. (I-27a) is substituted into the denominator of Eq. (I-27b) and the resulting expression is set equal to zero, an equation involving the mass-density ratio, $\mu$, to only the first power results. Solving for $\mu$ in terms of the other system parameters yields the value of $\mu$ for which the flutter speed is infinite, $\mu_a$. The resultant expression is, of course, the equivalent of Eq. (I-1) and may be written:

$$\mu_a = \frac{\frac{1}{2}\left[r_c^2 + (x_m - a)^2\right] + \Pi^2\left[\frac{a^2}{2} - \frac{a}{8} + \frac{1}{16}\right]}{\left[r_c^2 + (x_m - a)^2\right]\left[x_m + \frac{1}{2}\right]} \qquad \text{(I-28)}$$

$$- \Pi^2\left\{(x_m - a)(a^2 + a - \frac{1}{4}) + (\frac{1}{2} + a)\left[r_c^2 + (x_m - a)^2\right]\right\}$$

Since the parent expression to the above equation contains $\mu$ to only the first power, it is evident that for any single, physically possible combination of system parameters, only one $\mu_a$ will exist. Hence, all of the flutter boundaries discussed in the previous section which would have required at least a second asymptotic solution may immediately be discarded as valid possibilities. Thus the boundaries depicted in Figures 8a,

8c, and the boundary of Figure 9, which shows an infinite solution for some $\mu < \mu_a$ may all be eliminated as possibilities. Further, any of the other types of boundaries which are depicted as approaching an asymptote must approach the one determined from Eq. (I-28).

Since it has been shown in previous sections that no valid flutter points exist for, or approach asymptotically, the zero mass-density ratio line, it is clear that if some combinations of system parameters can be found which yield a negative value for $\mu_a$, the only valid finite flutter boundaries that might possibly exist are those shown to require one or more crossings of the abscissa. In the next section, this possibility will be discarded. Thus, although it has not as yet been definitely proven, it will be stated at this time that an infinite or a negative $\mu_a$ indicates that no physically meaningful flutter solutions exist for any positive mass-density ratio. This is in accordance with what was suggested by Herr, (Ref. 5), but which unfortunately was not proven. This entire matter will be discussed in detail in the next section, which also includes the evidence supporting the above statement.

Eq. (I-28) may be studied to determine the dependence of $\mu_a$ upon the various structural system parameters. That $\mu_a$ cannot be zero has already been established and discussed. Hence the determination of what minimum positive $\mu_a$ values may be expected for physically reasonable systems becomes of particular interest. In addition, the dependence and sensitivity of $\mu_a$ to changes in the various structural parameters is desired.

The physical constraints imposed for this investigation are listed and discussed below.

1. $\Pi^2$ must be equal to or greater than zero. Clearly no meaningful physical systems can possess negative natural frequencies.
2. $r_c^2$ must be positive and will be restricted to values less than or at most equal to one as this includes all meaningful physical systems.

3. The center of gravity will be constrained such that $-1 \leq x_m \leq 1$. This is somewhat arbitrary, but includes all systems with the c.g. on the section proper.
4. The limits imposed on the location of the axis of zero static coupling are again arbitrary. However, for reasons which have already been presented, the numerical analysis will consider values between $-4 \leq a \leq 3$.

The dependence of the calculated $\mu_a$ values upon the individual non-dimensional system parameters may be readily established by investigating the behavior of Eq. (I-28) as all but one of the structural parameters (say $x_m$) are regarded as being fixed. Clearly, this poses no problems. However, the determination of a positive minimum could become quite involved if it were approached in the classical manner whereby the above stated constraints would be imbedded into Eq. (I-28) and the partial derivatives of the combined expression examined. In addition, the boundaries of the mathematical space represented by the function and its constraints and the points for which Eq. (I-28) does not possess a derivative or where the function is not continuous would have to be examined. Fortunately, the classical approach is not required as the positive minimum may be deduced by combining the results of the individual dependence analyses with results which have already been discussed. That the deductions are correct is proven by numerical examples, some of which are included herein.

A glance at Eq. (I-28) will show that it may be put into the following form:

$$\mu_a = \frac{A + \Pi^2 B}{C + \Pi^2 D} \tag{I-29}$$

where A, B, C, and D are functions of $x_m$, $r_c^2$, and (a). For the present time, these may be regarded as constants. To determine whether any $\Pi^2$ values will result in a stationary point, the derivative of $\mu_a$ with respect to $\Pi^2$ is set equal to zero.

Accordingly, the following may be obtained:

$$\frac{\partial \mu_a}{\partial(\Pi^2)} = \frac{BC - AD}{(C + \Pi^2 D)^2} = 0 \qquad \text{(I-30)}$$

Therefore:

$$\frac{\partial \mu_a}{\partial(\Pi^2)} = 0$$

if $BC = AD$ (for all finite $\Pi^2$ if

$D\Pi^2 + C$ does not equal zero)

or if $\Pi^2 = \infty$

Thus, there exist no finite values of $\Pi^2$ for which $\partial \mu_a / \partial(\Pi^2)$ is zero although the limiting value of an infinite frequency ratio does appear as a possibility. The first solution noted above is, however, of some interest as it yields a condition for which the value of $\mu_a$ is independent of $\Pi^2$. This is discussed in detail later in this section.

Eq. (I-30) also shows that $\partial \mu_a / \partial(\Pi^2)$ approaches infinity as $D\Pi^2 + C$ approaches zero. This would yield combinations of parameters for which $\mu_a$ is very sensitive to changes in $\Pi^2$.

With regard to the immediate problem, it follows from the above that if some combination of (a), $r_c^2$, and $x_m$ can be associated with a minimum positive $\mu_a$, this value must occur for one of the limiting values of $\Pi^2$ or else must be determined by the behavior of the function, (Eq. I-28), as it approaches infinity. This latter possibility can be discarded as of no practical interest since an asymptotic behavior of $\mu_a$ as a function of $\Pi^2$ could only yield a positive minimum if a curve of $\mu_a$ versus $\Pi^2$ passed through zero for some value of $\Pi^2$ - in which case the minimum $\mu_a$ would

be zero. However, it has been shown that $\mu_a$ cannot be zero for any system of practical interest. Thus, only the former possibility need be given serious consideration.

Clearly, negative values of $\Pi^2$ are of no practical interest. Thus the limiting values of $\Pi^2$ that need be considered are zero and plus infinity. The case of $\Pi^2$ equal to zero is easily discerned from Eq. (I-28) and seen to yield the following result:

$$\mu_{a_{\Pi^2 = 0}} = \frac{1}{1 + 2x_m} \tag{I-31}$$

This is a particularly simple expression showing the $\mu_a$ for $\Pi^2 = 0$ to be entirely dependent upon the location of the center of gravity. Now to ascertain whether some positive $\mu_a$ can exist which is less than what could be obtained from Eq. (I-31), the other limiting value of $\Pi^2$ equal to infinity will be considered.

If Eq. (I-28) is investigated as $\Pi^2$ approaches infinity, an indeterminate expression results which, when evaluated, leads to the following:

$$\mu_{a_{\Pi^2 \to \infty}} = \frac{\frac{a^2}{2} - \frac{a}{8} + \frac{1}{16}}{(a - x_m)(a^2 + a - \frac{1}{4}) - (\frac{1}{2} + a)[r_c^2 + (x_m - a)^2]} \tag{I-32}$$

Clearly, the above expression is considerably more involved than that shown in Eq. (I-31). Since it contains all three of the remaining non-dimensional parameters, it follows that the minimum value which Eq. (I-32) might achieve is a function not only of the center of gravity, ($x_m$), but also of the location of the elastic axis (a), and the radius of gyration of the section ($r_c^2$). Thus, to determine the extremums of Eq. (I-32), these other

parameters must be considered. A fruitful approach is to consider Eq. (I-32) as a polynomial in (a) and arrange the expression accordingly:

$$\mu_{a_{\Pi^2 \to \infty}} = \frac{\frac{a^2}{2} - \frac{a}{8} + \frac{1}{16}}{a^2(x_m + \frac{1}{2}) - a(x_m^2 + r_c^2 + \frac{1}{4}) + (\frac{x_m}{4} - \frac{r_c^2}{2} - \frac{x_m^2}{2})} \qquad \text{(I-33)}$$

Now the extremums of $\mu_{a_{\Pi^2 \to \infty}}$ as a function of (a) will be sought. Again the extremums may occur where the derivative of the function to be extremized, ($\mu_{a_{\Pi^2 \to \infty}}$), taken with respect to (a), vanishes; for the limiting values of (a); or may be determined by the behavior of Eq. (I-33) as it approaches infinity. Since the desired quantity, if it exists, is to be a minimum positive value, the third possibility may be neglected for the same reasons given when discussing Eq. (I-29).

Since (a) is only arbitrarily restricted, the limiting value(s) of (a) may be taken as infinity. Clearly then, the second possibility would lead to an indeterminate form for Eq. (I-35), which, when evaluated, will yield the same expression as Eq. (I-31). Therefore, for very large values of (a), $\mu_{a_{\Pi^2 \to \infty}}$ approaches $\mu_{a_{\Pi^2 \to 0}}$. The typical numerical solutions of Eq. (I-28) which are included herein as Figures 11a through 11g clearly show this trend. Hence, Eq. (I-31) is seen to apply for still another limiting case. Thus, the first possibility is the only one of interest from the standpoint of any "new" positive minimum $\mu_a$.

Taking the required derivative of Eq. (I-33) and setting it equal to zero yields:

$$\frac{\partial \mu_{a_{\Pi^2 \to \infty}}}{\partial a} = (\frac{a^2}{2} - \frac{a}{8} + \frac{1}{16})(x_m^2 + r_c^2 + \frac{1}{4} - 2ax_m - a) + (a - \frac{1}{8})[a^2(x_m + \frac{1}{2})$$

$$- a(x_m^2 + r_c^2 + \frac{1}{4}) + (\frac{x_m}{4} - \frac{r_c^2}{2} - \frac{x_m^2}{2})] = 0$$

The above may be expanded and rearranged to yield the following expression:

$$a^2\left(\frac{x_m}{8} - \frac{x_m^2}{2} - \frac{r_c^2}{2} - \frac{1}{16}\right) + a\left(\frac{x_m}{8} - \frac{x_m^2}{2} - \frac{r_c^2}{2} - \frac{1}{16}\right)$$

$$- \frac{1}{4}\left(\frac{x_m}{8} - \frac{x_m^2}{2} - \frac{r_c^2}{2} - \frac{1}{16}\right) = 0$$

which may be expressed in particularly simple - and fortunately separated - form as:

$$\left(a^2 + a - \frac{1}{4}\right)\left(\frac{x_m}{8} - \frac{x_m^2}{2} - \frac{r_c^2}{2} - \frac{1}{16}\right) = 0 \qquad \text{(I-34)}$$

For physically plausible systems, the expression involving the center of gravity location and the radius of gyration cannot be zero. Thus, the required extremizing condition may be obtained by setting:

$$a^2 + a - \frac{1}{4} = 0 \qquad \text{(I-35)}$$

The roots to Eq. (I-35) are $-\frac{1}{2} \pm \frac{\sqrt{2}}{2}$ and represent two values of (a) for which Eq. (I-35) is stationary. The result is particularly interesting because it is independent of $x_m$ and $r_c^2$. Numerically these roots are approximately -1.2 and + .2.

If the roots of Eq. (I-35) are substituted into Eq. (I-33), the following two equations result:

1. $a = -\frac{1}{2} - \frac{\sqrt{2}}{2}$

$$\mu_{a_{\Pi^2 \to \infty}} = \frac{\frac{1}{2} + \frac{5}{16}\sqrt{2}}{\frac{\sqrt{2}}{2} x_m^2 + x_m\left(1 + \frac{\sqrt{2}}{2}\right) + \frac{1}{2} + \frac{3}{8}\sqrt{2} + \frac{\sqrt{2}}{2} r_c^2} \qquad \text{(I-36a)}$$

2. $a = -\frac{1}{2} + \frac{\sqrt{2}}{2}$

$$\mu_{a_{\Pi^2 \to \infty}} = \frac{\frac{1}{2} - \frac{5}{16}\sqrt{2}}{x_m(1 - \frac{\sqrt{2}}{2}) - \frac{\sqrt{2}}{2}x_m^2 + (\frac{1}{2} - \frac{3\sqrt{2}}{8} - \frac{\sqrt{2}}{2}r_c^2} \qquad \text{(I-36b)}$$

The numerators of both of the above expressions are positive. However, the denominator of Eq. (I-36a) cannot be negative for any real $x_m$ and any $r_c^2 > 0$ while, for the same conditions, the denominator of Eq. (I-36b) can never be positive. (This statement may be checked by regarding the denominators as quadratics in $x_m$ and checking the discriminant of each.) Accordingly, one may conclude that only Eq. (I-36a) can yield a positive $\mu_a$ and thus is really the only expression of interest. The second expression yields a minimum negative $\mu_a$ as $\Pi^2 \to \infty$.

These conclusions may be confirmed by referring to Figures 11a through 11g, from which it may be noted that no positive $\mu_a$ values exist for high values of $\Pi^2$ and an (a) of approximately + .2. It may be further noted by examining Figures 11a - 11e that the positive $\mu_{a_{\Pi^2 \to \infty}}$ obtained from Eq. (I-36a) is indeed lower, for the same $x_m < -\frac{1}{2}$, than the value obtained from Eq. (I-31) for the limiting $\Pi^2 = 0$ case. It is also interesting to note that although no positive $\mu_a$ could be obtained for the $\Pi^2 = 0$ case with the center of gravity ahead of the quarter chord, ($x_m \leq -\frac{1}{2}$), there are no center of gravity locations for which the extremum of the $\Pi^2 \to \infty$ case, (Eq. I-36a), will not yield a positive $\mu_a$ - provided only that $r_c^2$ is greater than zero. Figures 11f and 11g illustrate this fact.

For purposes of identification, the result obtained from Eq. (I-36a) will be referred to as $(\mu_{a_{\Pi^2 \to \infty}})_{min}$ as it may be confirmed from the numerical evidence presented in Figures 11a through 11g that the value

is indeed the minimum which may be obtained for any given physically sensible $x_m$ and $r_c^2$. By examining Eq. (I-36a), the following observations regarding the dependence of this minimum $\mu_a$ upon $x_m$ and $r_c^2$ may be made.

1. $(\mu_{a_{\Pi^2 \to \infty}})_{min}$ is lowered by increasing $r_c^2$. However, it may be seen that for the range of $r_c^2$ values normally encountered, $(.20 < r_c^2 < .33)$, the effect may be expected to be slight.
2. $(\mu_{a_{\Pi^2 \to \infty}})_{min}$ is lowered by increasing $x_m$ positively.
3. $(\mu_{a_{\Pi^2 \to \infty}})_{min}$ is raised by increasing $x_m$ negatively until $\sqrt{2}/2\, x_m^2$ becomes greater than $x_m\,(1 + \sqrt{2}/2)$. Beyond this point, increasing $x_m$ negatively will again decrease the extremum value in such a fashion that the extremum value approaches zero for very large positive or negative $x_m$. For the practical range of $-1 \le x_m \le 1$, the effect of center of gravity location is monotonic with a forward movement of the center of gravity tending to increase the flutter free region.
4. The extremum value can only be made to approach zero by having $x_m$ or $r_c^2$ approach infinity.
5. For the practical limiting value of the center of gravity at the trailing edge, $(x_m = 1)$, and with an $r_c^2$ equal to .25, $(\mu_{a_{\Pi^2 \to \infty}})_{min}$ is approximately .26.

Virtually all of the above statements are shown by the numerical results presented in Figures 11a-11g. However, before proceeding with a discussion of those results, it is interesting to return to Eq. (I-30). If the BC-AD of Eq. (I-30) is expanded, and rearranged, the following may be obtained:

$$\frac{1}{2}\left[r_c^2 + (x_m - a)^2\right]\left\{a^2\left(x_m + \frac{1}{2}\right) - a\left(x_m^2 + r_c^2 + \frac{1}{4}\right)\right.$$

$$\left. + \frac{x_m}{4} - \frac{r_c^2}{2} - \frac{x_m^2}{2} - \left(a^2 - \frac{a}{4} + \frac{1}{8}\right)\left(x_m + \frac{1}{2}\right)\right\} = 0 \qquad \text{(I-37)}$$

For physically possible systems, the first factor can never be zero. Thus, the second factor must vanish for the above equation to be valid.

The second factor may be written as a polynomial in (a) and set equal to zero. The resultant expression may be written as:

$$a\left(\frac{x_m}{4} - x_m^2 - r_c^2 - \frac{1}{8}\right) + \frac{1}{2}\left(\frac{x_m}{4} - x_m^2 - r_c^2 - \frac{1}{8}\right) = 0 \qquad \text{(I-38)}$$

For any physically possible system, the expression containing $x_m$ and $r_c^2$ cannot be zero. Thus, the only valid solution to Eq. (I-43) is: (a) = $-\frac{1}{2}$. Hence, an (a) of $-\frac{1}{2}$, (the elastic axis located at the quarter chord) represents a condition for which $\mu_a$ is independent of the frequency ratio, $\Pi^2$. From Figures 11a-11g, the validity of the above conclusion is apparent.

Figures 11a-11g show, as has been stated earlier, the results of solving Eq. (I-28) numerically. Because of the comparatively weak dependence of $\mu_a$ upon $r_c^2$ for typical $r_c^2$ values, ($.20 < r_c^2 < .33$), all of the calculations shown are based upon an $r_c^2$ of .25.

It is easy to see that the trends shown by Figures 11a-11g are in accordance with the analytical results which have been discussed. Further, the combination of the numerical and theoretical results allows the following statements to be made. It is again emphasized that these statements

are based upon the two-dimensional typical section analysis and hence may very well not apply for planforms which cannot be accurately represented in such a manner.

1. For configurations which have the elastic axis, (a), forward of the quarter chord, $\mu_a$ will decrease as $\Pi^2$ increases. For (a) aft of the quarter chord, the opposite is true.
2. For a given c.g. location and a given non-dimensional radius of gyration, the minimum $\mu_a$ will occur with an (a) of $\frac{-1-\sqrt{2}}{2}$ and $\Pi^2$ of infinity. However, it may be seen from the numerical results that the (a) required for a minimum $\mu_a$ is only slightly dependent upon $\Pi^2$.
3. With $\Pi^2 = 0$, no unstable solutions, regardless of the mass-density ratio, may be obtained if the center of gravity is forward of the quarter chord. However, for the case of $\Pi^2 \to \infty$, some unstable solution can always be obtained if the elastic axis is near the leading edge. A comparison is shown in Figure 12.
4. In general, aft c.g. locations lower $\mu_a$, (Figure 12). However, there are specific exceptions associated with the maximum $\mu_a$ values which occur for moderate values of $\Pi^2$ and aft elastic axis locations.
5. For center of gravity locations forward of the quarter chord, ($x_m < -.5$), no positive $\mu_a$ values exist for (a) locations aft of the quarter chord regardless of $\Pi^2$. Thus, it is extremely likely that configurations with a c.g. forward of the quarter chord and an elastic axis aft are flutter free for all $\mu$. However, these configurations might be particularly susceptible to static divergence.
6. Considering only the flutter aspects of the problem, it is apparent that for all practical values of $x_m$, certain configurations associated with comparatively large frequency

ratios, ($\Pi^2 > 1$), may be made flutter free for all $\mu$ by locating the elastic axis in an aft position.

The above statement regarding the dependence of $\mu_a$ upon the center of gravity has been made by other investigators (e.g., Refs. 3, 5, 12). Ref. 5 also included a figure depicting the dependence of $\mu_a$ upon $x_m$ and (a), for a moderate $\Pi^2$ of .64. Unfortunately, the calculations were performed using a constant $r_\alpha^2$ with the result that many of the configurations depicted were physically impossible, thus showing a questionable inter-dependence of $\mu_a$ upon $x_m$ and (a).

In effect, the last of the above statements says that for a given $x_m$ and $r_c^2$, certain combinations of $\Pi^2$ and (a) yield a negative $\mu_a$ which, for reasons which have been discussed, is an extremely strong indicator that the configuration will have no valid flutter points for any positive $\mu$. Hence, it is desirable to show for what parametric combinations a negative $\mu_a$ might be expected. Obviously, what is required is to determine what physically possible and plausible configurations can cause $\mu_a$ as expressed by Eq. (I-28) to change sign. Since the numerator of Eq. (I-28) must remain positive for meaningful systems, the sign of $\mu_a$ must be determined by the denominator; the boundary being those cases for which the denominator is equal to zero.

If the denominator of Eq. (I-28) is set equal to zero, the following expression may be obtained:

$$\Pi^2\{a^2(x_m + \frac{1}{2}) - a(x_m^2 + r_c^2 + \frac{1}{4}) + (\frac{x_m}{4} - \frac{r_c^2}{2} - \frac{x_m^2}{2})\}$$

$$+ [r_c^2 + (x_m - a)^2][x_m + \frac{1}{2}] = 0 \qquad \text{(I-39)}$$

Eq. (I-39) shows that for $\Pi^2 \to 0$, the algebraic sign of the $\mu_a$ solutions is entirely determined by $x_m$, with the change in sign occurring across $x_m = -\frac{1}{2}$.

For computational purposes, Eq. (I-39) may be re-written as:

$$\Pi^2 = \frac{[r_c^2 + (x_m - a)^2]\,[x_m + \frac{1}{2}]}{-a^2(x_m + \frac{1}{2}) + a(x_m^2 + r_c^2 + \frac{1}{4}) - (\frac{x_m}{4} - \frac{r_c^2}{2} - \frac{x_m^2}{2})} \qquad \text{(I-40)}$$

Now if $r_c^2$, a, and $x_m$ are specified, a valid boundary point will exist if the $\Pi^2$ calculated using the above is positive.

Some typical boundaries are shown in Figures 13a-13i. Figures 13a-13i, show that the location of the elastic axis can be very important. Also of interest is the complete change of character of the boundaries as the center of gravity is moved forward. For c.g. locations aft of the quarter chord, valid flutter solutions may, in general, be expected for some positive $\mu$; the exceptions being fairly well confined to configurations with an aft elastic axis and a frequency ratio greater than one. Further, the combination of a c.g. aft of and an elastic axis forward of the quarter chord will always result in unstable solutions for some $\mu$. Conversely, if the c.g. is forward of the quarter chord, valid flutter solutions may not, in general, be expected; the exceptions being confined to configurations with a forward elastic axis and a non-zero $\Pi^2$. Further, the combination of a c.g. forward of, and an elastic axis aft of the quarter chord is always stable for all mass-density ratios. These conclusions are, of course, in agreement with what was indicated in Figures 12a-12g. It is of interest to observe that certain all movable control surfaces have a comparatively high $\Pi^2$ and may be characterized by a center of gravity and an elastic axis forward of the quarter chord.

As has been previously stated, the primary reason for studying the expression for $\mu_a$, (Eq. I-28), has been the desire to obtain the practical limits of the "typical" flutter boundary depicted by Figure 7.

However, many of the remarks concerning the connection between the value obtained for $\mu_a$ and the existence of valid flutter solutions have implied that the validity of the flutter speed coefficients as determined from Eq. (I-27b) is solely dependent upon the algebraic sign of the denominator. Clearly, if the numerator were to change algebraic sign for some $\mu < \mu_a$, real solutions would again result. The possibility of the quasi-steady equations predicting a "new" flutter boundary for some $\mu < \mu_a$ does not need to be discussed in detail as other investigators, (e.g., Refs. 6, 12) have shown that solutions do indeed reappear. However, as has been stated earlier, the solutions which result are such that they invalidate the fundamental quasi-steady assumption. Further, the reappearance of valid solutions for $\mu < \mu_a$ implies that one of the boundaries sketched in Figure 8 must exist. The proof that none of these boundaries is possible will be completed in the next section. To clarify these last statements, an analysis similar to that contained in Ref. 12 will be presented. For computational ease, the analysis is based upon the assumption of $\Pi^2 = 0$ which is fairly representative of many structures. Further, the points discussed above are very well illustrated by this example.

If $\Pi^2$ is taken equal to zero, Eqs. (I-27a and 27b) may be written:

$$\Omega^2 = \frac{\mu\left[r_c^2 + x_m\left(x_m - \frac{1}{2}\right)\right] + \frac{1}{8}}{\mu\left[r_c^2 + (x_m - a)^2\right]} \tag{I-41a}$$

$$X^2 = \frac{\Omega^2\left\{\mu(\mu+1)\left[r_c^2 + (x_m - a)^2\right]\right\} - \mu\left(r_c^2 + x_m^2\right) - \mu^2 r_c^2 - \frac{\mu}{8} - \frac{1}{8}}{2\Omega^2\left[\mu\left(x_m + \frac{1}{2}\right) - \frac{1}{2}\right]} \tag{I-41b}$$

Substituting Eq. (I-41a) into the numerator of Eq. (I-41b) yields:

$$NUM = \mu x_m [\mu (x_m - \tfrac{1}{2}) - \tfrac{1}{2}] \tag{I-42}$$

From Eq. (I-42) it may be seen that for $\mu$ greater than $(\tfrac{1}{2})/(x_m - \tfrac{1}{2})$, the algebraic sign of the numerator will be the same as the sign of $x_m$. Conversely, for $\mu$ less than $(\tfrac{1}{2})/(x_m - \tfrac{1}{2})$, the sign of the numerator will be opposite to the sign of $x_m$.

Since $\Omega^2$ must be positive for a meaningful solution, the sign of the denominator may be seen to be governed by the now familiar expression:

$$\mu = \mu_a \Big|_{\Pi^2=0} = \frac{1}{2x_m + 1} \tag{I-31}$$

Thus the denominator is greater than zero for $\mu > \mu_a$ and less than zero for $\mu < \mu_a$.

The foregoing information allows a diagram (Figure 14) of the regions of real solution to be drawn. In Figure 14, the shaded portions indicate the regions of real solutions.

The interesting thing to be noted about Figure 14 is that real solutions are predicted for $\mu < \mu_a$ if the center of gravity is aft of midchord. Largely as a result of this fact, it was concluded in Ref. 14 that unswept sections with aft centers of gravity might have valid flutter solutions for $\mu < \mu_a$ and that these solutions would probably be characterized by very low reduced frequencies. This was indeed an attractive possibility as hydrofoils are characterized by aft centers of gravity and further the low mass-density modal flutter solutions obtained by the author and others, (Ref. 10), were characterized by very low reduced frequencies. Unfortunately, however, the conclusions are not valid. If Eqs. (I-41a and 41b) are solved for $x_m > 0$ and $\mu < \mu_a$, positive values will result. However,

if $\Omega^2$ and $X^2$ are then combined to find the resultant reduced frequency, it will be found that the quasi-steady ($k \to 0$) assumption is very poor everywhere except for $\mu$ very close to $\mu_a$. Thus, the results can only be regarded as another example of the inadequacy of the quasi-steady equations with regard to the prediction of valid flutter boundaries in the low mass-density ratio region. That the solutions indicated by Figure 14 for $\mu < \mu_a$ cannot exist will be definitely proven in the next section. Further, it will be shown that the correct trend can be predicted by the quasi-unsteady ($k \to \infty$) flutter equations.

Constraints on the Flutter Boundary of a Section Which are Imposed by the Character of the Zero Flutter Speed Solutions

It is shown in this section that a careful investigation of the dependence of the $\mu_o$ (mass-density ratio for which a system has a zero flutter speed coefficient) solutions upon the various non-dimensional system parameters completes the proof that a given section has only one flutter boundary, the "typical" boundary of Figure 7. This requires that the quasi-unsteady flutter equations be investigated.

The methods of obtaining the flutter equations associated with a reduced frequency (k) of infinity have been discussed earlier in this report with the resultant expressions presented as Eqs. I-19 and I-20. It is convenient, from the standpoint of the work to follow, to divide the numerator and the denominator of Eq. (I-20b) by $\Omega^2$. This leads to the following set of equations:

$$\Omega^2 = \frac{\mu\left[r_c^2 + \left(x_m - \frac{1}{2}\right)^2\right] + \frac{3}{8}}{\mu\left[r_c^2 + (x_m - a)^2 + \Pi^2\left(a - \frac{1}{2}\right)^2\right]} \qquad \text{(I-43a)}$$

$$\mu[(r_c^2 + [x_m - a]^2)(1 + \mu + \mu\Pi^2) + \Pi^2(\frac{1}{8} + a)]$$

$$- \Omega^2\mu^2\Pi^2[r_c^2 + (x_m - a)^2] - \frac{\mu}{\Omega^2}\{[r_c^2 + (x_m - a)^2][1 + \mu]$$

$$X^2 = \frac{- \mu(x_m - a)^2 + 2ax_m - a^2 + \frac{1}{8}\} - \frac{1}{8}\Omega^2}{\mu a(1 - \Omega^2\Pi^2) + \frac{\mu}{2}(1 - \Omega^2\Pi^2) + \mu x_m - \mu a - \frac{1}{2}} \qquad \text{(I-43b)}$$

For a physically meaningful set of system parameters, the above equations become "exact" as the flutter speed approaches zero. Hence, it is possible to use the above equations to obtain the value or values of the mass-density ratio, expressed as a function of the other system parameters, for which the flutter speed becomes zero. It is well to note that in the above system of equations, the $\Omega^2$ expression (Eq. I-43a) can never be negative for meaningful physical systems as $\mu$, $r_c^2$, and $\Pi^2$ cannot be negative. Therefore, the validity of any flutter solutions is entirely dependent upon the algebraic sign of the $X^2$ expression (Eq. I-43b).

For any meaningful physical system, a zero flutter speed coefficient is coincident with a zero flutter speed. Strictly speaking, a zero flutter speed coefficient results if either the denominator of Eq. (I-43b) is infinite or the numerator zero. Clearly the former possibility is of no practical interest for reasons which have been discussed in the previous section when comparable situations were encountered with the quasi-steady equations. Thus, any meaningful zero flutter speed solutions must be coincident with the vanishing of the numerator.

It may be recalled that certain of the flutter boundaries previously presented as possibilities, (Figures 8 and 9), were shown to originate or terminate, or both, with a zero flutter speed coefficient. In effect, the

existence of any of these boundaries would require that for certain specific geometrical configurations, $X^2$, (Eq. I-43b), be able to change smoothly from positive to negative by varying $\mu$. Thus, the behavior of $X^2$ as a function of $\mu$, near those points for which $X^2$ is zero, is as important as the determination of the parametric combinations yielding a zero flutter speed.

Before proceeding with an examination of the general quasi-unsteady flutter equations, it is instructive to again consider the case of $\Pi^2 = 0$. This is admittedly a special case and indeed certain of the specific conclusions are not applicable to the more general case of a non-zero frequency ratio. Still, the character of the flutter boundaries admitted by the limiting $\Pi^2 = 0$ case is, as will be shown later, quite typical.

If $\Pi^2$ is assumed to approach zero, Eqs. I-43a and 43b may be written as:

$$\Omega^2 = \frac{\mu\left[r_c^2 + \left(x_m - \frac{1}{2}\right)^2\right] + \frac{3}{8}}{\mu\left[r_c^2 + (x_m - a)^2\right]} \tag{I-44a}$$

$$X^2 = \frac{\Omega^2\left[\mu\left(r_c^2 + \left[x_m - a\right]^2\right)(1+\mu)\right] - \mu\left(r_c^2 + x_m^2\right) - \mu^2 r_c^2 - \frac{\mu}{8} - \frac{1}{8}}{\Omega^2\left[\mu\left(x_m + \frac{1}{2}\right) - \frac{1}{2}\right]} \tag{I-44b}$$

If Eq. (I-44a) is substituted into the numerator of Eq. (I-44b), the following expression may be obtained.

$$\text{NUM} = \mu^2\left(x_m - \frac{1}{2}\right)^2 - \mu\left(x_m - \frac{1}{2}\right) + \frac{1}{4} \tag{I-45a}$$

The above expression may be recognized as a perfect square which may be written as:

$$\text{NUM} = \left[\mu\left(x_m - \frac{1}{2}\right) - \frac{1}{2}\right]^2 \qquad \text{(I-45b)}$$

From this expression it may be seen that the numerator has a single zero which is obtained when:

$$\mu = \mu_{o_{\Pi^2 = 0}} = \frac{1}{2x_m - 1} \qquad \text{(I-46)}$$

What is of even greater importance is that for any meaningful system, the numerator of Eq. (I-44b) can never be negative. Thus, the algebraic sign of $X^2$, and hence, the significance of the result, is entirely determined by the denominator expression. This of course implies that, at least for the $\Pi^2 = 0$ case, none of the flutter boundaries which are depicted as originating or terminating with a zero flutter speed solution are possible, (Figures 8b, c, d, and 9), unless the change of sign of the denominator of Eq. (I-50b) is coincident with the vanishing of the numerator.

With regard to Eq. (I-46), the following observations may be made:

$$\mu_o > 0 \text{ for } x_m > \tfrac{1}{2}$$

$$\mu_o = 0 \text{ for } x_m = \tfrac{1}{2}$$

$$\mu_o < 0 \text{ for } x_m < \tfrac{1}{2}$$

Therefore, no meaningful zero flutter speed solutions can exist with a center of gravity forward of the three quarter chord.

Now the denominator of Eq. (I-44b) may be considered. Since for all meaningful systems the flutter frequency coefficient squared, $\Omega^2$, must be positive and non-zero, the zero, and hence the algebraic sign of the denominator must be determined by the expression:

$$\mu(x_m + \tfrac{1}{2}) - \tfrac{1}{2} \qquad \text{(I-47)}$$

This is seen to be identical to the expression obtained by the quasi-steady ($k \to 0$) theory and is seen to yield a denominator zero - or infinite $X^2$ - when:

$$\mu = \mu_{a_{\Pi^2=0}} = \frac{1}{2x_m + 1} \qquad \text{(I-31 and 48)}$$

Further,

$$\mu_a' > 0 \text{ for } x_m > -\tfrac{1}{2}$$

$$\mu_a' \to \infty \text{ for } x_m = -\tfrac{1}{2}$$

$$\mu_a' < 0 \text{ for } x_m < -\tfrac{1}{2}$$

Thus the denominator is positive for $\mu > \mu_a'$ and negative for $\mu < \mu_a'$. In addition, it may be seen that the numerator and the denominator will not vanish simultaneously, thus assuring that none of the "new" flutter boundaries previously discussed, (Figures 8b, 8c, 8d, and 9), exist.

As a summary of the examination of the quasi-unsteady ($k \to \infty$) flutter equations for the limiting case of $\Pi^2 = 0$, a diagram analogous to that shown in Figure 14 may be constructed. This is included herein as Figure 15. The shaded portion of Figure 15 is the region where real solutions exist.

From Figure 15 it may be noted that, unlike Figure 14, no valid solutions are predicted for $\mu < \mu_a$. Further, since all separate and "new" flutter boundaries have been shown to be impossible, it is obvious that the correct trend must be shown by Figure 15 and not by Figure 14. In addition, if Eqs. (I-44a and 44b) are solved for $x_m > -\frac{1}{2}$ and $\mu > \mu_a'$, the resultant reduced frequencies will tend to confirm the quasi-unsteady assumption except for a comparatively small $\mu$ range near $\mu_a'$. Since $\mu_a' = \mu_a$, this is no restriction but only indicates that the asymptotic approach to an infinite flutter speed indeed occurs. As might be expected, the quasi-unsteady assumption is particularly accurate for $x_m > \frac{1}{2}$ and for mass-density ratios approximately equal to $\mu$.

Since all separate and "new" flutter boundaries have been dismissed for the case where $\Pi^2 = 0$, it is concluded that the flutter boundary is of the "typical" form depicted in Figure 7. If $x_m > \frac{1}{2}$, a valid positive zero will exist and the boundary will approach, touch, and depart the zero flutter speed coefficient abscissa of Figure 7 as $\mu$ is decreased. Further decreasing $\mu$ will cause the boundary to approach an infinite flutter speed coefficient for $\mu = \mu_a = \mu_a'$. No real valid solutions can be found for $\mu < \mu_a$.

It might be here noted that the inclusion of structural damping into the analyses would prevent the calculation of a zero flutter speed which is, of course, physically impossible. Hence, the zero flutter speed points could be more correctly viewed (from a physical standpoint) as regions where the system may be expected to have a very low flutter speed.

The procedure to be followed in analyzing the more general case of a positive, non-zero frequency ratio is quite similar to what has been followed for the $\Pi^2 = 0$ case. Further, the conclusions regarding the non-existence of any "new" flutter boundaries will be shown to be valid in the general case. However, as with the quasi-steady case, the introduction of a non-zero frequency ratio results in expressions involving all of the structural system parameters.

To obtain the conditions which result in a zero flutter speed, the numerator of Eq. (I-43b) may be set equal to zero. If Eq. (I-43a) is substituted into the numerator of Eq. (I-43b) and the result equated to zero, the following equation may be obtained:

$$\{\mu^3\gamma + \frac{3}{8}\mu^2\}\{\mu\varphi(1 + \Pi^2) + (\varphi + \beta)\}\{\varphi + \epsilon\}$$

$$-\mu^2\Pi^2\varphi\{\mu^2\gamma^2 + \frac{3}{4}\mu\gamma + \frac{9}{64}\} - \mu^4 r_c^2 (\varphi + \epsilon)^2 \qquad \text{(I-49)}$$

$$-\mu^3(\varphi + \delta)(\varphi + \epsilon)^2 - \frac{\mu^2}{8}(\varphi + \epsilon)^2 = 0$$

where:

$$\varphi = r_c^2 + (x_m - a)^2$$

$$\beta = \Pi^2 (a^2 + \frac{1}{8})$$

$$\gamma = r_c^2 + (x_m - \frac{1}{2})^2$$

$$\epsilon = \Pi^2 (a - \frac{1}{2})^2$$

$$\delta = 2a\, x_m - a^2 + \frac{1}{8}$$

It may be noted that all of the factors in Eq. (I-49) contain the mass-density ratio $\mu$ to at least the second power. Since the case of $\mu = 0$ has been discussed and has been shown to be of no interest in this particular problem, a $\mu^2$ may be factored out of the above equation. The remaining expression can be arranged as a quadratic in $\mu$ as follows:

$$\mu^2\{(\varphi + \epsilon)(1 + \Pi^2)\varphi\gamma - \Pi^2\gamma^2\varphi - r_c^2(\varphi + \epsilon)^2\}$$

$$+ \mu\{(\varphi + \epsilon)[\gamma(\varphi + \beta) + \frac{3}{8}\varphi(1 + \Pi^2)] - \frac{3}{4}\Pi^2\varphi\gamma - (\varphi + \delta)(\varphi + \epsilon)^2\}$$

$$+ \frac{3}{8}(\varphi + \beta)(\varphi + \epsilon) - \frac{9}{64}\Pi^2\varphi - \frac{1}{8}(\varphi + \epsilon)^2 = 0 \qquad \text{(I-50)}$$

Equation (I-50) was solved for literally hundreds of combinations of the non-dimensional structural parameters and some of the results are included herein as Figures 16a-16o and will be discussed later. Of particular importance is the fact that the numerical solutions virtually proved that Eq. (I-50) is a perfect square of the form:

$$[\mu - f(r_c^2, x_m, \Pi^2, a)]^2 = 0 \qquad \text{(I-51)}$$

Because of the numerical work, the algebraic proof was undertaken with the result that after what can most conservatively be described as a great deal of algebraic manipulation, it was shown that the discriminant of Eq. (I-50) is identically zero. Thus, the numerator of the $X^2$ expression, (Eq. I-43b), can never be negative for any physically possible combination of the system parameters. Hence, the algebraic sign of the $X^2$ solution is entirely determined by the sign of the denominator. Further, a given combination of structural parameters will only admit to a zero flutter speed solution for one value of the mass-density ratio. Since the form of the numerator will not allow the $X^2$ solutions to proceed smoothly from positive, through zero, to negative - or vice versa - it may be concluded, as it was for the $\Pi^2 = 0$ case, that none of the boundaries requiring a zero flutter speed coefficient terminal point are possible, (Figures 8b, c, d, and 9). Since at most one meaningful $\mu_a$ and one meaningful $\mu_o$ can exist, at most one physically valid flutter boundary can exist for any given two-dimensional section. Thus, it must be concluded that

this boundary must be of the form depicted in Figure 7, or possibly Figure 10, except that in certain cases the boundary may touch the abscissa for some discrete value of the mass-density ratio.

The possibility of dual flutter speed solutions for $\mu < \mu_a$ - thus resulting in a flutter boundary of the type shown in Figure 10 - will be discussed later in this and in the following section. In general it will be shown that although some valid solutions are possible for $\mu < \mu_a$, it is very likely that the "undershoot," at least for a two-dimensional section, is always very slight, and thus of very little practical significance. Indeed, analyses using the "exact" theory have produced no examples to the contrary.

Because of the complexity of Eq. (I-50), the dependence of $\mu_o$ upon the various parameters was determined numerically. However, before discussing the numerical results, it is well to remember that only those $\mu_o$ solutions associated with a real flutter boundary ($X^2 \geq 0$) are of any practical interest. Hence the denominator of Eq. (I-43b) must be considered because for a given section, the $\mu_o$ can only be a point on the flutter boundary if for $\mu = \mu_o$ the denominator expression is greater than zero, (i.e., for $\mu_o > \mu_a'$). Clearly then, the values for which the denominator vanishes are of interest.

If the expression for $\Omega^2$, (Eq. I-43a), is substituted into the denominator of Eq. (I-43b) and the result set equal to zero, the following expression may be obtained:

$$\mu\left(a+\frac{1}{2}\right)\left\{\mu\left[r_c^2+(x_m-a)^2+\Pi^2\left(a-\frac{1}{2}\right)^2\right]\right.$$

$$\left.-\Pi^2\left[\mu\left(r_c^2+x_m^2-x_m+\frac{1}{4}\right)+\frac{3}{8}\right]\right\} \qquad \text{(I-52)}$$

$$+\mu\left(\mu x_m-\mu a-\frac{1}{2}\right)\left[r_c^2+(x_m-a)^2+\Pi^2\left(a-\frac{1}{2}\right)^2\right]=0$$

Since a $\mu$ appears as a factor in all of the terms, it may be factored out of the expression. The $\mu$ factor is of no interest as it may be regarded as being cancelled by a similar factor in the numerator expression, (see Eq. I-49). The remaining denominator expression contains $\mu$ to only the first power, thus indicating that for any given section, the quasi-unsteady theory will only admit to one mass-density ratio for which the flutter speed is infinite, ($\mu_a'$). This is in agreement with what the quasi-steady theory has shown. However, it will be shown that, in general, $\mu_a \neq \mu_a'$.

If the remaining expression is solved for $\mu$, the following expression may be obtained:

$$\mu = \mu_a' = \frac{\frac{1}{2}[r_c^2 + (x_m - a)^2] + \Pi^2[\frac{a^2}{2} - \frac{a}{8} + \frac{5}{16}]}{[x_m + \frac{1}{2}][r_c^2 + (x_m - a)^2]} \qquad \text{(I-53)}$$

$$- \Pi^2\{(a+\tfrac{1}{2})[r_c^2 + (x_m - \tfrac{1}{2})^2] - (x_m + \tfrac{1}{2})(a - \tfrac{1}{2})^2\}$$

For meaningful values of the system parameters, Eq. (I-52) is greater than zero for $\mu > \mu_a'$ and less than zero for $\mu < \mu_a'$. Thus, since the numerator is a perfect square, the quasi-unsteady theory will admit to no flutter solutions for $\mu < \mu_a'$. Further, if $\mu_o > \mu_a'$, it is a point on a valid flutter boundary while if $\mu_o < \mu_a'$ it is associated with a set of imaginary solutions. For the latter case, the physically interesting flutter boundary will not have a zero flutter speed point for any mass-density ratio.

The dependence of $\mu_a'$ upon the other system parameters may be determined for Eq. (I-53) by following the same procedure as that which was outlined in the previous section and used to analyze the $\mu_a$ expression, (Eq. I-28). Because of the complete similarity between the two

analyses, only the results that may be obtained by a study of Eq. (I-53) will be presented herein. These results may be summarized as follows:

1. $\mu_a'$ cannot be zero for any meaningful combination of non-dimensional structural parameters.
2. If the elastic axis is located at the quarter chord, ($a = -\frac{1}{2}$), $\mu_a'$ is independent of the section frequency ratio, $\Pi^2$.
3. The minimum positive value for $\mu_a'$ occurs as the frequency ratio, $\Pi^2$, approaches infinity and for an elastic axis located one quarter chord forward of the leading edge ($a = -1.5$).
4. The actual minimum numerical value taken by $\mu_a'$ is dependent upon the location of the center of gravity and upon the non-dimensional radius of gyration. The dependence is expressed by the following relationship.

$$\mu_{a\,MIN}' = \frac{\frac{13}{8}}{(x_m + \frac{3}{2})^2 + r_c^2} \qquad \text{(I-54)}$$

For an $r_c^2$ of .25 and the center of gravity of the section at the trailing edge, the above expression yields a $\mu_{a\,min}'$ of .25. This is very slightly less than the comparable $\mu_a$.

5. Since the numerator of Eq. (I-53) cannot be negative for any physically possible section, the algebraic sign of $\mu_a'$ is determined by the denominator. If the denominator is set equal to zero, the following expression may be obtained.

$$\Pi^2_{\mu_a' \to \infty} = \frac{[r_c^2 + (x_m - a)^2][x_m + \frac{1}{2}]}{-a^2(x_m + \frac{1}{2}) + a(x_m^2 + r_c^2 + \frac{3}{4}) - (\frac{3}{4}x_m - \frac{1}{2}r_c^2 - \frac{1}{2}x_m^2)} \qquad \text{(I-55)}$$

The positive $\Pi^2$ values obtained from the above for combinations of a, $x_m$, and $r_c^2$ define a boundary for which $\mu_a'$ is infinite. For $x_m > -\frac{1}{2}$, (c.g. aft of quarterchord), positive $\mu_a'$ values exist for frequency ratios less than the frequency ratio for which $\mu_a'$ is infinite. For $x_m < -\frac{1}{2}$, the opposite is true.

Strictly speaking, the only reason for computing a $\mu_a'$ is to determine whether the $\mu_o$ associated with the given section is associated with the real flutter boundary of the section, inasmuch as the quasi-unsteady theory ($k \to \infty$) is, in general, not valid as $U_f/b\omega_\alpha$ approaches infinity. However, as will be pointed out when discussing Figures 16a-16o, there are cases for a $\mu_a' < \mu_a$ where the flutter boundary may tend toward the lower value before approaching an infinite flutter speed at $\mu = \mu_a$.

Figures 16a-16o show plots of $\mu_o$, $\mu_a$, and $\mu_a'$ versus the elastic axis location for various values of $x_m$ and $\Pi^2$. For all plots, the value of $r_c^2$ is considered to be .25. For center of gravity locations aft of the three quarter chord, ($x_m > \frac{1}{2}$), and low values of the frequency ratio ($\Pi^2 < 1$), all three curves behave in much the same manner with $\mu_o > \mu_a'$ and $\mu_a$ for most elastic axis locations. For higher $\Pi^2$ values, $\mu_o$ tends to become less than $\mu_a'$ and $\mu_a$ for many of the important elastic axis locations between plus and minus one. Other characteristics are also evident. It can be seen that $\mu_a$ and $\mu_a'$ both equal $1/(2x_m + 1)$ for an elastic axis at the quarter chord and also both approach the same value as (a) becomes large - either positively or negatively. Likewise $\mu_o$ equals $1/(2x_m - 1)$ for an elastic axis location at the three quarter chord ($a = \frac{1}{2}$) and seems to approach the same value as (a) becomes large. It is interesting to note, for the higher frequency ratios, the sensitivity of $\mu_o$ to elastic axis locations in the vicinity of the three quarter chord. However, it must be mentioned that this behavior is only of academic interest as it may be seen from the $\mu_a$ and $\mu_a'$ curves that no valid flutter solutions exist for the combinations of parameters required to

produce such an extraordinary behavior. It may also be seen from the curves that the minimum positive values of $\mu_a$ and $\mu_a'$ are comparatively weak functions of the frequency ratio and occur for an elastic axis location which can be generally located as slightly forward of the leading edge. On the other hand, the minimum value of $\mu_o$ is a much stronger function of the frequency ratio and occurs for an elastic axis location near the mid-chord. Of course, the minimum $\mu_o$ is only of practical interest if it may be associated with a family of real flutter solutions, $(\mu_o > \mu_a')$.

For centers of gravity forward of the three quarter chord but aft of the quarter chord, the character of the $\mu_o$ curves is seen to change while the curves for $\mu_a$ and $\mu_a'$ remain essentially the same as for the more aft c.g. locations. For a $\Pi^2$ of zero, $\mu_o$ is infinite for $x_m = \frac{1}{2}$. However, for $\Pi^2 > 0$, valid positive $\mu_o$ points are seen to exist for many elastic axis locations forward of the three quarter chord. For center of gravity locations forward of the three quarter chord, the frequency ratio range for which no positive $\mu_o$ values may be obtained is seen to increase. As an example, for the center of gravity at the mid-chord ($x_m = 0$), no positive $\mu_o$ values exist for $\Pi^2 \leq 1$. Furthermore, the elastic axis range for which physically interesting $\mu_o$ values may be obtained is seen to be extremely limited; the range being generally located in the vicinity of the quarter chord.

If the center of gravity is considered to be forward of the quarter chord, the character of the $\mu_a$ and $\mu_a'$ plots changes to the extent that valid positive values only exist for forward ($a < -\frac{1}{2}$) elastic axis locations. The region for which the $\mu_o$ solutions are of interest remains limited both with respect to the frequency ratio and the location of the elastic axis.

Having discussed the general character of the zero and asymptotic solutions depicted by Figures 16a-o, it is of some interest to consider some of the specific information that may be obtained from the curves.

For $\mu_o > \mu_a'$, the zero flutter speed solution is a valid point on a real flutter boundary. Hence, a configuration may be expected to have a low flutter speed for mass-density ratios in the vicinity of $\mu_o$, if $\mu_o > \mu_a'$.

For $\mu_o$ just slightly less than $\mu_a'$, the zero flutter speed point is not on the flutter boundary. However, the flutter boundary will tend toward the zero and probably attain a rather low flutter speed coefficient before increasing toward an infinite flutter speed as $\mu_a$ is approached. If $\mu_o$ is much less than $\mu_a'$, it is likely that the quasi-unsteady theory will be of little value in accurately predicting the flutter behavior of the given section. Rather, the complete "exact" unsteady theory is needed to correctly determine the flutter behavior at most mass-density ratios with the practical lower limit to the flutter boundary being established by $\mu_a$.

Something about the flutter boundary may also be learned by noting how much larger $\mu_o$ is than $\mu_a'$ and consequently $\mu_a$. If $\mu_o >> \mu_a$, the slope of the flutter boundary $\left(\partial \frac{U_f}{b\omega_\alpha} \Big/ \partial\mu\right)$ about $\mu_o$ may be expected to be moderate. Thus a slight difference in $\mu$ may be expected to have only a slight affect upon the flutter behavior of the section. Conversely, if $\mu_o$ and $\mu_a$ are nearly equal, an extremely sensitive dependence of the flutter speed upon the mass-density ratio may be expected - at least for the mass-density ratio range between the two values. Thus flutter predictions made for mass-density ratios near $\mu_a$ and $\mu_o$ may easily be in considerable error unless the parameters are very carefully ascertained. It may be noted that the likelihood of such an extra sensitive behavior increases as the frequency ratio is increased.

Little has as yet been said about the fact that, in general, $\mu_a = \mu_a'$. Strictly speaking, the asymptotic approach of the flutter boundary to an infinite flutter speed will occur at $\mu_a$ since the theory from which $\mu_a'$ is derived is not valid as $k \to 0$. Hence, if $\mu_a' > \mu_a$, the approach to an asymptotic solution at $\mu_a$ may be expected to be smooth and of the type characterized by Figure 7. In this case, the value of $\mu_a'$ is unimportant.

However, if $\mu_a' < \mu_a$, and further if $\mu_o$ is sufficiently close to $\mu_a$ and $\mu_a'$ that the quasi-unsteady theory may be expected to be valid, the boundary may tend toward $\mu_a'$ before approaching infinity for $\mu = \mu_a$. Hence, two flutter solutions can occur for some range of $\mu < \mu_a$. Checks using the "exact" unsteady theory have confirmed this fact and an example is included herein in Figure 19. However, it may be seen from Figure 19 that the range of double solutions is slight. Further, it may be seen from Figures 16a-16o that when $\mu_a' < \mu_a$, it is generally only slightly less; this statement being particularly true for very low mass-density ratios. Hence, it is extremely unlikely that real flutter solutions will be obtained for any mass-density ratios significantly lower than $\mu_a$ - particularly in the very low mass-density ratio region. This is deemed to be another indicator that the type of flutter boundary depicted by Figure 10 is unlikely. In addition, as has been previously stated, none of the many "exact" solutions were found to yield any counter-examples.

Just what general types of flutter boundaries may be expected as a result of the relative values determined for $\mu_o$, $\mu_a$, and $\mu_a'$ may be shown by a series of simple diagrams, (Figures 17a-17e).

Combinations other than those depicted by Figures 17a-17e are, of course, possible, but the five which are shown include most of the more interesting combinations.

It may be seen from Figures 16a-16o that, for certain completely realistic systems, the mass-density ratio for which the lowest flutter speeds may be expected can change drastically with only small changes in the system parameters. This statement is particularly true with regard to the location of the elastic axis for all but the very lowest frequency ratios. Hence, it is obvious that general statements regarding the dependence of the flutter velocity upon the various non-dimensional structural parameters cannot be made unless the mass-density ratio is specified. For example, it was stated in Ref. 3, and is in fact an almost universally accepted "rule of thumb," that a rearward movement of the

elastic axis is generally accompanied by a lower flutter speed. A glance at Figures 16a-16o reveals many contradictions to the above statement.

It is evident that the flutter boundary of a given section is not only a function of the relative values of $\mu_o$, $\mu_a$, and $\mu_a'$, but is also dependent upon the sensitivity of the flutter speed coefficient to changes in the mass-density ratio, $(\partial X/\partial \mu)$. Since the lowest flutter speed coefficients may logically be expected to occur near $\mu_o$ - if $\mu_o > \mu_a$ - this is the region that is discussed herein. Examples of some flutter boundary calculations are included herein as Figures 18a-18h. These figures are all based upon the approximate quasi-unsteady theory. However, only those solutions for which the resultant reduced frequencies are calculated to be greater than six are included. Hence, the departure from the boundary predictable from the "exact" unsteady theory is slight. This statement has been, in fact, confirmed by comparing certain of the boundaries obtained from the "exact" unsteady theory to some of the results shown in Figures 18a-18h. Figure 19 is included herein as a typical comparison.

It may be seen that almost all of the configurations shown in Figures 18a-18h are characterized by aft locations of the center of gravity. This is hardly surprising as most of the valid $\mu_o$ points are associated with aft centers of gravity - particularly for structures having a low frequency ratio, $\Pi^2$. Figure 18h is the only exception with an $x_m$ of zero.

The configurations shown in Figure 18a are all characterized by a zero frequency ratio. Hence $\mu_o$ and $\mu_a$ are independent of the elastic axis location. For this case, it may be seen that with the elastic axis aft, lower flutter speed coefficients may be expected for mass-density ratios on either side of $\mu_o$. However, as $\Pi^2$ is increased to even the nominal value of .4, the dependence of the flutter coefficient upon the elastic axis location is seen to be very much a function of the mass-density ratio being considered. Figures 18e-18g show the same trends for a slightly more forward center of gravity.

Figure 18c shows a set of boundaries for the same elastic axis location but different frequency ratios. It is particularly interesting to note the extreme sensitivity to small changes in the mass-density ratio that is exhibited by the boundaries of the higher frequency ratio configurations. Because of the extreme sensitivity to small changes, it is likely that accurate flutter analyses of real systems characterized by high frequency ratios would be difficult to perform for mass-density ratios near $\mu_o$. Admittedly the location of the center of gravity of the configuration in Figure 18c is extreme. However, an unfortunate choice of parameters could result in a similar behavior for centers of gravity considerably more forward, (e.g., Figure 18h). Figure 18h is also interesting because it shows how sensitive a low mass-density ratio flutter boundary can be to small changes in the location of the elastic axis. Again the comments regarding the analytical difficulties apply. When one considers the many approximations made in the flutter analysis of a practical structure, it becomes apparent that a flutter behavior which is extraordinarily sensitive to small changes in any of the system parameters can make an accurate prediction of the flutter speed extremely difficult to obtain. It certainly appears that some all movable control surfaces might exhibit just such a sensitive behavior. This fact may be the reason why theoretical attempts to analyze observed instabilities have generally proven to be unsuccessful. The mere fact that two-dimensional unsteady hydrodynamic coefficients are normally used immediately suggests a potential source of considerable error. This particular possibility will be discussed in more detail in a section to follow.

Results Obtained by Utilizing the "Exact" Two-Dimensional Unsteady Hydrodynamic Theory

The methods of obtaining the flutter equations associated with an arbitrary reduced frequency (k) have been discussed with the resultant expressions presented as Eqs. I-24 and I-25. Since the non-existence

of any "new" flutter boundaries has been assured by the results obtained using the approximate quasi-steady and quasi-unsteady flutter equations, the use of the "exact" equations is confined to amplifying the conclusions drawn from the aforementioned analyses. Because of the transcendental nature of the "exact" equations, it is obvious that only a reasonable number of numerical checks could be made. It may be stated that none of the numerical checks yielded any significant contradictions to what was concluded from the analyses of the approximate equations - particularly with regard to the flutter free regions. In addition, it may be stated that the "exact" results agreed very well with the results obtained from the quasi-unsteady theory for the portion of the flutter boundary characterized by a reduced frequency greater than six. A typical comparison of the flutter boundaries shown in Figures 18a-18h with the boundaries predicted by the exact theory may be obtained from Figure 19.

From Figure 19 it may be noted that the approximate theory predicts a more conservative flutter boundary everywhere except for mass-density ratios very near $\mu_a$. However, it may also be noted that the exact theory shows that two flutter solutions are predicted for some mass-density ratios less than $\mu_a$ but that the "undershoot" is quite small. Calculations using Eqs. I-28 and I-53 show that for the combination of parameters considered in Figure 18, $\mu_a'$ is slightly less than $\mu_a$.

It may be recalled that the quasi-steady hydrodynamic theory indicated that for aft centers of gravity, solutions could be expected for $\mu < \mu_a$. Indeed Figure 19 shows the approach of the "exact" boundary to $\mu_a$ to be from the side of lower mass-density ratios. There were not enough boundaries calculated to ascertain whether this behavior could always be expected for configurations possessing an aft c.g. However, it is interesting to note that this would assure compliance with the quasi-steady trends predicted to be applicable for mass-density ratios very near $\mu_a$ without requiring the existence of any "new" flutter boundaries.

Hence, the region of dual solutions may be expected to be confined to a narrow range of mass-density ratios near $\mu_a$. Such was, in fact, the case for all the configurations actually checked. Thus there is every indication that, for all practical purposes, $\mu_a$ may be regarded as the mass-density ratio below which the two-degree-of-freedom section analysis will not predict any valid flutter solutions. In short, it is deemed to be extremely unlikely that any physically reasonable combinations of non-dimensional structural parameters will cause the typical section analysis to yield an exaggerated flutter boundary of the type shown in Figure 10.

To summarize, it may be stated that the numerical work incorporating the "exact" unsteady flutter equation confirms the results of the approximate theories. Thus, a lengthy discussion of many of the actual numerical results is unnecessary.

On the Apparent Contradictory Aspects of the Flutter Behavior of a Typical Section as the Low Mass-Density Ratio Region is Approached

Results included herein have shown that some of the lowest $\mu_a$ values - and $\mu_o$ values - are associated with high frequency ratios and forward locations of the elastic axis. This would seem to be in apparent contradiction to what has come to be accepted as the result of a body of aircraft experience. However, a simple sketch will serve to show that, in fact, no contradiction exists and the configurations conducive to flutter in the range of mass-density ratios peculiar to aircraft can logically be extrapolated to yield the higher $\mu_a$ and $\mu_o$ values. This fact is illustrated by Figure 20.

It is a well known fact that the flutter speed coefficient will vary approximately as the square root of the mass-density ratio (constant dynamic pressure boundary for a given section) in the range peculiar to aircraft. Thus, it is logical to expect that the configuration have the lower flutter speed in the aircraft range will tend toward a zero or

minimum flutter speed for a mass-density ratio higher than its more stable counterpart. For mass-density ratios less than $\mu_o$, (or the $\mu$ which corresponds to a minimum flutter speed if $\mu_o < \mu_a'$), the trends may be reversed, as shown in Figure 20. Thus, the seemingly paradoxical behavior peculiar to the low mass-density ratio region is seen to be, qualitatively, a very natural extension of what has come to be accepted on the basis of aircraft experience. However, as may be seen, it is an extension that must be made with care as it is the flutter boundaries that may be extrapolated and not the comparative flutter behavior at some fixed mass-density ratio.

A more interesting example can be discussed with regard to the use of two-dimensional unsteady derivatives in a flutter analysis. Aircraft experience has shown that, in general, the use of two-dimensional derivatives results in a predicted flutter speed somewhat lower than that predicted if three-dimensional derivatives are used.

Ref. 2 includes some experimental and theoretical comparisons which show that for the higher mass-density ratios, the theoretical data are definitely conservative. However, for the lower mass-density ratios near $\mu_a$, some unconservative predictions are noted. In particular, what could be regarded as the experimental $\mu_a$ values were seen to occur at a mass-density ratio less than the $\mu_a$ predictable from the two-dimensional theory. This apparent contradiction to what has come to be regarded as accepted fact can be explained by considering the basic flutter determinant, (Eq. I-4).

If the two homogeneous equations from which the flutter determinant is derived are divided by the mass-density ratio $\mu$, the flutter determinant may be written in the following manner:

$$\begin{vmatrix} \left\{\left[1 + \frac{\omega_h^2}{\omega_\alpha^2} \cdot \frac{\omega_\alpha^2}{\omega_f^2}\right] + \frac{L_h}{\mu}\right\} & \left\{x_\alpha + \frac{L_\alpha}{\mu} - \frac{L_h}{\mu}\left(\tfrac{1}{2} + a\right)\right\} \\ \left\{x_\alpha + \frac{M_h}{\mu} - \frac{L_h}{\mu}\left(\tfrac{1}{2} + a\right)\right\} & \left\{r_\alpha^2\left[1 - \frac{\omega_\alpha^2}{\omega_f^2}\right] + \frac{M_\alpha}{\mu} - \left(\frac{L_\alpha + M_h}{\mu}\right)\left(\tfrac{1}{2} + a\right) + \frac{L_h}{\mu}\left(\tfrac{1}{2} + a\right)^2\right\} \end{vmatrix} = 0 \qquad \text{(I-56)}$$

It may be noted that in the above expression, all of the unsteady derivatives appear divided by the mass-density ratio and further, that the mass-density ratio only appears in combination with one of the derivatives. Hence, if it is assumed that each of the four derivatives can be modified, to account for finite span effects, by applying the same correction factor ($\eta$), it is clear that the finite span effect may be duplicated by increasing $\mu$ some given amount. In such a case, the effect upon the flutter boundary of using the three-dimensional coefficients would be to displace the boundary as shown in Figure 21.

Figure 21 shows that the two-dimensional theory may indeed be expected to be unconservative for certain of the lower mass-density ratios. In particular, it may be seen that the $\mu_a$ obtained from the two-dimensional theory may well be too high - particularly if the actual structure has a fairly low aspect ratio.

It is interesting to consider some of the results previously noted from the standpoint of what effects a finite span might have on the results. It may be recalled that the flutter boundaries of certain configurations characterized by high frequency ratios and forward elastic axis locations were found to be extremely sensitive to mass-density ratio

changes. Since it has been shown that finite span effects may be regarded qualitatively as mass-density ratio changes, it is logical to expect that systems known to be sensitive to small mass-density ratio changes may also be sensitive to finite span effects. Thus an accurate analysis of such systems may be very difficult to perform. Since the extraordinarily sensitive systems are more characteristic of all movable control surfaces than main support or lifting surfaces, these remarks are even more pertinent as control surfaces normally have a comparatively low aspect ratio. The extraordinary sensitivity of control surface type structures, coupled with the possible finite span effects, may well explain why certain observed instabilities have defied theoretical explanation. An obvious remedy is to use the correct three-dimensional coefficients. However, this is very difficult and may even be impossible for overly sensitive systems. Thus a series of analyses covering a range of mass-density ratios seems to be in order for control surface type structures designed to operate at or near the $\mu_a$ of the system.

## I-E Conclusions Resulting from Part I

Before proceeding with the conclusions resulting from Part I of this investigation, it is again emphasized that the statements to be made apply only to fully wetted, two-dimensional sections acted upon by two-dimensional unsteady hydrodynamic forces and moments and that any extrapolation of the conclusions must be made with great care. Further, it is to be understood that the structures which the typical section are assumed to represent are unswept in the sense that no spanwise variations in the vibratory behavior of the structure are considered. That is, certain of the inertial - or mechanical - effects of a swept structure have been considered by regarding the section as being a streamwise section and using the concept of an axis of zero static coupling rather than of a section elastic axis. However, none of the possible effects

of sweep on the spanwise variation of the unsteady hydrodynamic forces and/or the spanwise pitch to plunge ratio have been considered.

It may be recalled that other investigators have indicated, on the basis of a limited number of experimental and numerical results, that lifting surfaces amenable to a two-dimensional section representation appeared to have a minimum mass-density ratio below which flutter could not occur, (Refs. 3, 5). On the other hand, it has been definitely established that certain swept cantilevered struts will flutter at very low mass-density ratios and further that numerically sophisticated theoretical results have shown that no low $\mu$ flutter free region exists for such structures, (Ref. 10). This fundamental difference is in contrast to extrapolations based upon aircraft experience. Hence, this investigation may be regarded as having been an attempt to establish, in as general a sense as possible, whether the swept cantilevered struts and the unswept structures which may be represented by a two-dimensional section indeed pose separate and distinct problems with regard to operations characterized by low mass-density ratios.

In the light of the above statements, undoubtedly the most important and most fundamental conclusion resulting from Part I of this investigation is that the two-degree-of-freedom section analysis will not, for all practical purposes, admit to any dynamically unstable solutions for mass-density ratios below what may be termed a "critical" value. This "critical" mass-density ratio may be closely approximated by determining the mass-density ratio for which the approximate quasi-steady hydrodynamic theory associated with a zero reduced frequency will predict an infinite flutter speed, ($\mu_a$). In the course of verifying the above fact, several interesting and related characteristics of the section analysis have been noted. These may be stated as follows:

1. For any physically meaningful geometrical configuration, only one mass-density ratio exists for which the flutter boundary will asymptotically approach an infinite flutter

speed, ($\mu_a$). Further, $\mu_a$ cannot be made to approach zero unless $x_m$ or $r_c^2$ are considered to approach infinity. For sections of reasonable geometry, (meaning an $r_c^2$ of between .2 and .4 and with the center of gravity located on the section proper), the minimum $\mu_a$ is approximately .25 and occurs with an (a) value of approximately -1.2, and $x_m$ of 1.0, and for very high values of $\Pi^2$. However, the minimum $\mu_a$ is a weak function of the frequency ratio $\Pi^2$.

2. The numerator of the expression for the flutter speed coefficient ($U_f/b\omega_\alpha$) which is derivable from the approximate theory associated with an infinite reduced frequency ($k \to \infty$) may be written as the product of the mass-density ratio $\mu$ and a quadratic in $\mu$ which is by itself a perfect square. Hence, for any given section only one mass-density ratio greater than zero may admit to a real zero flutter speed solution. Further no meaningful flutter boundaries may terminate on the zero flutter speed abscissa (see e.g., Figure 7), as the numerator of the flutter speed expression cannot change algebraic sign. Hence, the physical validity of the $\mu_o$ flutter speed solutions is determined by the denominator; the algebraic sign change occurring at that value of $\mu$ for which the denominator is zero, ($\mu_a'$). In the low mass-density ratio region, $\mu_a'$ and $\mu_a$ are nearly equal for any meaningful combination of structural parameters. Hence, if $\mu_o$ is greater than $\mu_a'$ (and thus for practical purposes $\mu_a$), it is associated with a family of real solutions and will yield a mass-density ratio region for which a given section can be expected to exhibit a very low flutter speed.
3. If the center of gravity is considered to be confined to the section proper, $\mu_a$, $\mu_a'$, and $\mu_o$ are, in general, all lowered as the center of gravity is moved aft.

4. If the frequency ratio, $\Pi^2$, is zero, $\mu_a$, $\mu_a'$, and $\mu_o$ are completely independent of the axis of zero static coupling, (a). However, the value of (a) quickly becomes important as the frequency ratio, $\Pi^2$, is increased; with forward axis locations (negative (a) values) tending to produce the lowest $\mu_a$ values. It may be noted that certain systems exhibit an extreme sensitivity to comparatively small changes in the axis location. As an example, certain configurations employing a forward axis location and moderate or high frequency ratios ($\Pi^2$ approximately equal to or greater than one) will yield very low flutter speeds over a relatively restricted range of mass-density ratios while the same parametric values but with an aft axis location may well not yield any dynamically unstable solutions for any mass-density ratio.

It may be noted that statements one and two above are sufficient to assure that for any meaningful system, "new" or distinct flutter boundaries cannot exist and be entirely confined within the mass-density ratio region below $\mu_a$.

The above conclusions certainly imply that, contrary to what aircraft experience would dictate, the historically insignificant differences between a swept cantilevered lifting surface and its two dimensional "typical section" representation are indeed extremely important factors in determining the actual low mass-density ratio flutter behavior of the surface in question.

# PART II - THE LOW MASS-DENSITY RATIO HYDROELASTIC BEHAVIOR OF A UNIFORM CANTILEVERED LISTING SURFACE

## II-A Background

It was shown in Part I of this investigation that the simplified two-degree-of-freedom typical section analysis will not admit to any separate and/or distinctive flutter boundaries for mass-density ratios significantly less than $\mu_a$. Hence, the obvious conclusion which may be drawn is that certain of the low mass-density ratio flutter boundaries previously encountered both theoretically and experimentally, (see e.g., Ref. 10), must have been the result of system details that were entirely lost in the simplified typical section representation. Therefore, even though the primary purpose of this investigation is to provide a basic understanding of the fundamental mechanism of low mass-density ratio flutter, it is clear that the simplified mathematical model required for such a purpose must contain more of the salient features of the structure and the resulting hydrodynamic loadings than what is provided by the typical section representation.

Before continuing, it must be noted that the above statements are not to be interpreted as meaning that all dynamic instabilities associated with comparatively low mass-density ratios are completely beyond the scope of the simplified theory. Indeed it was demonstrated in Part I of this study that certain classes of structures which can be well represented by a typical section may be expected to encounter dynamic stability problems for comparatively low mass-density ratios. This was shown to be true in spite of the fact that the complete flutter boundary of these structures could be described, as a function of the mass-density ratio, by the "usual" boundary of Figure 7. As was indicated, at least some of the analytical difficulties associated with these structures, for mass-density ratios close to $\mu_a$, may well have been due to the extreme

sensitivity of the flutter solutions to small changes in certain parameters. The attendant results were that the effects of the usual approximations (e.g., two-dimensional hydrodynamic theory) were magnified and in some cases, certain commonly expected trends were reversed.

Nevertheless, the specific low mass-density ratio flutter occurrences which formed the background and, in fact, the motivation for this entire investigation (see e.g., Ref. 10) could not be explained by extending the results discussed above. Rather, a study of the flutter cases of interest indicated that some could be associated with mass-density ratios as much as an order of magnitude below the respective $\mu_a$ of the structure. Further, all of the related numerical analyses showed that the structural parametric combinations associated with the low $\mu$ flutter cases exhibited comparable flutter points for mass-density ratios approaching zero. In essence, this meant that the calculated $\mu_a$ value (Eq. I-28) of the structure did not represent a lower mass-density ratio limit to the flutter boundary of the specific lifting surfaces under consideration. Rather, some form of boundary completely predictable by production type modal analyses incorporating the usual two-dimensional, unsteady, strip theory existed in the low mass-density region well below the $\mu_a$ value predicted by the simplified analysis. The portion of the flutter boundary for mass-density ratios less than the $\mu_a$ of the structure which cannot be predicted by the simplified typical section analysis marks precisely the region of interest of Part II of this study. Hence, it is here noted that the term "low mass-density ratio" as used in Part II is meant to imply an association with the mass-density ratio region below the characteristic $\mu_a$ of the system in question and for which the simplified section analysis has been proven to be partially inadequate.

A review of the well documented experimentally and/or theoretically observed low mass-density ratio flutter occurrences of primary interest quickly revealed that all of the structures involved were thin, uniform, swept, cantilevered lifting surfaces with the length significantly

greater than the width, (minimum 1/b ratio of 8). These facts had been previously noted. In particular, the probable importance of sweep had been previously stated or implied by the author and several other investigators. (See e.g., Ref. 5.) Landahl, et al (Ref. 26) had, in fact, used a specific example to show the probable dependence of low $\mu$ flutter on sweep. However, in spite of these facts, the mechanism of low mass-density ratio flutter remained unknown. Hence, the extrapolation of results from the specific to the general could not be done with confidence.

The observation that certain rather special structural features might be an important part of the low $\mu$ flutter mechanism certainly indicates that these features must be retained in the mathematical model to be used to study the mechanism. Conversely, a truly basic understanding of the flutter phenomenon requires that unnecessary complexity be avoided. Just what features could be expected to be important may be reasoned rather simply by considering the inter-relationships of the structures of interest and the hydrodynamic forces acting upon them.

In the case of a two-dimensional swept lifting surface, the hydrodynamic forces can, in general, be very well approximated by considering only the axis-normal component U cos $\Lambda$ of the free stream. This leads to the simple result that if a two-dimensional lifting surface is assumed to be swept by rotating the surface relative to the free stream, the critical flutter speed $U_f$ may be expected to vary approximately as the secant of the sweep angle. According to this simplest of approximations, the only effect of sweep upon the flutter behavior of a system is to increase the critical flutter speed. Thus, it is clear that this most basic effect of sweep cannot be responsible for the occurrence of low mass-density ratio flutter. Hence, the fact that the structures of interest had been flexible cantilevers has to be regarded as significant. As a result, it is obvious that a satisfactory mathematical model must retain the salient features of both the flexible cantilever rigidly supported at the root and the angle of sweepback of the elastic axis without becoming so complex that cause and effect relationships are lost.

Accordingly, Part II of this investigation is based upon a simple binary representation of a uniform cantilevered lifting surface which includes the provision for incorporating an angle of sweep and retains a spanwise variation in the pitch to bending ratio.

## II-B The Axis-Normal and Streamwise Formulations

The problem of obtaining a simplified mathematical model capable of accurately representing an oscillating, uniform, cantilevered lifting surface may be approached in two separate but related ways. One method may be considered to be a logical refinement of the simplest effect of sweep, which has been described in the previous section. This method arises from the consideration that a flexible cantilevered lifting surface experiences spanwise deformations and that in consequence the spanwise component of the free stream velocity - U sin $\Lambda$ - cannot be ignored with respect to the hydrodynamic forces produced. Hence, in the case of the oscillating cantilever, the spanwise component of the free stream also produces downwash. The full downwash on the surface is thus considered to be the sum of the two downwash components. The technique has then been to start from the full downwash but to apply to it only the axis-normal component of the free stream. Consequently, axis-normal strips form the basis of this analysis. The result of following an approach of this type has been what may be termed a first order approximation to the swept cantilever problem which has become known as the "axis-normal" method. This method was developed and used by Barnby, Cunningham, and Garrick (Ref. 19). As may be noted from Ref. 19, the refinements upon the two-dimensional analysis introduced by this approach primarily take the form of additional unsteady hydrodynamic terms, the importance of which is largely determined by the "sweep parameter" $\chi$ which appears as a multiplying factor with each of the "new" terms. The sweep parameter $\chi$ is a consequence of the local bending slope of the structure and hence incorporates both the sweepback and the cantilevered aspects of the

structure. It may be mentioned that Herr (Ref. 5) used the method of Ref. 19 in his calculations and was thus able to produce some of the first theoretical results indicative of the possible important role of sweep in low mass-density ratio flutter.

A second approach has been to consider the full free stream velocity and apply it to streamwise strips. This method, which has become known as the "streamwise approach" must lead to the simplest approximation as the swept lifting surface approaches an infinite aspect ratio, just as the "axis-normal" approach does. Hence, it follows that the hydrodynamic forces to be used on a streamwise strip which is part of a swept structure are cos $\Lambda$ times the forces that would be calculated for the same strip, and for its identical motion, in the unswept case. The details of combining strip theory and the streamwise approach with a cantilevered lifting surface were included by Jordan in Ref. 20. As with the axis-normal method, the result of following the approach just described is an approximation to the swept cantilever problem which may again be termed as of first order. However, unlike the axis-normal approach, the refinements do not introduce any unsteady hydrodynamic derivatives other than those of the usual unswept or "typical section" formulations discussed in Part I. Rather, the effects of sweep are introduced structurally. In particular, the angle of sweep of the elastic axis results in a skewness between the elastic axis - which is assumed to be straight and held rigidly at the root - and the streamwise strip. As a result, the entire streamwise strip is not associated with one point on the elastic axis but rather with a range of points and, therefore, a range of bending values. Hence, a bending of the elastic axis produces both translation and pitch of the streamwise strip; the pitching motion being proportional to the local bending slope and thus, in general, a function of the spanwise location of the strip under consideration. In addition, the moment of the hydrodynamic forces acting on the strip produces both a torsional moment and a bending moment on the elastic axis. The

details of the equation that arises from the streamwise formulation of the problem are shown in Ref. 20 (see also Appendix B).

Obviously, the two methods are not entirely similar, particularly for cantilevered lifting surfaces of modest aspect ratio. The streamwise approach seems to have an advantage in that the entire flow is considered. In addition, none of the strips end at the side boundaries of the surface as is the case with the axis-normal approach at the tip and the root. A disadvantage of the streamwise approach arises if the structure has axis-normal ribs, or if the structure is solid but an appreciable sweep angle is involved, since in these cases a camber of the streamwise strip may result. This latter difficulty can also arise with the axis-normal approach if rigid streamwise ribs are used. To examine the inherent differences between the two methods any more carefully is quite pointless since experience has shown that both methods lead to practically identical flutter speeds if the span to chord ratio of the lifting surface is large enough to justify the strip theory involved in either method and if the sweep angle is considered to be moderate. Indeed, for swept surfaces with a low span to chord ratio, there is little doubt but what the use of strip theory and the assumption of a straight elastic axis represent a degree of approximation considerably greater than any differences resulting from the choice of either the axis-normal or the streamwise approach. Thus it is apparent that either approach could form the basis for this investigation. This latter statement is further substantiated when it is realized that the flutter cases which form the background for this investigation are characterized by structures having relatively high $l/b$ ratios and low sweep angles - and hence low values of $\chi$. However, it is felt that the approach incorporating the streamwise strips is more easily visualized and hence better suited to an investigation seeking a physical interpretation of the basic low mass-density ratio flutter mechanism. The cause and effect relationships are easier to isolate and interpret if the forms of the unsteady hydrodynamic terms remain unchanged by the sweeping process.

Furthermore, the streamwise method is closely related to the multi-panel point modal analyses commonly used in industrial production work and known, by virtue of experimental evidence, to be capable of reasonably accurate low mass-density ratio flutter predictions. Hence, the streamwise approach forms the basis of this investigation.

## II-C The Salient Features of the Streamwise Approach Applied to the Uniform Cantilevered Lifting Surface

The combination of incompressible, unsteady, strip theory and the streamwise approach as applied to the uniform cantilevered lifting surface forms the theoretical basis of Part II of this investigation. The fact that the unsteady hydrodynamic theory is as stated implies a number of assumptions, such as potential flow, which are stated in virtually all modern flutter texts and need not be repeated herein, (see e.g., Ref. 14). In addition, assumptions must be made with regard to the structure and how the swept and unswept configurations are assumed to be related. For this study, the unswept reference cantilevered strut and the swept strut are related as shown in Figure 22 and as stated below after the fashion proposed by Jordan in Ref. 18.

The strut in Figure 22 is assumed to have a straight elastic axis which is rigidly held at the root. As the transition from the unswept to the swept takes place, each spanwise strip keeps its length and mass composition. While the strip rotates about its root point, this point slides along the root chord. In addition, the structure is assumed to be of such a nature that the streamwise strips remain rigid. By sweeping in this manner, the halfchord at a given spanwise station of the swept strut is related to the halfchord of the straight strut counterpart as follows:

$$b_{\Lambda} = b \sec \Lambda \qquad \text{(II-1)}$$

The details of the integro-differential equation that is the result of applying strip theory to the streamwise strip of a cantilever which is swept as noted above, and then integrating over the span are shown in Ref. 20. The flutter determinant may then be obtained by using the Rayleigh-Ritz method to approximate the vibratory character of the structure in question. Inasmuch as modal analyses using as few as two modes have successfully predicted the existence of low mass-density ratio flutter, the mathematical model chosen for this investigation is the binary flutter determinant of a uniform, swept strut; the assumed flutter modes being the fundamental bending and torsional modes of the uniform cantilever. The salient features of the flutter determinant, based on the above representation, can be summed up briefly as follows. Again, the details are contained in Ref. 20 with an abbreviated development of the determinant included herein as Appendix B.

As noted in Part I and Appendix A, the flutter determinant of the strictly two-dimensional typical section may be written as:

$$\begin{vmatrix} A - \mu\left(\frac{\omega_h}{\omega_f}\right)^2 & B \\ C & D - \mu r_\alpha^2\left(\frac{\omega_\alpha}{\omega_f}\right)^2 \end{vmatrix} = 0 \qquad \text{(II-2)}$$

where:

$A = \mu + L_h$

$B = \mu x_\alpha + L_\alpha - L_h(\frac{1}{2} + a)$

$C = \mu x_\alpha + M_h - L_h(\frac{1}{2} + a)$

$D = \mu r_\alpha^2 + M_\alpha - (L_\alpha + M_h)(\frac{1}{2} + a) + L_h(\frac{1}{2} + a)^2$

(See Appendix A for definition of unsteady derivatives $L_h$, etc.)

Now the counterpart of Eq. II-2 for the uniform and unswept cantilever strut may be considered. The flutter determinant for this system is obtained if certain spanwise integrals over the bending and torsional modes are introduced in Eq. II-2. For convenience, the resultant equations may be normalized to yield:

$$\begin{vmatrix} A - \mu \left(\frac{\omega_h}{\omega_f}\right)^2 & .96\,B \\ .96\,C & D - \mu\, r_\alpha^2 \left(\frac{\omega_\alpha}{\omega_f}\right)^2 \end{vmatrix} = 0 \qquad \text{(II-3)}$$

This determinant is seen to be identical to Eq. (II-2) except for the coefficients of the off-diagonal terms. The nearness of .96 to 1.0 has in the past been regarded as evidence that the two-dimensional typical section and the cantilever flutter problems are closely related. Indeed, it may be stated that the practical usefulness of the simplified typical section analysis before high speed digital computers became available, was largely due to the fact that it could be used to adequately represent a cantilevered aircraft wing. However, it will be shown later in this study that the close relationship between the two-dimensional and the flexible cantilever flutter problems does not hold in the low mass-density ratio region due to an extreme sensitivity of the flutter behavior of a lifting surface to its vibratory character - and hence to its assumed flutter modes. The exact value of the off-diagonal coefficients depends upon the particular choice of flutter modes.

Now if Eq. (II-3) is regarded as the flutter determinant of an unswept strut and the corresponding swept strut is assumed to be formed as discussed earlier in this section, the flutter determinant of the swept, cantilever strut may be written as:

$$\begin{vmatrix} A - \mu\left(\frac{\omega_h}{\omega_f}\right)^2 + \varkappa(B+C) + 1.16\,\varkappa^2 D & .96B + 1.07\varkappa D \\ .96C + 1.07\varkappa D & D - \mu r_\alpha^2 \left(\frac{\omega_\alpha}{\omega_f}\right)^2 \end{vmatrix} = 0 \qquad \text{(II-4)}$$

It may be noted that the changes introduced by this first order approximation of the swept cantilever are entirely determined by terms containing the sweep parameter $\varkappa$. The sweep parameter $\varkappa$ combines both the sweep angle $\Lambda$ and the length to semichord ratio of the equivalent or "reference" unswept strut as follows:

$$\varkappa = 2 \tan \Lambda \Big/ \ell / b \qquad \text{(II-5)}$$

(See also the List of Symbols and Figure 22.)

Conversely, it may be seen that the sweep parameter value may be changed by altering any one of the three structural parameters of sweep, span, or semichord. However, it must be recalled that Eq. (II-4) is based upon certain assumptions regarding the structure and the two-dimensional unsteady hydrodynamic theory. Clearly, these assumptions limit the classes of structures which may be regarded as being represented by Eq. (II-4) regardless of the value of the sweep parameter $\varkappa$.

It may be seen from the swept strut determinant under discussion that if $\varkappa$ is assumed to be zero, as is the case if the angle of sweep is zero or the span infinite, Eq. (II-4) reduces to Eq. (II-3). Further, the A, B, etc. of Eq. (II-4) are the same as equations (II-3) and (II-2). Also, all of the non-dimensional parameters - including $\mu$ - are referred to the unswept strut and thus invariant with respect to the sweep parameter $\varkappa$.

Hence, the effects upon the flutter behavior of a structure which are entirely due to sweep - or more correctly, the introduction of a non-zero sweep parameter - are easily studied. However, the flutter speed of the swept strut is now related to the reduced frequency k by the relation:

$$U_f = \frac{\omega_f b \Lambda}{k} = \frac{\omega_f b \sec \Lambda}{k} \qquad \text{(II-6)}$$

Hence, it may be seen that the above approximation includes the most fundamental effect of sweep.

As mentioned in the last section, the terms which include the sweep parameter $\mathcal{K}$ arise from the pitch of the streamwise section that is coupled to the local slope of the bending mode and from the bending moment acting on the elastic axis which is a component of the streamwise moment. The fact that the same parameter $\mathcal{K}$ governs both effects might be expected as both are essentially the result of one structural change. Nevertheless, it is fortunate that any additional complexity may be avoided.

A plot of the sweep parameter $\mathcal{K}$ for various configurations is included herein as Figure 23. A glance will suffice to show that for practical structures for which the fundamental assumptions of strip theory, a straight elastic axis, and a rigid streamwise section apply; $\mathcal{K}$ is normally a small number. Further, it may be noted that the majority of flutter cases - theoretical and experimental - which, in fact, provided the motivation for this investigation ( see e.g., Ref. 7 or 10) involved extremely low values of $\mathcal{K}$, (on the order of $10^{-1}$ to $10^{-2}$). Use is made of these facts to simplify the swept strut flutter equations.

## II-D Simplification of the Flutter Determinant

Before considering the development of a simplified swept strut equation, a few remarks regarding the reasons for seeking a simplified

version are in order. In this era of high speed digital computers, the flutter determinant represented by Eq. (II-4), could obviously be easily handled without eliminating any of the terms. Further, it might be argued that any trends determined as a result of a parametric study of the unsimplified determinant would inherently be more accurate than what might be expected from any simplified version. However, it must be remembered that the purpose of this study is not to obtain numerical answers to specific problems. It is a known fact that reasonably accurate answers may be obtained by production type model analyses. However, the very completeness and complexity that produces the degree of accuracy associated with the production analyses makes a study of the general cause and effect relationships difficult. Rather, an insight into the fundamental mechanism of low mass-density ratio flutter is sought. To this end, the simplest - or nearly simplest - mathematical model which retains the salient features of the mechanism is required. Fortunately, the pitfall of oversimplification presents no problem as the results of more elaborate techniques - and experiments - are available for comparison. Indeed, it is the very fact that known results have shown that low values of the sweep parameter can be associated with known flutter occurrences that suggests that a simplified version of Eq. (II-4) may be used.

If Eq. (II-4) is expanded, certain of the terms may be combined to produce the following result:

$$\left(A - \mu \Pi^2 \frac{\omega_\alpha^2}{\omega_f^2}\right)\left(D - \mu r_\alpha^2 \frac{\omega_\alpha^2}{\omega_f^2}\right) - .96^2 BC$$

$$- \varkappa \mu r_\alpha^2 \frac{\omega_\alpha^2}{\omega_f^2}(B+C) - 1.16 \varkappa^2 \mu r_\alpha^2 \frac{\omega_\alpha^2}{\omega_f^2} D$$

$$+ (1.0 - 1.0272)\varkappa D(B+C) + (1.16 - 1.1449)\varkappa^2 D^2 = 0 \qquad \text{(II-7)}$$

It may be seen from Eq. (II-7) that the coefficients of the last two terms are two orders of magnitude less than the coefficients of the other terms. This fact, combined with the fact that low mass-density ratio flutter has been predicted and experimentally verified for struts having sweep parameter values on the order of $10^{-1}$ to $10^{-2}$, serves to strongly indicate that the last two terms may be entirely eliminated without the character of the problem being lost. Similar reasoning leads to the use of 1.0 as the coefficient of the fourth term. In addition to strictly numerical reasons, a physical justification to the above stated simplification is seen to exist when it is realized that the exact values of the numerical coefficients in Eq. (II-7) are functions of the assumed flutter modes. Thus, the terms neglected can be viewed as the results of the effects of sweep upon the mode shapes and the hydrodynamic force changes resulting therefrom. Clearly, these effects could well be expected to be negligible for small angles of sweep. As will be shown in the next section of this investigation, the above reasoning is fully justified by the accuracy of the results obtained from the simplified equation.

By making the simplifications discussed above, the expansion of the flutter determinant may be written as follows:

$$(A - \mu \Pi^2 \frac{\omega_\alpha^2}{\omega_f^2})(D - \mu r_\alpha^2 \frac{\omega_\alpha^2}{\omega_f^2}) - .96^2\, BC$$

$$- \varkappa \mu r_\alpha^2 \frac{\omega_\alpha^2}{\omega_f^2}(B + C + \varkappa D) = 0 \qquad \text{(II-8a)}$$

In effect, the above is similar to Eq. (II-3), but with a term due to sweep added and thus is seen to contain all of the essential features of the swept cantilever.

It may be seen from Eq. (II-8a) that the effect of the spanwise integrals over the assumed mode shapes appears only as the coefficient of the second term - or more explicitly as the coupling coefficient of the off-diagonal terms of the determinant of the unswept cantilever. Since production type modal analyses have shown a strong sensitivity to the number and character of the assumed flutter modes, it is desired to set up the equations so that the effect of varying the off-diagonal coupling constant may be studied. Accordingly, the second term of Eq. (II-8a) is expressed as a sum and difference as follows:

$$(A - \mu \Pi^2 \frac{\omega_\alpha^2}{\omega_f^2})(D - \mu r_\alpha^2 \frac{\omega_\alpha^2}{\omega_f^2}) - (BC - .0784\ BC)$$

$$- \aleph \mu r_\alpha^2 \frac{\omega_\alpha^2}{\omega_f^2}(B + C + \aleph D) = 0 \qquad \text{(II-8b)}$$

By substituting the appropriate unsteady aerodynamic terms in the above equation as indicated by the definitions following Eq. (II-2) and Appendix A, and separating the resultant complex equation into its real and imaginary parts, the equations shown on the next page may be obtained, (Eqs. II-9a and 9b).

As in Part I, the following substitutions are made:

$\Omega^2 = \frac{\omega_\alpha^2}{\omega_f^2}$, the flutter frequency coefficient squared; and

$X^2 = (\frac{U_f}{b\omega_\alpha})^2$, the flutter speed coefficient squared.

$$\Omega^2 = \frac{\begin{array}{l} k[2 - F + \mu 2(1 - F - 2a + 4a^2F + 8aFx_\alpha - 2x_\alpha + 4Fr_\alpha^2)] + 4G[1 - \mu(1 + 2a + 2x_\alpha)] \\ - .3136[\mu x_\alpha(4aFk - k - 2G) + \frac{2}{k}(1 + 2a)(G^2 - F^2) \\ + 2FG(1 - 4a^2) + G(1 + 4a) + ak(1 - 4aF)] \end{array}}{\begin{array}{l} \mu k[8Fr_\alpha^2 + \Pi^2(2 - 2F - 4a + 8a^2F)] - \mu 4\Pi^2 G(2a + 1) \\ - \varkappa\mu r_\alpha^2\{k[16aF - 4] - 8G + \varkappa[k(2F - 2 + 4a - 8a^2F) + 8aG + 4G]\} \end{array}}$$

$$X^2 = \frac{\begin{array}{l} \mu^2 8\Pi^2 r_\alpha^2\Omega^2 - \varkappa\mu 8r_\alpha^2[\mu 2x_\alpha - \frac{2F}{k^2} - 2a - \frac{4aG}{k} + \varkappa(\mu r_\alpha^2 + \frac{1}{8} - \frac{G}{2k} + \frac{2aF}{k^2} + \frac{2a^2G}{k} + \frac{F}{k^2} + a^2)] \\ + \frac{.6272}{\Omega^2}\{(\mu x_\alpha - \frac{2F}{k^2} + \frac{G}{k} - a - \frac{2aG}{k})(\mu x_\alpha - a - \frac{G}{k} - \frac{2aG}{k}) \\ + (\frac{1}{k} + \frac{F}{k} - \frac{2aF}{k} + \frac{2G}{k^2})(\frac{F}{k} + \frac{2aF}{k})\} \end{array}}{\begin{array}{l} \mu 8k^3\Omega^2\{(1+\mu)r_\alpha^2 + \Pi^2(\frac{1}{8} + a^2 + \mu r_\alpha^2)\} + \mu 8k\{2Gr_\alpha^2 + G\Pi^2(2a^2 - \frac{1}{2})\}\Omega^2 + \mu 8\Pi^2 F(1+2a)\Omega^2 \\ - \{k^2 - 2Gk - 8F + \mu k^2[1 + 8a^2 + 16ax_\alpha - \mu 8x_\alpha^2 + 8r_\alpha^2(1 + \mu)] \\ + \mu 4Gk[4a(a + 2x_\alpha) + 4r_\alpha^2 - 1] + \mu 8F(1 + 2a + 2x_\alpha)\} \end{array}}$$

Equations (II-9a) and (II-9b)

In both of these equations, the terms introduced by the inclusion of the sweep parameter are readily identifiable. The terms which express the difference of the off-diagonal coupling constants from unity are in the numerator in both cases, and are preceded by the decimal values. As with the equations obtained for the typical section and discussed in Part I, Eqs. (II-9a) and (II-9b) are transcendental and require a trial and error solution. Some results of solving Eqs. (II-9a) and (II-9b) are discussed in the following section.

## II-E Some Typical Results Based Upon the Simplified Theory

Since previous work had shown that production type modal analyses are capable of predicting the low mass-density ratio flutter of uniform, cantilever struts, and further since at least part of the prior theoretical work had been experimentally verified, results are available which may be used to check the validity of the simplified approach used to obtain Eqs. (II-9a) and (II-9b). Accordingly, several of the models for which results exist have been investigated using the simplified approach outlined in the previous two sections. In addition to checking the simplified flutter equation, these investigations show the character of the flutter solutions as a function of the two parameters of primary interest, namely the sweep parameter $\aleph$ and the mass-density ratio $\mu$. Specifically, the structural non-dimensional parametric values used for a major portion of the preliminary numerical work outlined herein are those of Model #2 used by Baird, et al, (Ref. 10) and Model #2 used by Herr (Ref. 5). In addition, certain of the conclusions of this investigation, which will be discussed in the sections to follow, are compared to some as yet unpublished results which have been obtained by C. E. Squires, Jr., of Grumman Aircraft Engineering Corporation for a third model. These models are referred to herein as Baird's Model #2, Herr's Model #2, and Squires' Model, respectively. That Eq. (II-8b) represents a

satisfactory mathematical representation of the low mass-density flutter problem was verified when the resultant solutions were found to agree quite well with the results of the more elaborate techniques used by the above named investigators. It naturally follows that the agreement with experimental results was also found to be acceptably good.

Figure 24 shows a comparison of the results obtained by Herr (Ref. 5), using the theory of Ref. 19, with results obtained using the simplified analysis for the unswept Herr #2 model. In both cases, no low mass-density ratio flutter ($\mu < \mu_a$) is predicted, while a range of flutter speeds is predicted for the higher mass-density ratios. It can be seen that the agreement is quite good, particularly with respect to the lower boundary which is the one of greatest practical interest. Since the two underlying unsteady hydrodynamic theories approach each other as the sweep angle approaches zero, it is very likely that the slight differences shown in Figure 24 are due to 1) the slightly different off-diagonal coupling constants used, and 2) the fact that the frequencies used in the simplified analysis were not the fundamental bending and torsional frequencies of the unswept strut but rather the swept measured frequencies of the first and third coupled modes, which were predominantly fundamental bending and fundamental torsion respectively. It might be mentioned that Figure 24 is typical in that no finite low mass-density ratio solutions could be obtained with a sweep parameter, $K$, of zero for any of the many combinations of system parameters investigated. This was in keeping with what other investigators had suggested, (see e.g., Ref. 26) and was a factor which contributed to the formulation of the physical interpretation of the low mass-density ratio flutter mechanism which is presented in a section to follow.

Figure 25 shows that both theories predict a low mass-density ratio flutter boundary for the Herr Model #2 with a 10 degree sweep angle. As may be seen, the agreement is quite good. The character

of the low mass-density ratio solutions shown in Figure 25 may be regarded as typical for parametric combinations possessing such solutions. In particular, Figure 25 illustrates the local maximum of the flutter speed that occurs for some mass-density ratios near the $\mu_a$ of the system. This local maximum may be said to divide the "usual" from the low mass-density ratio flutter boundaries, (see also Ref. 11). It might be mentioned that Herr tested this model with a sweep angle of 15 degrees and a mass-density ratio $\mu$ of .13 and did not obtain flutter. However, the maximum speed obtained during the test was less than one half of the predicted flutter speed and thus the absence of experimental verification is understandable. It will be shown in a section to follow that the comparatively high flutter speed predicted and quite possibly physically existent flutter speed was at least partially due to the unfortunate choice of a forward elastic axis location.

Figure 26 shows a comparison of solutions for the Baird Model #2 with 15 degrees of sweep. The solutions obtained by Squires and Baird were obtained by using production type modal analyses incorporating the lowest three, four, or five coupled modes of the strut. Again, the agreement was quite good, particularly with regard to the low mass-density ratio quartic - or four mode - analysis. As may be seen, the agreement with the two experimental points was excellent. In addition, Figure 26 demonstrates the "unusual" sensitivity of the low mass-density ratio modal solutions to the modal representation of the structure. The sensitivity has been termed "unusual" because of the comparatively weak dependence of the "usual" ($\mu > \mu_a$) flutter boundary upon the assumed flutter modes. This characteristic of low mass-density ratio flutter will be discussed in considerable detail in the sections to follow. It will be shown that such a behavior can be readily explained.

In addition to the flutter speed or flutter speed coefficient comparisons discussed above, the flutter frequency solutions were also checked at the discrete points for which comparable solutions were available. Again, the agreement was good.

The results which have been discussed represent a typical sampling of the calculations performed to assure the validity of Eq. (II-8b) and have been presented to illustrate why it was concluded that the simplified equation could be used to study the fundamental mechanism of low mass-density ratio flutter. Having established the validity of the simplified approach, certain of the specific characteristics of the solutions resulting from the use of the approach will be discussed.

Figure 27 is a typical plot of the flutter speed coefficient as a function of the mass-density ratio for several sweep parameter values. This plot shows that although the physically meaningful flutter boundary is only slightly affected by small changes in the value of the sweep parameter when mass-density ratios appreciably greater than $\mu_a$ are involved, (the $\mu_a$ of the system depicted is .76), a radical change in the low mass-density ratio behavior occurs as the sweep parameter is increased beyond what might be termed the "critical" $\chi$ of the system in that a finite valued flutter boundary is seen to appear. As the sweep parameter is further increased - at least within the physically meaningful range - the low mass-density ratio boundary is seen to remain essentially unchanged. Thus the flutter speed, for configurations possessing a sweep parameter greater than the critical value, is predicted to rise approximately as a function of the secant of the sweep angle. The results of more elaborate analytical techniques and, in fact, experimental results have shown the rise in the flutter speed as a function of sweep to be somewhat greater. However, it must be recalled that both the simplified and the complete binary flutter determinants involve assumptions which deteriorate in validity as the angle of sweep is increased. These assumptions have been discussed in previous sections.

Another feature of the low mass-density ratio solutions which is typified by Figure 27 is that if the mass-density ratio can be assumed to be varied by varying the fluid density, the low mass-density ratio

boundary is seen to be a constant dynamic pressure phenomenon. It should be noted that certain of these characteristics have been noted by other investigators for this and other models, (see e.g., Ref. 12).

Although Figure 27 may be regarded as typical for those parametric combinations which possess a valid low mass-density ratio boundary, many combinations do not possess low mass-density ratio solutions (and thus might be presumed to be flutter free in the low $\mu$ region) for any reasonable sweep parameter values. Qualitative and quantitative reasons for this behavior are discussed in sections to follow. In all cases, the effect of varying the sweep parameter upon the "usual" ($\mu > \mu_a$) flutter boundary will be shown to be slight.

Figure 28 is a magnification of the low $\mu$ portion of Figure 27, and shows the behavior as the zero mass-density ratio is approached. In addition, the numerical values give some indication of the range of reduced frequencies (k) typically encountered with the low mass-density ratio flutter solutions. It may be noted that for any given low mass-density ratio, the reduced frequency rises as the sweep parameter is increased.

Figure 29 is the flutter frequency counterpart of Figure 27 and may again be regarded as typical. As can be seen, the flutter frequency for those parametric combinations possessing a low $\mu$ boundary approaches zero as the mass-density ratio approaches zero. Further, the flutter frequency at any given low mass-density ratio decreases as the sweep parameter decreases. Figure 30 is the flutter frequency coefficient counterpart of Figure 28.

With regard to the characteristics discussed above, by far the most interesting fact is that the flutter frequency due to any given parametric combination is seen to approach zero as the sweep parameter approaches the "critical" value. Hence, the flutter is seen to degenerate to a pure divergence. This behavior is illustrated by Figure 31 which has been computed for the Baird #2 model at a mass-density ratio of .1. As

may be seen from the figure, the "critical" sweep parameter value is approximately .03. This corresponds to approximately 6.8 degrees of sweep which agrees very well with the statement in Ref. 10, that, "a sweep of 7.5 degrees was sufficient to assure freedom from static divergence." Figure 32 is the corresponding flutter speed coefficient plot which is seen to be a very weak function of the sweep parameter for values above the "critical" value.

In an effort to obtain some idea of what value the approximate quasi-steady ($k \to 0$) and the quasi-unsteady ($k \to \infty$) hydrodynamic theories might be, a few sample calculations were performed. The procedure followed was simply to utilize Eqs. (II-9a) and (II-9b) with the appropriate F and G values inserted. (The quasi-steady and unsteady approximations were discussed in considerable detail in Part I.) Figure 33 shows a comparison of the flutter speed coefficients predicted by the "exact" and by both approximate theories for the Baird #2 model at zero degrees of sweep. As can be seen, the quasi-unsteady theory ($k \to \infty$) agrees reasonably well with the "exact" theory while the quasi-steady theory ($k \to 0$) actually predicts a non-existent set of flutter points in the low mass-density ratio region. It may be seen that the reduced frequencies associated with the low mass-density ratio solutions suggest that the quasi-steady assumption might not be valid. Figure 34 is the flutter frequency counterpart of Figure 33.

Figure 35 shows the same comparison but for a sweep parameter value greater than the "critical" value of the system. Once again, the quasi-unsteady theory ($k \to \infty$) is seen to be qualitatively correct over the entire mass-density ratio range while the quasi-steady theory is valid only in the low mass-density ratio range and even there only if careful attention is paid to the reduced frequencies associated with the predicted flutter points. It might be mentioned that the quasi-steady boundaries form a loop which meets at the origin. Because of the typically low reduced frequencies normally associated with low $\mu$ flutter, the quasi-

steady branch associated with the low reduced frequencies is very nearly exact. Figure 36 is the flutter frequency counterpart.

Because of the limited number of calculations performed utilizing the approximate theories, it cannot be stated with certainty that the figures discussed above are typical of all parametric combinations. In fact, it is quite likely that the inconsistencies encountered in conjunction with the quasi-steady theory are at least partially due to the combination of an aft center of gravity and a very low frequency ratio. Indeed, analyses discussed in Part I of this study showed that such a behavior could be expected with a "typical section" having such properties. Nevertheless, it is interesting to note that once again the quasi-unsteady theory ($k \to \infty$) was found to be qualitatively reliable while the quasi-steady theory could only be used with considerable caution.

When all of the results which have been discussed thus far are viewed as a whole, one fact quickly emerges. Namely, the rather radical changes in the flutter behavior which occur as a function of the mass-density ratio and the sweep parameter suggest that low mass-density ratio flutter does not have the same physical origin as the "usual" coupled bending-torsion flutter familiar to aircraft flutter analysts.

## II-F Investigation of the Sensitivity of Solutions to the Assumed Flutter Modes

The simplified two-degree-of-freedom, uniform cantilever, flutter equation (Eq. II-8a) was developed by ignoring the effect of sweep upon the assumed flutter mode shapes. As a result, only the direct effect of the spanwise integrals over the unswept mode shapes appears in Eq. (II-8a); this being the value taken by the numerical coefficient of the second group of terms. A glance at Eq. (II-8a) reveals that if the numerical coefficient of $(.96)^2$ is replaced by unity, the first two terms of the equation are identically the mathematical model of the familiar "typical section." The

equation which is the result of altering Eq. (II-8a) by replacing $(.96)^2$ by 1.0 may then be viewed as the representation of a simple pitch-plunge section with the major sweep effect of pitch-bending added.

The altered equation discussed above was investigated; the results being that no low mass-density ratio solutions could be obtained regardless of the sweep parameter assumed although the high mass-density ratio results were virtually unaltered from what could be obtained by using Eq. (II-8a). The nature of the solutions is shown by Figure 37, which may again be regarded as typical. As can be seen from Figure 37, the only effect of increasing the sweep parameter, from a low mass-density ratio point of view, was to lower the $\mu_a$ of the system an almost insignificant amount. The obvious implication of the nature of the results depicted by Figure 37 is that the pitch-plunge "typical section" analysis, even with the sweep effect of pitch-bending included, is incapable of predicting the low mass-density ratio ($\mu < \mu_a$) flutter behavior of a swept, flexible cantilevered strut. This conclusion is not entirely unexpected as it has been known that single panel point modal analyses in which the sweep condition has been simulated by introducing a streamwise angle of attack into the bending mode have also failed to predict the existence of low mass-density ratio flutter for configurations known to be susceptible to the phenomenon. Note that this result implies that experimental tests conducted by using semi-rigid models are of questionable value in predicting the low mass-density ratio flutter behavior of flexible structures.

Figure 38 shows a typical set of flutter boundaries obtained by varying the off-diagonal coupling constant of Eq. (II-8a) from $.9^2$ to 1.0. It may be seen that although the high $\mu$ flutter boundary remains unchanged, the low $\mu$ flutter boundary is extremely sensitive to the coupling constant utilized. Quite obviously, the low $\mu$ boundary trend is such that an infinite flutter speed coefficient is rapidly approached as the coupling constant approaches unity. Hence, a low mass-density ratio

($\mu < \mu_a$) flutter boundary is non-existent for a coupling of 1.0. When it is recalled that the value of the coupling constant arises from spanwise integrals over the assumed mode shapes, it is clear that low $\mu$ flutter is extremely "mode shape sensitive." Indeed, Figure 26 illustrates that the results of production type model analyses have exhibited a strong sensitivity to the number and type of assumed modes used in the flutter analysis. From the standpoint of the production analyses, the extreme sensitivity of the solutions to the coupling constant used implies that not only must a considerable number of modes be assumed, but the number of panel points must be sufficient to insure accurate and representative spanwise numerical integration. In short, the vibratory character of the structure must be representative to a degree far in excess of what has come to be regarded as acceptable for aircraft work. The problems inherent with this extreme sensitivity when complex structures are involved are obvious.

## II-G The Zero Mass-Density Ratio Analysis

All discussion thus far in Part II has been based upon the physical assumption that a mass-density ratio variation is achieved by considering a variable fluid density. Indeed, the statement that the low mass-density ratio solutions exhibited a constant critical dynamic pressure implied that such must be the case. If the above reasoning is extended to the limiting case, it is clear that a zero mass-density ratio implies a fluid of infinite density. As one might intuitively expect, the flutter behavior as the zero mass-density case is assumed to be approached in the above stated manner is for the flutter speed and flutter frequency to both approach zero. This results in an indeterminate solution for the reduced frequency. These tendencies are both very well illustrated by Figures 28 and 29 which are, of course, based upon parametric studies which assumed constant structural mass and stiffness properties throughout the mass-density ratio range.

However, a zero mass-density ratio can also be approached by decreasing the section mass while holding the fluid density constant. The details of these two physically different approaches were discussed in some detail in Part I of this investigation and the advantages of each were pointed out at that time. Briefly, a meaningful investigation of the limiting zero mass-density case is possible by writing the flutter equations in terms of "in-fluid" frequencies and then using the concept of a "decreasing section mass." The physical interpretation of finite "in fluid" frequency ratios coupled with a zero section mass is quite simply that the strut is assumed to retain its stiffness properties as the section mass approaches zero.

Using the relationships shown herein as Eqs. (I-7), Eq. (II-9a) may be converted to its "in fluid" equivalent which may be written as shown on the following page as Eq. (II-10a). Similarly, Eq. (II-9b) may be written as Eq. (II-10b).

It is obvious from the simple substitutions which result in Eqs. (II-10a) and (II-10b) that the two sets of equations are mathematically equivalent. However, a glance at Eqs. (II-9a) and (II-9b) will suffice to show that the equations become worthless, in a practical sense, as a zero mass-density ratio is approached inasmuch as the reduced frequency k is indeterminate regardless of the choice of structural parameters. However, Eqs. (II-10a) and (II-10b) may yield finite and determinate reduced frequency k solutions if the zero mass-density ratio is considered to be approached by decreasing the section mass while retaining the stiffness properties; i.e., $\mu \rightarrow 0$ while $\Pi_*^*$ remains real and finite.

Assuming the limiting case of a zero mass-density ratio to be approached in the above manner results in the Eqs. (II-11a) and (II-11b) which are shown on page 111.

$$\frac{\omega_\alpha^{*2}}{\omega_f^2} = \Omega_*^2 = \frac{\begin{array}{l} k[2 - F + \mu\, 2(1 - F - 2a + 4a^2F + 8aFx_\alpha - 2x_\alpha + 4Fr_\alpha^2)] + 4G[1 - \mu\,(1 + 2a + 2x_\alpha)] \\ -.3136\{\mu\, x_\alpha(4aFk - k - 2G) + \frac{2}{k}(1 + 2a)(G^2 - F^2) + 2FG(1 - 4a^2) \\ \quad + G(1 + 4a) + ak(1 - 4aF)\} \end{array}}{\begin{array}{l} 8Fk(\frac{1}{8} + a^2 + \mu\, r_\alpha^2) + k\Pi_*^2(1 + \mu)(2 - 2F - 4a + 8a^2F) - 4G(2a + 1)(1 + \mu)\Pi_*^2 \\ -\varkappa(\frac{1}{8} + a^2 + \mu\, r_\alpha^2)\{k[16aF - 4] - 8G + \varkappa[k(2F - 2 + 4a - 8a^2F) + 8aG + 4G]\} \end{array}}$$

$$\left(\frac{U_f}{b\omega_\alpha}\right)^2 = X_*^2 = \frac{\begin{array}{l} 8\Pi_*^2\Omega_*^2(1 + \mu)(\frac{1}{8} + a^2 + \mu\, r_\alpha^2) - \varkappa(1 + 8a^2 + \mu\, 8r_\alpha^2)[\mu\, 2x_\alpha - \frac{2F}{k^2} - 2a - \frac{4aG}{k} \\ + \varkappa(\mu\, r_\alpha^2 + \frac{1}{8} - \frac{G}{2k} + \frac{2aF}{k^2} + \frac{2a^2G}{k} + \frac{F}{k^2} + a^2)] \\ + \frac{.6272}{\Omega_*^2}\{(\mu\, x_\alpha - \frac{2F}{k^2} + \frac{G}{k} - a - \frac{2aG}{k})(\mu\, x_\alpha - a - \frac{G}{k} - \frac{2aG}{k}) \\ \quad + (\frac{1}{k} + \frac{F}{k} - \frac{2aF}{k} + \frac{2G}{k^2})(\frac{F}{k} + \frac{2aF}{k})\} \end{array}}{\begin{array}{l} 8k^2\Omega_*^2(\frac{1}{8} + a^2 + \mu\, r_\alpha^2)\{(1+\mu) + \Pi_*^2(1+\mu)\} + 8k\{2G(\frac{1}{8} + a^2 + \mu\, r_\alpha^2) + (2a^2 - \frac{1}{2})G\Pi_*^2(1+\mu)\}\Omega_*^2 \\ + 8F(1+2a)\Pi_*^2(1+\mu)\Omega_*^2 - \{k^2 - 2Gk - 8F + \mu k^2[1 + 8a^2 + 16ax_\alpha - \mu\, 8x_\alpha^2 + 8r_\alpha^2(1+\mu)] \\ + \mu\, 4Gk[4a(a + 2x_\alpha) + 4r_\alpha^2 - 1] + \mu\, 8F(1 + 2a + 2x_\alpha)\} \end{array}}$$

Equations (II-10a) and (II-10b)

$$\Omega_*^2 = \frac{k(2 - F) + 4G - .3136\left[\frac{2}{k}(1 + 2a)(G^2 - F^2) + 2FG(1 - 4a^2) + G(1 + 4a) + ak(1 - 4aF)\right]}{8Fk\left(\frac{1}{8} + a^2\right) + k\Pi_*^2(2 - 2F - 4a + 8a^2F) - 4G(2a + 1)\Pi_*^2}$$

$$- \mathcal{K}\left(\frac{1}{8} + a^2\right)\{k[16aF - 4] - 8G + \mathcal{K}[k(2F - 2 + 4a - 8a^2F) + 8aG + 4G]\}$$

$$X_*^2 = \frac{8\Pi_*^2\Omega_*^2\left(\frac{1}{8} + a^2\right) - \mathcal{K}(1 + 8a^2)\left[-\frac{2F}{k^2} - 2a - \frac{4aG}{k} + \mathcal{K}\left(\frac{1}{8} - \frac{G}{2k} + \frac{2aF}{k^2} + \frac{2a^2G}{k} + \frac{F}{k^2} + a^2\right)\right]}{8k^2\Omega_*^2\left(\frac{1}{8} + a^2\right)\{1 + \Pi_*^2\} + 8k\{2G\left(\frac{1}{8} + a^2\right) + \left(2a^2 - \frac{1}{2}\right)G\Pi_*^2\}\Omega_*^2}$$

$$+ \frac{.6272}{\Omega_*^2}\left\{\left(-\frac{2F}{k^2} + \frac{G}{k} - a - \frac{2aG}{k}\right)\left(-a - \frac{G}{k} - \frac{2aG}{k}\right) + \left(\frac{1}{k} + \frac{F}{k} - \frac{2aF}{k} + \frac{2G}{k^2}\right)\left(\frac{F}{k} + \frac{2aF}{k}\right)\right\}$$

$$+ 8F(1 + 2a)\Pi_*^2\Omega_*^2 - [k^2 - 2Gk - 8F]$$

Equations (II-11a) and (II-11b)

Hence, a simple mathematical interpretation of what has been shown is that the "in vacuum" approach causes all solutions to be collapsed onto the origin while the "in fluid" approach stretches the solutions from a point to a line. From a practical standpoint, the latter approach offers two significant advantages. First, all flutter frequencies do not approach zero as the mass-density ratio approaches zero. Rather, even for the limiting zero mass-density case, only the "critical" sweep parameter values yield zero flutter frequency solutions. (This point is illustrated by Figure 39; Figure 40 being the flutter speed counterpart.) As may be seen from Figure 39, real finite flutter frequencies may be calculated for sweep parameter values greater than the critical value while no solutions exist for lesser values. Secondly, the structural non-dimensional parameters $\Pi^2$, $r_c^2$, and $x_m$ do not appear independently in the zero mass-density equations, but rather only appear in combined form as the "in fluid" frequency ratio $\Pi_*^2$. (To avoid any misunderstanding it is recalled that $\Pi_*^2$ is a form of stiffness ratio.) For the limiting case of interest, the relationship may be written as:

$$\Pi_{*_{\mu \to 0}}^2 = \frac{(\frac{1}{8} + a^2)\Pi^2}{r_c^2 + (x_m - a)^2} \qquad \text{(II-12)}$$

As was shown in Part I, this reduces the task of conducting a parametric study by several orders of magnitude. In particular, the above stated fact allows the complete zero mass-density ratio solution pattern for uniform cantilever struts to be discerned by considering only the three parameters $\Pi_*^2$, a, and $\mathcal{K}$. This fact, coupled with the use of high speed digital computers, allows a complete parametric study covering the physically useful ranges of parameters to be conducted quite easily and efficiently. The result is a compact representation of what

parametric combinations possess zero mass-density ratio solutions and, of particular interest, the minimum sweep parameter value required for a valid flutter solution. This information is included herein as Figure 41, which shows the critical sweep parameter value as a function of the elastic axis location for various values of $\Pi_*^2$.

If Figure 41 were only valid for the limiting zero mass-density ratio case, it would only be of academic interest. However, it may be recalled that the zero mass-density ratio case is merely the extreme limit of the low mass-density ratio region and as such, any physical effects due to the decreasing of the mass-density ratio are retained and, in fact, magnified as the limiting condition is approached. Indeed, it is intuitively obvious and is, in fact, illustrated by many of the figures included herein that the low mass-density ratio flutter boundaries ($\mu < \mu_a$) terminate at the zero mass-density ratio. (Literally hundreds of solutions by the author and others, in addition to what has been included herein, furnish the numerical proof that the above statements are correct.) Hence, the non-existence of a zero mass-density ratio flutter solution implies the non-existence of low mass-density ratio flutter for the configuration in question. Therefore, Figure 41 is seen to be a completely practical plot of which configurations may be expected to have a low mass-density ratio flutter problem for some real, finite, free stream velocity; and further, the minimum sweep parameter value required for a dynamic instability to develop. At this point it is again emphasized that Figure 41 is based upon the assumptions of a uniform, cantilevered, fully wetted, lifting surface and further that all the assumptions involved in two-dimensional, unsteady, incompressible, potential flow are inherent in the development. Further, the simplified equation used to obtain Figure 41 inherently decreases in accuracy as the "critical" sweep parameter increases. However, it may be noted that Figure 41 checked very well with all applicable cases found in the literature, including the three models specifically mentioned in an earlier section.

As an illustration of the applicability of Figure 41 to a low but non-zero mass-density ratio case, Figure 42 in included herein. Figure 42 shows the flutter frequency as a function of the sweep parameter for a set of structural parameters equivalent to those of Figure 39. Two of the structural parameters used to construct Figure 42 were chosen at random as, in fact, were the two mass-density ratios plotted. This figure may be regarded as typical. Figure 43 shows the corresponding flutter speed coefficients.

Returning to Figure 41, several interesting facts may be noted. First, no low mass-density ratio flutter is predicted if the elastic axis is forward of the quarter chord. Second, it may be noted that the structural configurations most likely to encounter a low mass-density ratio flutter problem (i.e., for minimal values of $\mathcal{K}$ and the largest range of elastic axis (a) locations) are those much less stiff in bending than in torsion, i.e., low $\Pi_*^2$ values. Conversely, if the elastic axis is just aft of the quarter chord, virtually all combinations of stiffness may be expected to yield valid flutter solutions for comparatively low values of the sweep parameter. However, Figure 44 shows that the flutter speed coefficient asymptotically approaches infinity as the elastic axis is assumed to move forward toward the quarter chord. To obtain Figure 44, the sweep parameter value is always assumed to be the minimum required for a valid flutter solution. This plot illustrates why the choice of a forward elastic axis by Herr (Ref. 5) was previously termed unfortunate from the standpoint of an experimental verification of his theoretical results. Figure 45 is a similar plot for a strut assumed to retain the mass properties of the Baird model #2 with the mass-density ratio assumed to be .1. It can be seen that there is little difference between the general zero mass-density ratio plot and the specific plot of Figure 45. However, as the mass-density ratio is assumed to increase, the influence of the location of the center of gravity of the section mass may be expected to increase. Accordingly, the shape of the curve may be expected to be altered somewhat.

As has been previously noted, the zero mass-density ratio analysis shows the "critical" sweep parameter value to be associated with a zero flutter frequency. This is not unexpected as a similar trend has been noted and has been discussed for the several specific non-zero mass-density ratio cases included herein. For the special case of a zero flutter frequency, the "exact" unsteady hydrodynamic theory degenerates to the simpler quasi-steady ($k \to 0$) theory. Hence, it is apparent that the "critical" sweep parameter values may be determined by considering the quasi-steady zero mass-density ratio flutter equation.

If the quasi-steady values of F and G are substituted into Eqs. (II-11a) and (II-11b), the following may be obtained.

$$\Omega_*^2 = \frac{1 + .3136\{2(1 + 2a)X_*^2\Omega_*^2 - a(1 - 4a) - \varkappa(\frac{1}{8} + a^2)\{16a - 4 + \varkappa[4a - 8a^2]\}}{1 + 8a^2 + \Pi_*^2 (8a^2 - 4a)} \tag{II-13a}$$

$$X_*^2 = \frac{\Pi_*^2\Omega_*^2(1 + 8a^2) + \varkappa(1 + 8a^2)[2a - \varkappa(\frac{1}{8} + a^2)] + \frac{.6272}{\Omega_*^2}\, a^2 + \frac{1}{\Omega_*^2} - (1 + 8a^2)(1 + \Pi_*^2)}{8(1 + 2a)\Pi_*^2\Omega_*^2 + 8 - \varkappa\Omega_*^2(1 + 8a^2)[2 - \varkappa(2a + 1)] - .6272(2 + 4a - 4a^2)} \tag{II-13b}$$

It may be recalled that a similar simplification of the flutter equations of the "typical section" (see Part I) immediately resulted in a set of uncoupled equations. However, such is not now the case as Eq. (II-13a)

contains an $X^2$ term. Thus the independent determination of the flutter frequency coefficient requires that Eq. (II-13b) be substituted into Eq. (II-13a). Performing this substitution results in a quadratic in $\Omega_*^2$ which may be written as follows:

$$\Omega_*^4\{4(1+2a)\Pi_*^2 Z - \mathcal{K}(1+8a^2)[1-\mathcal{K}(a+\tfrac{1}{2})]Z - .3136(1+2a)\Pi_*^2(1+8a^2)\}$$

$$+\Omega_*^2\{4Z - .6272(1+2a-2a^2)Z - .3136(1+2a)(1+8a^2)[\mathcal{K}[2a-\mathcal{K}(\tfrac{1}{8}+a^2)]$$

$$-(1+\Pi_*^2)] - [1+.3136\,a(4a-1)][4(1+2a)\Pi_*^2 - \mathcal{K}(1+8a^2)[1-\mathcal{K}(a+\tfrac{1}{2})]]\}$$

$$-.3136(1+2a)(.6272\,a^2+1) - [1+.3136\,a(4a-1)][4-.6272(1+2a-2a^2)] = 0$$

(II-14)

where Z, the denominator of Eq. (II-13a), is written as:

$$Z = \{1+8a^2+\Pi_*^2(8a^2-4a)\} - \mathcal{K}\{(\tfrac{1}{8}+a^2)(16a-4)\}$$

$$-\mathcal{K}^2\{(\tfrac{1}{8}+a^2)(4a-8a^2)\}$$

Eq. (II-14) may be easily solved by the quadratic formula. Since the critical sweep parameter value results in a zero flutter frequency, the critical value may be determined by letting the quadratic solution of Eq. (II-14) approach infinity. For finite values of the structural parameters, an infinite solution is approached as the coefficient of the $\Omega_*^4$ term approaches zero. This coefficient may be written as follows:

$$\mathcal{K}^4\{(1+8a^2)(2a-1)(\tfrac{1}{8}+a^2)(4a-8a^2)\}$$

$$+\mathcal{K}^3\{(1+8a^2)(2a-1)(\tfrac{1}{8}+a^2)(16a-4)+(1+8a^2)(\tfrac{1}{8}+a^2)(2a-1)8a\}$$

$$-\mathcal{K}^2\{(1+8a^2)(2a-1)(1+8a^2+4a\Pi_*^2[2a-1])$$

$$+(1+8a^2)(\tfrac{1}{8}+a^2)(4a-1)8-(1+8a^2)(1+2a)(1-2a)4a\Pi_*^2\}$$

$$+\mathcal{K}\{(1+8a^2)(1+2a)(4a-1)4\Pi_*^2+2(1+8a^2)(1+8a^2+4a\Pi_*^2[2a-1])\}$$

$$-8(1+2a)(1+8a^2+4a\Pi_*^2[2a-1]\Pi_*^2+.6272(1+2a)(1+8a^2)\Pi_*^2=0$$

(II-15)

Hence, the above may be solved for $\mathcal{K}$ to yield Figure 41.

It may be seen from Figure 23 that, in general, practical sweep parameter values are less than unity while Figure 41 shows that many critical sweep parameter values are an order of magnitude less than unity. Accordingly, the quartic and cubic terms of Eq. (II-15) may be expected to be negligible for many cases of practical interest. This leaves a comparatively simple quadratic expression. The remaining quadratic expression may be solved for $\mathcal{K}$; the results being included herein as Figure 46. As might be expected, Figures 46 and 41 agree very well for those combinations possessing a low $\mathcal{K}$ critical while the agreement deteriorates for those combinations of $\Pi_*^2$ and (a) which have a comparatively large $\mathcal{K}$ critical. Extending the comparison leads to the conclusion that the simplified flutter equation upon which this investigation is based may be expected to predict somewhat erroneous results for configurations possessing an aft elastic axis and an equivalent zero mass-density ratio "in fluid" frequency ratio squared, $\Pi_*^2$, on the order of one

tenth. However, it is evident that the fundamental features of the phenomenon of low mass-density ratio flutter are retained even in the much simplified equation used to obtain Figure 46.

## II-H A Physical Interpretation of the Low Mass-Density Ratio Flutter Mechanism

If the results of the parameter studies discussed in Part II of this investigation are considered as a whole, an explanation of the physical origin of the coupled bending-torsion, low mass-density ratio flutter of uniform, cantilevered, fully wetted lifting surfaces may be formulated. The most important features of the low mass-density ratio solutions which lead to the explanation to follow are:

1. A positive, non-zero sweep parameter value is required for a low mass-density ratio dynamic instability to occur. This implies a structure of finite length, the elastic axis of which is swept back.
2. The structures most likely to encounter a low mass-density ratio flutter problem are those much less stiff in bending than in torsion.
3. The structure must be flexible in the spanwise direction and properly represented as such. This is implied by the fact that an off-diagonal coupling constant less than unity is required for the proper prediction of low mass-density ratio flutter, and,
4. The minimum sweep parameter value for which a dynamic instability can occur yields a zero flutter frequency. Thus the flutter instability degenerates to a pure divergence as the sweep parameter is decreased.

Item 1 suggests that the streamwise angle of attack which results from the bending of a swept strut is an important part of the mechanism. Item 2 supplements the suggestion of Item 1 since a strut much less stiff

in bending than in torsion would have the largest ratio of streamwise angle due to bending to streamwise angle due to torsion. Item 3 suggests that the spanwise pitch to bending ratio is important, while Item 4 indicates that the dynamic instability is a direct outgrowth of a tendency of the strut to diverge. The fact that no low mass-density ratio flutter may be predicted for struts having an elastic axis forward of the quarter chord further strengthens the latter indication. Hence, it is suggested that the flutter condition occurs in the following manner. First, a perturbation in angle of attack causes a moment about the elastic axis which tends to further increase the angle of attack of the strut. This in turn results in an incremental increase in lift which tends to bend the strut, while the translation resulting from the lift force tends to produce an opposing streamwise angle of attack. Since the relieving angle of attack is a function of the local bending slope and the translational velocity, it is not uniform over the span. Hence, the instantaneous spanwise leading is also not uniform - and may even be non-unidirectional. Therefore, it is suggested that the flutter condition develops - at least for the low flutter frequency cases associated with sweep parameter values near the critical value - when the positive hydrodynamic spring on the outer end of a strut overcomes the negative hydrodynamic spring of the fixed end and causes an oscillatory motion to develop. Obviously, the direction of the hydrodynamic spring is a function of the streamwise angle of attack. In all probability, the oscillation is sustained by the inertia effects of the structural and virtual masses and the negative hydrodynamic spring which exists over a portion of the strut. Naturally the balance of forces must be such that a complete cycle results in positive work being performed on the strut.

It may be noted that the rather delicate balance of loading required to produce the condition described above is a direct function of the local spanwise pitch to bending ratio. This would account for the extreme sensitivity of the analyses to the vibratory mode shapes assumed

in the representation of the structure. In addition, the proposed necessity of having both a positive and a negative hydrodynamic spring acting on the strut would seem to explain why the production modal analyses such as those discussed in Ref. 10, have always shown the second bending mode branch to be the critical branch leading to the flutter condition.

If the inertia load of the translating virtual mass which is centered at the midchord is considered in even the most rudimentary fashion, it may be seen that the proposed mechanism accounts for the shape of the curves shown in Figure 41. It may be seen from Figure 41 that the highest critical sweep parameter values are associated with parametric combinations having an elastic axis location near the midchord position. Clearly, the effect of the inertia force of the virtual mass is such that it tends to increase the diverging angle of attack for forward elastic axis locations while it has a relieving effect for the aft axis configuration. Hence, the aft axis configurations require that less of the total relieving angle be provided by the pitch-bending effect.

It must be once again mentioned that the proposed flutter mechanism has been formulated along the lines of the streamwise approach followed throughout this investigation. However, there is little doubt that an entirely equivalent explanation can be formulated from the "axis-normal" approach. Further, it must be stated that the above explanation does not consider the unsteady fluid forces which are the natural result of an oscillatory motion. Hence, it is possible that the mechanism may be somewhat more complex as the sweep parameter is increased substantially beyond the critical value as the increase is accompanied by a rise in the flutter frequency.

Figure 47 shows the calculated divergence or flutter speeds as a function of the sweep angle for Squires' strut model. It may be noted that the divergence speed of the unswept strut is considerably less than the minimum flutter speed, which is associated with $\chi$ critical. Landahl,

et al, showed a similar plot in Ref. 26, for the Herr #2 model. When these results are combined with the proposed theory, one is drawn to the conclusion that an unswept, uniform, cantilevered strut which will not diverge at some given free stream velocity will not, for any reasonable sweep angle, experience a low mass-density ratio flutter problem for at least as great a free stream velocity. This statement is made because the flutter condition appears to develop directly from an initial attempt of the structure to diverge.

## II-J Conclusions Resulting from Part II

Part II of this investigation has dealt specifically with fully wetted, uniform, cantilevered lifting surfaces. Further, it has been assumed that the surfaces could be considered rigid in the streamwise direction with the span to chord ratio large enough to justify the use of two-dimensional strip theory. Accordingly, the specific conclusions to be stated below may be considered to be entirely valid only when dealing with such structures.

However, this last statement is not meant to imply that a low mass-density ratio flutter mechanism such as that discussed in the previous section cannot exist for any structures other than those supported in a cantilevered fashion. Clearly, other types of structures could experience a non-unidirectional spanwise force distribution; the only requirement being a spanwise variation in the pitch to plunge ratio. Rather, the reason for qualifying the conclusions stated in this section is simply that the sensitivity of the flutter mechanism to small parametric changes could make certain extrapolations of the results presented in Part II of questionable value. Some extrapolations and generalizations of the results which <u>are</u> believed to be valid will be treated in the next section which deals with the conclusions resulting from the consideration of this entire investigation in combination with the results obtained by other investigators.

As a direct result of Part II of this investigation, the following conclusions may be drawn:

1. A comparatively simple modal analysis using the fundamental bending and torsion modes as the assumed flutter modes may be expected to predict the existence of a potential low mass-density ratio flutter problem provided the spanwise variation in coupling between the pitch and bending modes is considered and further provided that any sweep of the elastic axis is considered. Conversely, the prediction will not be reliable if the system is reduced to the so-called "typical section," as one or more features important to the fundamental flutter mechanism will be lost. In particular, the local spanwise pitch to bending ratio is an important parameter. It further follows that semi-rigid strut models are not susceptible to low mass-density ratio dynamic instabilities of the type discussed herein, and hence, tests performed with semi-rigid models are of questionable value.
2. Although the simplified analysis mentioned above is sufficient to predict the existence of a potential problem, the sensitivity of the flutter speed prediction to small changes in the assumed vibratory character of the structure implies that an accurate prediction of flutter speed may require a relatively complex analysis involving a considerable number of modes and panel points. Again, this is the result of the extreme dependence of the mechanism upon the local spanwise pitch to bending ratio.
3. No low mass-density ratio flutter may be predicted - and none is believed to be physically possible - unless the structure has a positive, non-zero sweep parameter value. For

physically plausible structures, this implies that the elastic axis must be swept back relative to the normal to the free stream. The minimum sweep parameter value for which a dynamic instability can occur yields a zero flutter frequency.

4. The streamwise relieving angle of attack of a swept cantilever subjected to bending is an important part of the flutter mechanism. Accordingly, the structures most likely to encounter a low mass-density ratio flutter problem are those much less stiff in bending than in torsion.
5. No low mass-density ratio flutter may be predicted - and none is believed to be physically possible - for structures having an elastic axis forward of the quarter chord.
6. A structure which may experience a low mass-density ratio flutter problem will encounter the instability at approximately the same dynamic pressure throughout the low mass-density ratio range.

It is further concluded that the analysis of the limiting zero mass-density ratio case which has been shown herein allows a rapid determination of whether a structure can experience a low mass-density ratio dynamic instability at any finite free stream velocity and further, that parametric trends obtained from the analysis of the limiting case are qualitatively valid throughout the low mass-density ratio range.

In short, it may be stated that the low mass-density ratio flutter cases which motivated this study (see e.g., Ref. 10) can be said to be both qualitatively and quantitatively understood as a direct result of this investigation.

## GENERAL CONCLUSIONS AND RECOMMENDATIONS

If the results of this investigation and the previously documented experiences of other investigators are considered as a whole, one is drawn to the conclusion that, in principle, the existing unsteady hydrodynamic and flutter theories may be used to predict the low mass-density ratio flutter behavior of fully wetted lifting surfaces. However, the physical origin of the low mass-density ratio flutter phenomenon is such that the hydro-elastic behavior of a lifting surface is extraordinarily dependent upon its vibratory character. Hence an accurate prediction requires a much more accurate structural representation that what might be expected on the basis of well documented aircraft experience. Conversely, it may be stated that the early low mass-density ratio investigations which were based upon the mathematical model of a "typical section" were not fundamentally wrong. However, the conclusions which resulted from such studies were extended, on the basis of aircraft experience, to such a degree that completely erroneous notions followed. It follows that the most important lesson to be learned from all of the low mass-density ratio work performed to date is that the region is typified by the extremely sensitive nature of the hydro-elastic behavior of a system to small changes in the system parameters. Thus, it is a region for which it is dangerous to generalize. It is the very sensitivity of the dynamic behavior of lifting surfaces operating in low mass-density ratio region that suggests some areas which might be fruitfully investigated in the future.

Both Part I and Part II of this investigation showed qualitatively the sensitivity of $\mu_a$ or the $\mu$ peak to small changes in the system parameters. It is suggested that a quantitative investigation of this phenomenon might be valuable. If reliable theoretical techniques could be developed, it would be possible, in certain cases, to make a slight structural change and greatly improve the hydro-elastic behavior of a surface.

It is likely that an investigation such as the one suggested would require that considerable effort be expended upon the probable improvements in theory made possible by the use of three dimensional unsteady derivatives.

As an extension of the work presented in Part II, it is suggested that a cantilevered structure with an aft mounted control surface be considered, as many aft mounted hydrofoil struts are of this design. In addition, the transient response of typical hydrofoil designs could be investigated to determine whether fatigue problems might exist even when an actual instability does not occur.

All of the work performed to date has considered the structure to be rigid in either the streamwise or axis-normal directions. In view of the demonstrated sensitivity of the predicted hydro-elastic behavior of a structure to its assumed vibratory character, a study considering the possible effects of a completely elastic structure would seem to be in order.

Lastly, it must be once again stated that almost all of the work performed to date has been concerned with fully wetted surfaces. As higher speeds are attained, it will be necessary to investigate the effects of cavitation upon the hydro-elastic behavior of a system.

## APPENDIX A

### An Abbreviated Development of the Complex "Flutter Determinant" of a Two-Degree-of-Freedom Section Oscillating in Incompressible Flow

The equations of motion of the representative section of Figure 2, may be written in the following form:

$$\begin{aligned} m\ddot{h} + S_\alpha \ddot{\alpha} + m\omega_h^2 h &= -L \\ S_\alpha \ddot{h} + I_\alpha \ddot{\alpha} + I_\alpha \omega_\alpha^2 \alpha &= M \end{aligned} \tag{A-1}$$

The determination of the aerodynamic forces which serve as the forcing functions of the above set of equations is a lengthy one. However, it has been well documented in a number of references including Refs. 1, 13, 14, 15, 16, and hence need not be considered here in any detail. Qualitatively it may be mentioned that for the case of unsteady motion the lift on a foil section is no longer a simple function of the circulation. For one thing, hydrodynamic inertia forces and moments can result due to the acceleration and deceleration of the fluid moving with the foil - even at zero forward velocity. Secondly, there is a contribution known as the quasi-steady lift. This is the lift which would be produced by the motion of the foil if the wake were assumed to have no effect. The third contribution may be regarded as a correction to the quasi-steady lift resulting from considering the normal velocities in the neighborhood of the foil which are produced by the trailing vortices. Hence, the lift and moment are a function of the motion and the configuration of the system.

Theodorsen and others considered the motion of the foil at the inception of flutter to be simple harmonic and after some rather involved mathematics showed that the aerodynamic forces and moments can be expressed as:

$$L = \pi\rho b^2[\ddot{L} + U_f\dot{\alpha} - ba\ddot{\alpha}] + 2\pi\rho U_f bC(k)[\dot{h} + U_f\alpha + b(\tfrac{1}{2} - a)\dot{\alpha}]$$

$$M = \pi\rho b^2[ba\ddot{h} - U_f b(\tfrac{1}{2} - a)\dot{\alpha} - b^2(\tfrac{1}{8} + a^2)\ddot{\alpha}]$$

$$+ 2\pi\rho U_f b^2(a + \tfrac{1}{2})C(k)[\dot{h} + U_f\alpha + b(\tfrac{1}{2} - a)\dot{\alpha}] \qquad (A-2)$$

where C(k) is the well known Theodorsen function expressible as the couplex number F + jG. The Theodorsen function is a function of only the reduced frequency k. F and G may both be expressed as a ratio of Bessel functions of the first and second kinds, of argument k. C(k) can also be expressed in terms of Hankel functions. The dependence of C(k) upon k can most easily be shown by a complex polar plot.

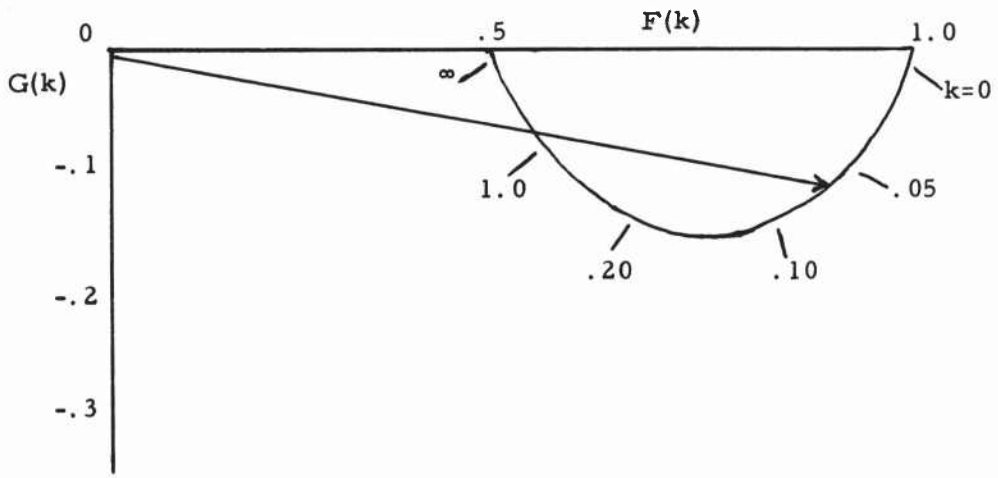


Figure A-1

Eq. (A-2) may now be combined with Eq. (A-1) and the harmonic motion assumption again introduced to yield the following:

$$-\omega_f^2 mh - \omega_f^2 S_\alpha \alpha + \omega_h^2 mh = -\pi\rho b^2 [-\omega_f^2 h + jU_f\omega_f\alpha + \omega_f^2 ba]$$

$$+ 2\pi\rho U_f bC(k)[j\omega_f h + U_f\alpha + j\omega_f b(\tfrac{1}{2} - a)\alpha]$$

$$-\omega_f^2 S_\alpha h - \omega_f^2 I_\alpha \alpha + \omega_\alpha^2 I_\alpha \alpha = \pi\rho b^2 [-\omega_f^2 bah - j\omega_f U_f b(\tfrac{1}{2} - a)\alpha + \omega_f^2 b^2(\tfrac{1}{8} + a^2)\alpha$$

$$+ \pi 2\rho U_f b^2(a + \tfrac{1}{2})C(k)[j\omega_f h + U_f\alpha + j\omega_f b(\tfrac{1}{2} - a)\alpha] \qquad (A-3)$$

The lift and moment expressions may be put into the notation of Ref. 16 by the introduction of the unsteady derivatives, this yields the following set of expressions:

$$-\omega_f^2 mh - \omega_f^2 S_\alpha \alpha + \omega_h^2 mh = \pi\rho b^3\omega_f^2 \{L_h \frac{h}{b} + [L_\alpha - L_h(\tfrac{1}{2} + a)]\alpha\}$$

$$-\omega_f^2 S_\alpha h - \omega_f^2 I_\alpha \alpha + \omega_\alpha^2 I_\alpha \alpha = \pi\rho b^4\omega_f^2 \{[M_h - L_h(\tfrac{1}{2} + a)]\frac{h}{b}$$

$$+ [M_\alpha - (L_\alpha + M_h)(\tfrac{1}{2} + a) + L_h(\tfrac{1}{2} + a)^2]\alpha\} \qquad (A-4)$$

where:

$$L_h = 1 - j2\frac{U_f}{b\omega_f}(F + jG)$$

$$L_\alpha = \frac{1}{2} - j\frac{U_f}{b\omega_f}[1 + 2(F + jG)] - 2(\frac{U_f}{b\omega_f})^2 (F + jG)$$

$$M_h = \frac{1}{2}$$

$$M_\alpha = \frac{3}{8} - j\frac{U_f}{b\omega_f}$$

Each of the above equations may now be suitably non-dimensionalized by dividing the first by $-\pi\rho b^3\omega_f^2$ and the second by $-\pi\rho b^4\omega_f^2$ and introducing the non-dimensional expressions $x_\alpha$ and $r_\alpha^2$.

$$\frac{m}{\pi\rho b^2}\frac{h}{b} + \frac{m}{\pi\rho b^2}x_\alpha\alpha - \frac{m}{\pi\rho b^2}\frac{\omega_h^2}{\omega_f^2}\frac{h}{b} = -L_h\frac{h}{b} - [L_\alpha - L_h(\tfrac{1}{2}+a)]\alpha$$

$$\frac{m}{\pi\rho b^2}x_\alpha\frac{h}{b} + \frac{m}{\pi\rho b^2}r_\alpha^2\alpha - \frac{\omega_\alpha^2}{\omega_f^2}\frac{m}{\pi\rho b^2}r_\alpha^2\alpha = -[M_h - L_h(\tfrac{1}{2}+a)]\frac{h}{b}$$

$$-[M_\alpha - (L_\alpha + M_h)(\tfrac{1}{2}+a) + L_h(\tfrac{1}{2}+a)^2]\alpha$$

(A-5)

Transposing, collecting coefficients of the same motion coordinates, and letting $\mu = \frac{m}{\pi\rho b^2}$ - the mass-density ratio - will yield the following set of homogeneous algebraic equations:

$$\{\mu[1 - \frac{\omega_h^2}{\omega_\alpha^2}\cdot\frac{\omega_\alpha^2}{\omega_f^2} + L_h]\frac{h}{b} + \{\mu x_\alpha + L_\alpha - L_h(\tfrac{1}{2}+a)\}\alpha = 0$$

$$\{\mu x_\alpha + M_h - L_h(\tfrac{1}{2}+a)\}\frac{h}{b} + \{\mu r_\alpha^2[1 - \frac{\omega_\alpha^2}{\omega_f^2}] + M_\alpha$$

$$-(L_\alpha + M_h)(\tfrac{1}{2}+a) + L_h(\tfrac{1}{2}+a)^2\}\alpha = 0$$

(A-6)

For a meaningful solution, the determinant of the above set must vanish. This determinant is the familiar "flutter determinant" of Eq. (I-4).

# APPENDIX B

## An Abbreviated Development of a Binary Flutter Determinant for a Uniform, Swept, Cantilever Lifting Surface

The calculation of the steady lift distribution of a uniform, swept, cantilever lifting surface of large aspect ratio presents little difficulty apart from the root and tip since, if the flow is assumed to be frictionless, the spanwise component of the free stream has little influence. However, such is not the case when the unsteady hydrodynamic forces acting on such surfaces are of interest as the downwash will, in general, vary along the span of an oscillating surface even if the root and tip effects are neglected.

Ideally, an unsteady hydrodynamic theory applicable to a swept surface should include all of the effects mentioned above. However, an approach which is both simplifying and, in general, conservative is to neglect the root and tip effects when dealing with surfaces which have a moderate to large aspect ratio. Thus, a two-dimensional "strip" theory is assumed to apply. This strip theory is similar to what is commonly used in the flutter calculations of unswept surfaces.

When the strip method is to be applied to a swept surface, the question arises as to whether the strips should be taken normal to the elastic axis or in the streamwise direction. For reasons which have been discussed in the text, the latter approach is used in the abbreviated development to follow. Ref. 20 may be consulted if more details are desired.

With regard to the surface being considered, the effects of sweeping a surface on the relation between the forces and the flutter speed can be considered in a convenient manner if the axial length (unswept span) and the normal chord are taken to be invarient during the sweeping process. The retention of these dimensions can be accomplished if the

surface is swept by rotation in the manner described in the text and shown in Figure 22.

For this development, the point of origin of the axis system is taken to be the root of the elastic axis, i.e., point 0 in Figure 22. x and $\bar{y}$ are non-dimensional coordinates.[#] The length xb sec $\Lambda$ is measured in the streamwise direction from the elastic axis, positive backward. The length $\bar{y}\ell$ is measured along the elastic axis. b and $\ell$ are both taken as defined in the general list of symbols, i.e., invariant with sweep. The lift per unit span $L(\bar{y})$ is taken to be opposite to the positive normal displacement z and a "nose-up" twist is regarded as positive while the moment $M(\bar{y})$ is positive "nose-down." It is to be understood that the forces involved imply a harmonic motion of the structure. Hence, any reference to the harmonic factor is omitted in the subsequent treatment.

Now if the lift per unit span is $L(\bar{y})$ and the torsional moment per unit span is $M(\bar{y})$, the force and moment acting on the elastic axis per unit length of the elastic axis are:

$$\bar{L}(\bar{y}) = L(\bar{y}) \cos \Lambda$$

and (B-1)

$$\bar{M}(\bar{y}) = M(\bar{y}) \cos^2 \Lambda$$

The lift and moment are expressed in terms of non-dimensional load functions as:

$$\bar{L}(\bar{y}) = b\int x^0 F(x, \bar{y})dx = \rho \omega_f^2 b^3 \bar{Z}_o(\bar{y})$$

and (B-2)

$$\bar{M}(\bar{y}) = b^2\int x^1 F(x, \bar{y})dx = \rho \omega_f^2 b^4 \bar{Z}_1(\bar{y})$$

The subscripts o and 1 refer to translation and pitch or bending and torsion respectively as indicated in the supplementary list of symbols.

---

[#] See supplementary list of symbols at end of Appendix B.

The deformations of the elastic axis are represented by the non-dimensional "modes" $\bar{z}_s(\bar{y})$.

$$\text{Vertical Translation} = \bar{z}_o(\bar{y})b$$

$$\text{Nose up Angle of Twist} = \bar{z}_1(\bar{y}) \qquad \text{(B-3)}$$

The local stiffnesses are represented by the function $\bar{\sigma}_o$ and $\bar{\sigma}_1$ of dimensions time $^{-2}$ as follows:

$$\text{Bending Stiffness} = EI = \rho b^3 \ell^4 \bar{\sigma}_o$$

$$\text{Torsional Stiffness} = GJ = \rho b^4 \ell^2 \bar{\sigma}_1 \qquad \text{(B-4)}$$

By combining expressions B - 2, 3, 4, the elastic equations relating the deformations of the elastic axis to the external forces may be written. These equations are written by considering the fact that the bending moment $\bar{M}(\bar{y})\tan\Lambda$ acts on the axis in addition to the bending force $\bar{L}(\bar{y})$. Further, the equations below are written by considering the phase angle of the structural damping to be zero and without regard to the boundary conditions at the point $\bar{y} = 0$.

$$\int_{\bar{y}}^{1} [(\bar{\eta}-\bar{y})Z_o(\bar{\eta}) + \frac{\varkappa}{2}\bar{Z}_1(\bar{\eta})]d\eta = -\frac{\bar{\sigma}_o}{\omega_f^2}\frac{d^2[\bar{z}_o(\bar{y})]}{d\bar{y}^2}$$

$$\int_{\bar{y}}^{1} \bar{Z}_1(\eta)d\eta = -\frac{\bar{\sigma}_1}{\omega_f^2}\frac{d[\bar{z}_1(\bar{y})]}{d\bar{y}} \qquad \text{(B-5)}$$

In the above, $\bar{\eta}$ is used as a dummy variable along the $\bar{y}$ axis.

Equations (B-5) refer to quantities measured in the axis-normal system. However, the loads $\bar{Z}_r(\bar{y})$ are referred to the external forces on the streamwise strip through Eq. (B-2).

The coefficient $\varkappa$ which appears above has been termed the "sweep parameter" in the text. It is written as:

$$\varkappa = 2 \frac{b}{\ell} \tan \Lambda \tag{B-6}$$

A relationship between the displacement $z(x, \bar{y})b$ along the streamwise strip and the modes $\bar{z}_s(\bar{y})$ of the elastic axis may be written as follows:

$$z(x, \bar{y})b = \bar{z}_o(\bar{y})b + xb \tan \Lambda \frac{d[\bar{z}_o(\bar{y})b]}{d(\bar{y}\ell)} + \frac{xb}{\cos \Lambda} \cos \Lambda \bar{z}_1(\bar{y})$$

Dividing by b and noting the second term of the right hand side contains the "sweep parameter," the above may be written:

$$z(x, \bar{y}) = \bar{z}_o(\bar{y}) + x\left[\frac{\varkappa}{2} \frac{d[\bar{z}_o(\bar{y})]}{d\bar{y}} + \bar{z}_1(\bar{y})\right] \tag{B-7}$$

Having obtained the elastic and the kinematic relationships, the determination of the external forces on the streamwise strip which are caused by a given displacement of the strip remains.

The external forces consist of inertia forces and hydrodynamic forces. All of these forces may be combined by writing the local external force as:

$$F(x, \bar{y}) = - \omega_f^2 \tilde{m}(x, \bar{y}) z(x, \bar{y}) b \tag{B-8}$$

Here $\tilde{m}(x, \bar{y})$ is not the local structural mass but rather that "complex mass" which, if fixed to the structure at the point $(x, \bar{y})$, would produce the inertia force $F(x, \bar{y})$. Hence, $\tilde{m}(x, \bar{y})$ is the sum of the structural mass, virtual hydrodynamic mass, and further components corresponding to hydrodynamic stiffness and hydrodynamic damping, (see Appendix A).

The displacement $z(x, \bar{y})$ of the streamwise strip is now split up into elementary deformations, $x^n$, assuming a rigid streamwise section:

$$z(x, \bar{y}) = \sum_{n=0}^{1} z_n(\bar{y}) x^n \tag{B-9}$$

Note that in the above functions $z_n(\bar{y})$ are non-dimensional amplitudes of the streamwise strips and not the "modes" of the elastic axis.

In integrating $F(x, \bar{y})$ along the streamwise strip, use may be made of Eq. (B-2). Thus the forces on the elastic axis are:

$$\rho\omega_f^2 \bar{Z}_r(\bar{y}) = \int x^r F(x, \bar{y}) dx = -\omega_f^2 b \sum_n z_n(\bar{y}) \int_{x_{L.E.}}^{x_{T.E.}} \tilde{m}(x, \bar{y}) x^{r+n} dx$$

Now from the above and by replacing the "complex mass" by the coefficients $A_{rn}$, the following expression may be obtained:

$$-\rho b \bar{Z}_r(\bar{y}) = \rho b \sum_n A_{rn} z_n(\bar{y}) = \sum_n z_n(\bar{y}) \int_{x_{L.E.}}^{x_{T.E.}} \tilde{m}(x, \bar{y}) x^{r+n} dx \tag{B-10}$$

The "complex mass" not only depends upon the reduced frequency k but also on the motion $x^n$ being considered. Hence, in general, $A_{rn} \neq A_{nr}$. However, under certain conditions, (see Ref. 20) the "complex mass" is invariant with sweep just as is the structural mass. The physical explanation for the invariability of the hydrodynamic reactions is that if the sweeping is accomplished by rotation, the cos $\Lambda$ term which is the result of the most fundamental effect of sweep is just cancelled by the sec $\Lambda$ factor in the semichord, i.e., $b_\Lambda = b \sec \Lambda$.

By combining the results which have been shown; the equation relating the modes $z_s(\bar{y})$ to the load functions $Z_r(\bar{y})$ may be obtained. For streamwise strips, these may be written:

$$-\bar{Z}_r(\bar{\eta}) = A_{ro}\bar{z}_o(\bar{\eta}) + A_{ri}\left[\frac{\chi}{2}\frac{d[\bar{z}_o(\bar{\eta})]}{d\bar{\eta}} + \bar{z}_1(\bar{y})\right] \qquad \text{(B-11)}$$

The flutter equations result if Eqs. (B-11) are combined with Eqs. (B-5).

The complete set of flutter equations, for a given reduced frequency, is a complex eigenvalve problem with the unknown eigen-solutions being the complex modes $\bar{z}_s(\bar{y})$. In most flutter calculations these modes are replaced by a set of dynamic coordinates.

For the binary case being considered here, the modes are replaced by one coordinate each in bending and torsion.

$$\bar{z}_o(\bar{y}) = q_o h(\bar{y})$$

$$\bar{z}_1(\bar{y}) = q_1 \alpha(\bar{y}) \qquad \text{(B-12)}$$

Now the amplitudes $q_o$ and $q_1$ become the unknowns in the problem.

For simplicity, and because the case discussed in the text was that of a rigidly supported cantilever, the boundary conditions which are assumed are:

$$h(o) = \frac{dh}{d\bar{y}}(o) = \alpha(o) = 0$$

The Lagrangian equations can now be obtained if the elastic equations, (Eqs. B-5), are multiplied by $\frac{d^2h}{d\bar{y}^2}$ and $\frac{d\alpha}{d\bar{y}}$, respectively, and then integrated along the span $0 \le \bar{y} \le 1$.

Integration by parts, using the boundary conditions previously stated, results in the following:

$$\int_0^1 [h\bar{Z}_o(\bar{y}) + \frac{K}{2}\frac{dh}{d\bar{y}}\bar{Z}_1(\bar{y})]d\bar{y} + \frac{q_o}{\omega_f^2}\int_0^1 \bar{\sigma}_o(\frac{d^2h}{d\bar{y}^2})^2 d\bar{y} = 0$$

$$\int_0^1 \alpha\bar{Z}_1(\bar{y})d\bar{y} + \frac{q_1}{\omega_f^2}\int_0^1 \bar{\sigma}_1(\frac{d\alpha}{d\bar{y}})^2 d\bar{y} = 0 \qquad \text{(B-13)}$$

The integrals on the right side of the above set represent the stiffness and can be expressed by the uncoupled "in vacuum" natural frequencies $\omega_h$ and $\omega_\alpha$. This results in the following:

$$\int_0^1 [h\bar{Z}_o(\bar{y}) + \frac{K}{2}\frac{dh}{d\bar{y}}Z_1(\bar{y})]d\bar{y} + q_o\frac{\omega_h^2}{\omega_f^2}\pi\int_0^1 \mu h^2 d\bar{y} = 0$$

$$\int_0^1 \alpha\bar{Z}_1(\bar{y})d\bar{y} + q_1\frac{\omega_\alpha^2}{\omega_f^2}\pi\int_0^1 \mu r_\alpha^2\alpha^2 d\bar{y} = 0 \qquad \text{(B-14)}$$

Eqs. (B-14) are the binary flutter equations. For a uniform listing surface, Eqs. (B-14) and Eqs. (B-11) can be combined to yield the following flutter determinant.

$$\begin{vmatrix} A_{oo} + (c_1A_{o1} + c_2A_{1o})\frac{K}{2} + c_3A_{11}\frac{K^2}{4} - \frac{\omega_h^2}{\omega_f^2}\mu & c_4A_{o1} + c_5A_{11}\frac{K}{2} \\ c_4A_{1o} + c_6A_{11}\frac{K}{2} & A_{11} - \frac{\omega_\alpha^2}{\omega_f^2}\mu r_\alpha^2 \end{vmatrix} = 0 \qquad \text{(B-15)}$$

In Eq. (B-15) the $A_{oo}$ etc. are the "complex mass" coefficients, or more precisely, the individual structural mass, virtual mass, and hydrodynamic reaction terms of the "typical section" or unswept analysis, i.e., $\mu + L_h$, etc. (See Appendix A.) The coefficients $c_1$ are integrals taken over the mode shapes and can be calculated numerically for a given design. Jordan (Ref. 20) calculated the values for a uniform surface by using as the normal modes h and $\alpha$ the fundamental modes of a uniform beam. This yielded the following values.

$$c_1 = c_2 = 2$$

$$c_3 = 4.648$$

$$c_4 = .959$$

$$c_5 = c_6 = 2.146$$

It may be noted that if the above coefficients are used Eq. (B-15) becomes the fundamental determinant used in Part II, (see Eq. II-4).

Additional Symbols Used in Appendix B

| | |
|---|---|
| $A_{rn}$ | "Complex mass" coefficient, see Eq. (B-15) |
| $F(x, \bar{y})$ | External force per unit area |
| L | Lift per unit span |
| M | Moment per unit span |
| $m(x, \bar{y})$ | Structural mass per unit area |
| $\tilde{m}(x, \bar{y})$ | "Complex mass" per unit area, see Eq. (B-8) |
| $x, \bar{y}, z$ | Non-dimensional coordinates |
| $\bar{z}_o(\bar{y})$ | Bending mode, non-dimensional |
| $\bar{z}_1(\bar{y})$ | Torsional mode, non-dimensional |
| $\bar{Z}_o(\bar{y})$ | Non-dimensional lift per unit length of elastic axis |
| $\bar{Z}_1(\bar{y})$ | Non-dimensional moment per unit length of elastic axis |
| $\eta$ | Dummy variable equal to $\bar{y}$ in integrals |
| $\bar{\sigma}_o$ | Bending stiffness function, invariant for uniform structure |
| $\bar{\sigma}_1$ | Torsional stiffness function, invariant for uniform structure |

Indices

| | |
|---|---|
| i | General index ( i = 0, 1, 2. . . . ) |
| r | Denotes force (o lift; 1 moment) |
| s | Denotes elastic axis deformation (o bending; 1 torsion) |
| n | Denotes streamwise strip deformation (o translation; 1 pitch) |

A superimposed bar $\bar{\ }$ denotes quantities referred to "axis-normal" directions except for "axis-normal" or unswept length $\ell$ and semi-chord b.

## REFERENCES


1. Theodorsen, T. and Garrick, I. E., The Mechanism of Flutter, A Theoretical and Experimental Investigation of the Flutter Problem, NACA Report 685, 1940.

2. Woolston, D. and Castile, G., Some Effects of Variations in Several Parameters Including Fluid Density on the Flutter Speed of Light Uniform Cantilever Wings, NACA TN 2558, 1951.

3. Henry, C. J., Dugundji, L., and Ashley, H., Aeroelastic Stability of Lifting Surfaces in High Density Fluids, OSR Tech. Note No. 58 - 626, June 1958.

4. Abramson, H. N. and Chu, W. H., A Discussion of the Flutter of Submerged Hydrofoils, Journal of Ship Research, Vol. 3, No. 2, October 1959.

5. Herr, R. W., A Study of Flutter at Low Mass Ratio with Possible Application to Hydrofoils, NASA TN D-831, May 1961.

6. Brunelle, E. J., An Informal Letter to the Office of Naval Research Concerning Hydrofoil Instability, Princeton University, May 1962.

7. Hilborne, D. V., The Hydroelastic Stability of Struts, Admiralty Research Lab. Dept. ARL/RI/G/HY/S/3, Great Britain, November 1958.

8. Brunelle, E. J., A Proposal to the Office of Naval Research Concerning the Investigation of Hydrofoil Instability at Low Mass Density Ratios, Princeton University, 8 October 1962.

9. Brunelle, E. J., Unpublished remarks delivered to the ad hoc committee for Hydroelastic Stability and Flutter on 29 August 1962 at the Fourth Symposium on Naval Hydrodynamics, Washington, D.C.

10. Baird, E. F., Squires, C. E., Jr., and Caporali, R. L., Investigation of Hydrofoil Flutter - Final Report, Report No. DA 10-4803, Grumman Aircraft Corp., 7 February 1962.

11. Squires, C. E., Jr., and Baird, E. F., The Flutter Characteristics of a Hydrofoil Strut, Vol. 3 of Preprints of Fourth Symposium on Naval Hydrodynamics, August 27-31, 1962.

12. Squires, C. E., Jr., On the Role of Mass-Density Ratio in Classical Flutter Theory with Application to Hydrofoil Flutter Prediction, Grumman Aircraft Engineering Corp. Report No. ADR 06-12-62.1, 15 January 1963.

13. Bisplinghoff, R. L., Ashley, H., and Halfman, R. L., Aeroelasticity, Addison-Wesley, Cambridge, Mass., 1955.

14. Bisplinghoff, R. L. and Ashley, H., Principles of Aeroelasticity, John Wiley and Sons, Inc., New York, 1962.

15. Scanlan, R. H., and Rosenbaum, R., Introduction to the Study of Aircraft Vibration and Flutter, the Macmillan Company, New York, 1951.

16. Smilg, B. and Wasserman, L. S., Application of Three-Dimensional Flutter Theory to Aircraft Structures, Air Force Technical Report 4798, 1942.

17. Cunningham, H. J., Analysis of Pure-Bending Flutter of a Cantilever Swept Wing and Its Relation to Bending Torsion Flutter, NACA TN 2461, September 1951.

18. Jordan, Peter F., On the Flutter of Swept Wings, I.A.S. Preprint 619, January 1956.

19. Barmby, J. G., Cunningham, H. J., and Garrick, I. E., Study of Effects of Sweep on the Flutter of Cantilever Wings, NACA Report 1014, 1950.

20. Jordan, Peter F., General Consideration of the Flutter of Swept Wings, Report No. Structures 61 Royal Aircraft Establishment, Farnborough, England. Also published as British ARC, R & M No. 2892.

21. Broadbent, E. G., Some Considerations of the Flutter Problem of High-Speed Aircraft, Proceedings of the Second International Aeronautical Conference, New York, pp. 556-581, 1949.

22. Jordan, Peter F., Four Years' Flutter Research, Air Documents Division T-2, AMC Wright Field, Microfilm No. R 2031 F. Previously Cataloged as Captured Document No. ZWB/AVAG/C, June 1946.

23. Molyneux, W. G., The Flutter of Swept and Unswept Wings with Fixed-Root Conditions, R & M No. 2796, 1954.

24. Flax, A. H., Aeroelastic Problems at Supersonic Speeds, Proceedings of 2nd International Aeronautical Conference, New York, 1949.

25. Miles, J. W., A Formulation of the Aeroelastic Problem for a Swept Wing, Journal of the Aeronautical Sciences, August 1949.

26. Landahl, M. T., Ashley, H., and Widnall, S. M., Some Free Surface Effects on Unsteady Hydrodynamic Loads and Hydroelasticity, Vol. 2, Fourth Symposium on Naval Hydrodynamics, August 1962.

# A TYPICAL SECTION FLUTTER BOUNDARY

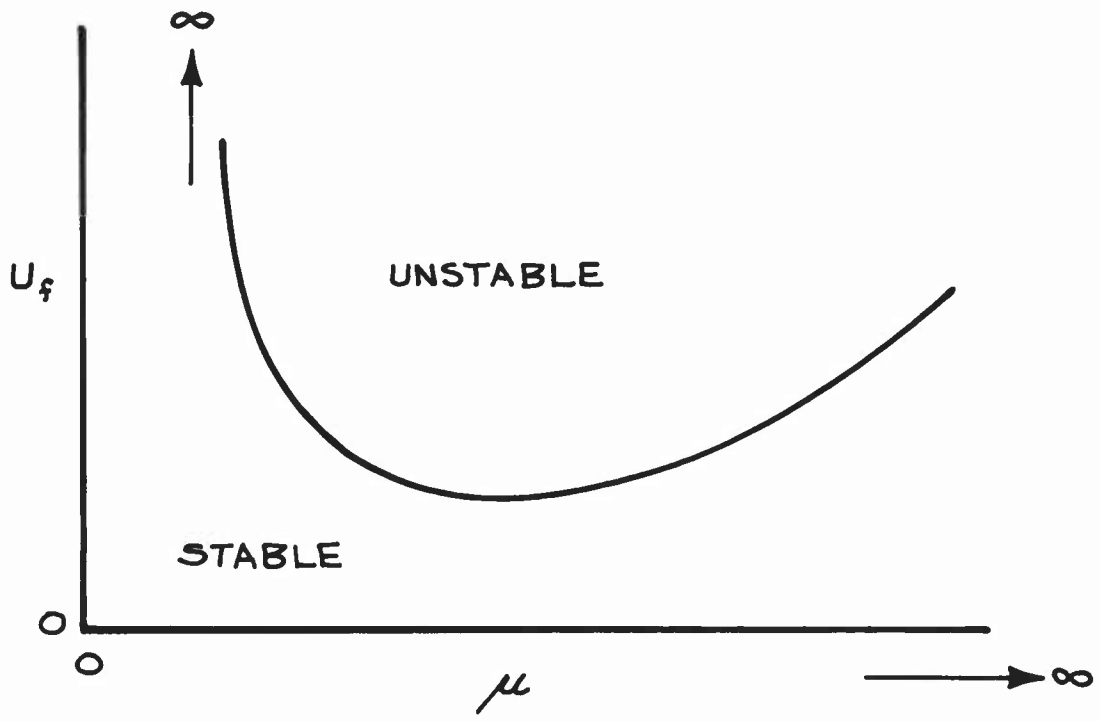


FIGURE 1

# COORDINATE SYSTEMS EMPLOYED

## DIMENSIONAL COORDINATE SYSTEM:

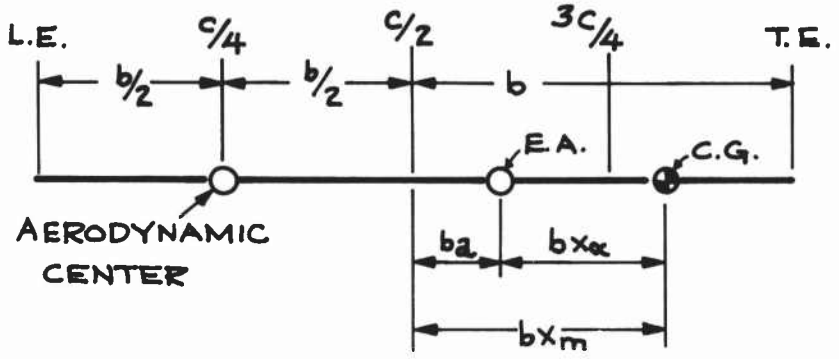


## NON-DIMENSIONAL COORDINATE SYSTEM:

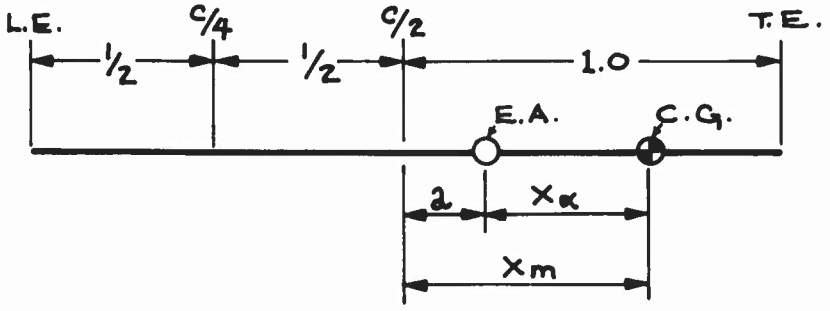


## MOTION COORDINATES:

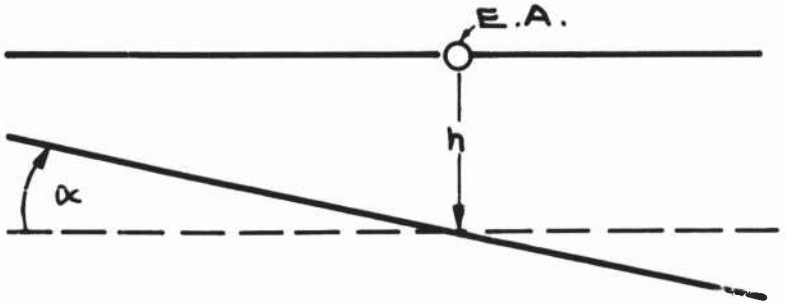


FIGURE 2

A PLOT OF $\pi_*^2$ vs. $a$ FOR WHICH THE FLUTTER SPEED IS ZERO @ $\mu = 0$
-BASED UPON ANALYSIS OF TYPICAL SECTION -

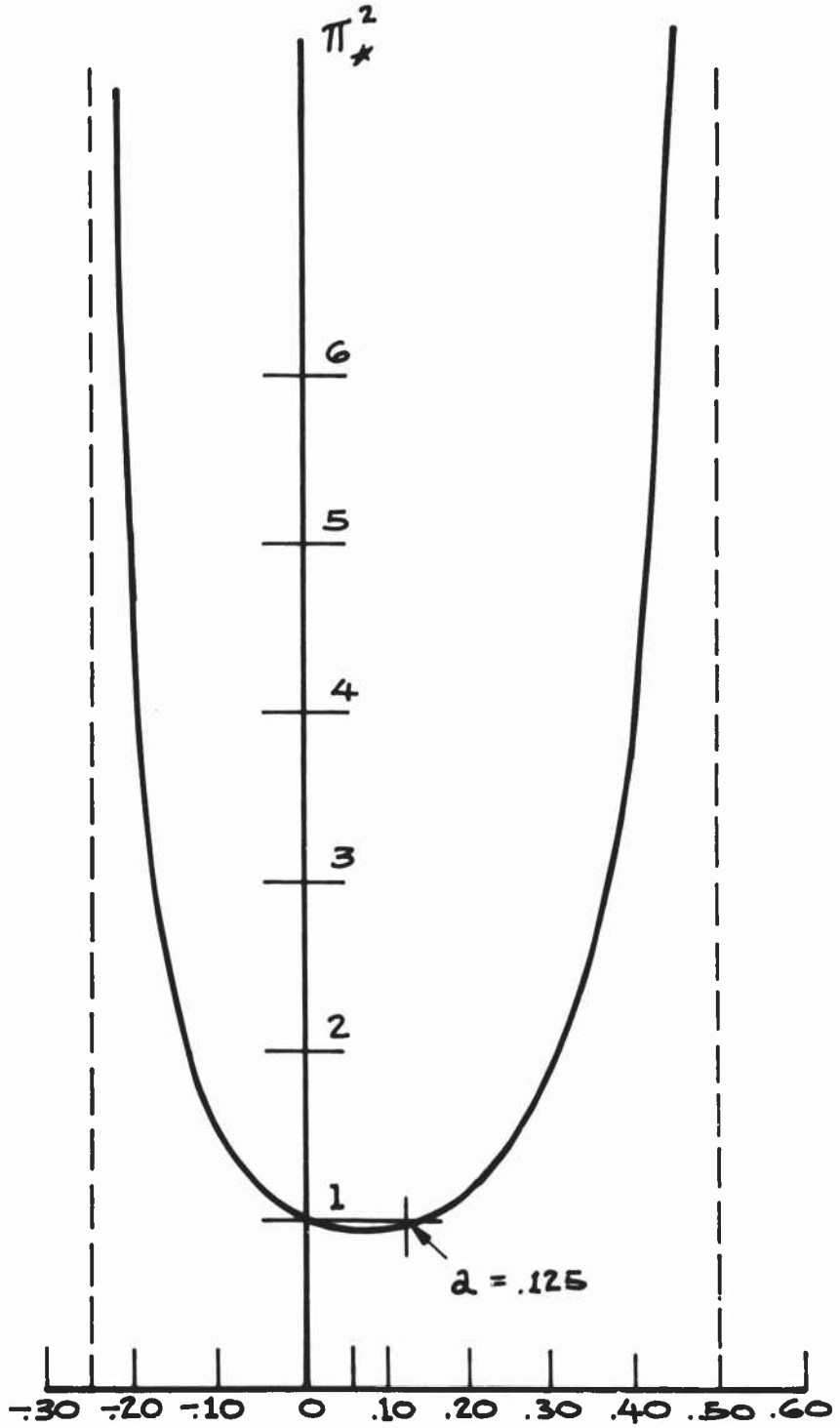


FIGURE 3

AXIS SYSTEM USED TO PORTRAY THE RESULTS OF THE ZERO MASS-DENSITY RATIO ANALYSIS FOR A TYPICAL SECTION

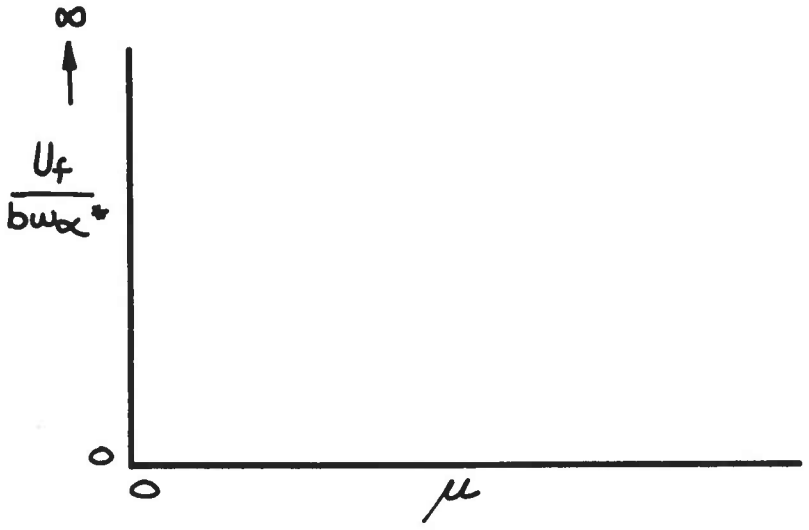


FIGURE 4

POSSIBLE "BOUNDARIES" TERMINATING IN ZERO-ZERO SOLUTIONS

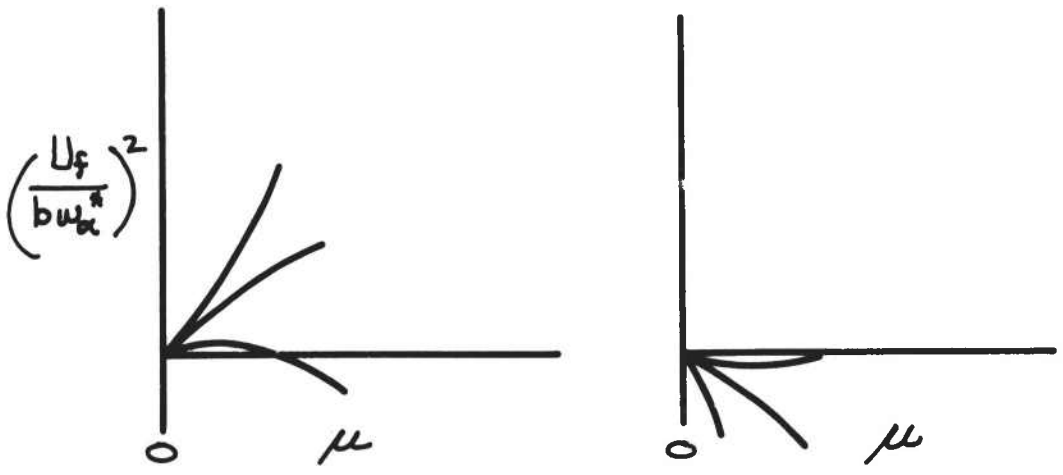


5a 5b

FIGURE 5

COMPARISON OF ELASTIC AXIS AND AXIS OF ZERO STATIC COUPLING

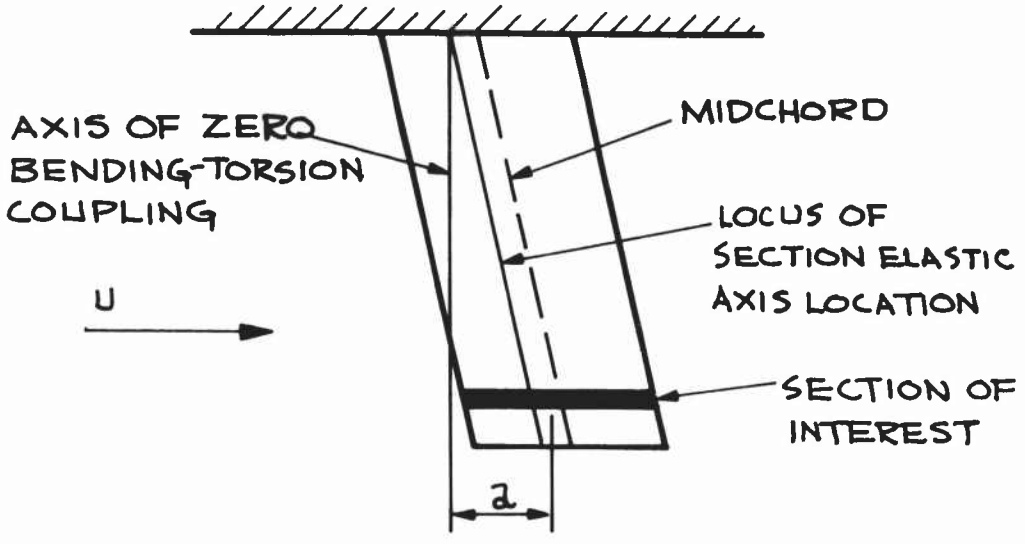


FIGURE 6

TYPICAL FLUTTER BOUNDARY AND ITS ACCOMPANYING "REGION OF INTEREST"

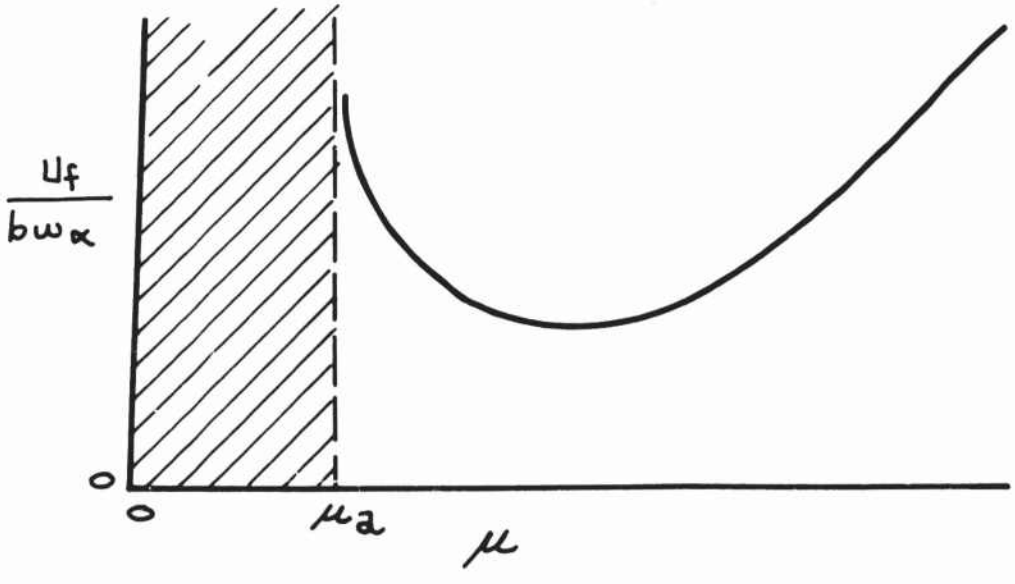


FIGURE 7

POSSIBLE FLUTTER BOUNDARIES CONFINED TO MASS-DENSITY RATIOS LESS THAN THE "CRITICAL" VALUE.

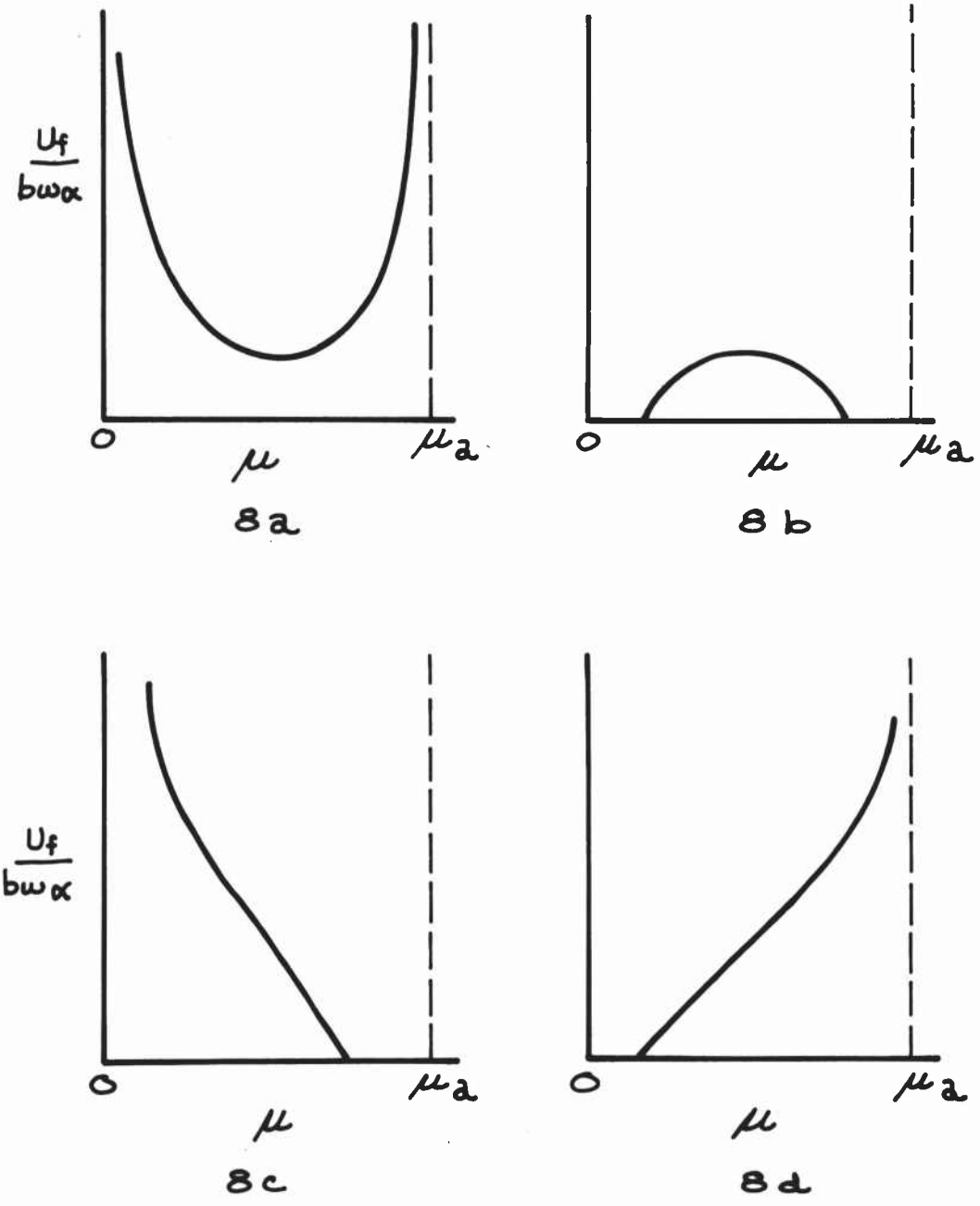


FIGURE 8

POSSIBLE "NEW" BOUNDARIES NOT ENTIRELY CONFINED TO MASS-DENSITY RATIO REGION BELOW THE "CRITICAL" VALUE

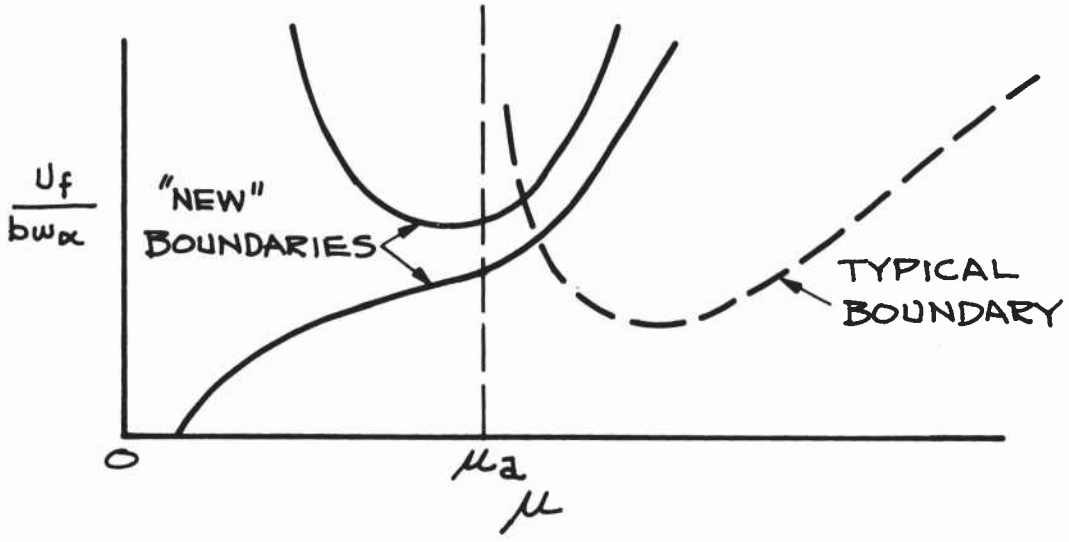


FIGURE 9

POSSIBLE DOUBLE VALUED FLUTTER BOUNDARY

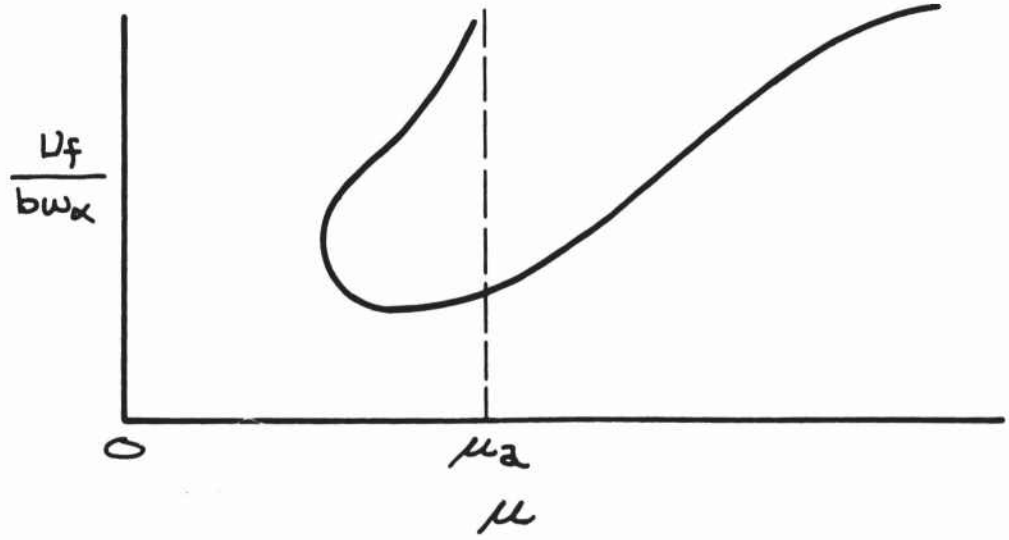


FIGURE 10

Figures 11a-11g show how the "critical" mass-density ratio varies as a function of the location of the elastic axis for various center of gravity positions and a non-dimensional radius of gyration squared of .25.

$\mu_a$ vs. $a$ FOR VARIOUS $\pi^2$

$X_m = 1.0$

$r_c^2 = .25$

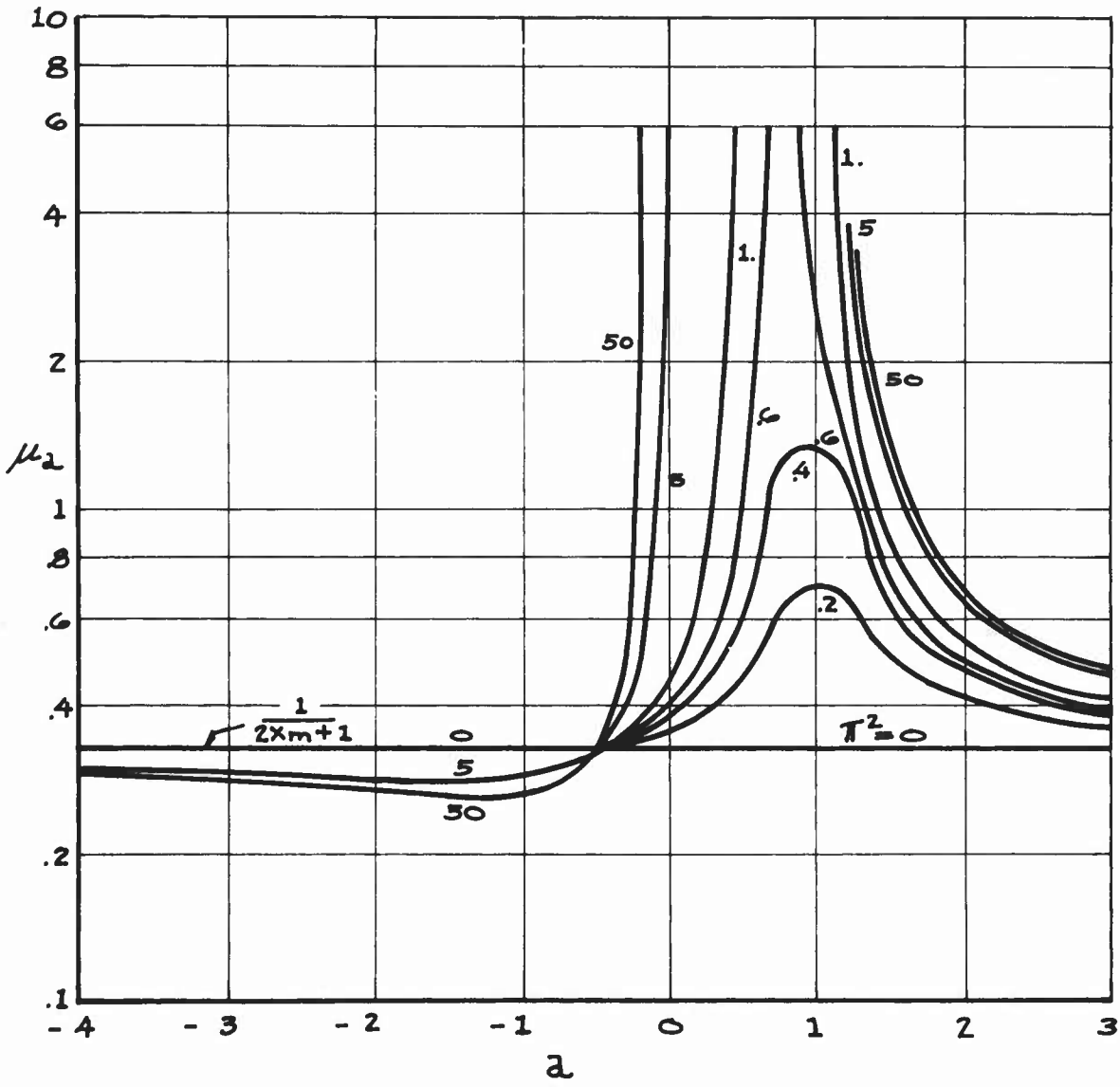


FIGURE 11a

$\mu_d$ vs. d FOR VARIOUS $\pi^2$

$X_m = .75$

$r_c^2 = .25$

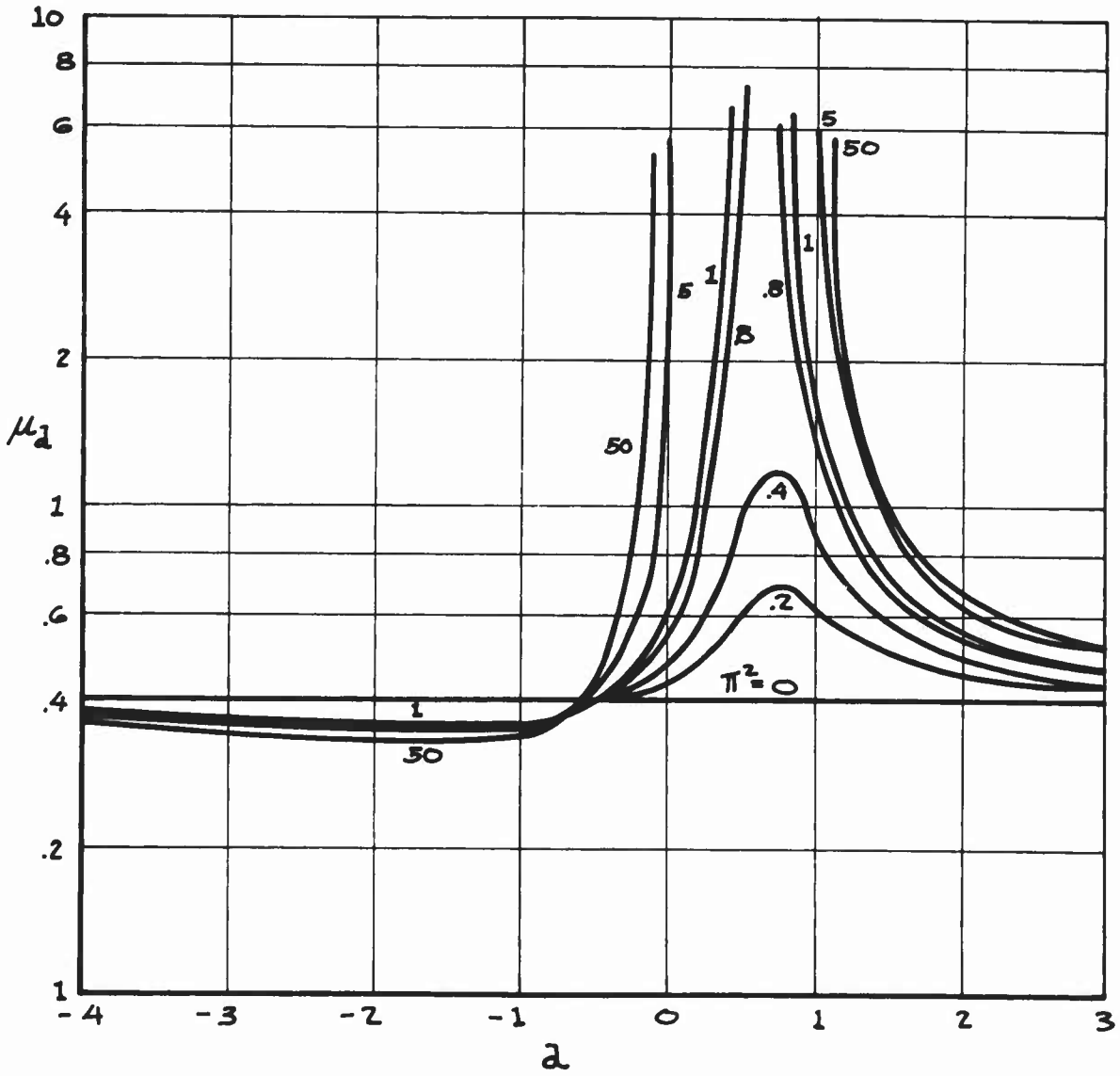


FIGURE 11b

$\mu_a$ vs. $a$ FOR VARIOUS $\pi^2$

$X_m = .50$

$r_c^2 = .25$

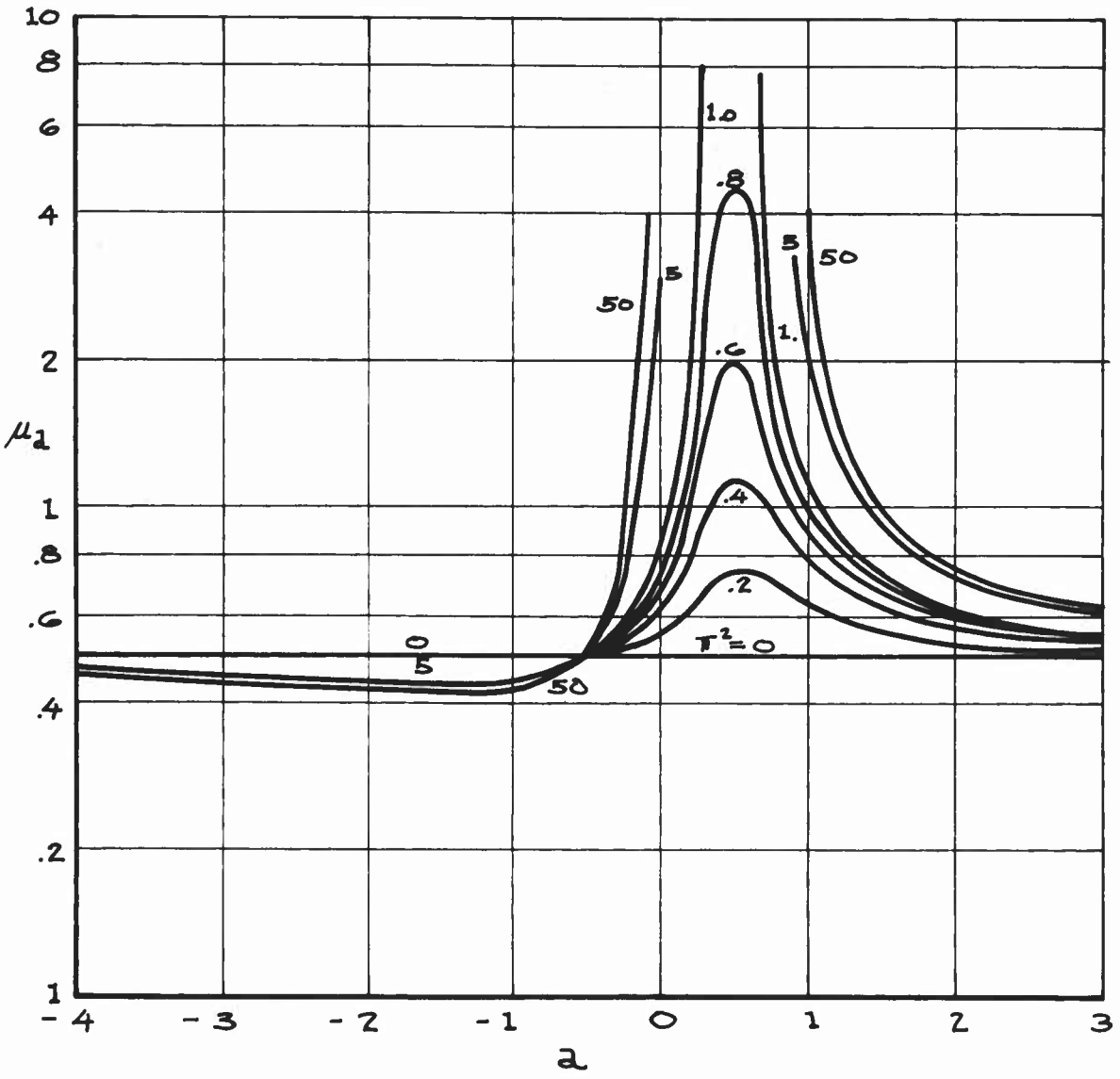


FIGURE 11c

$\mu_2$ vs. $a$ FOR VARIOUS $\pi^2$

$X_m = .25$

$r_c^2 = .25$

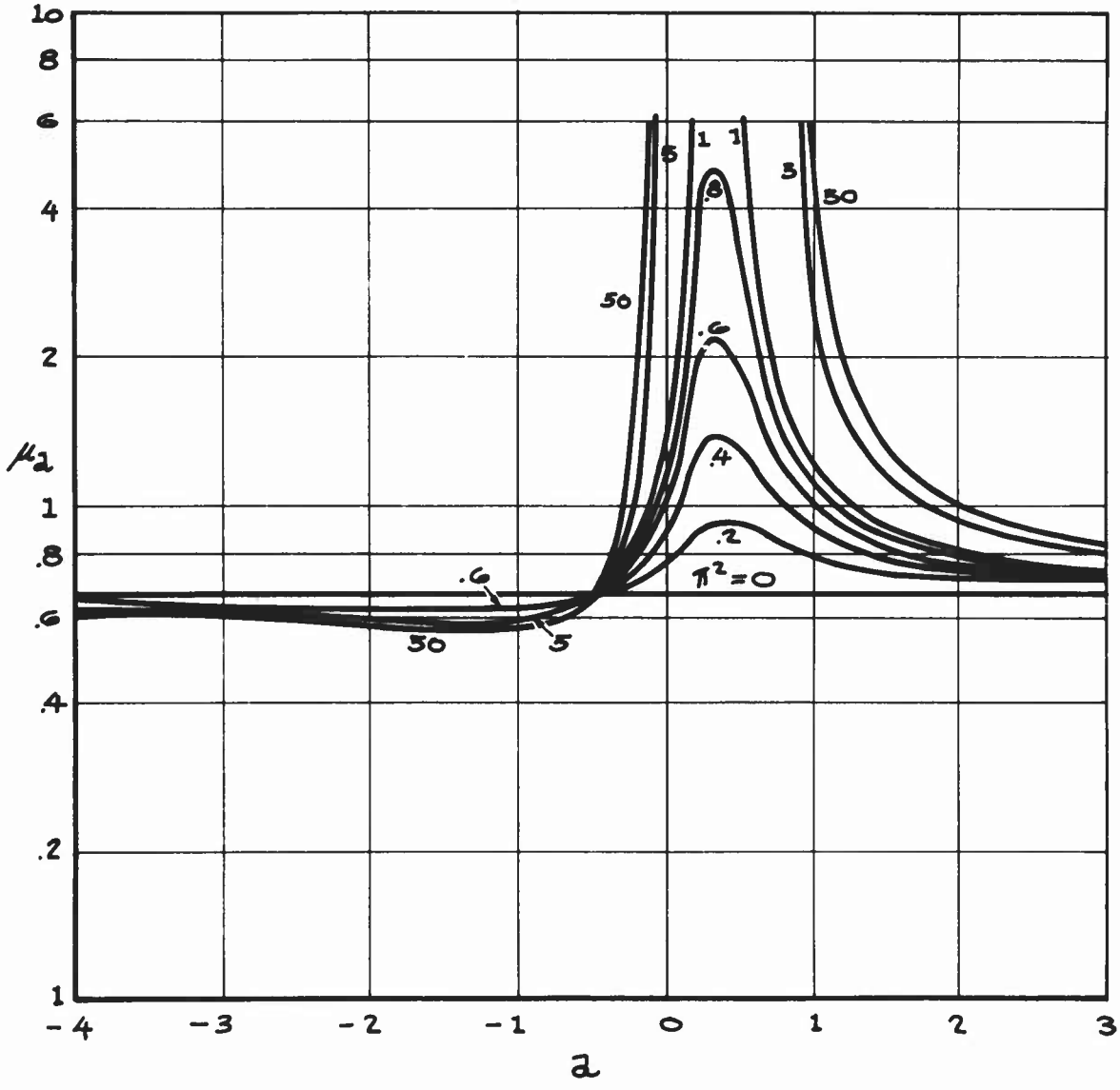


FIGURE 11d

# $\mu_a$ vs. $a$ FOR VARIOUS $\pi^2$

$X_m = 0$
$r_c^2 = .25$

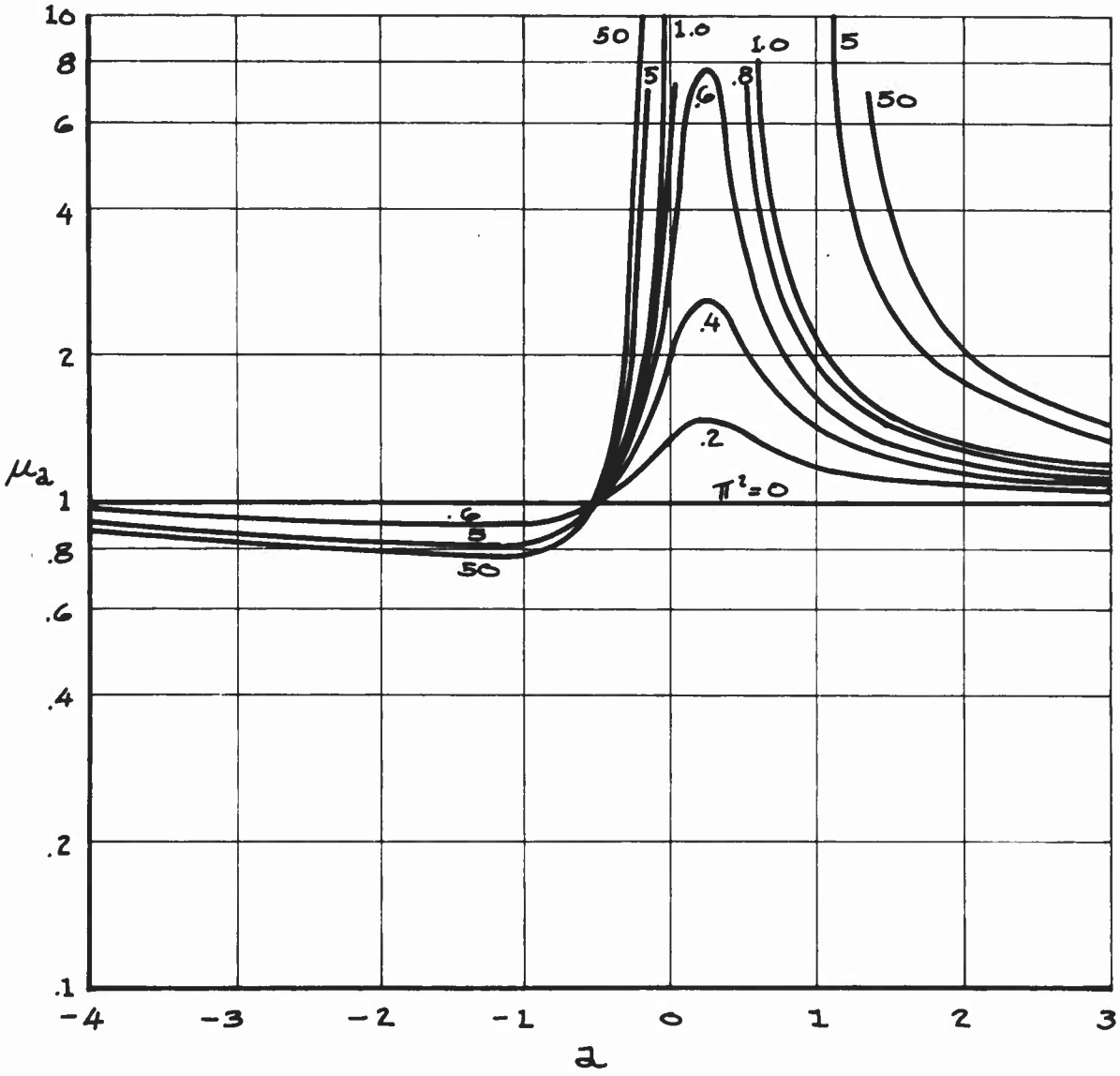


FIGURE 11e

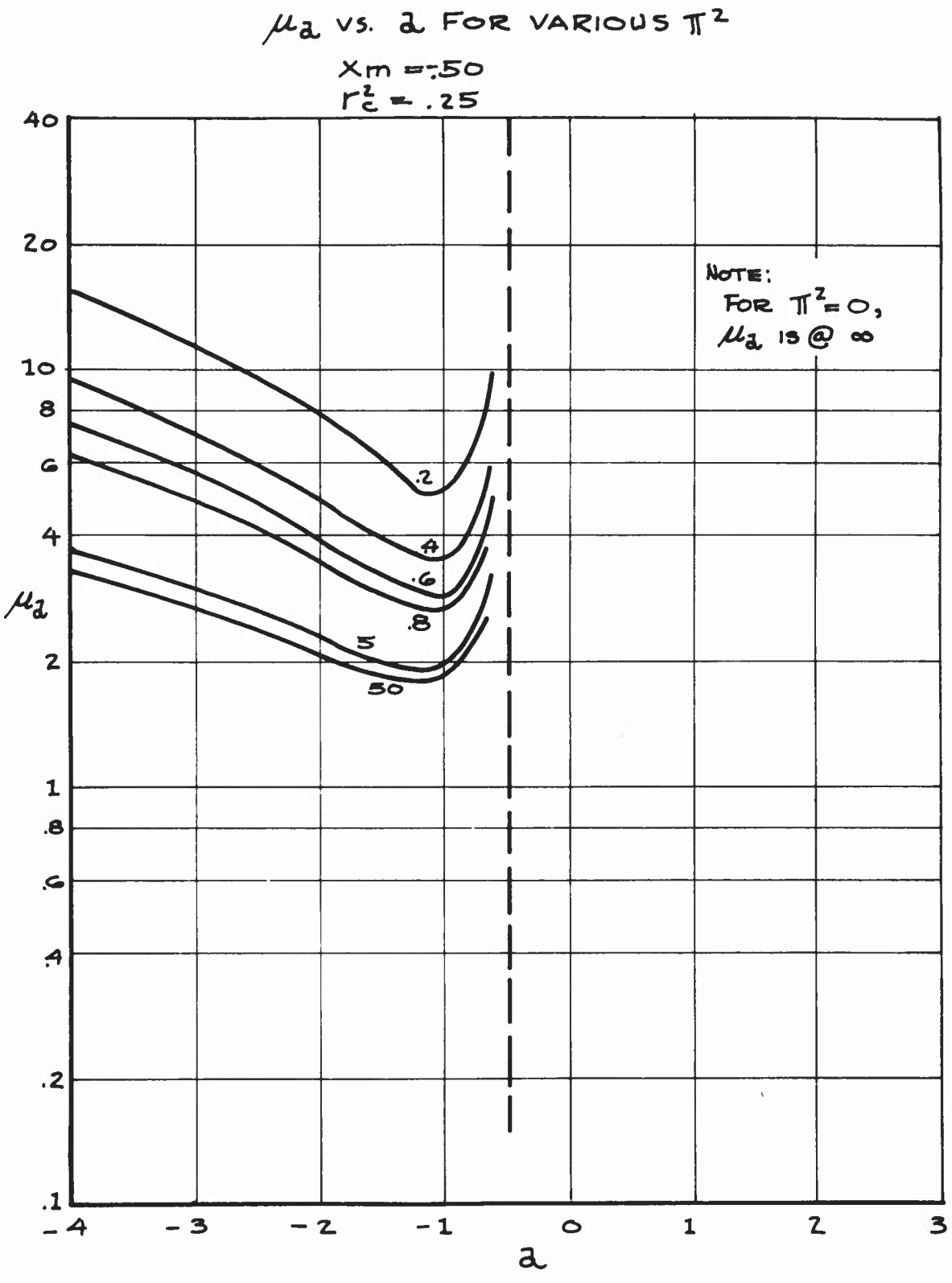
$\mu_d$ vs. $a$ FOR VARIOUS $\pi^2$
Xm = .50
$r_c^2$ = .25
NOTE:
FOR $\pi^2 = 0$,
$\mu_d$ IS @ ∞
40
20
10
8
6
4
2
1
.8
.6
.4
.2
.1
$\mu_d$
.2
.4
.6
.8
5
50
-4
-3
-2
-1
0
1
2
3
$a$

FIGURE 11 f

$\mu_a$ vs. a FOR VARIOUS $\pi^2$

$X_m = -.75$

$r_c^2 = .25$

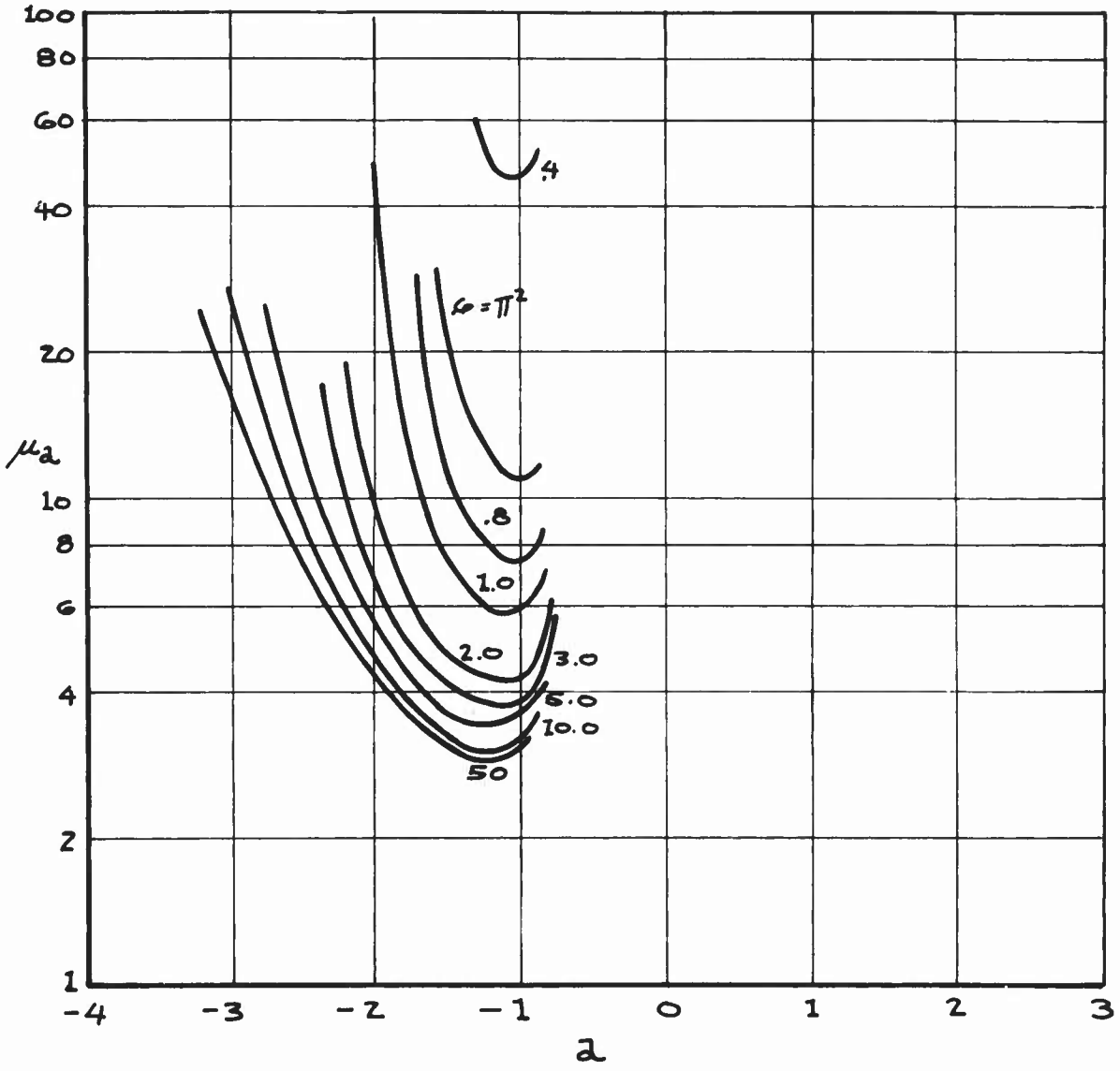


FIGURE 11g

# A COMPARISON OF $\mu_a$ VS. Xm PLOTS FOR THE FREQUENCY RATIO EXTREMES

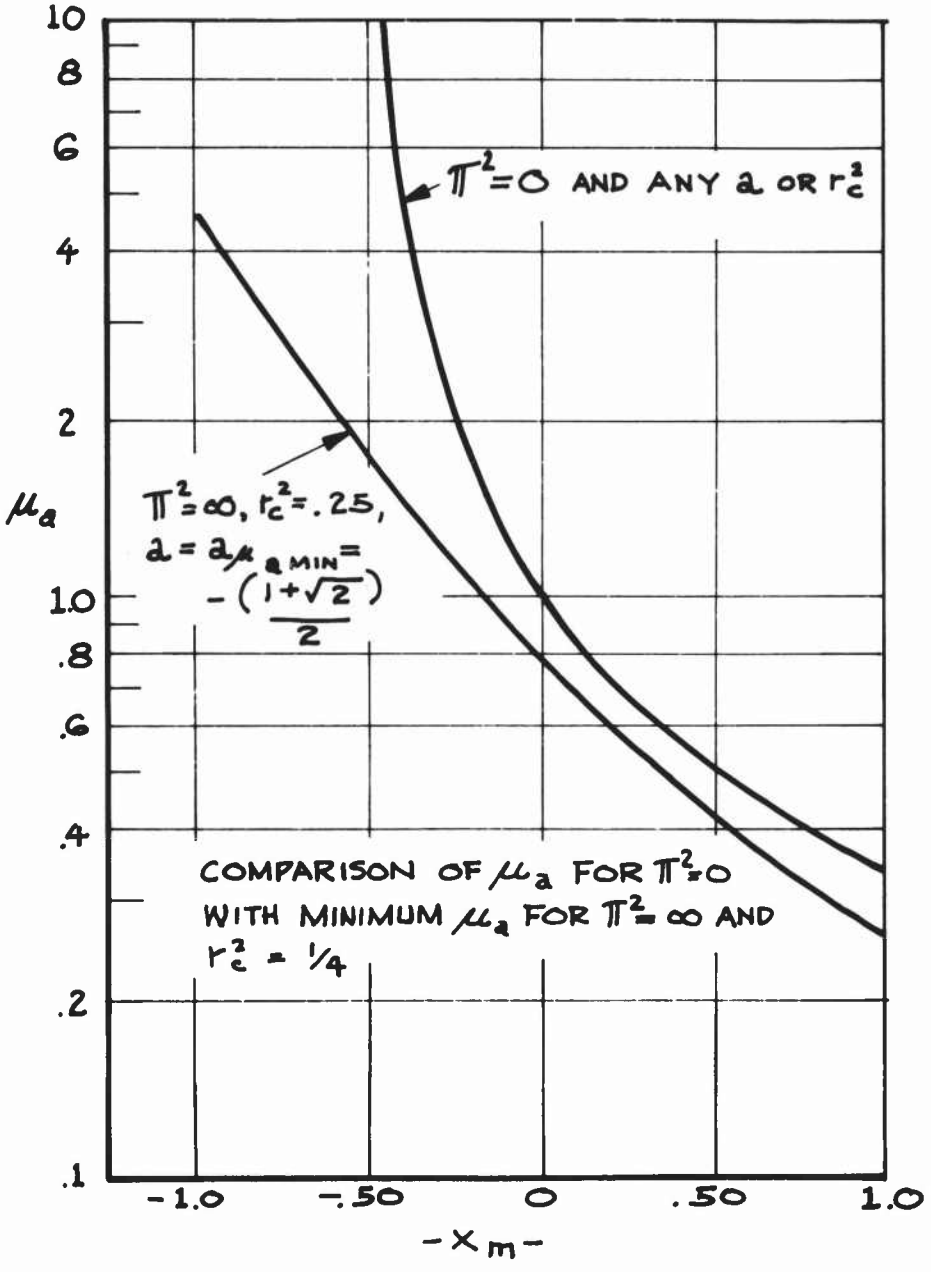


FIGURE 12

Figures 13a-13i show what combinations of the frequency ratio and the elastic axis location will yield a finite, positive value for the "critical" mass-density ratio. These plots are for various locations of the center of gravity and for a non-dimensional radius of gyration squared of .25.

A PLOT OF $\pi^2$ VS. $a$ DEPICTING A REGION OF POSITIVE $\mu_a$ SOLUTIONS

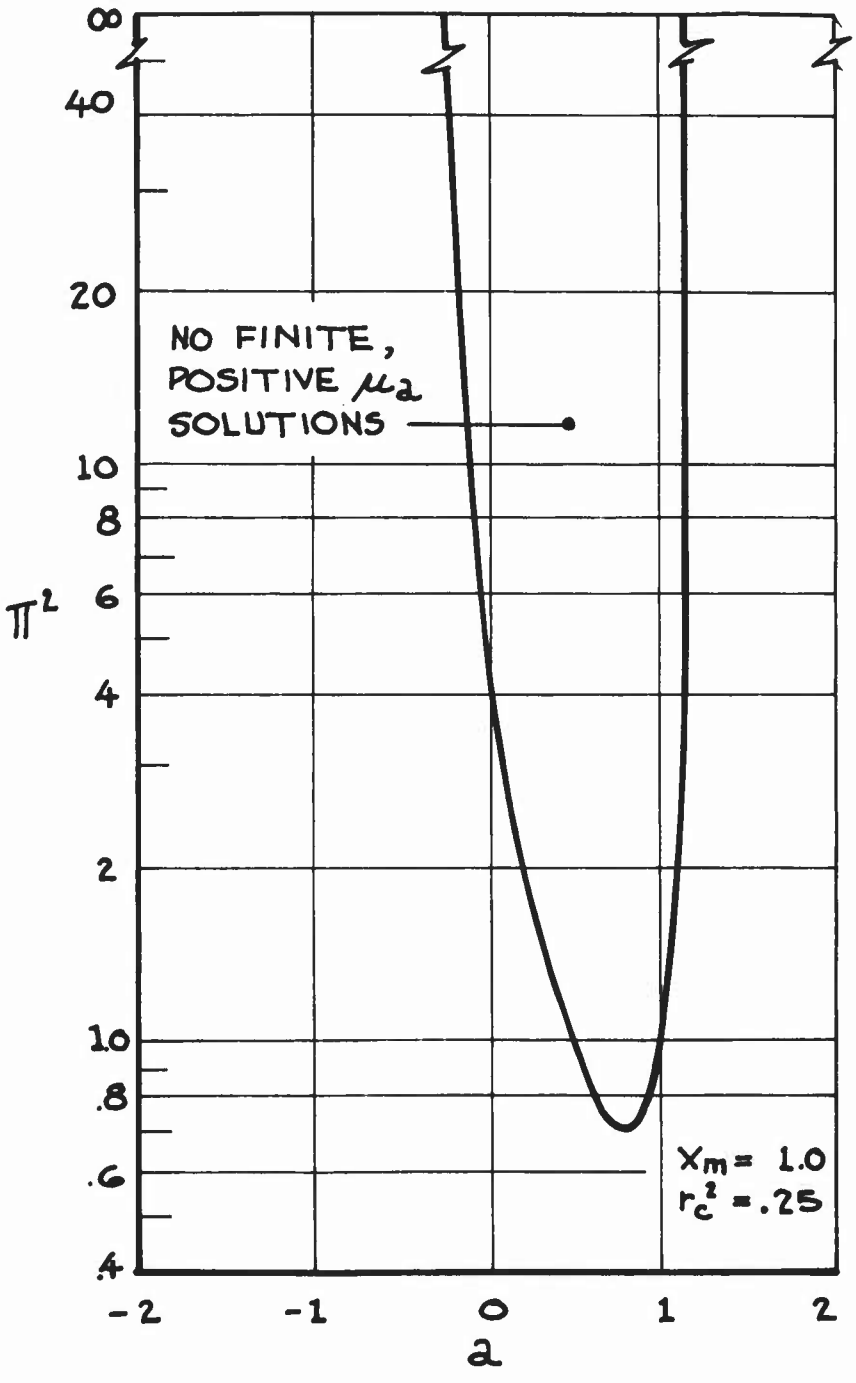


FIGURE 13a

A PLOT OF $\pi^2$ VS. a DEPICTING A REGION OF POSITIVE $\mu_a$ SOLUTIONS

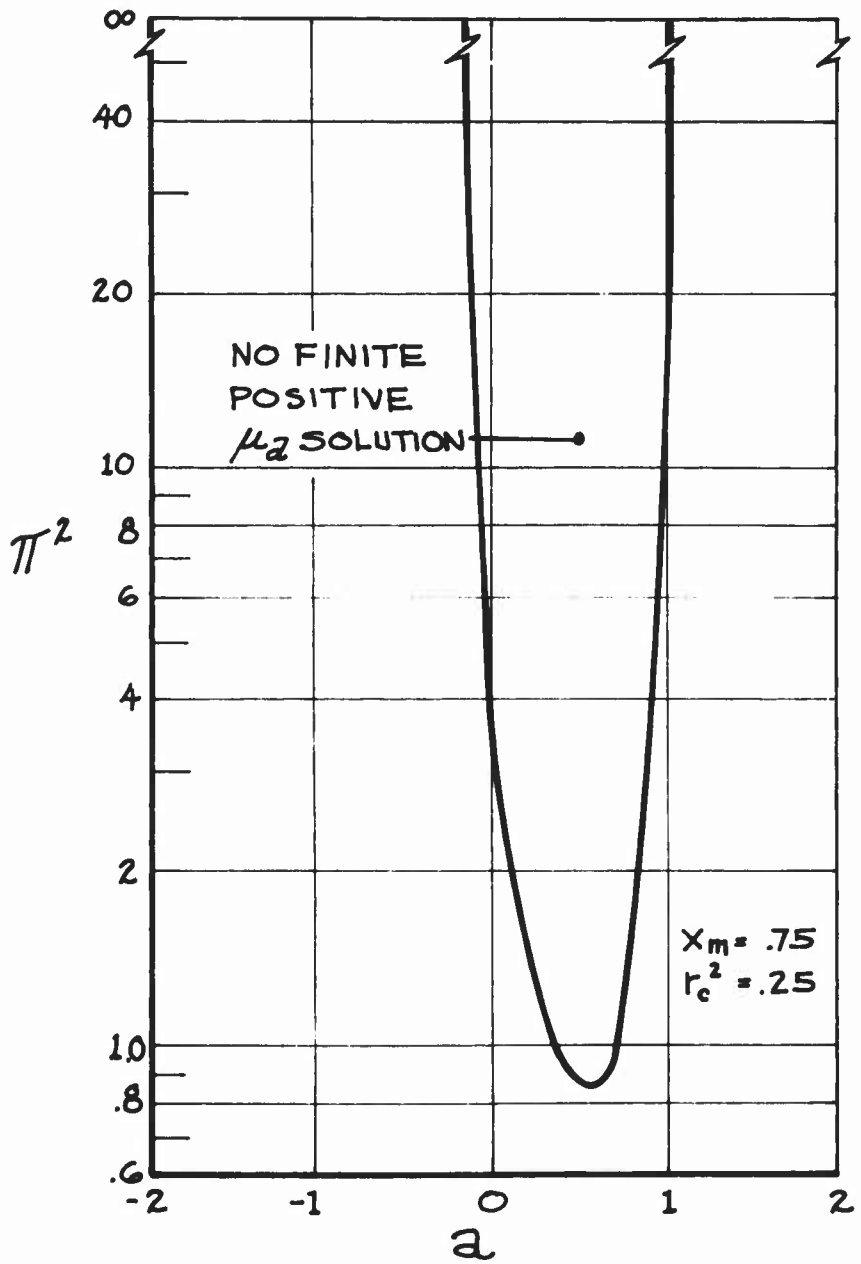


FIGURE 13b

A PLOT OF $\pi^2$ VS. $a$ DEPICTING A REGION OF POSITIVE $\mu_a$ SOLUTIONS

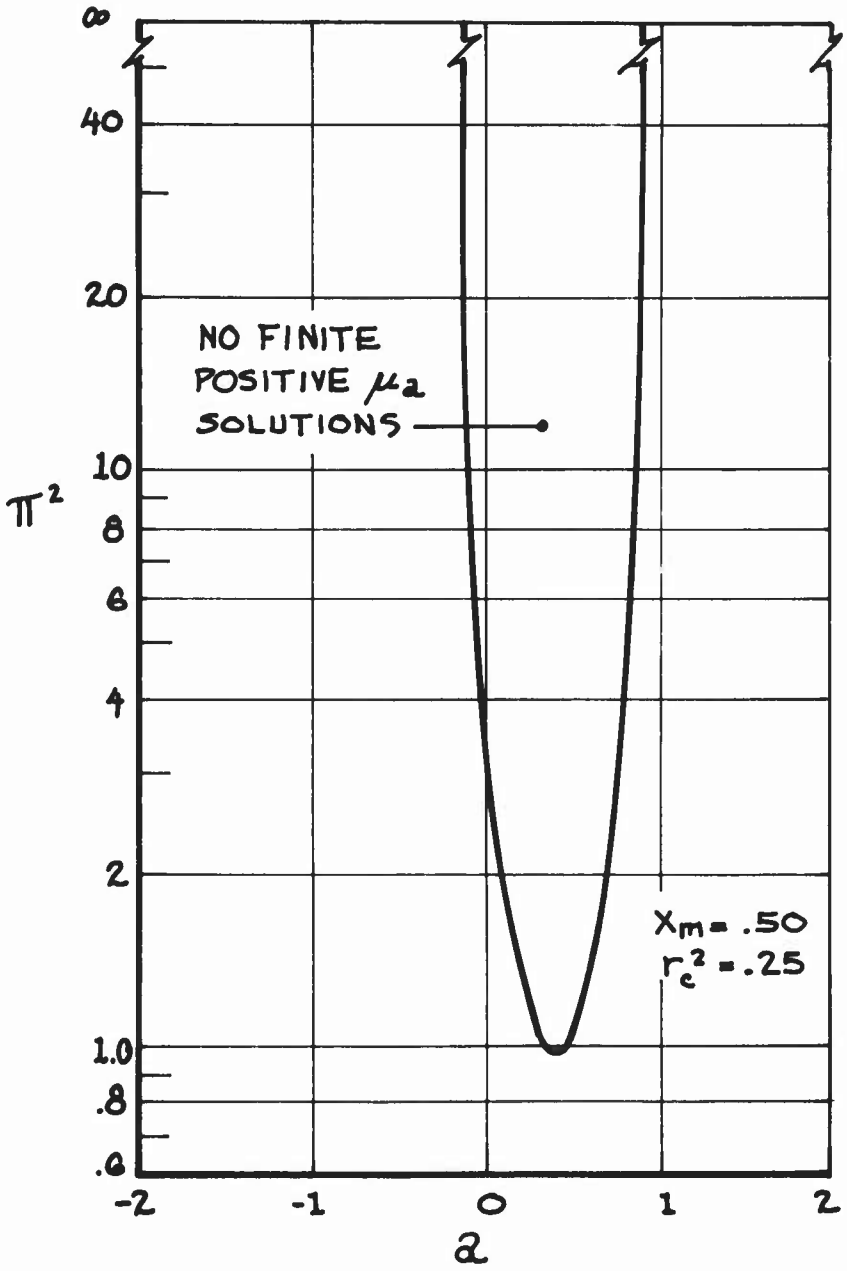


FIGURE 13C

A PLOT OF $\pi^2$ VS. $a$ DEPICTING A REGION OF POSITIVE $\mu_a$ SOLUTIONS

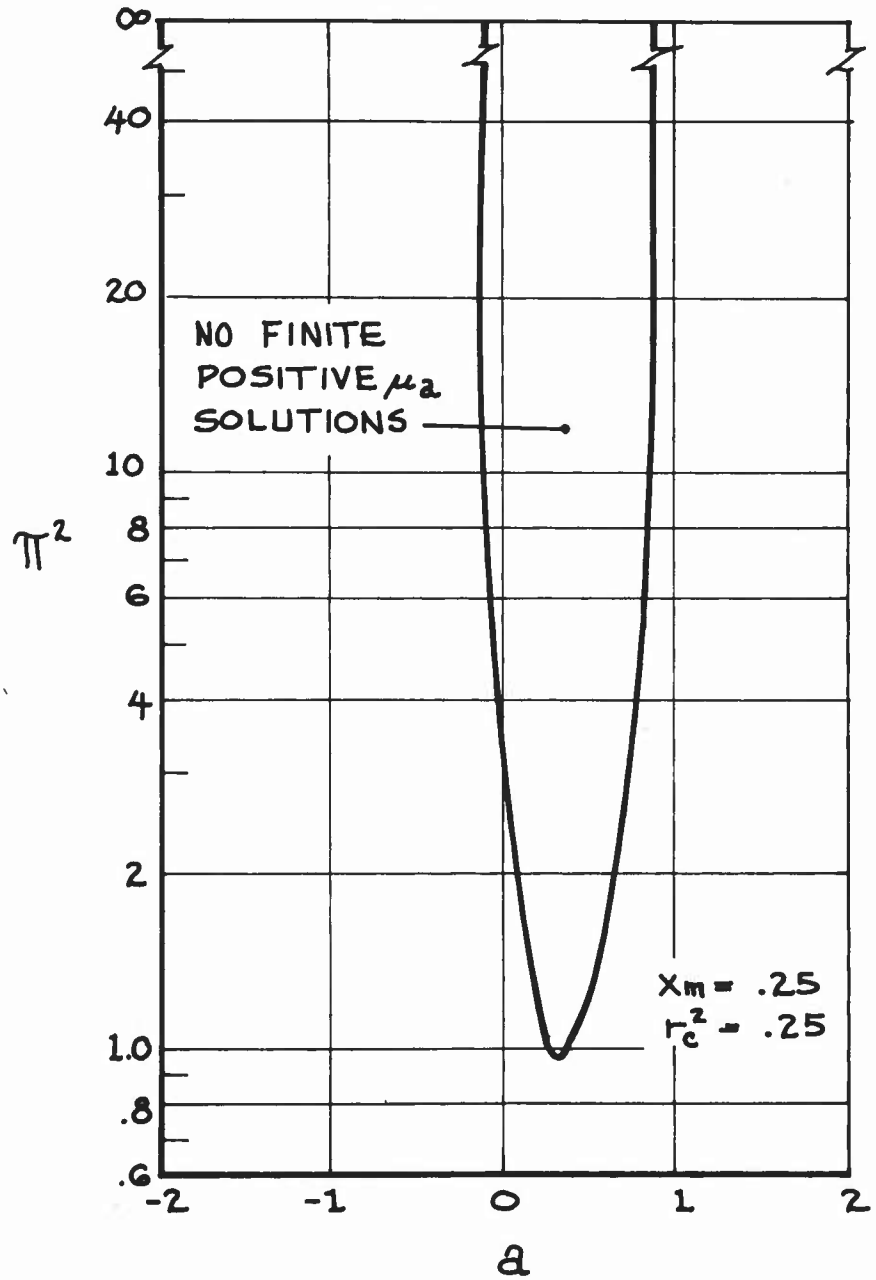


FIGURE 13d

A PLOT OF $\pi^2$ VS. $a$ DEPICTING A REGION OF POSITIVE $\mu_a$ SOLUTIONS

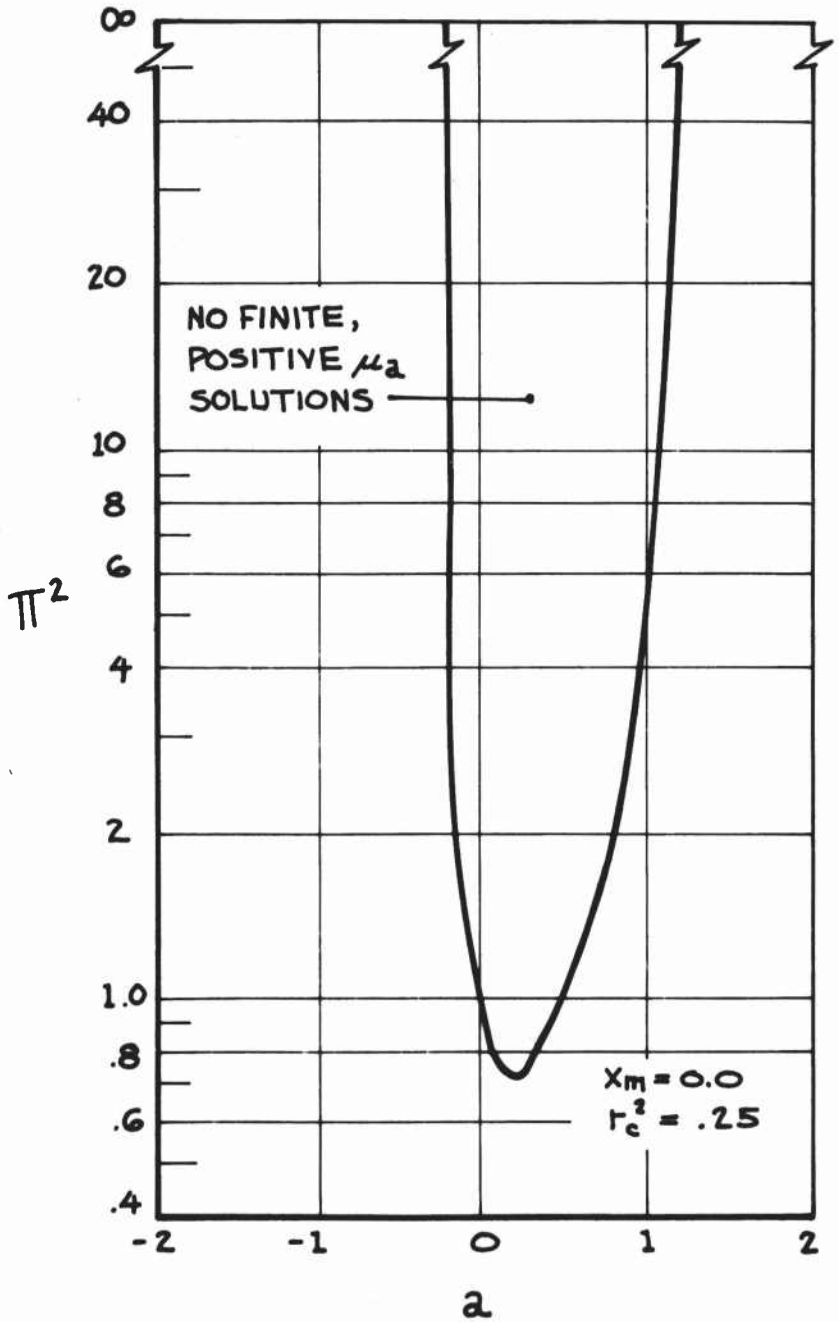


FIGURE 13e

A PLOT OF $\pi^2$ VS. $a$ DEPICTING A REGION OF POSITIVE $\mu_a$ SOLUTIONS

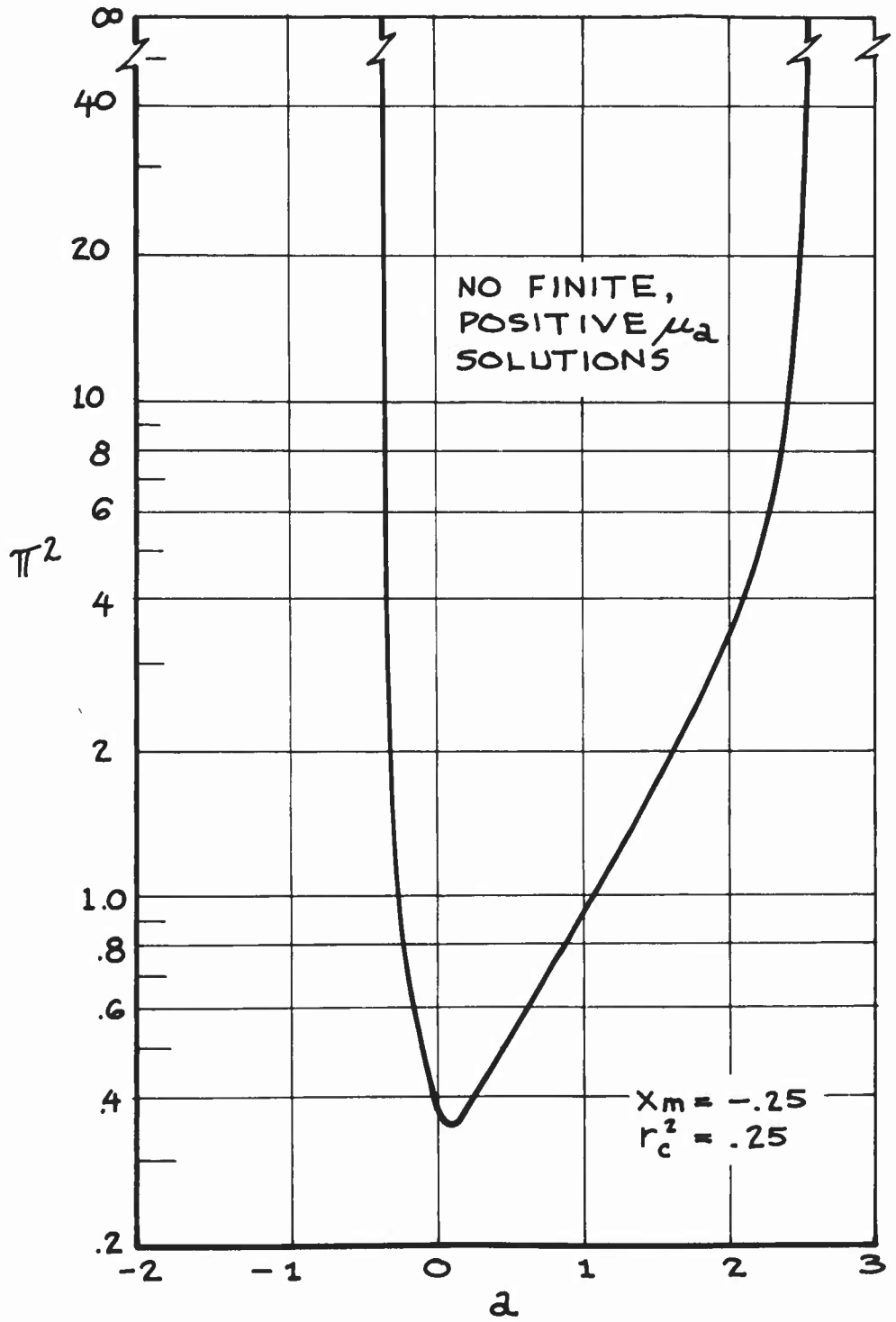


FIGURE 13f

A PLOT OF $\pi^2$ VS. $a$ DEPICTING A REGION OF POSITIVE $\mu a$ SOLUTIONS

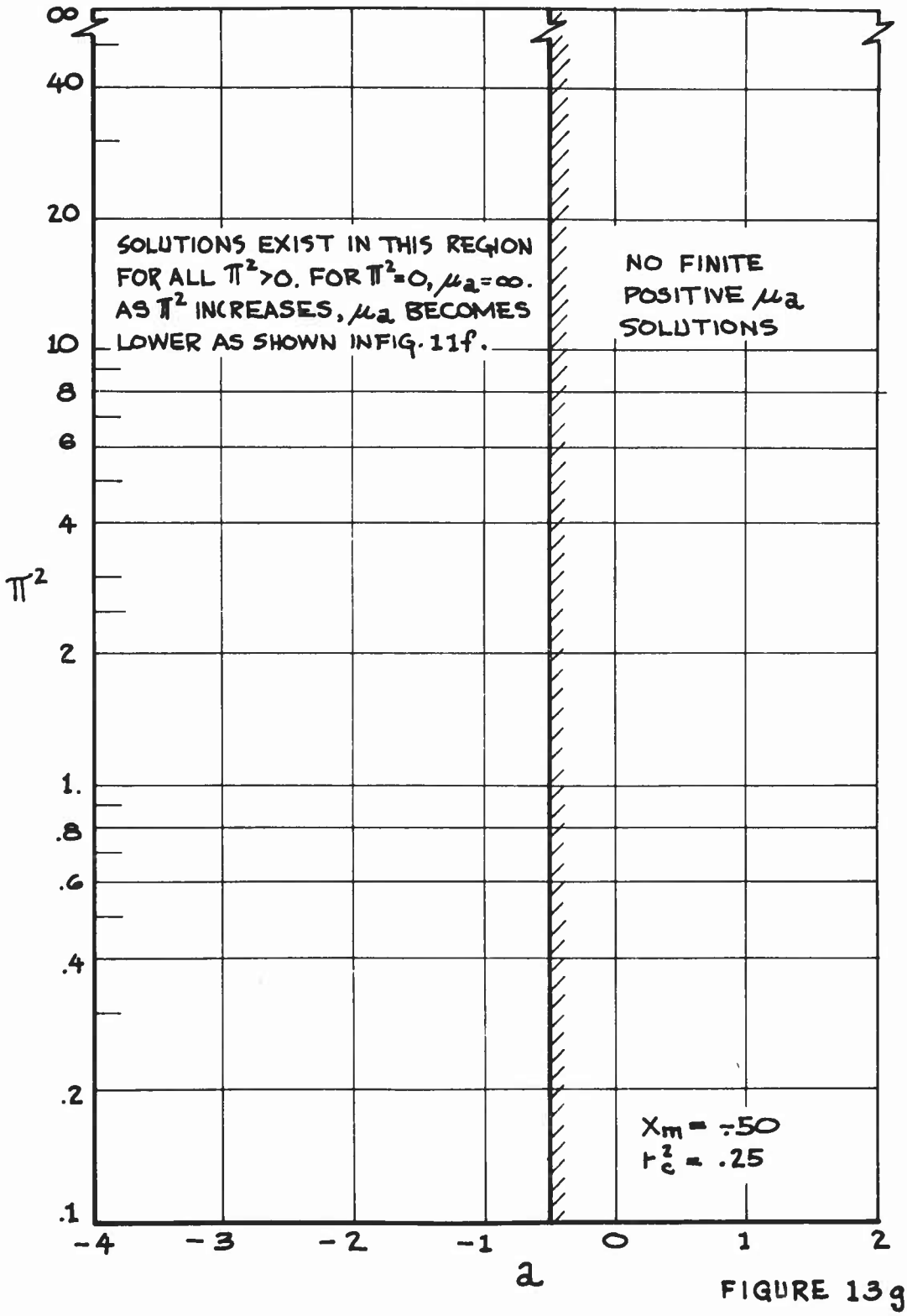


FIGURE 13g

A PLOT OF $\pi^2$ vs. $a$ DEPICTING A REGION OF POSITIVE $\mu_a$ SOLUTIONS

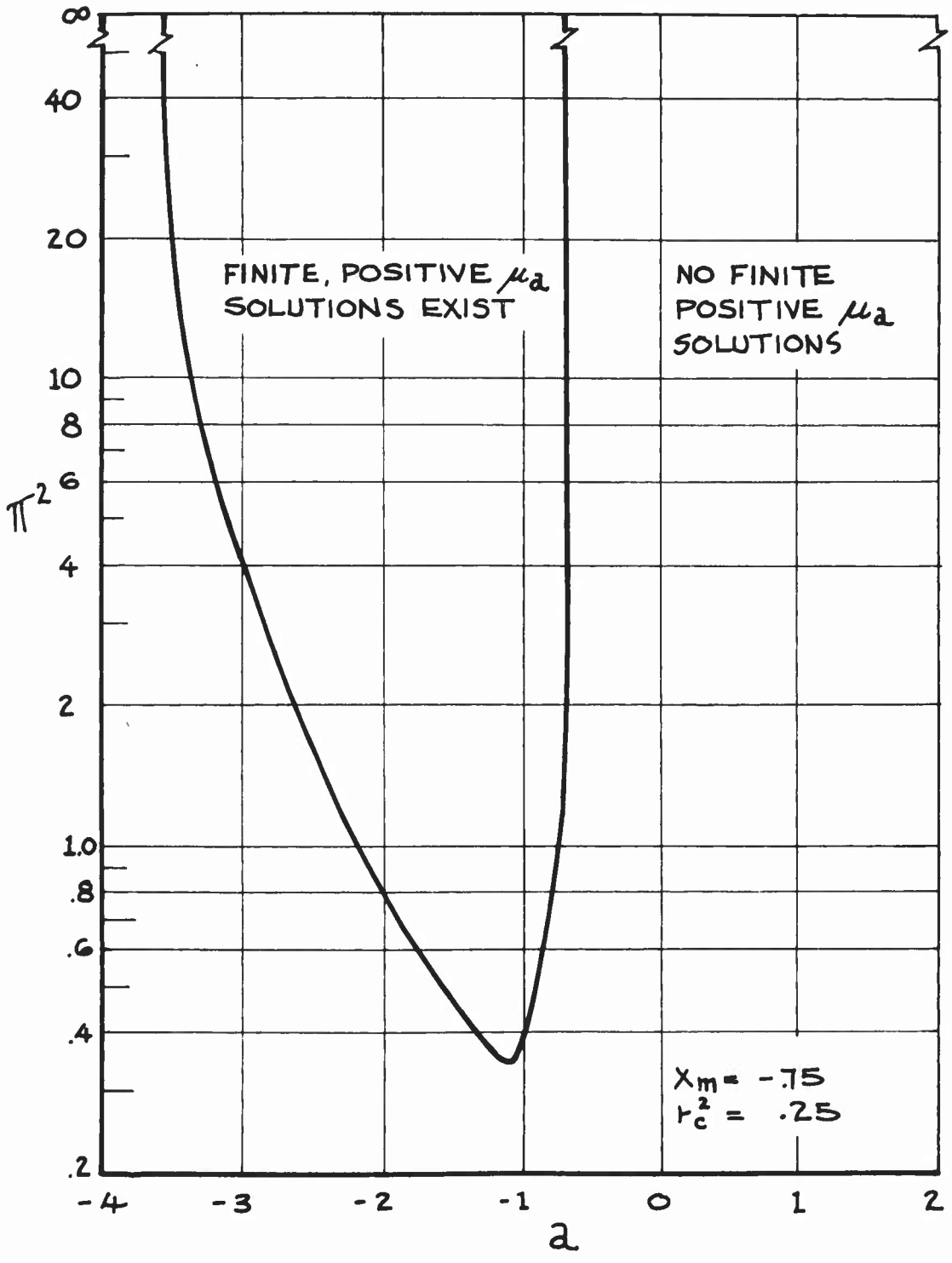


FIGURE 13h

A PLOT OF $\pi^2$ VS. $a$ DEPICTING A REGION OF POSITIVE $\mu_a$ SOLUTIONS

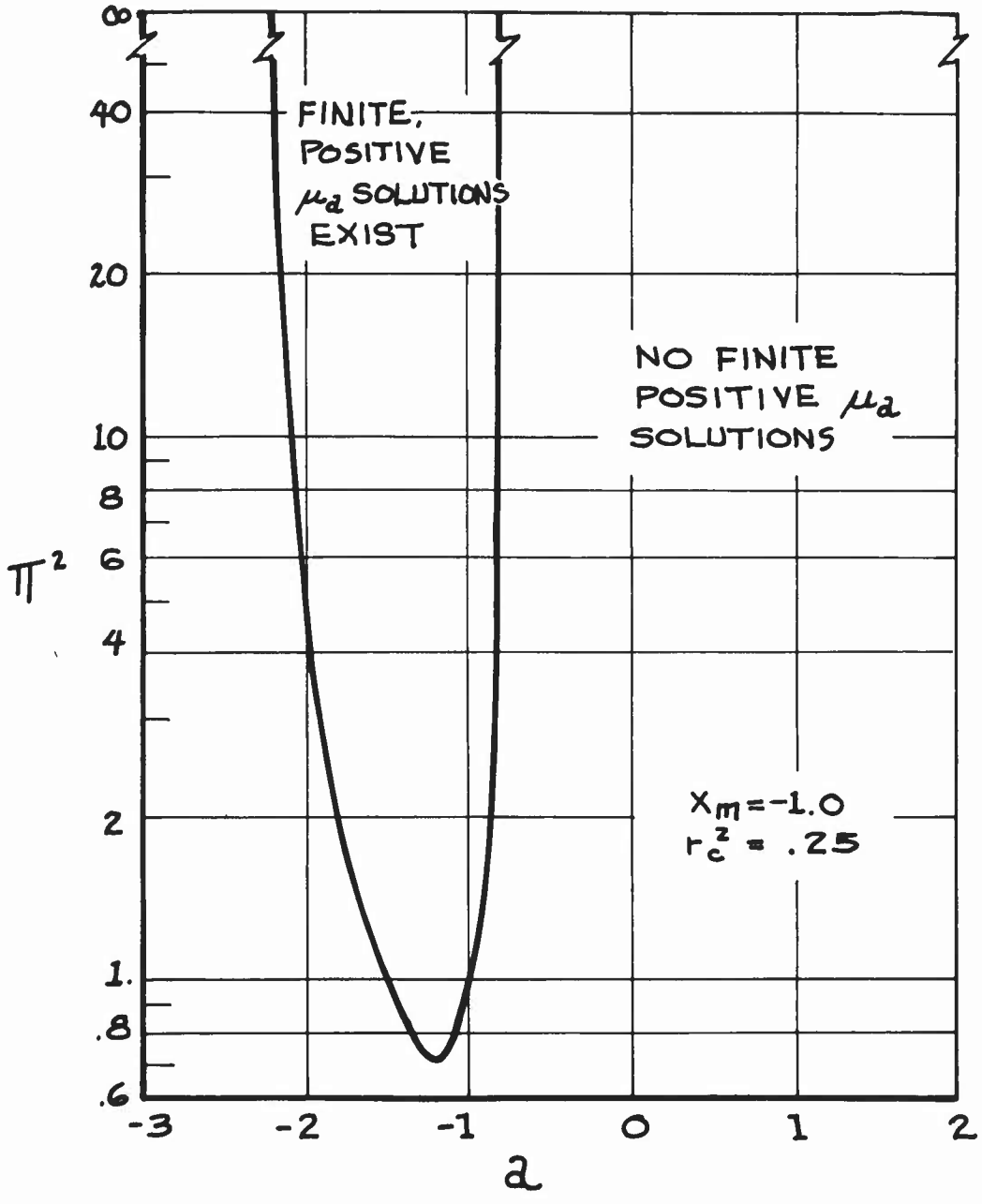


FIGURE 13i

PREDICTED REGIONS OF REAL SOLUTIONS FOR
ZERO FREQUENCY RATIO CASE
(BASED ON QUASI- STEADY THEORY)

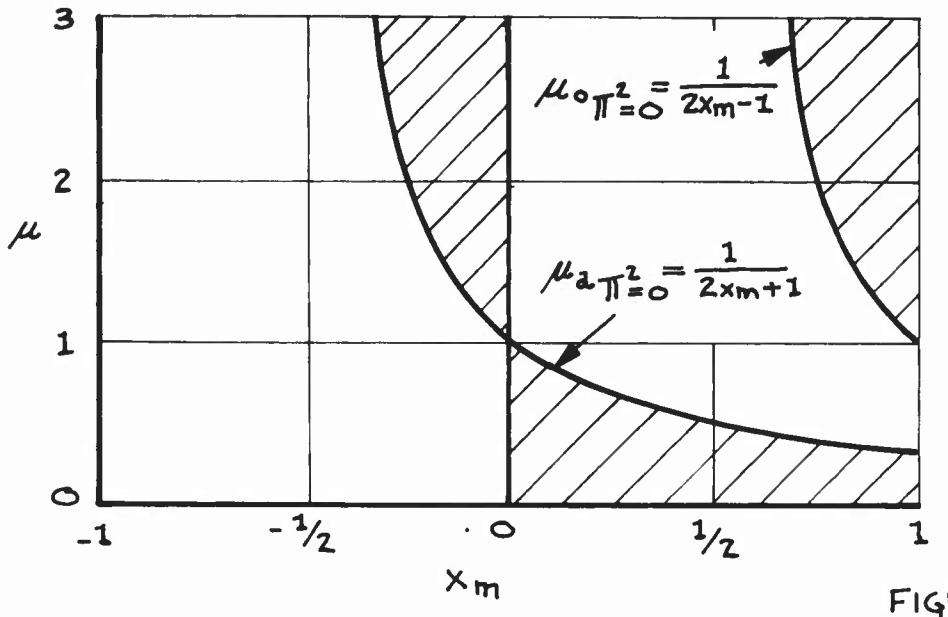


FIGURE 14

PREDICTED REGIONS OF REAL SOLUTIONS FOR
ZERO FREQUENCY RATIO CASE
(BASED ON QUASI-UNSTEADY THEORY)

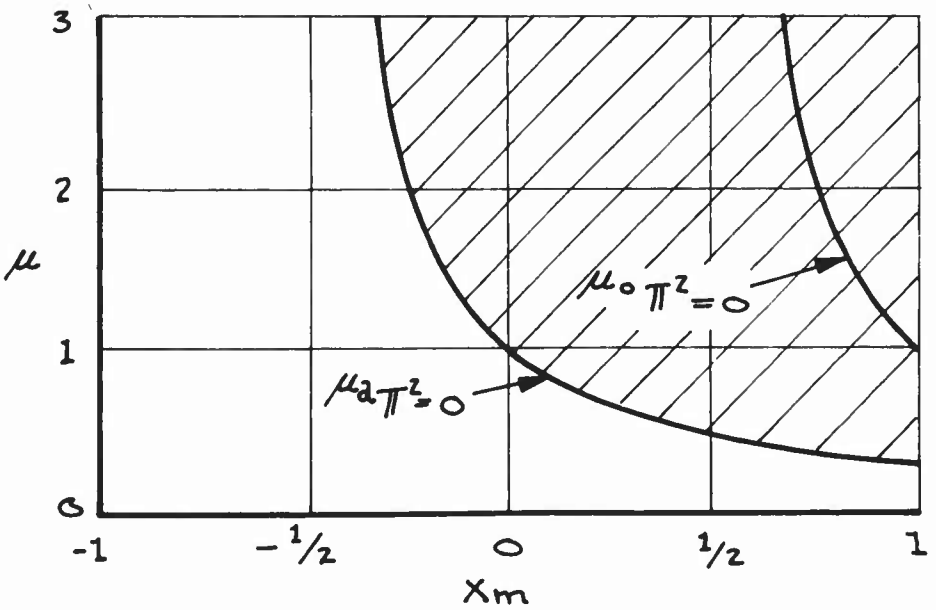


FIGURE 15

Figures 16a-16o show the quasi-steady and quasi-unsteady "critical" mass-density ratios and the quasi-unsteady "zero" mass-density ratio as a function of the location of the axis of zero static coupling. The plots are for various locations of the center of gravity and for various frequency ratios. In all cases, the non-dimensional radius of gyration about the c.g. was considered to be .50.

MASS-DENSITY RATIO VALUES VS. ELASTIC AXIS LOCATIONS

$r_c^2 = .25$

$xm = .75$

$\pi^2 = 0.0$

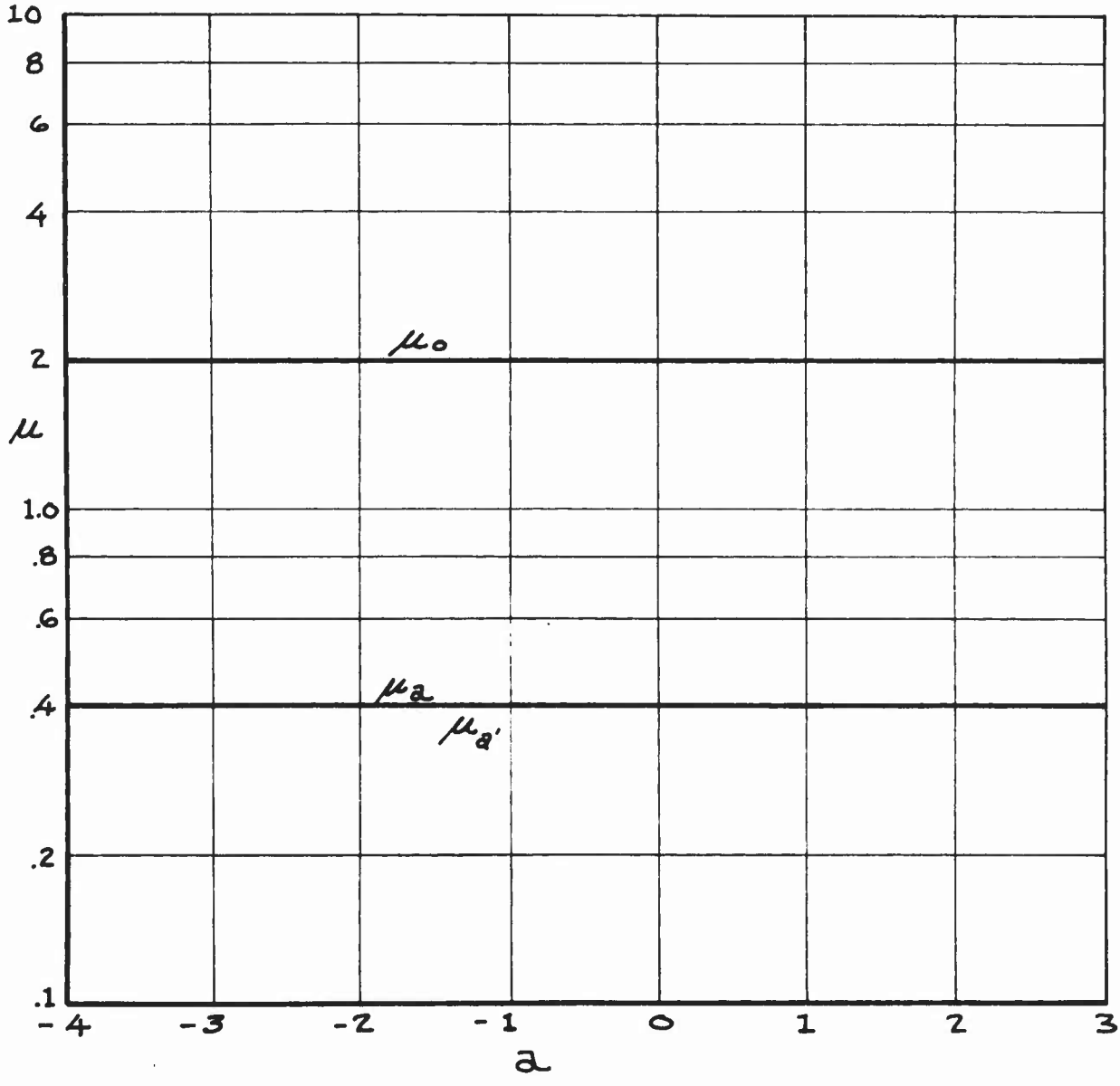


FIGURE 16A

MASS-DENSITY RATIO VALUES VS. ELASTIC AXIS LOCATIONS

$r_c^2 = .25$

$Xm = .75$

$\pi^2 = .2$

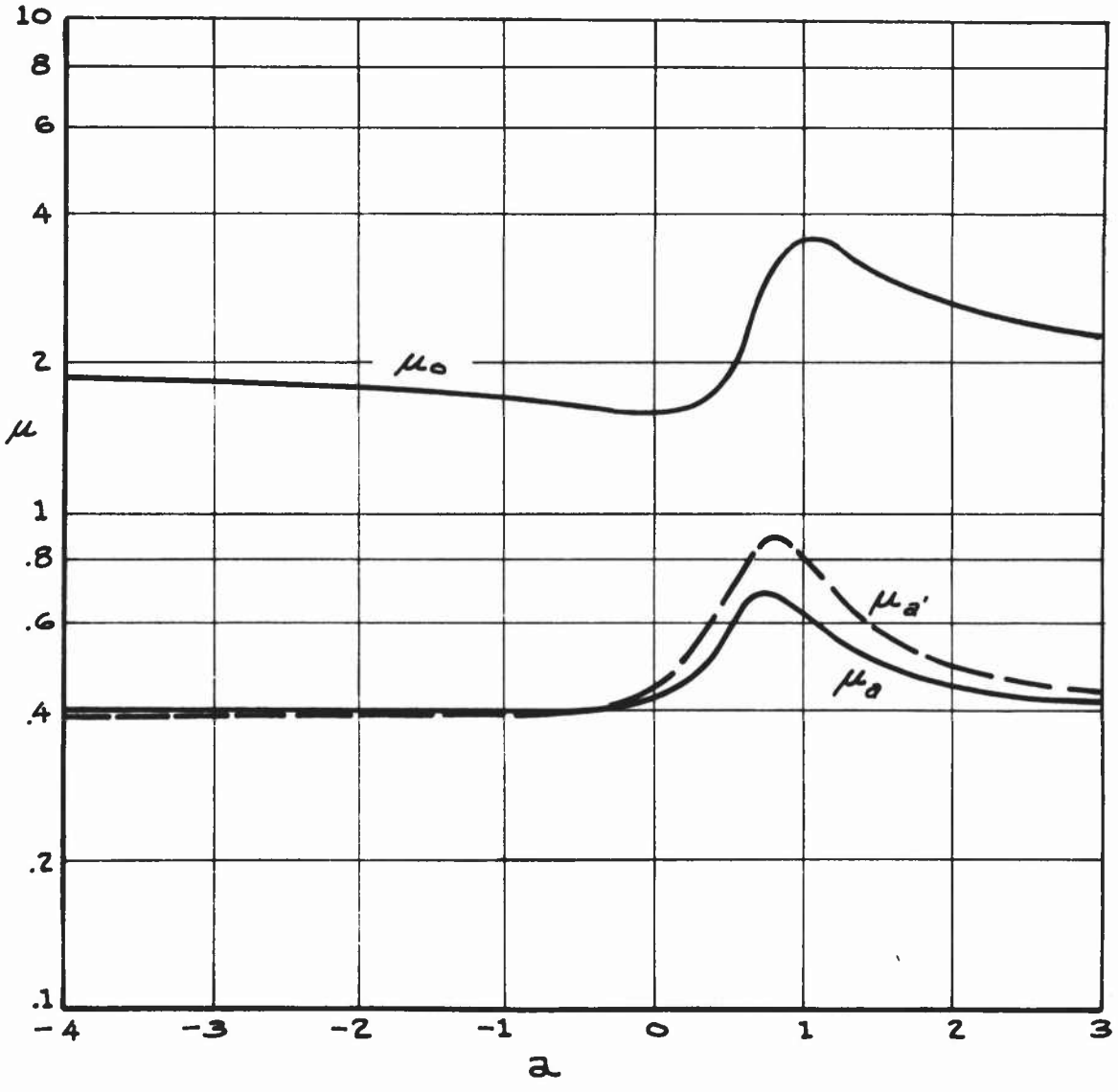


FIGURE 16b

MASS-DENSITY RATIO VALUES VS. ELASTIC AXIS LOCATIONS

$r_c^2 = .25$

$X_m = .75$

$\pi^2 = .4$

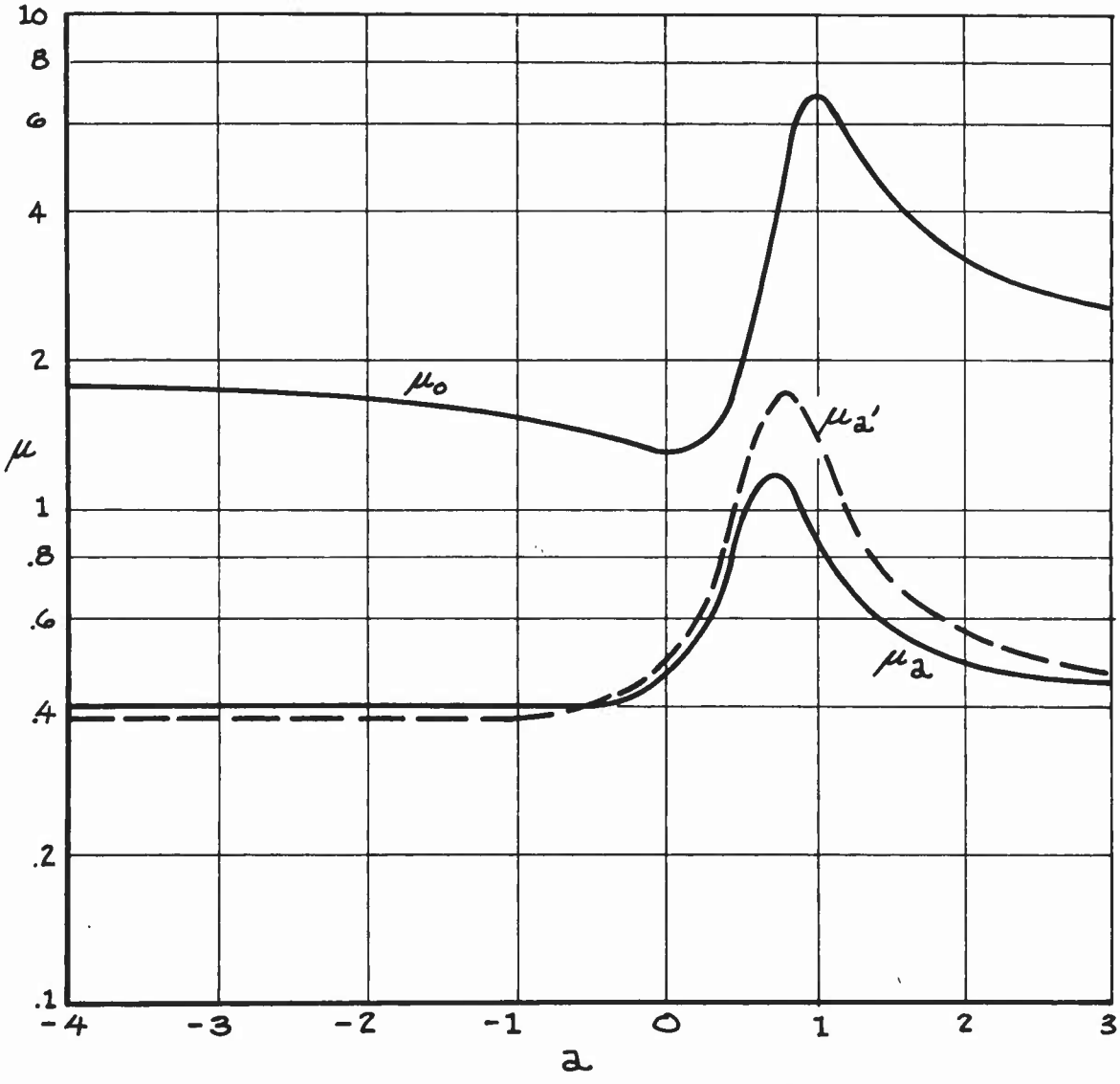


FIGURE 16c

MASS-DENSITY RATIO VALUES VS ELASTIC AXIS LOCATIONS

$r_c^2 = .25$

$x_m = .75$

$\pi^2 = 1.0$

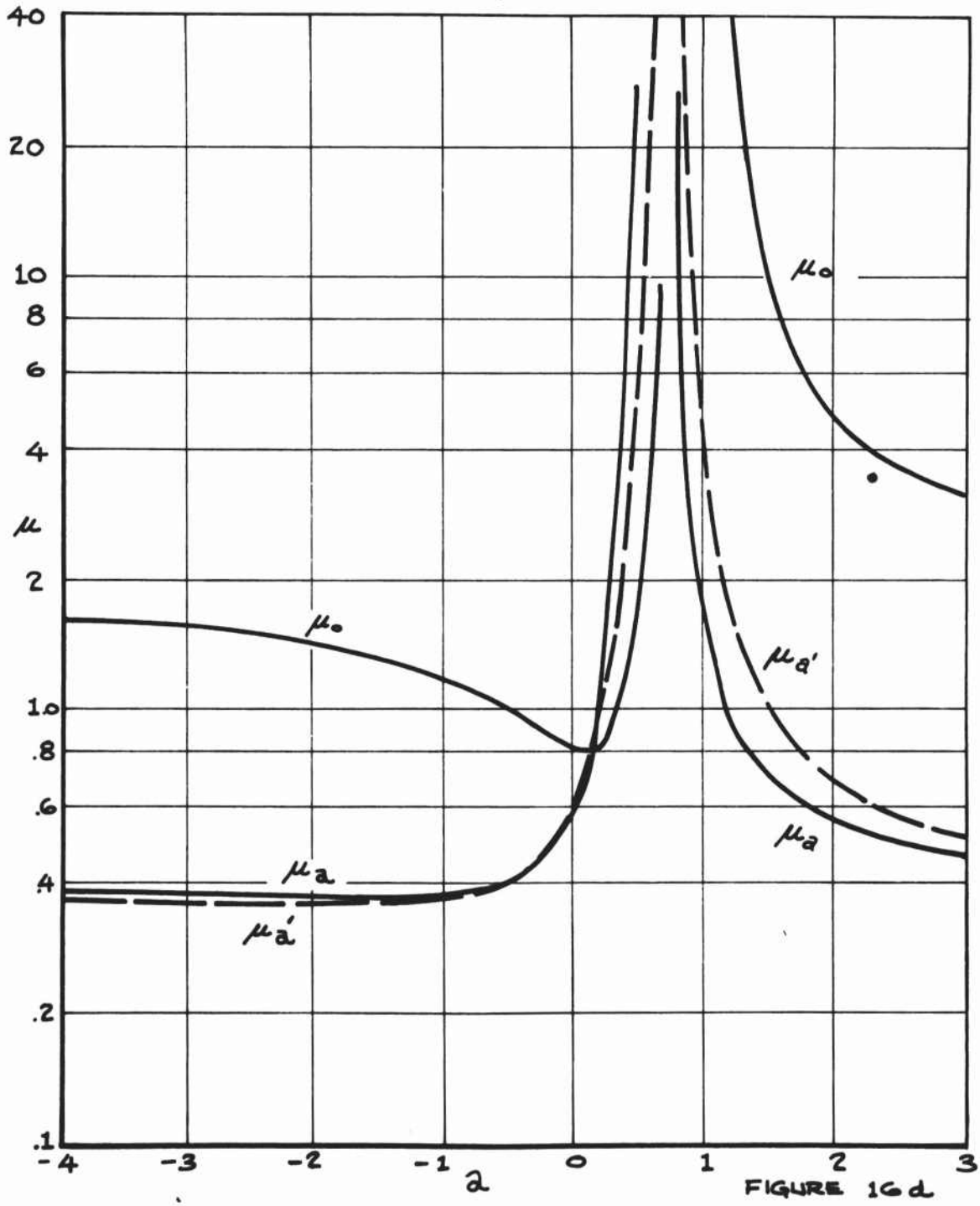


FIGURE 16 d

MASS-DENSITY RATIO VALUE VS. ELASTIC AXIS LOCATIONS $r_c^2 = .25$ $Xm = .75$ $\pi^2 = 5.0$

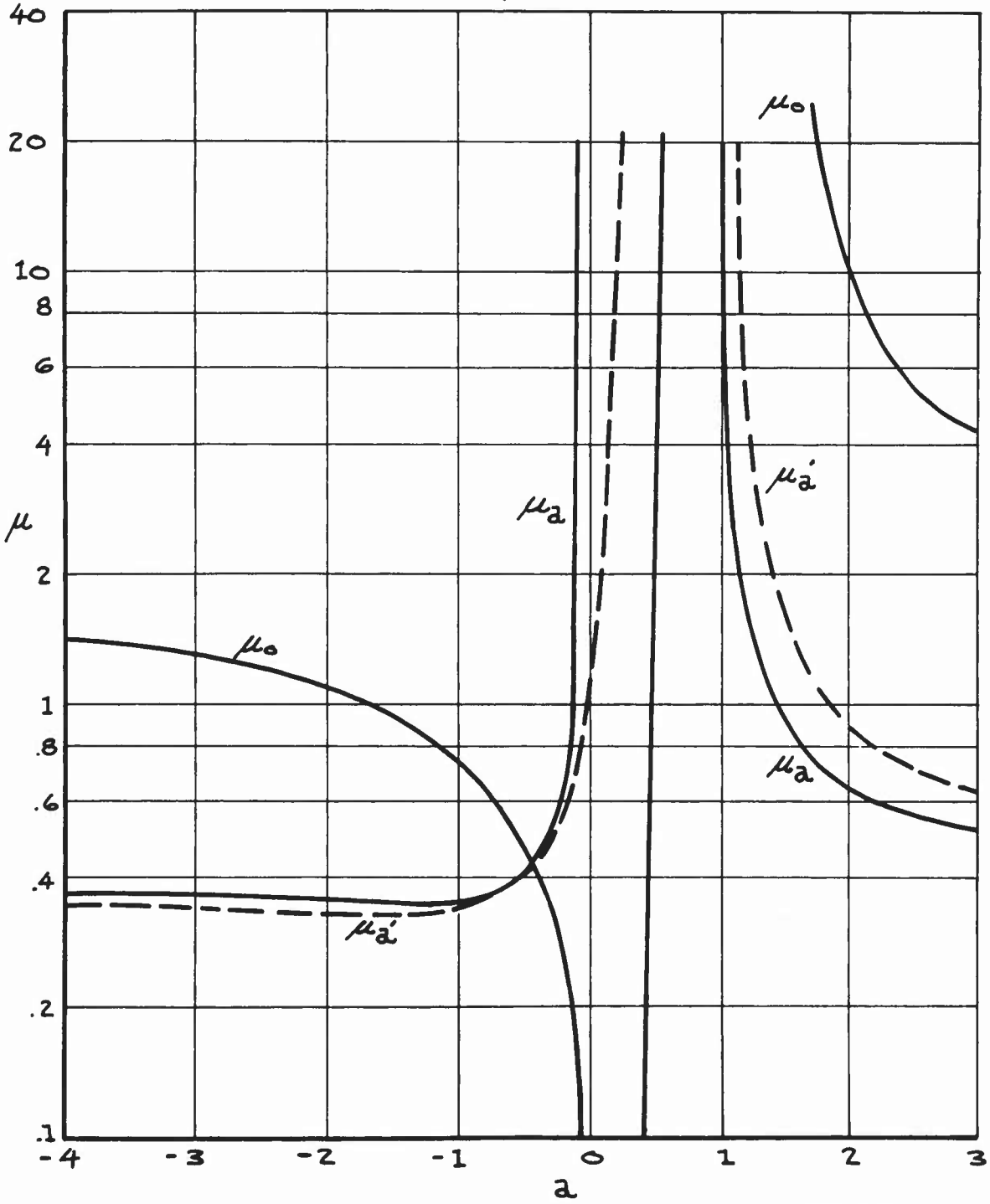


FIGURE 16e

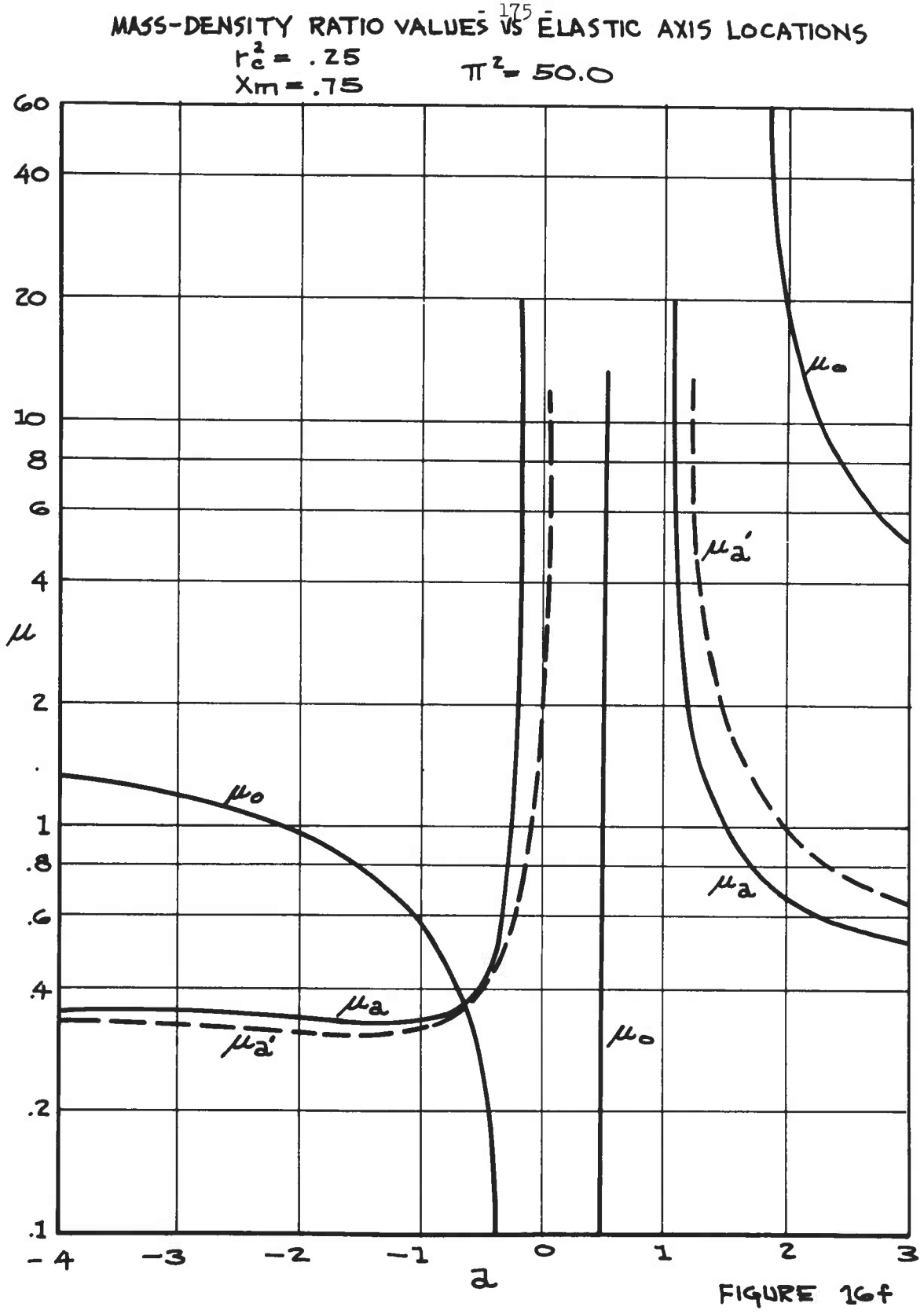
MASS-DENSITY RATIO VALUES VS ELASTIC AXIS LOCATIONS
$r_e^2 = .25$
$X_m = .75$
$\pi^2 = 50.0$
60
40
20
10
8
6
4
2
1
.8
.6
.4
.2
.1
$\mu$
$\mu_o$
$\mu_a$
$\mu_{a'}$
$\mu_o$
$\mu_{a'}$
$\mu_a$
$\mu_o$
-4
-3
-2
-1
0
1
2
3
a

FIGURE 16f

MASS-DENSITY RATIO VALUES VS. ELASTIC AXIS LOCATIONS

$r_c^2 = .25$

$x_m = .5$

$\pi^2 = 0$

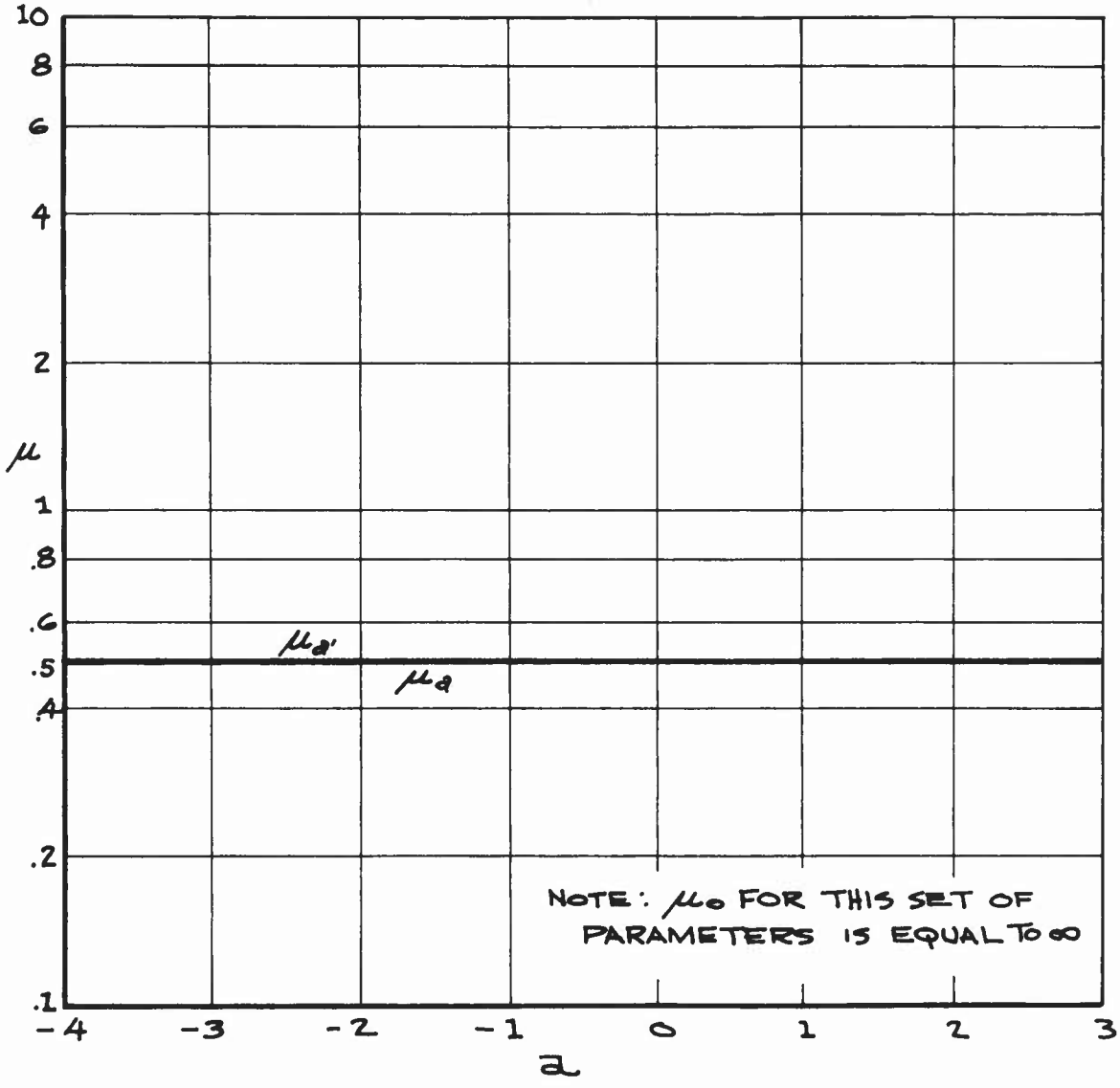


FIGURE 16g

MASS-DENSITY RATIO VALUES Vs. ELASTIC AXIS LOCATIONS $r_c^2 = .25$ $\pi^2 = .2$ $X_m = .5$

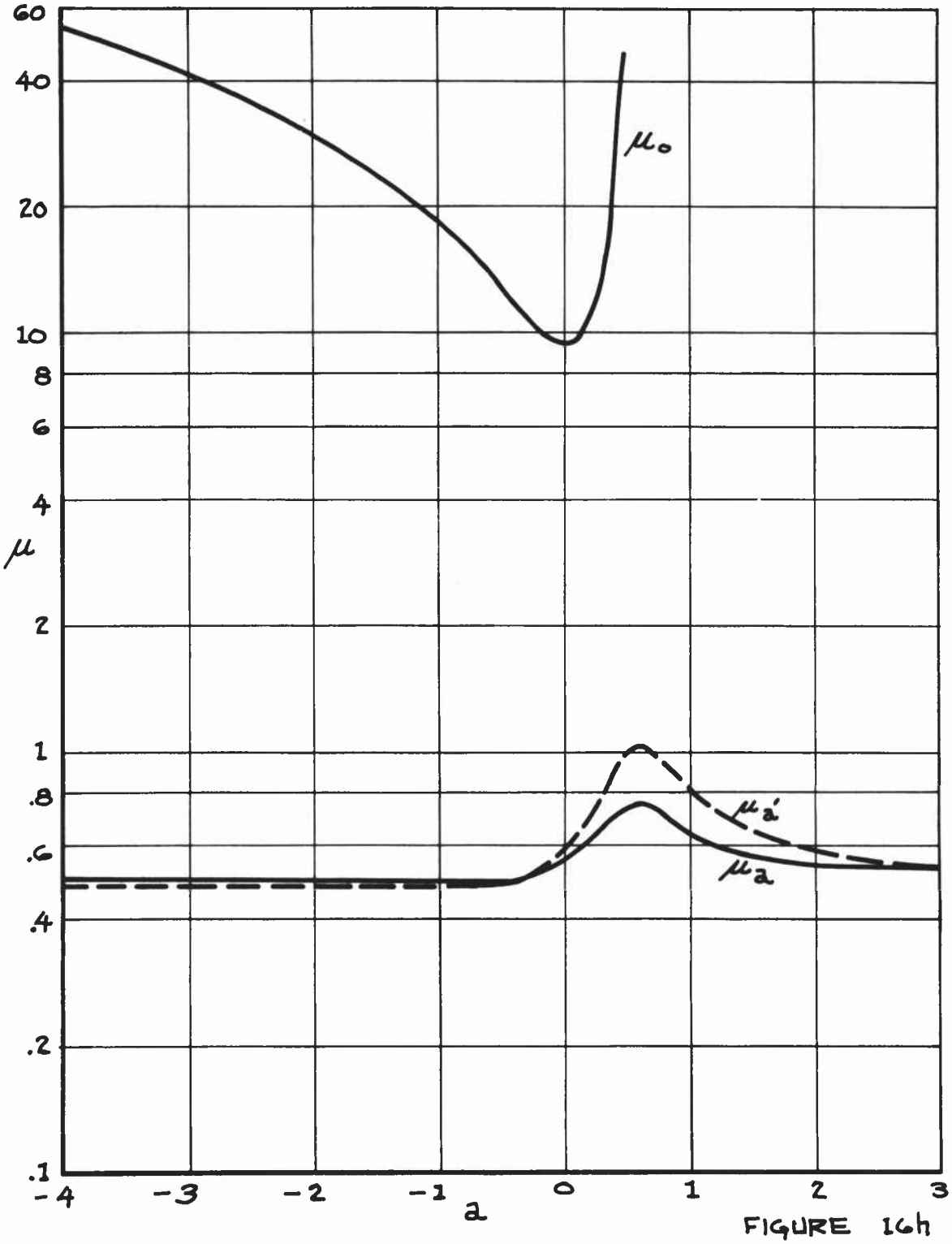


FIGURE 16h

MASS-DENSITY RATIO VALUES VS ELASTIC AXIS LOCATIONS

$r_c^2 = .25$ $\pi^2 = .4$

$X_m = .5$

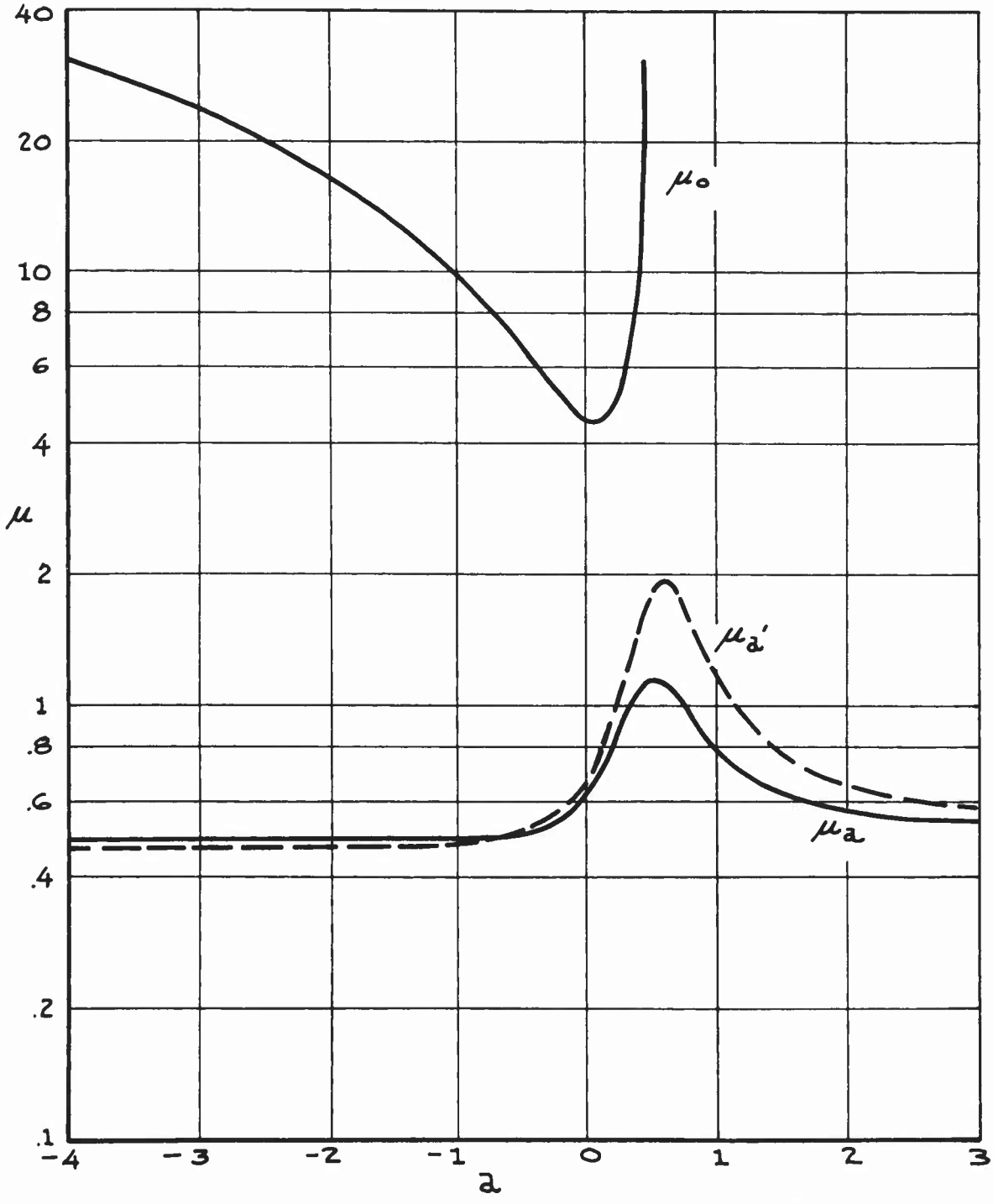


FIGURE 16i

MASS-DENSITY RATIO VALUES VS ELASTIC AXIS LOCATIONS

$r_c^2 = .25$

$X_m = -.5$

$\pi^2 = 1.0$

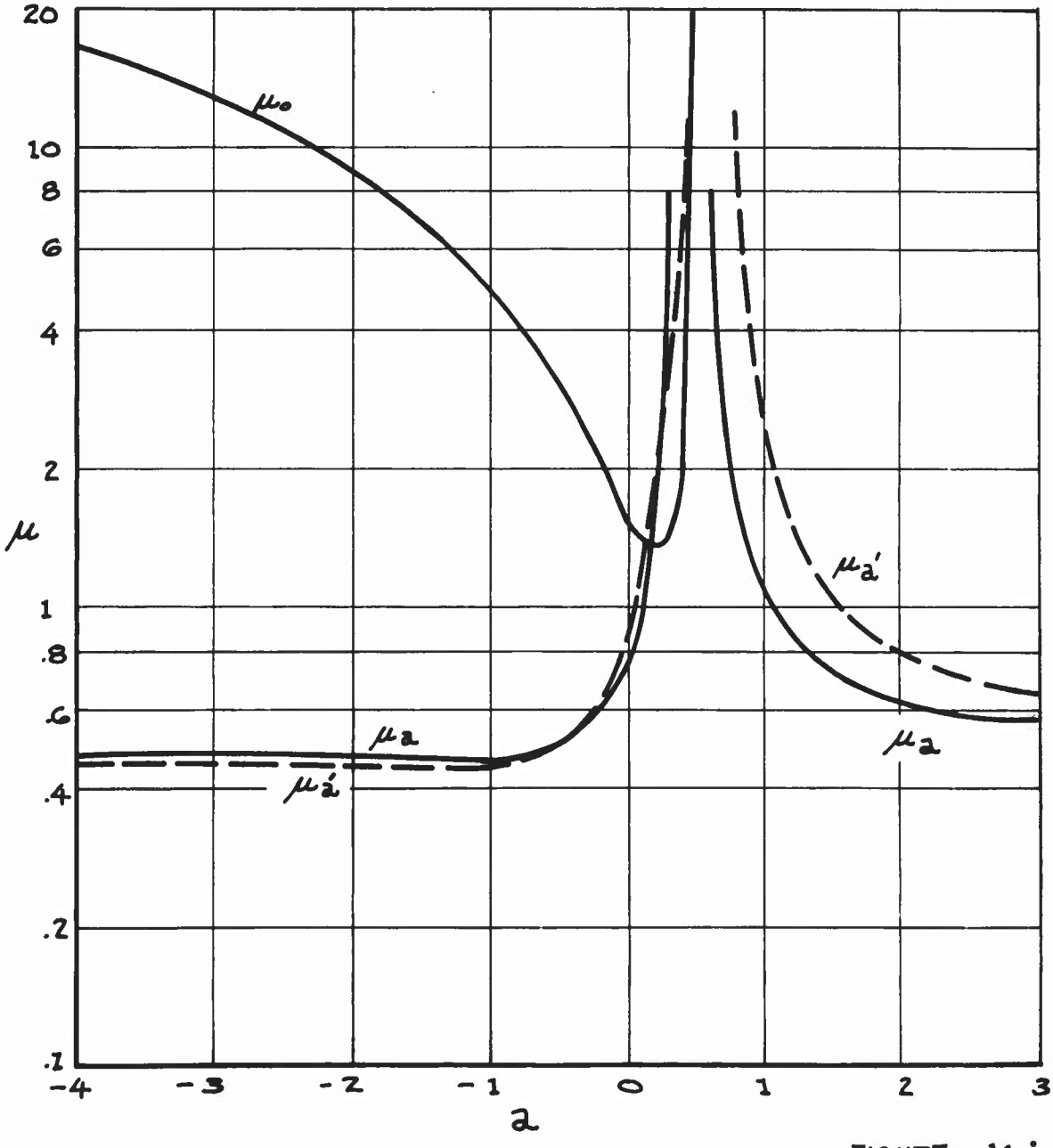


FIGURE 16j

MASS-DENSITY RATIO VALUES VS ELASTIC AXIS LOCATIONS

$r_c^2 = .25$

$Xm = .5$

$\pi^2 = 5.0$

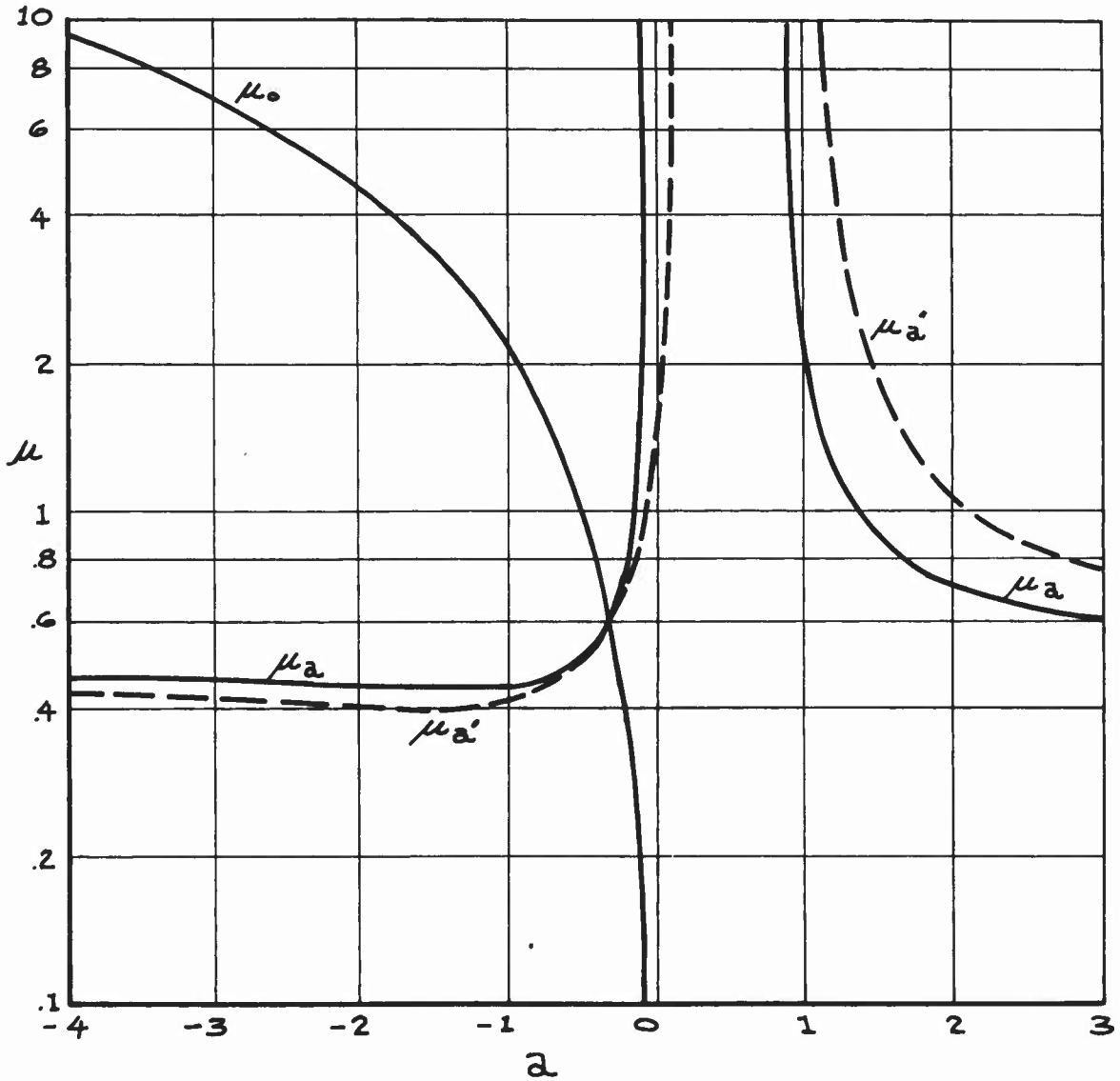


FIGURE 16k

MASS-DENSITY RATIO VALUES VS ELASTIC AXIS LOCATIONS

$r_c^2 = .25$ $\pi^2 = 50$

$Xm = .5$

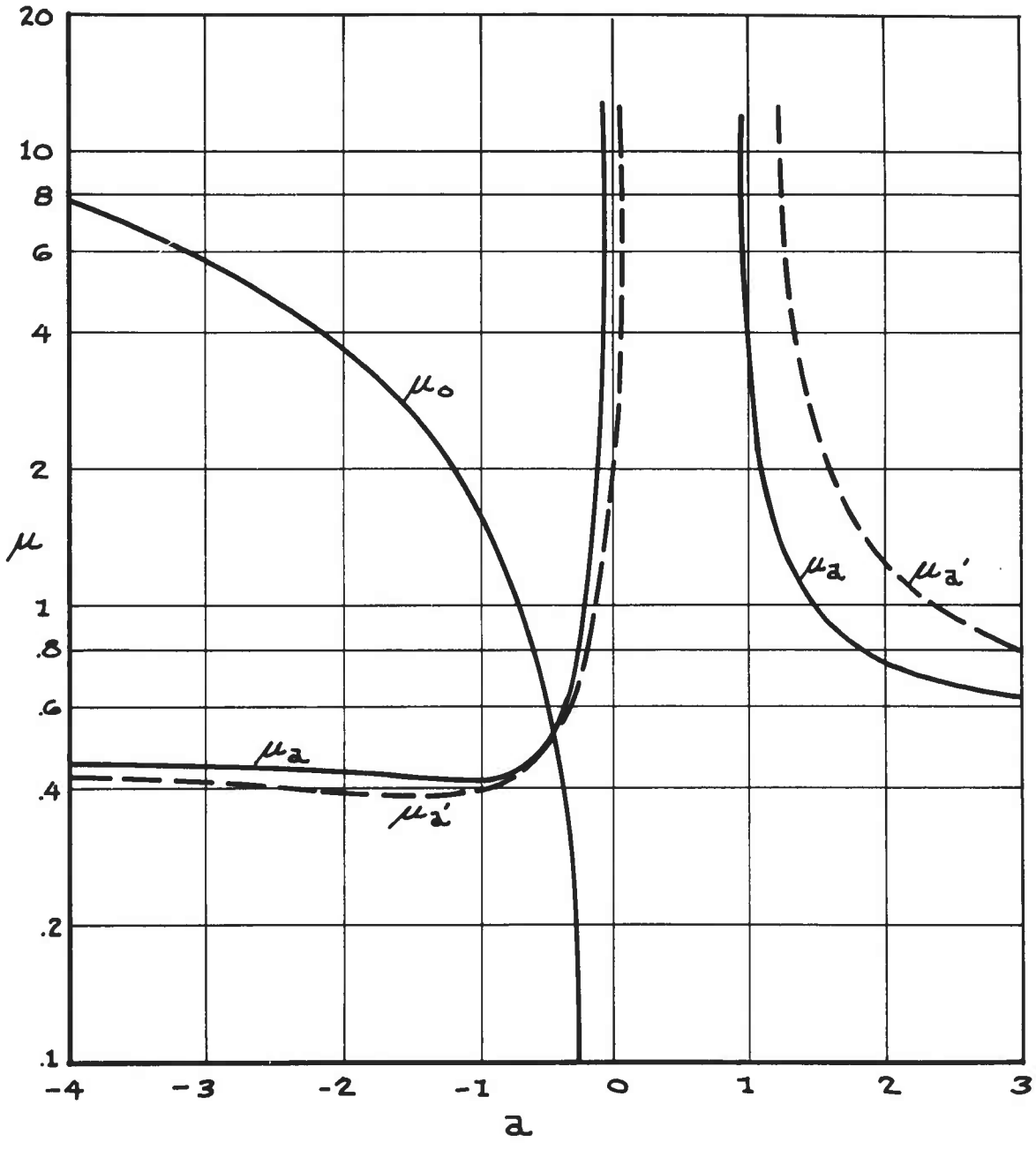


FIGURE 16 l

MASS-DENSITY RATIO VALUES VS ELASTIC AXIS LOCATIONS

$r_c^2 = .25$
$x_m = -.75$
$\pi^2 = 1.0$

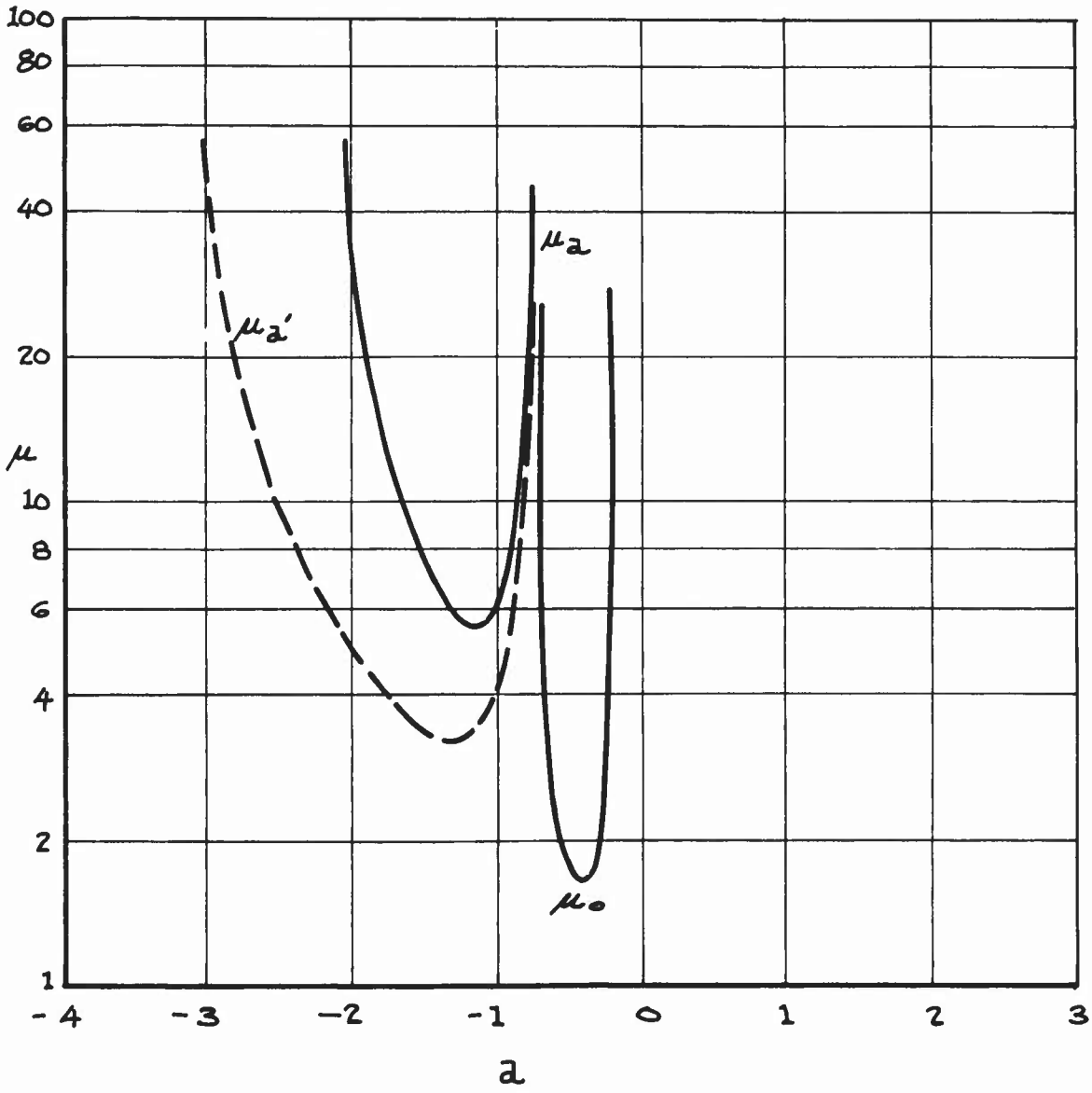


FIGURE 16m

MASS-DENSITY RATIO VALUES VS ELASTIC AXIS LOCATIONS $r_c^2 = .25$ $\pi^2 = 5.0$ $X_m = -.75$

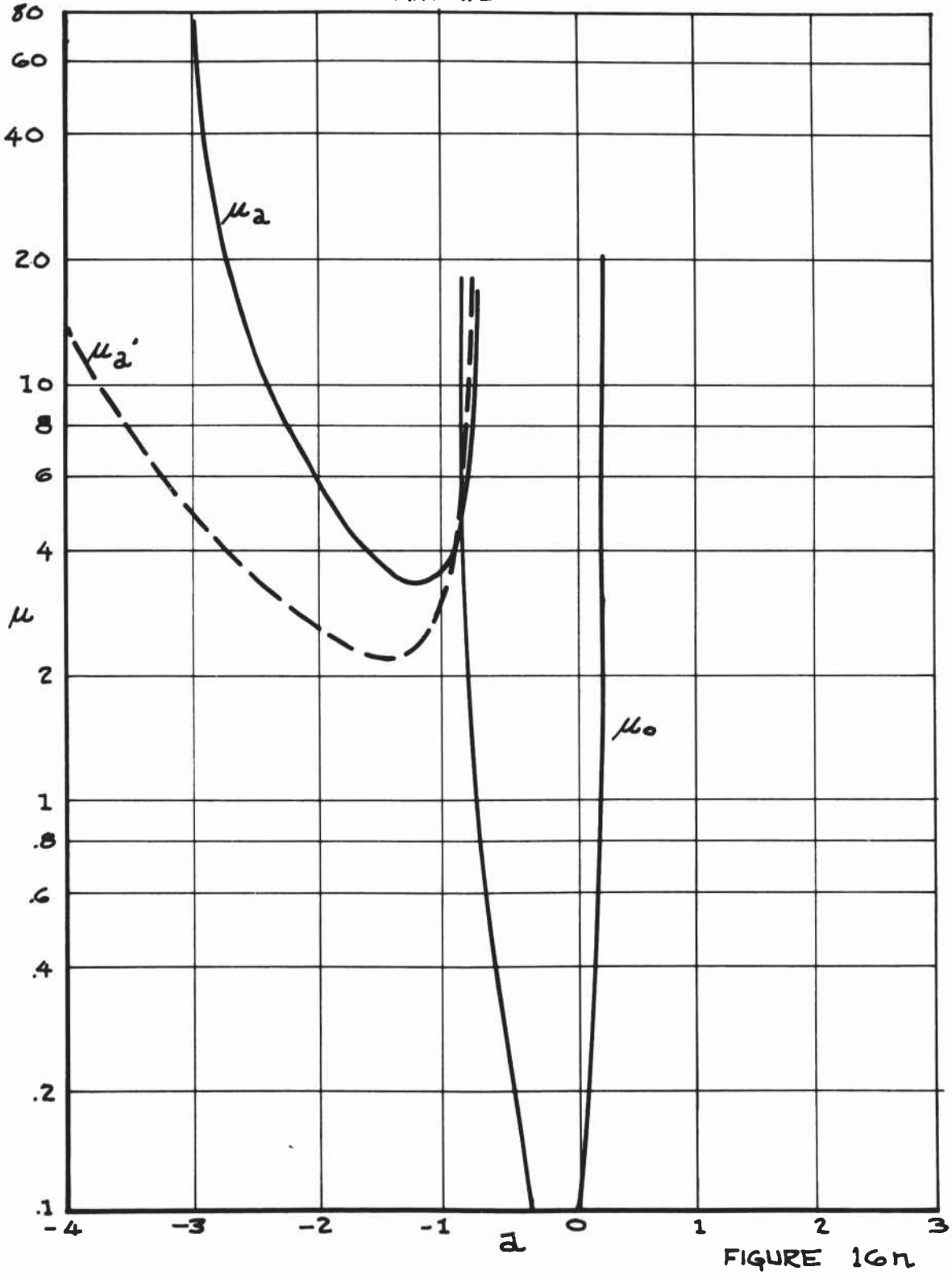


FIGURE 16n

MASS-DENSITY RATIO VALUES VS. ELASTIC AXIS LOCATIONS $r_c^2 = .25$ $\pi^2 = 50.0$ $X_m = -.75$

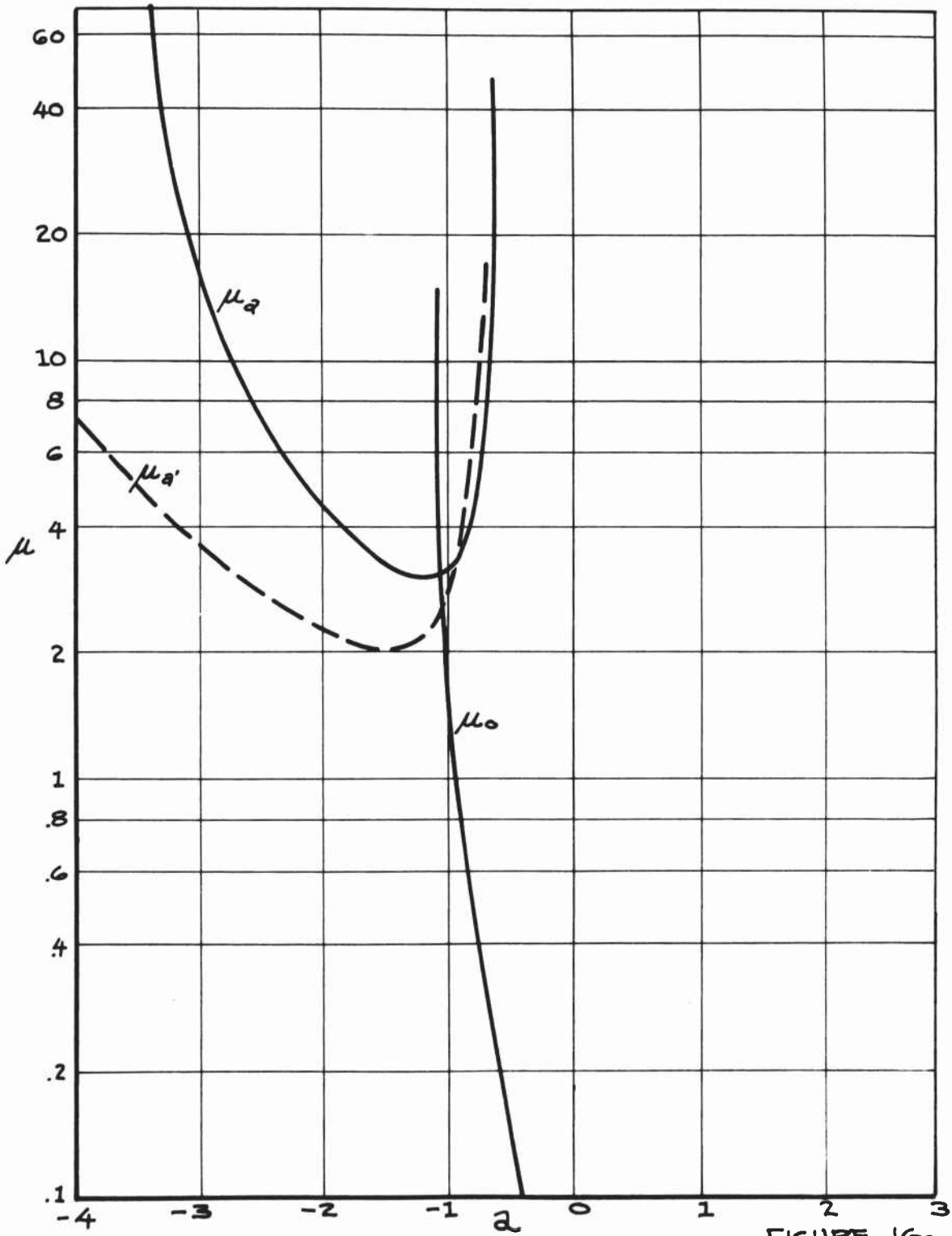


FIGURE 16.

PLOTS SHOWING THE QUALITATIVE DEPENDENCE OF A SECTION FLUTTER BOUNDARY UPON THE SECTION $\mu_o$, $\mu_{a'}$, AND $\mu_a$ VALUES

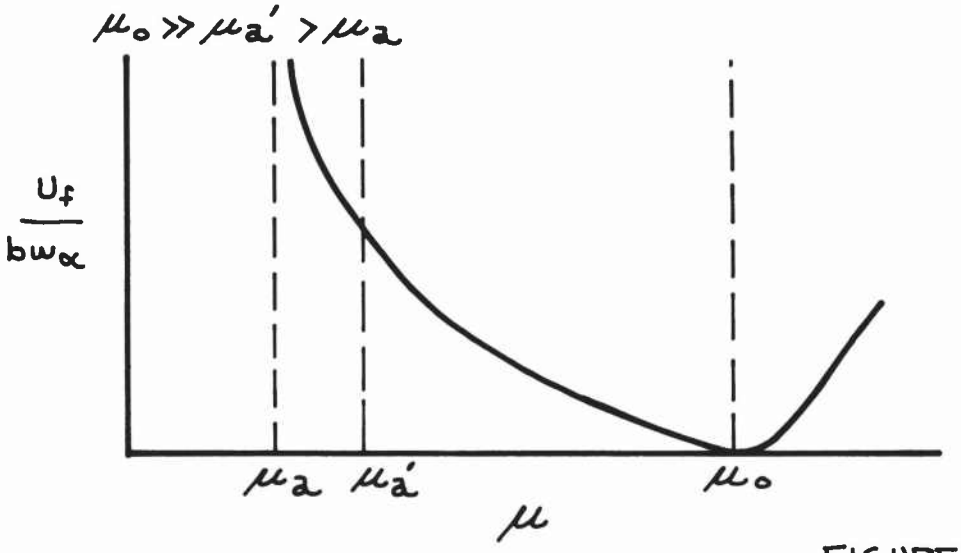


FIGURE 17a

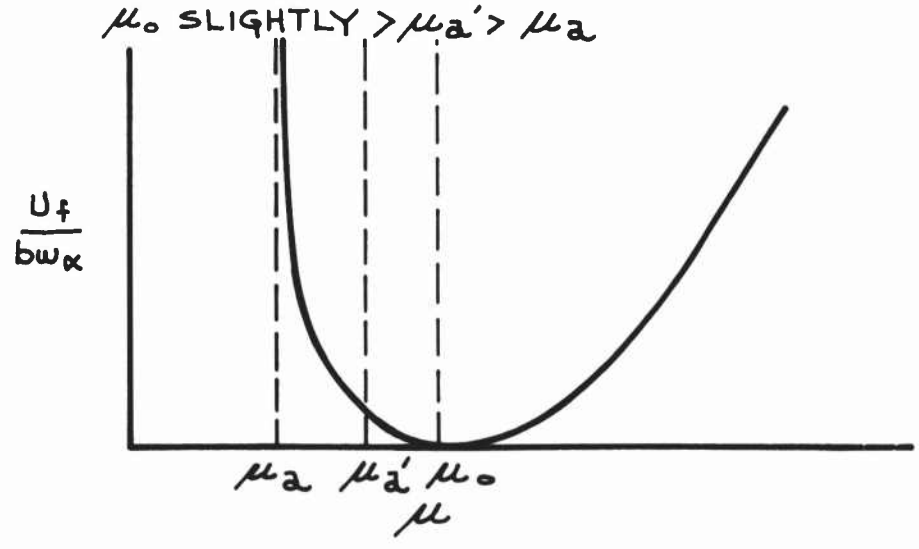


FIGURE 17b

PLOTS SHOWING THE QUALITATIVE DEPENDENCE OF A SECTION FLUTTER BOUNDARY UPON THE SECTION $\mu_o$, $\mu_a'$, AND $\mu_a$ VALUES


FIGURE 17C

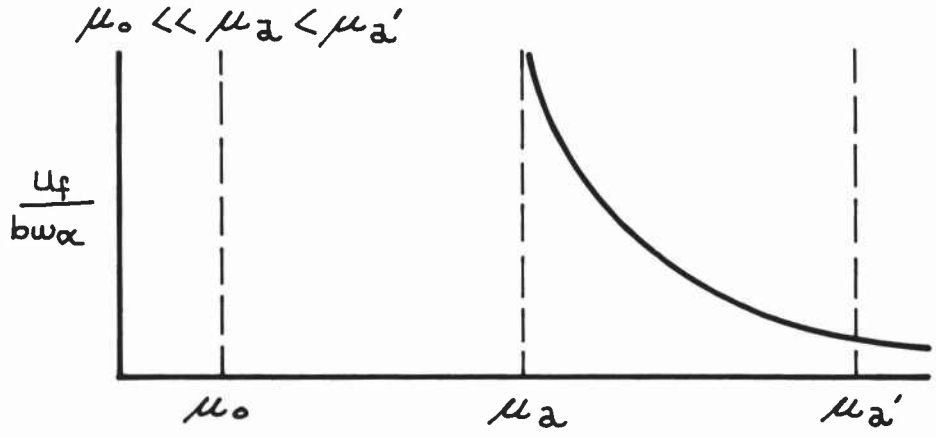


FIGURE 17d

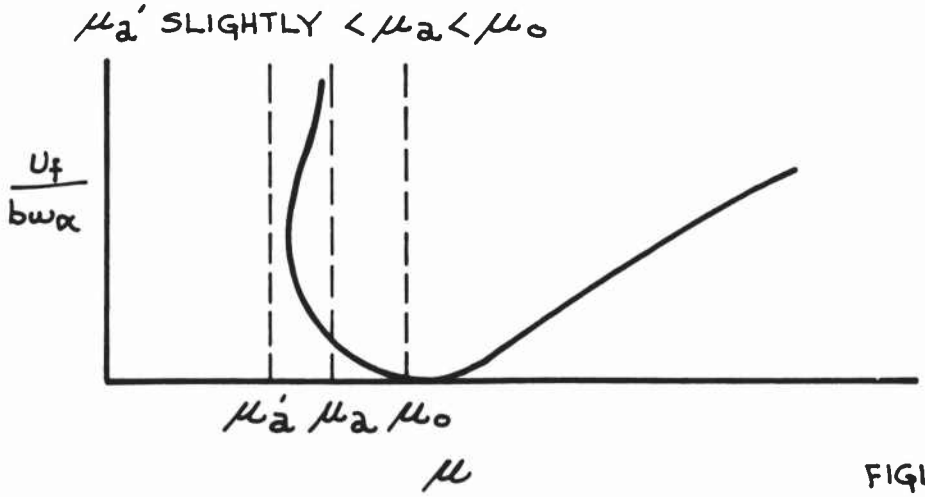


FIGURE 17e

Figures 18a-18h show the relative sensitivity of various flutter boundaries to changes in the non-dimensional system parameters. These plots are based upon quasi-unsteady theory.

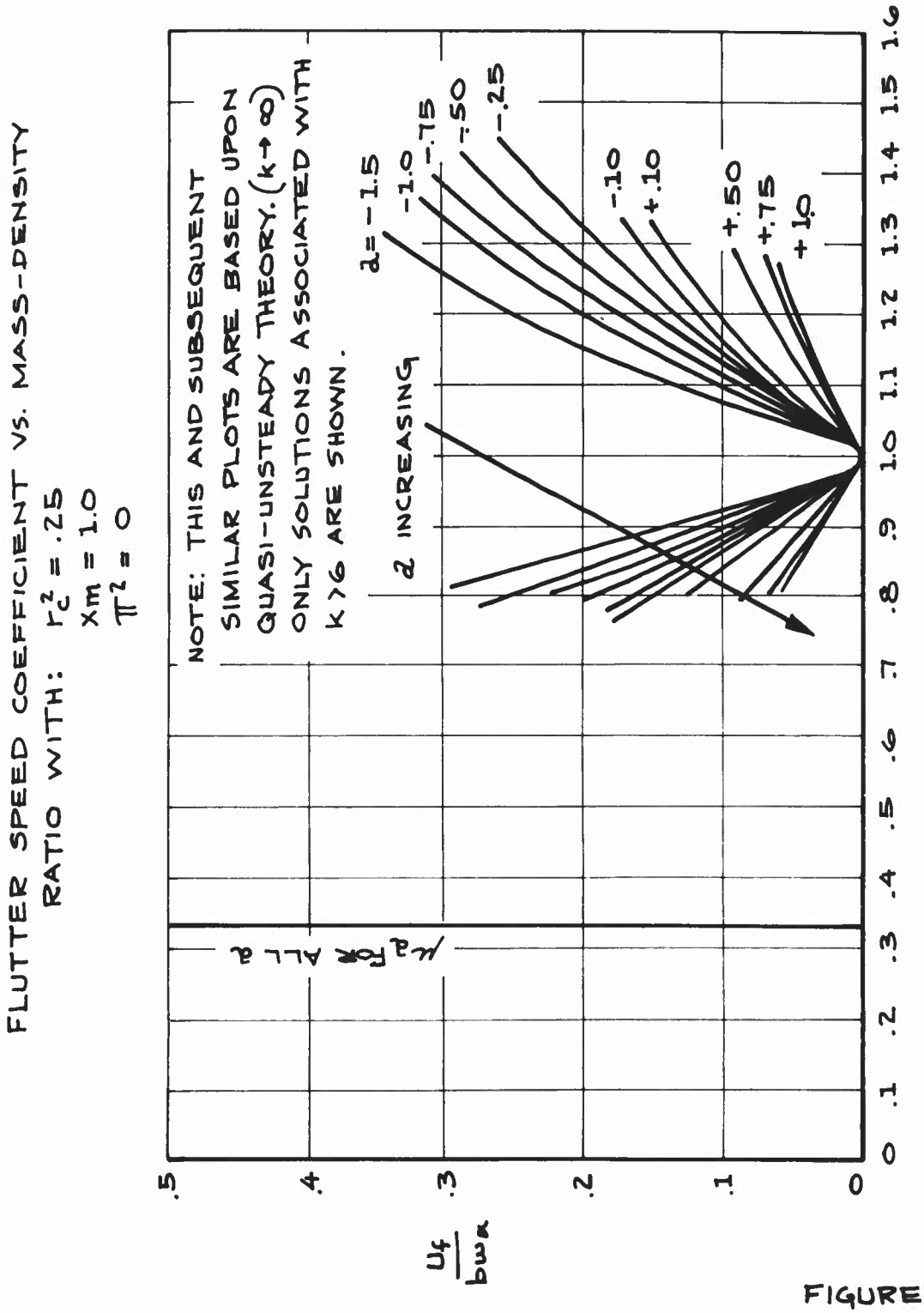
FLUTTER SPEED COEFFICIENT VS. MASS-DENSITY RATIO WITH: $r_c^2 = .25$, $x_m = 1.0$, $\pi^2 = 0$
NOTE: THIS AND SUBSEQUENT SIMILAR PLOTS ARE BASED UPON QUASI-UNSTEADY THEORY. $(k \to \infty)$ ONLY SOLUTIONS ASSOCIATED WITH $k > 6$ ARE SHOWN.
d INCREASING
d = -1.5
-1.0
-.75
-.50
-.25
-.10
+.10
+.50
+.75
+1.0
$\mu_a$ FOR ALL a
$\frac{U_f}{bw_\alpha}$
$\mu$
0
.1
.2
.3
.4
.5
.6
.7
.8
.9
1.0
1.1
1.2
1.3
1.4
1.5
1.6

FIGURE 18a

FLUTTER SPEED COEFFICIENT VS. MASS-DENSITY RATIO

WITH: $r_c^2 = .25$
$x_m = 1.0$
$\mathfrak{T}^2 = .4$

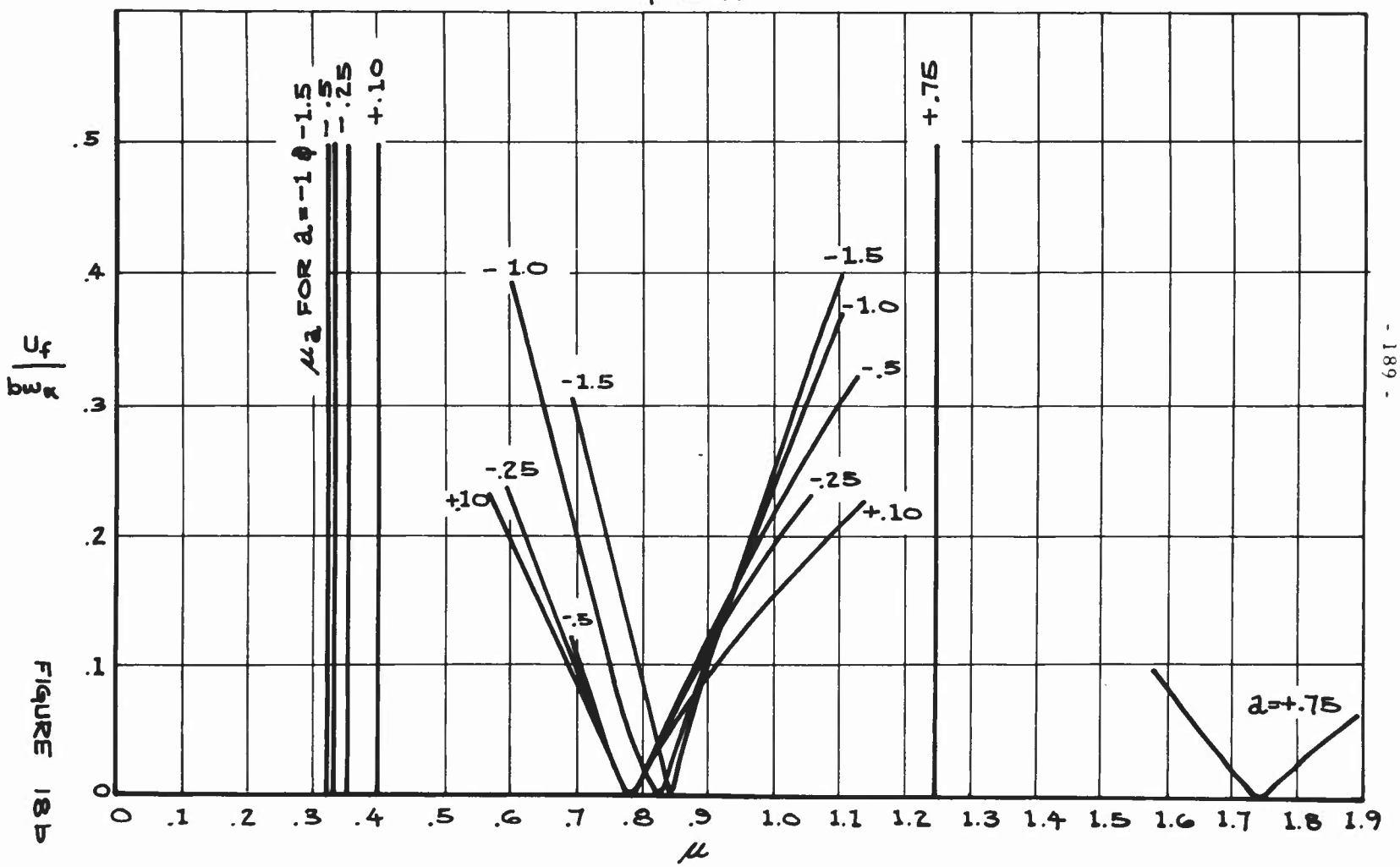


FIGURE 18b

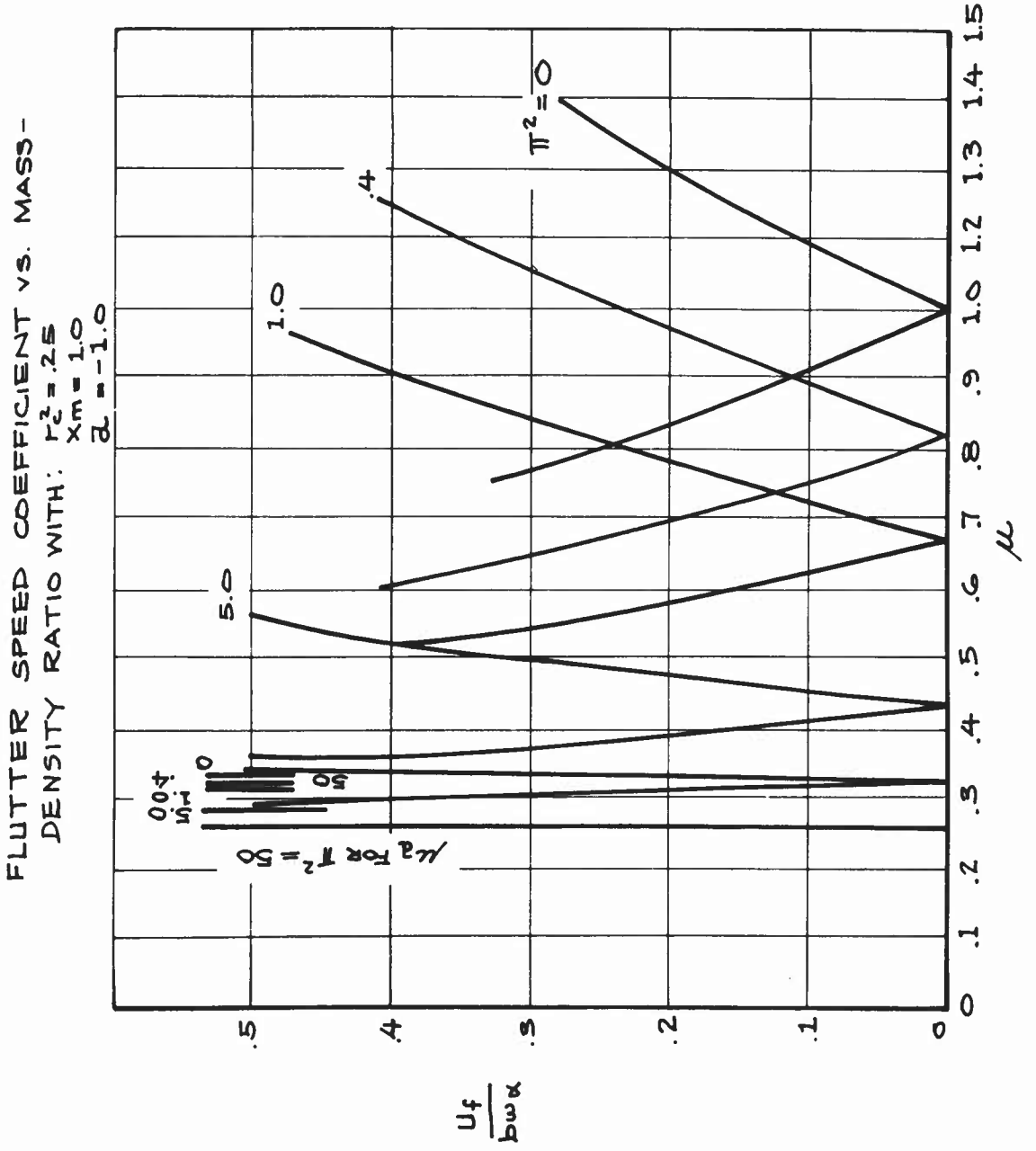
FLUTTER SPEED COEFFICIENT vs. MASS-DENSITY RATIO WITH: $r_c^2 = .25$ $x_m = 1.0$ $a = -1.0$
$\pi^2 = 0$
.4
1.0
5.0
$\mu_a$ FOR $\pi^2 = 50$
0
50
100
$\frac{U_f}{b\omega_\alpha \sqrt{\mu}}$
$\mu$
0 .1 .2 .3 .4 .5 .6 .7 .8 .9 1.0 1.2 1.3 1.4 1.5
0 .1 .2 .3 .4 .5

FIGURE 18c

FLUTTER SPEED COEFFICIENT VS. MASS-DENSITY RATIO WITH: $r_c^2 = .25$, $X_m = 1.0$, $a = -.5$

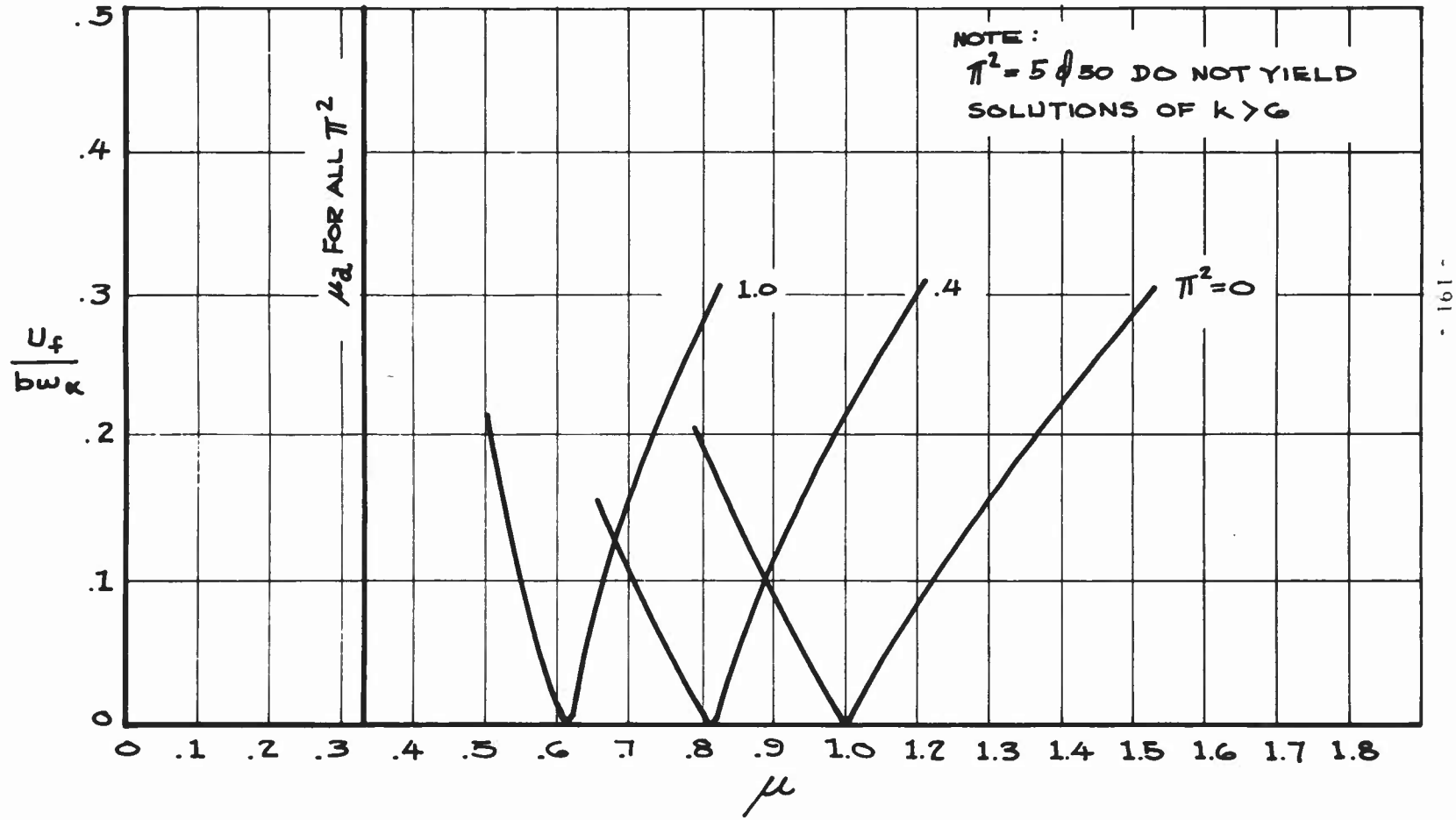


FIGURE 18 d

FLUTTER SPEED COEFFICIENT VS. MASS-DENSITY RATIO WITH: $r_c^2 = .25$, $x_m = .75$, $\pi^2 = 0$

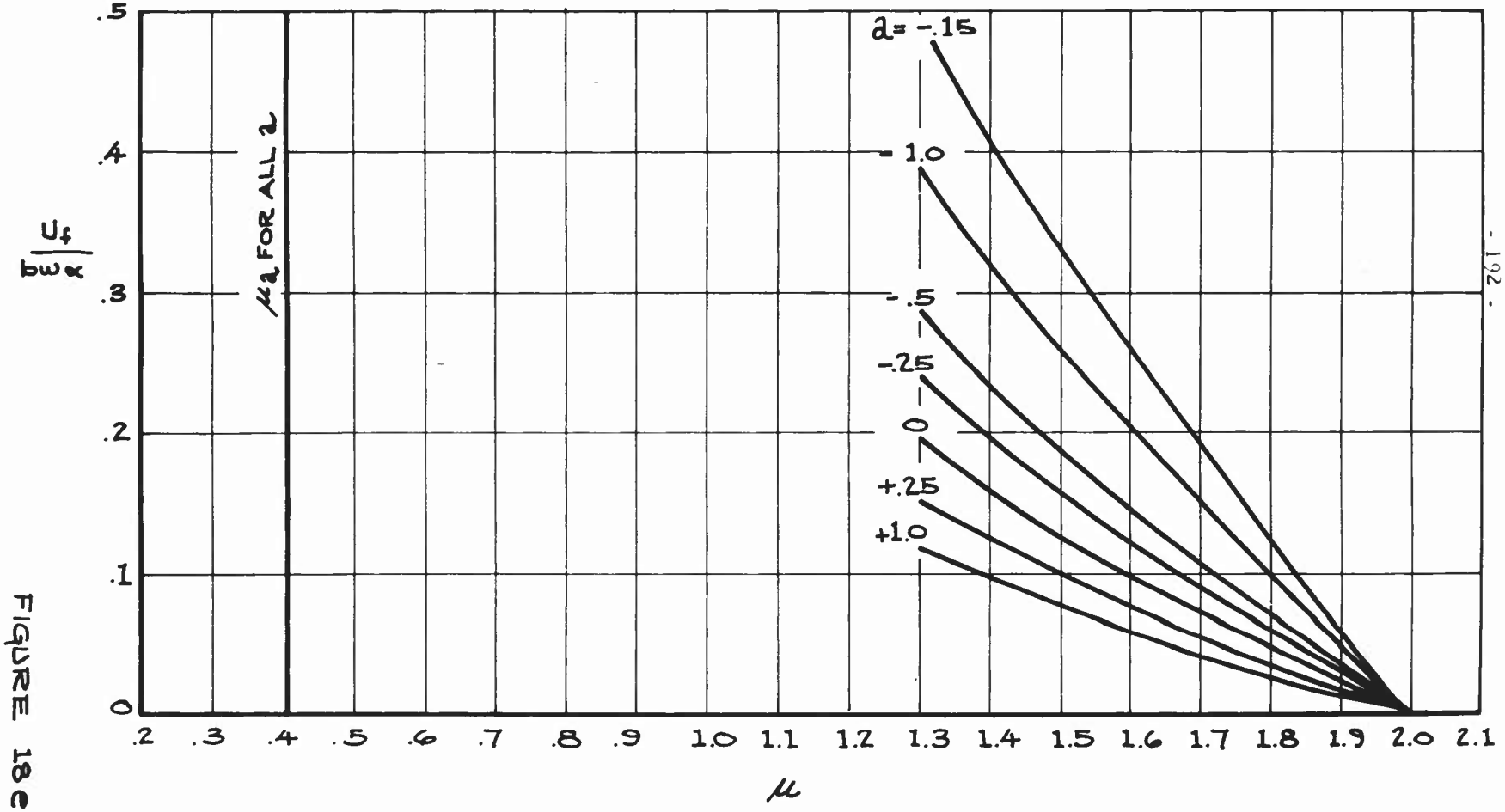


FIGURE 18c

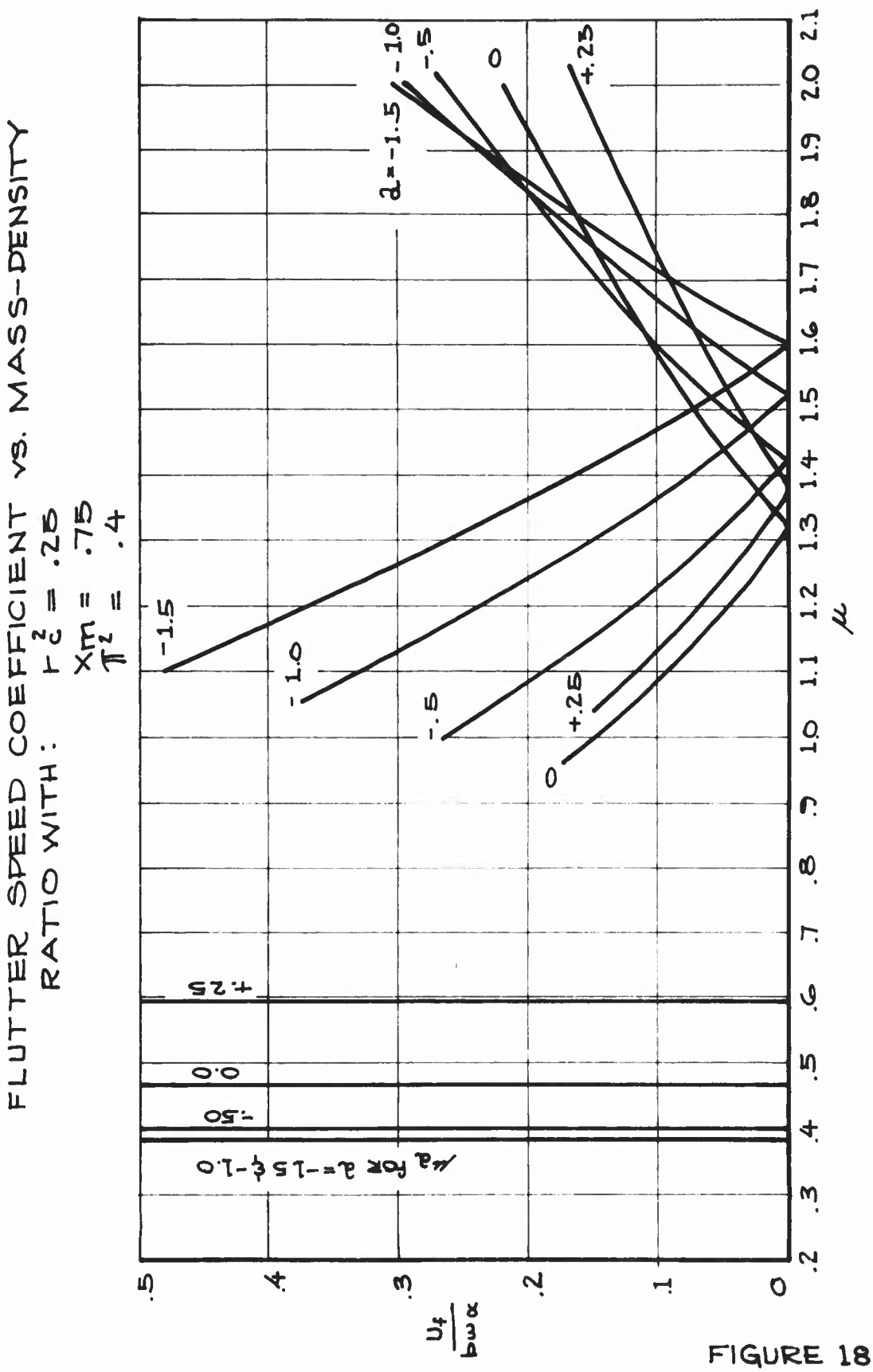
FLUTTER SPEED COEFFICIENT VS. MASS-DENSITY RATIO WITH: $r_c^2 = .25$ $x_m = .75$ $\pi^2 = .4$
$\frac{U_f}{b\omega_\alpha}$
$\mu$
$\mu_a$ FOR $a = -1.5$ & $-1.0$
-1.50
0.0
+.25
a=-1.5
-1.0
-.5
0
+.25
-1.5
-1.0
-.5
0
+.25
.5
.4
.3
.2
.1
0
.2
.3
.4
.5
.6
.7
.8
.9
1.0
1.1
1.2
1.3
1.4
1.5
1.6
1.7
1.8
1.9
2.0
2.1

FIGURE 18f

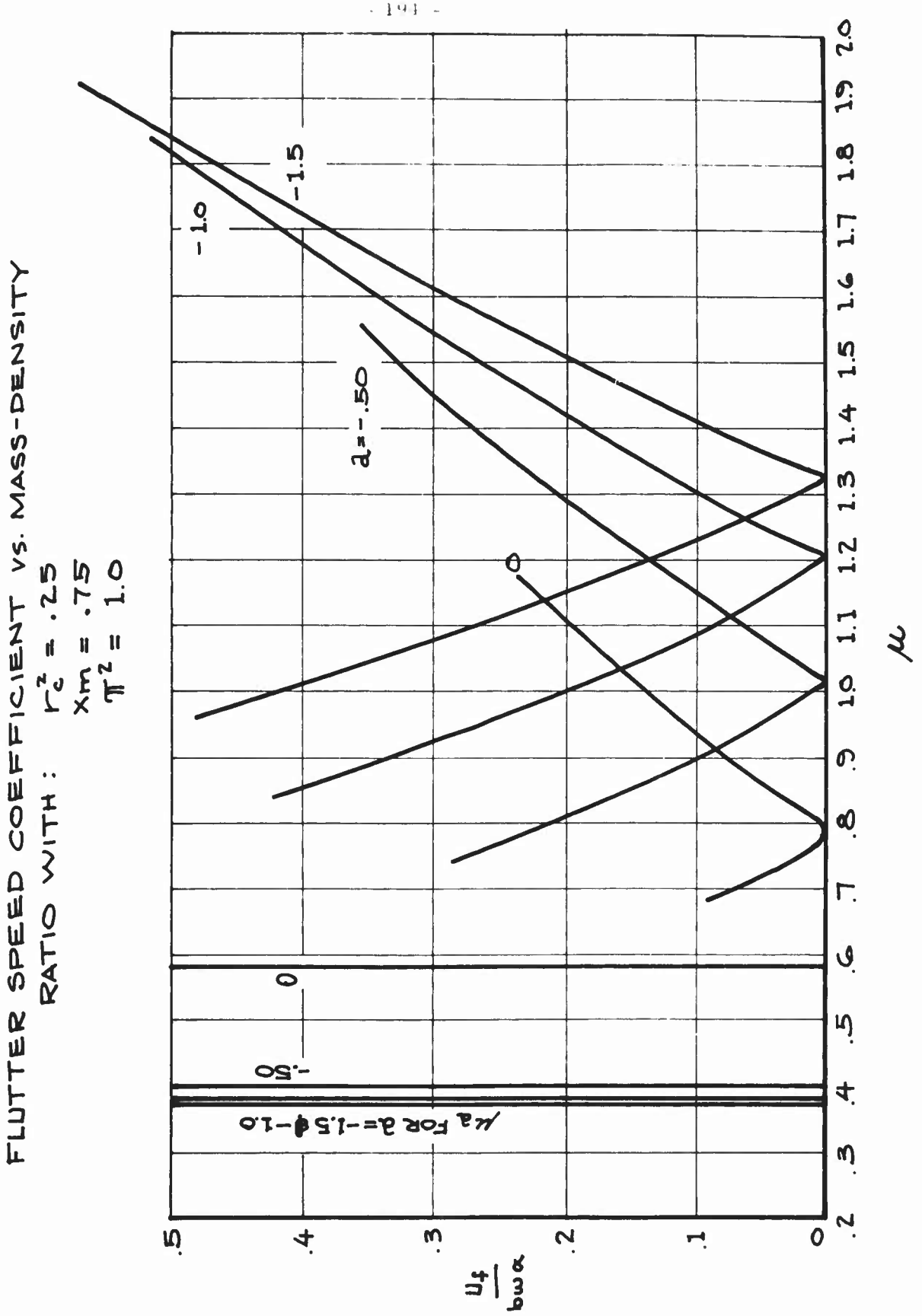
FLUTTER SPEED COEFFICIENT VS. MASS-DENSITY RATIO WITH: $r_c^2 = .25$ $x_m = .75$ $\pi^2 = 1.0$
$\frac{V_f}{b\omega_\alpha\sqrt{\mu}}$
$\mu$
$\mu_a$ FOR $\delta = -1.5$ & $-1.0$
$\delta = -.50$
0
-.50
-1.0
-1.5
.5
.4
.3
.2
.1
0
.2 .3 .4 .5 .6 .7 .8 .9 1.0 1.1 1.2 1.3 1.4 1.5 1.6 1.7 1.8 1.9 2.0

FIGURE 18g

FLUTTER SPEED COEFFICIENT VS. MASS-DENSITY RATIO WITH: $r_c^2 = .25$
$x_m = 0$
$\pi^2 = 50$

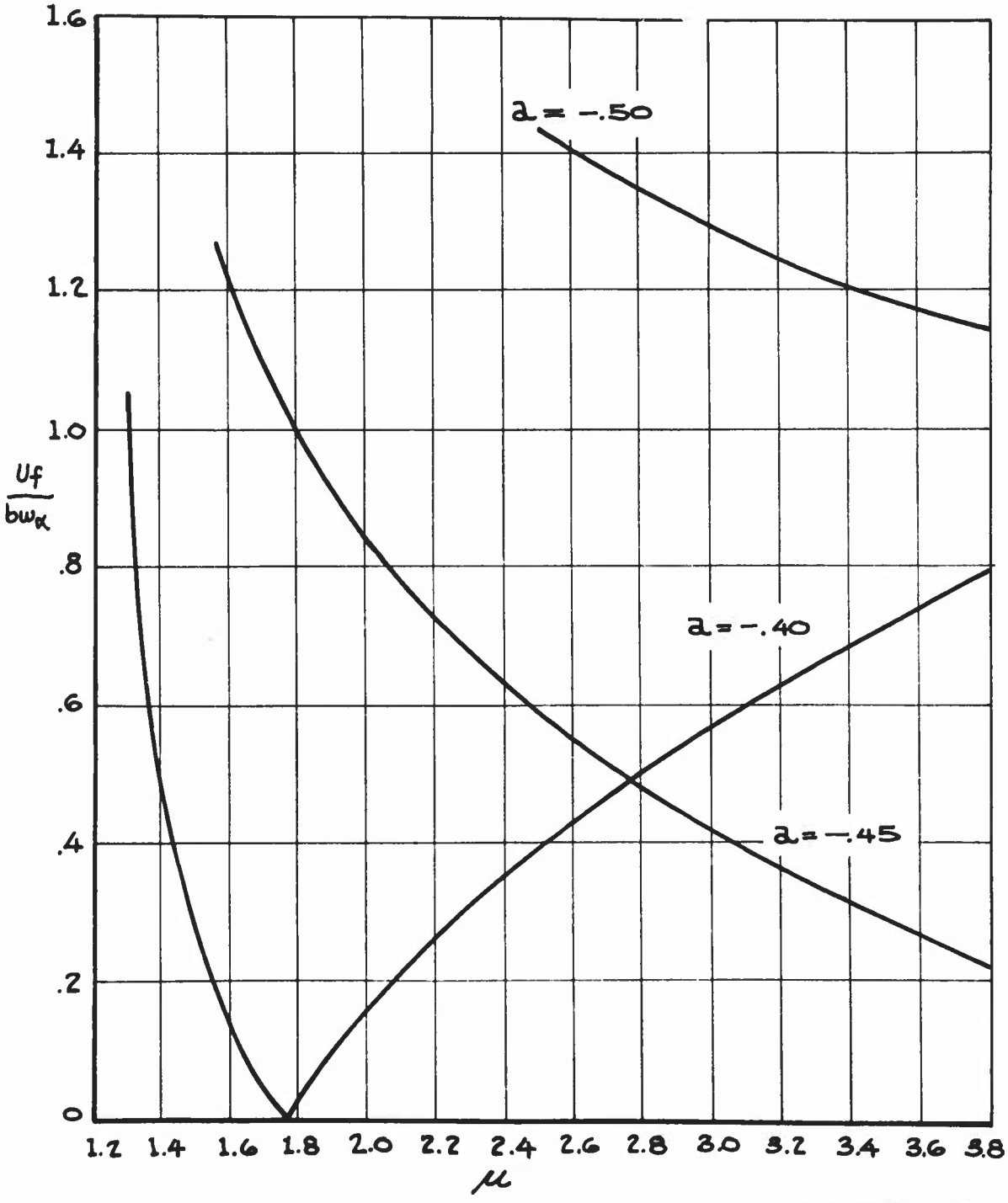


FIGURE 18 h

A COMPARISON OF QUASI-UNSTEADY AND "EXACT" BOUNDARIES FOR: $r_c^2 = .25$ $\pi^2 = .4$ $X_m = 1.0$ $a = -1.5$

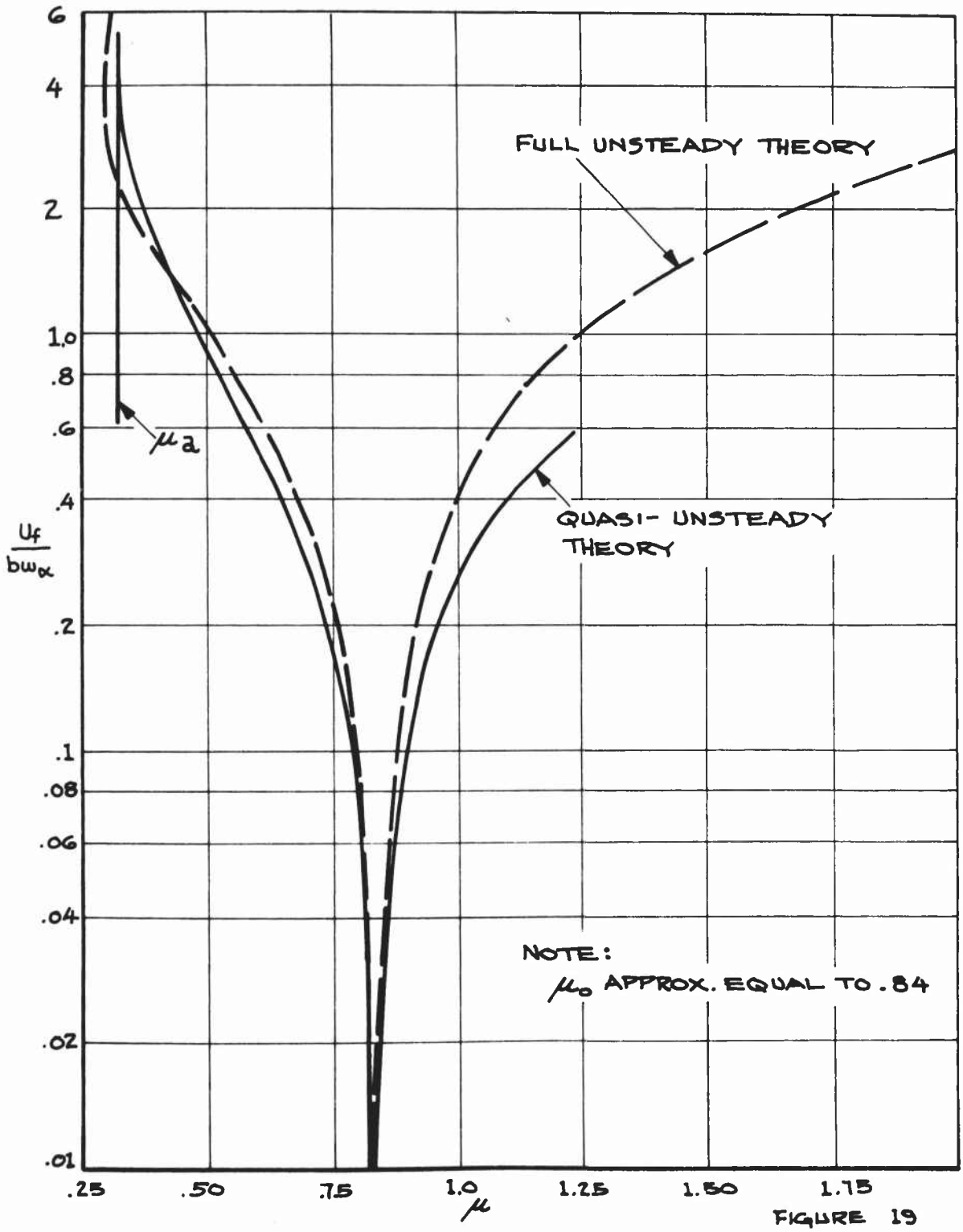


FIGURE 19

A TYPICAL COMPARISON OF SECTION FLUTTER BOUNDARIES

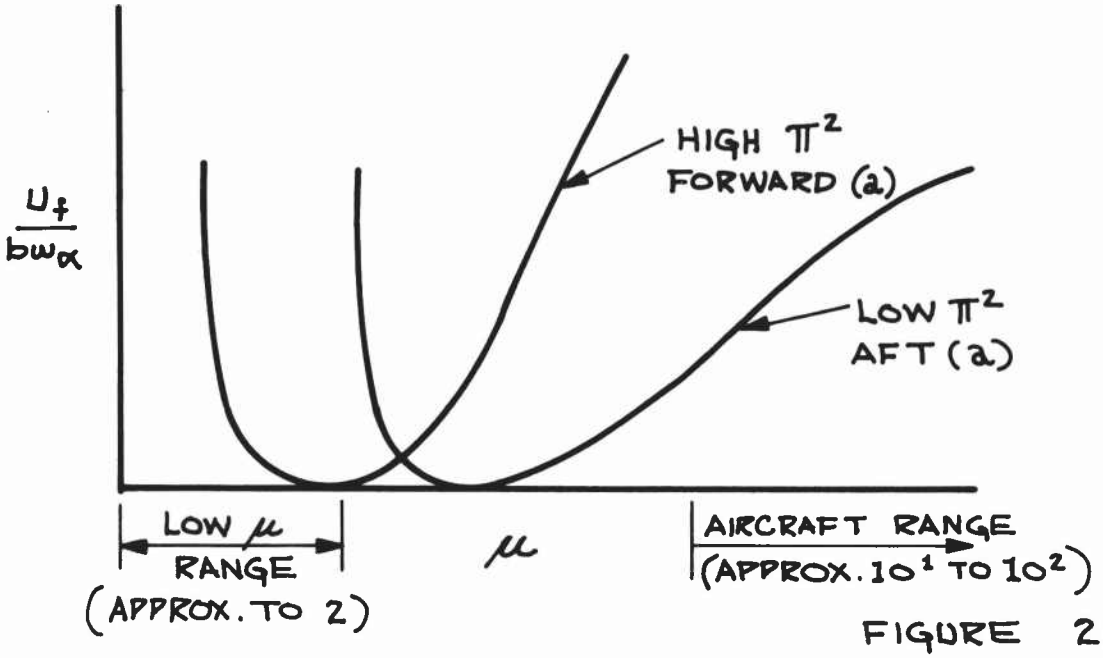


FIGURE 20

A QUALITATIVE PORTRAYAL OF FINITE SPAN EFFECTS

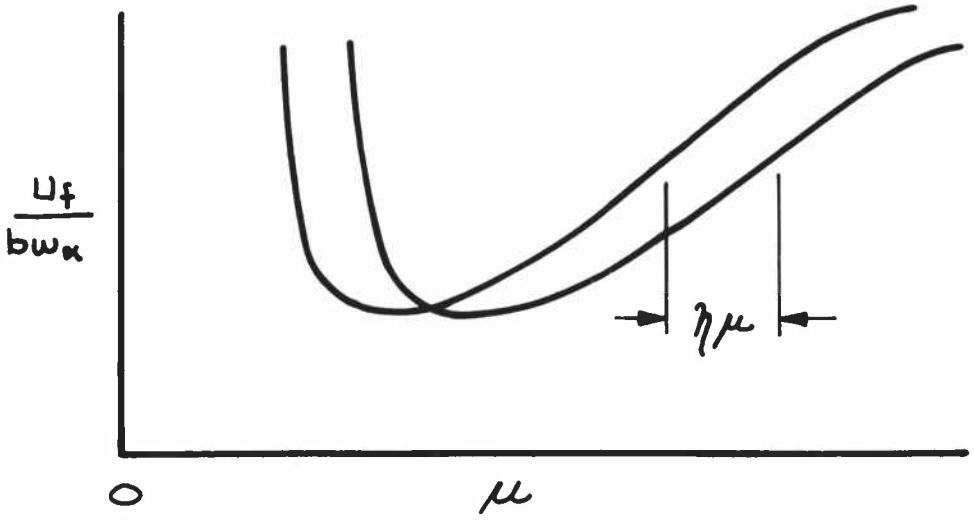


FIGURE 21

UNSWEPT REFERENCE STRUT AND ITS SWEPT COUNTERPART

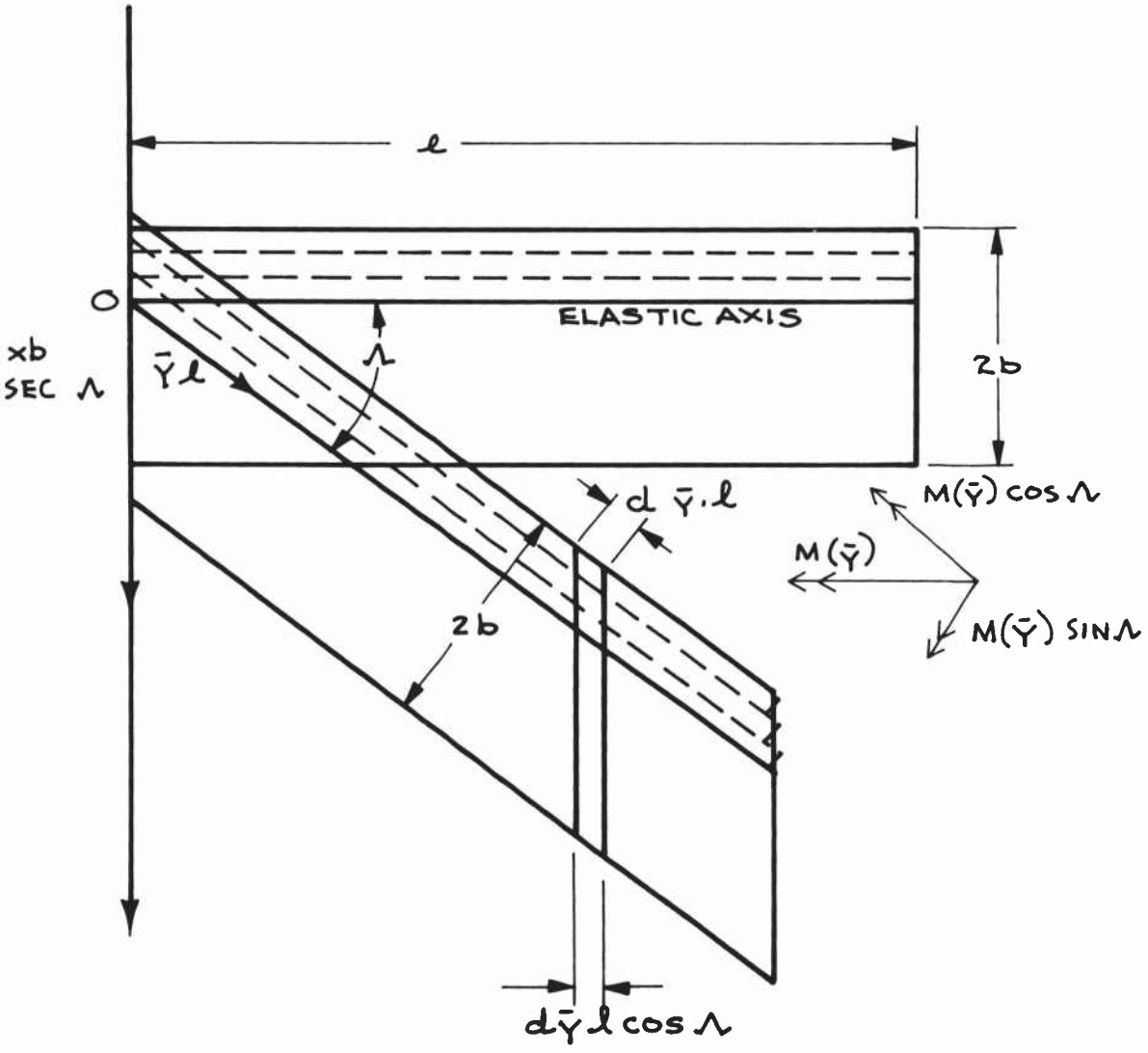


FIGURE 22

A PLOT OF THE SWEEP PARAMETER AS A FUNCTION OF THE UNSWEPT CANTILEVERED LENGTH TO SEMI-CHORD RATIO FOR VARIOUS ANGLES OF SWEEP.

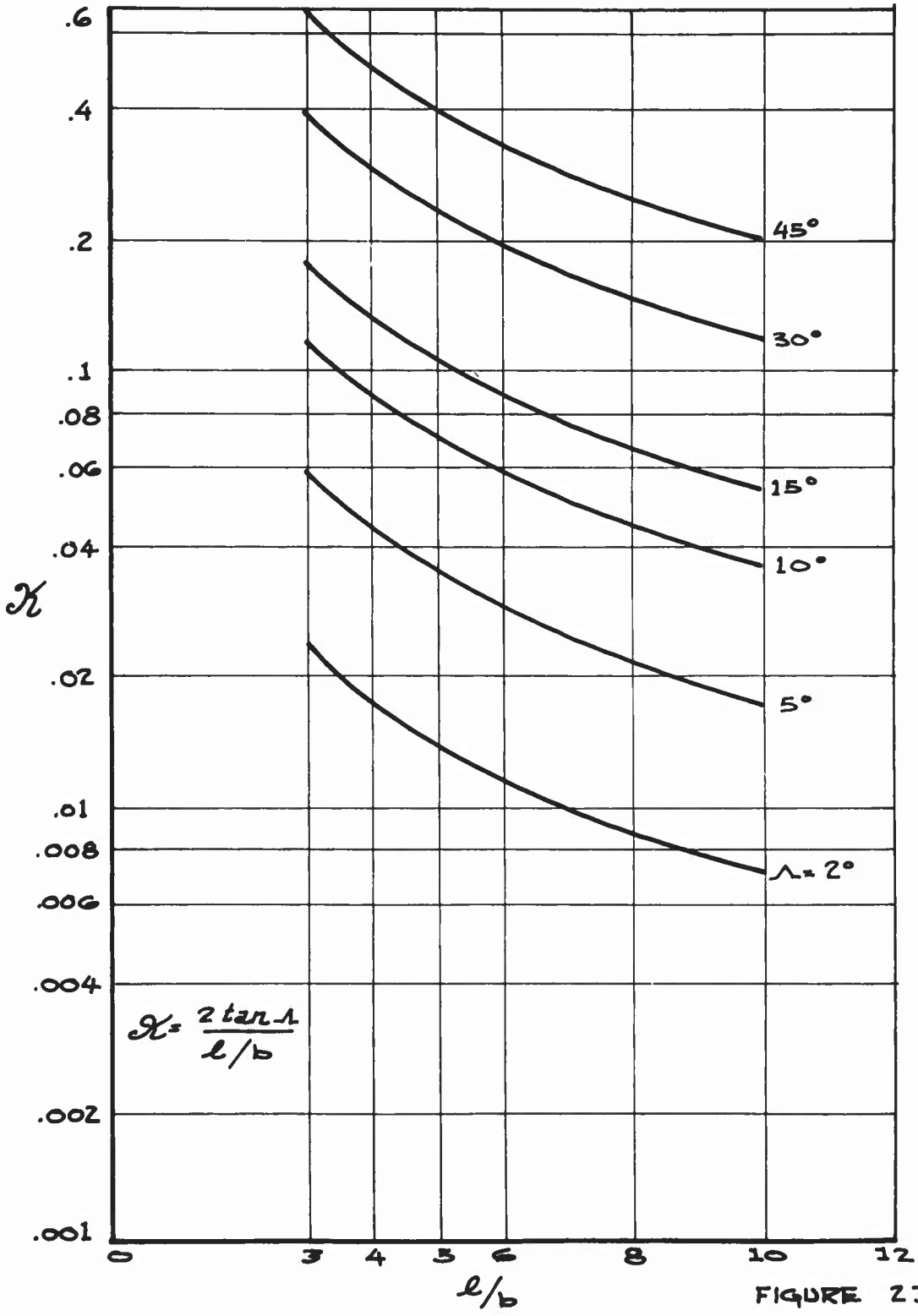


FIGURE 23

A COMPARISON OF A FLUTTER BOUNDARY PREDICTED BY THE SIMPLIFIED ANALYSIS WITH A BOUNDARY PREDICTED BY HERR USING THE AXIS-NORMAL APPROACH.

MODEL — UNSWEPT HERR # 2

PARAMETERS — $r_c^2 = .2142$ $a = -.172$

$X_m = .318$ $\mathcal{K} = 0.0$

$\pi^2 = .0114$

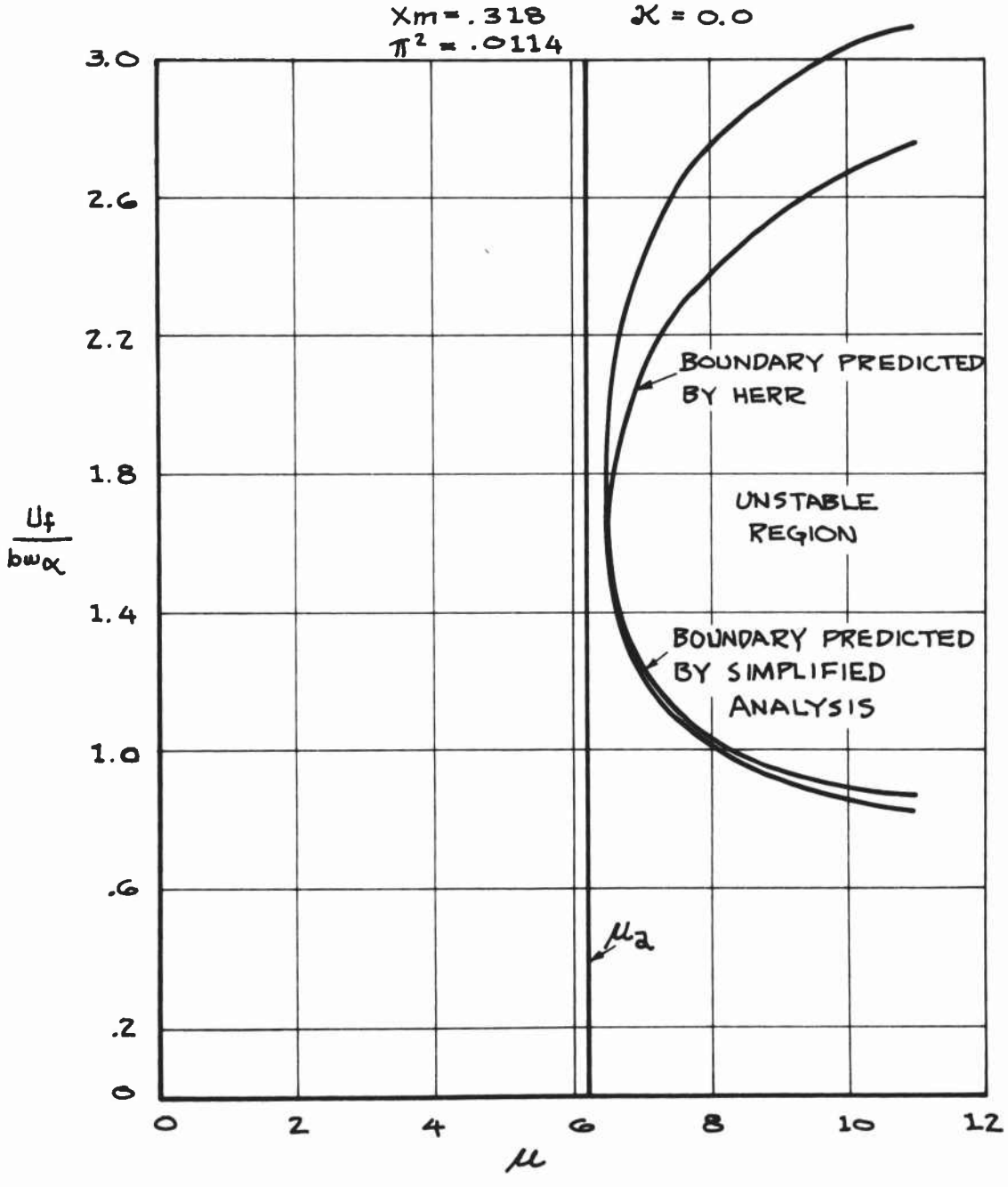


FIGURE 24

A COMPARISON OF A FLUTTER BOUNDARY PREDICTED BY THE SIMPLIFIED ANALYSIS WITH A BOUNDARY PREDICTED BY HERR USING THE AXIS-NORMAL APPROACH.

MODEL- HERR #2 WITH 10 DEGREES OF SWEEP

PARAMETERS- $r_c^2 = .2142$ $a = -.172$

$X_m = .318$ $\kappa = .03$

$\pi^2 = .0114$

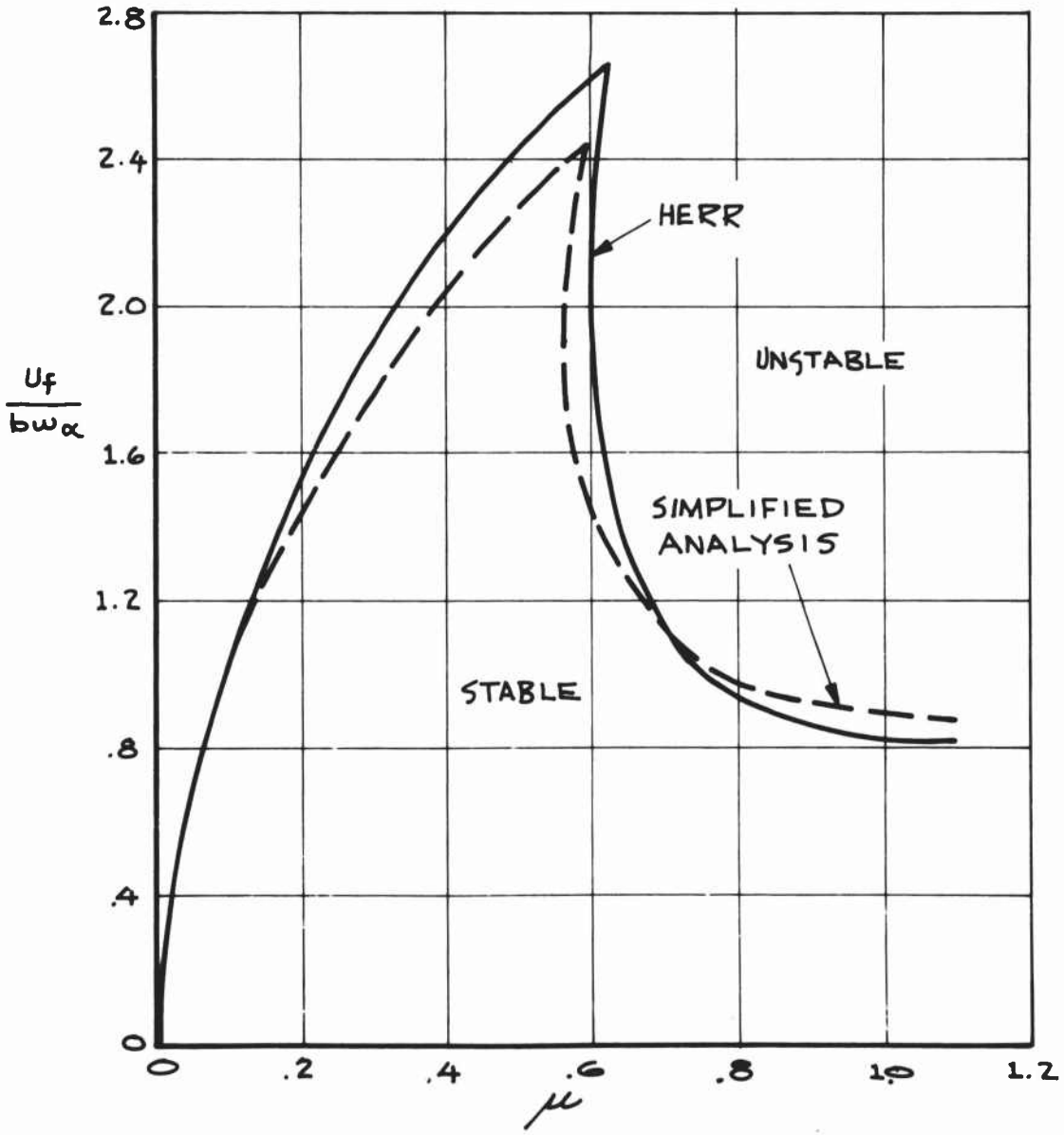


FIGURE 25

A COMPARISON OF A FLUTTER BOUNDARY PREDICTED BY THE SIMPLIFIED ANALYSIS WITH BOUNDARIES PREDICTED BY BAIRD AND SQUIRES USING MODAL ANALYSES

MODEL – BAIRD # 2 @ 15 DEGREES OF SWEEP

PARAMETERS – $r_c^2 = .26$ $\pi^2 = .011$

$X_m = .166$ $a = .38$

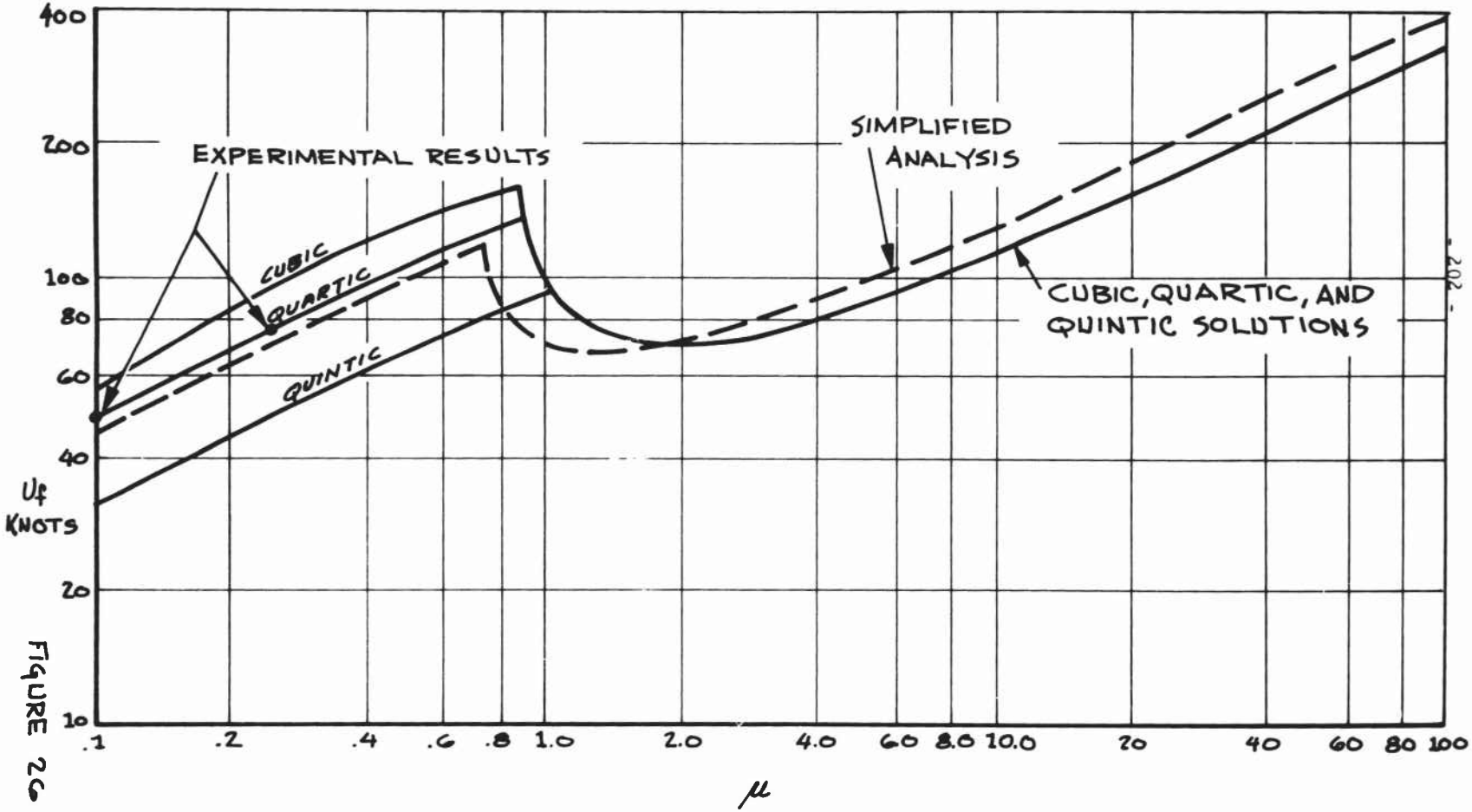


FIGURE 26

FLUTTER SPEED COEFFICIENT AS A FUNCTION OF THE MASS-DENSITY RATIO FOR VARIOUS VALUES OF THE SWEEP PARAMETER.

MODEL — BAIRD #2

PARAMETERS — $r_c^2 = .26$ $\pi^2 = .011$

$X_m = .166$ $a = .38$

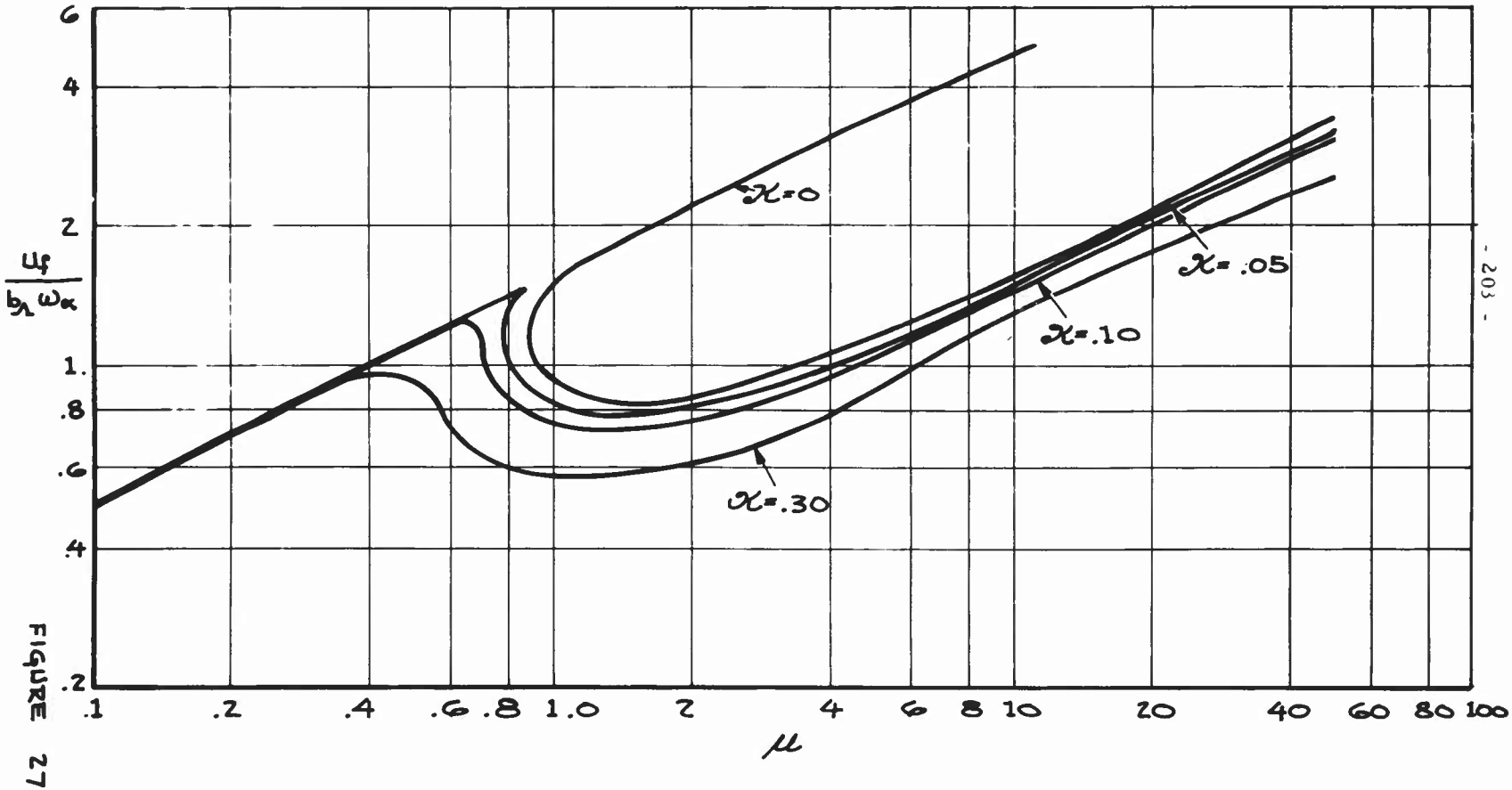


FIGURE 27

LOW MASS-DENSITY RATIO FLUTTER BOUNDARIES FOR VARIOUS VALUES OF THE SWEEP PARAMETER.

MODEL - BAIRD #2

PARAMETERS - $r_c^2 = .26$
$Xm = .166$
$\pi^2 = .011$
$\lambda = .38$

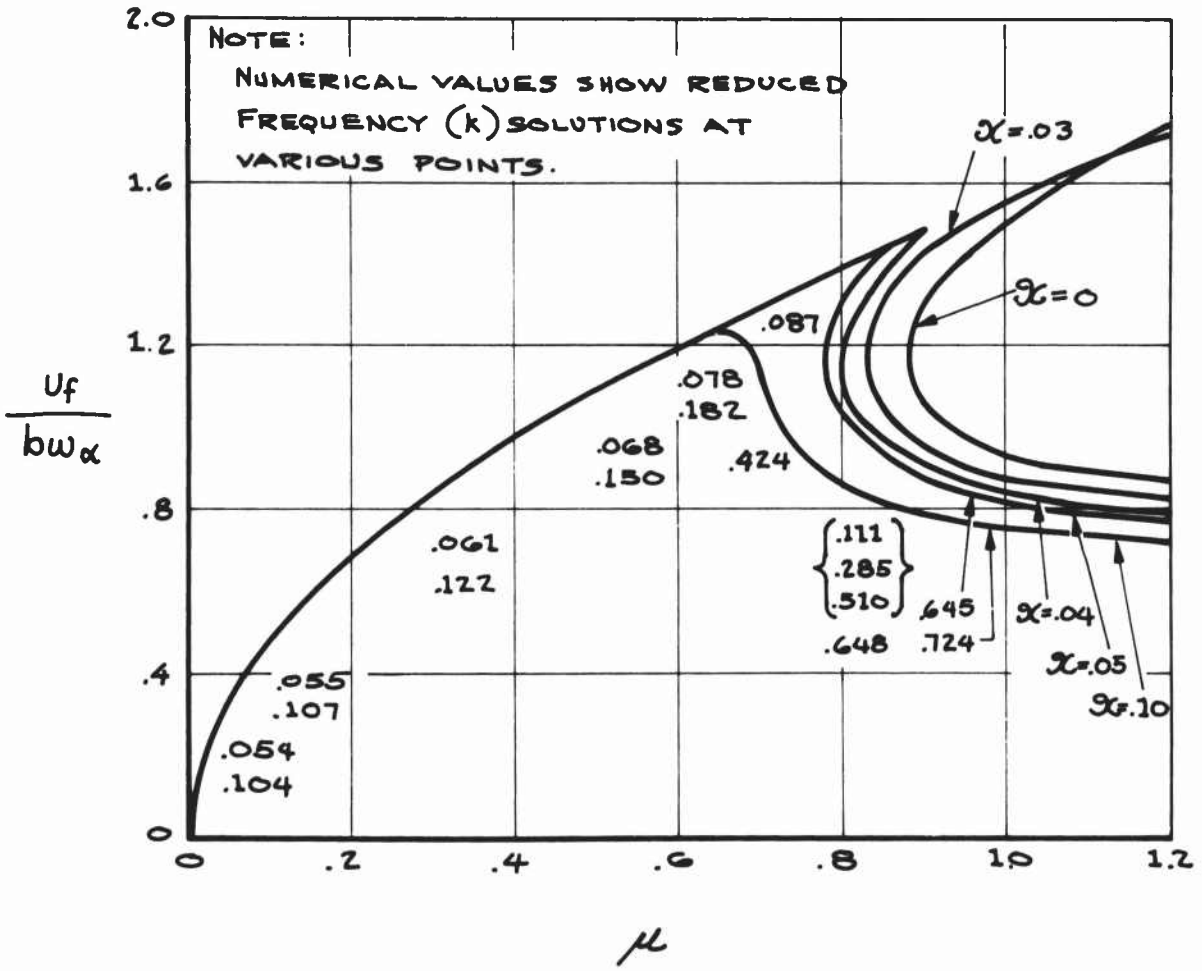


FIGURE 28

THE INVERSE OF THE FLUTTER FREQUENCY COEFFICIENT AS A FUNCTION OF THE MASS-DENSITY RATIO.

MODEL- BAIRD #2

PARAMETERS — $r_c^2 = .26$ $\pi^2 = .011$

$x_m = .166$ $a = .38$

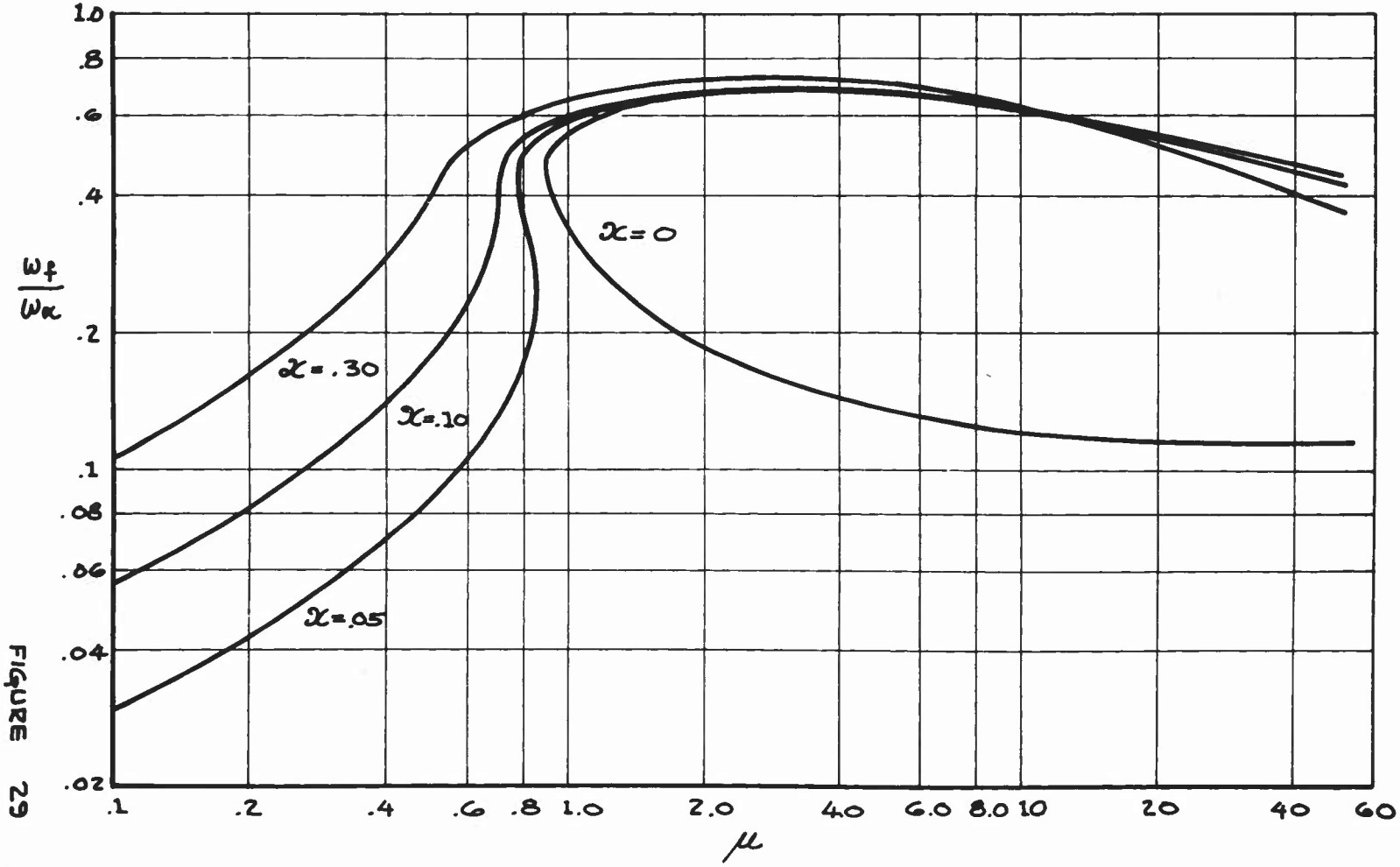


FIGURE 29

THE INVERSE OF THE FLUTTER FREQUENCY COEFFICIENT AS A FUNCTION OF THE MASS-DENSITY RATIO
MODEL-BAIRD # 2, PARAMETERS- $r_c^2 = .26$ $\pi^2 = .011$
$x_m = .166$ $a = .38$

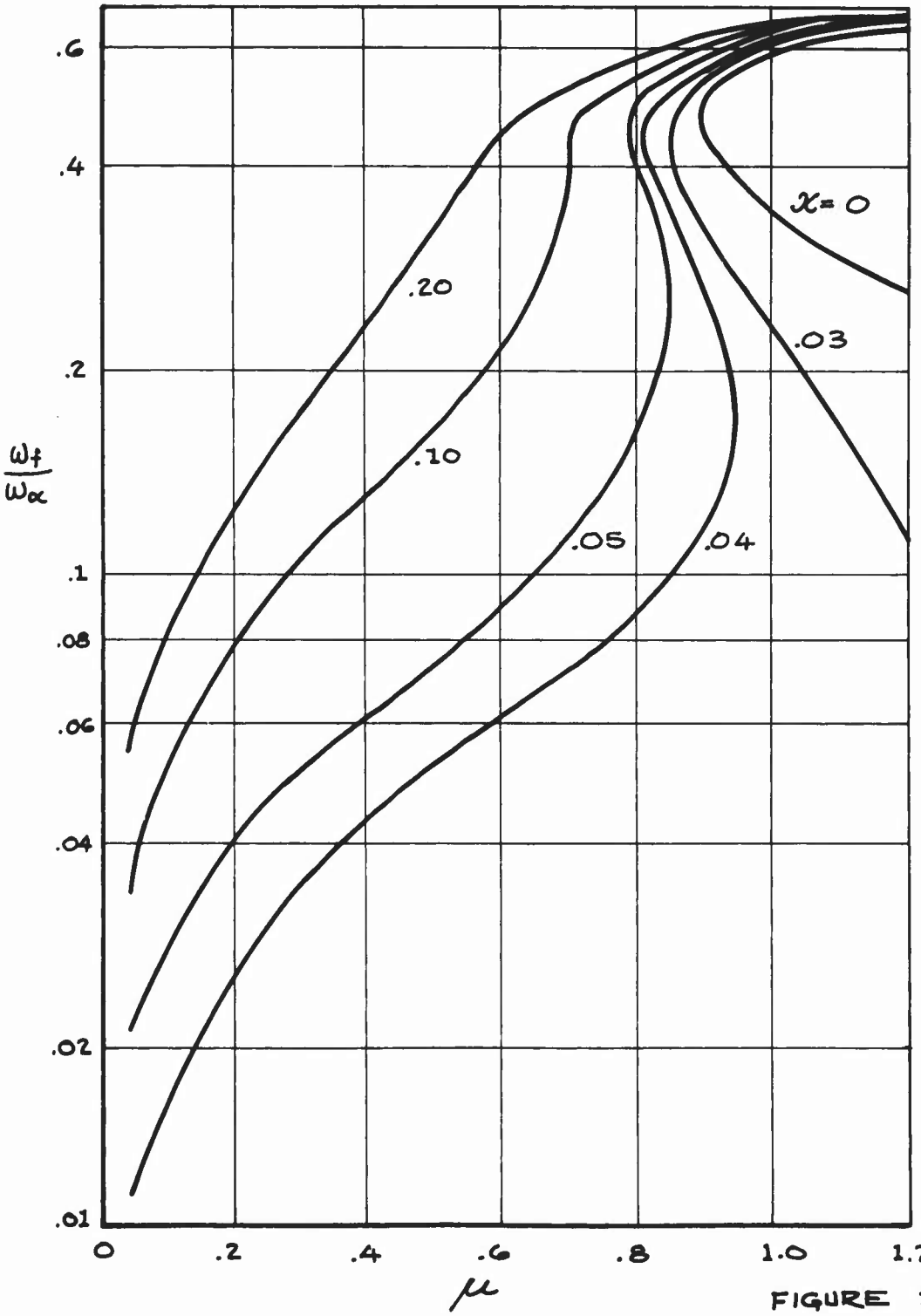


FIGURE 30

THE INVERSE OF THE FLUTTER FREQUENCY COEFFICIENT AS A FUNCTION OF THE SWEEP PARAMETER

MODEL – BAIRD # 2

PARAMETERS – $r_c^2 = .26$

$X_m = .166$

$\pi^2 = .011$ $\mu = .1$

$a = .38$

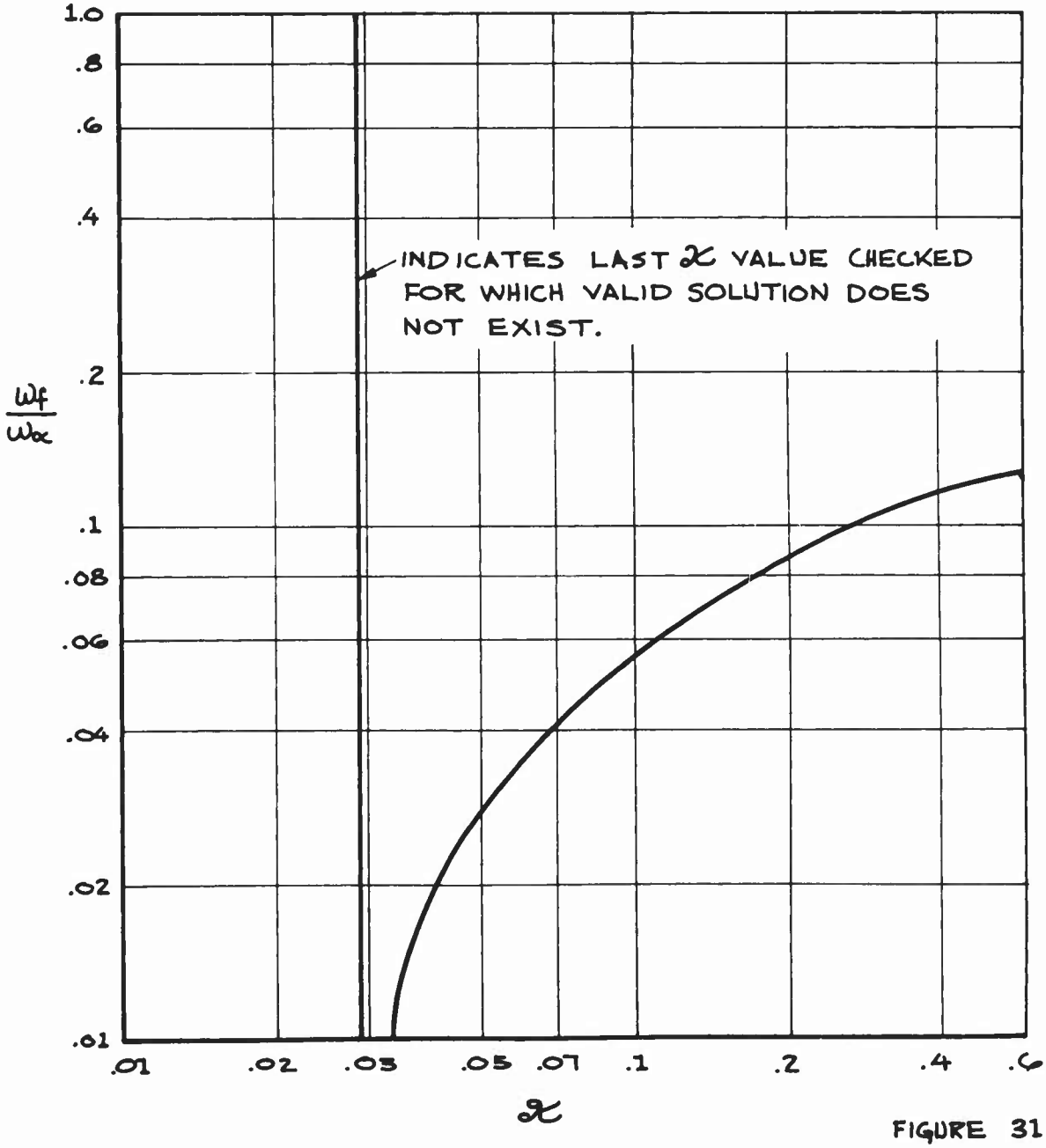


FIGURE 31

FLUTTER SPEED COEFFICIENT AS FUNCTION OF THE SWEEP PARAMETER.

MODEL— BAIRD #2

PARAMETERS — $r_c^2 = .26$ $\pi^2 = .011$ $\mu = .1$

$X_m = .166$ $a = .38$

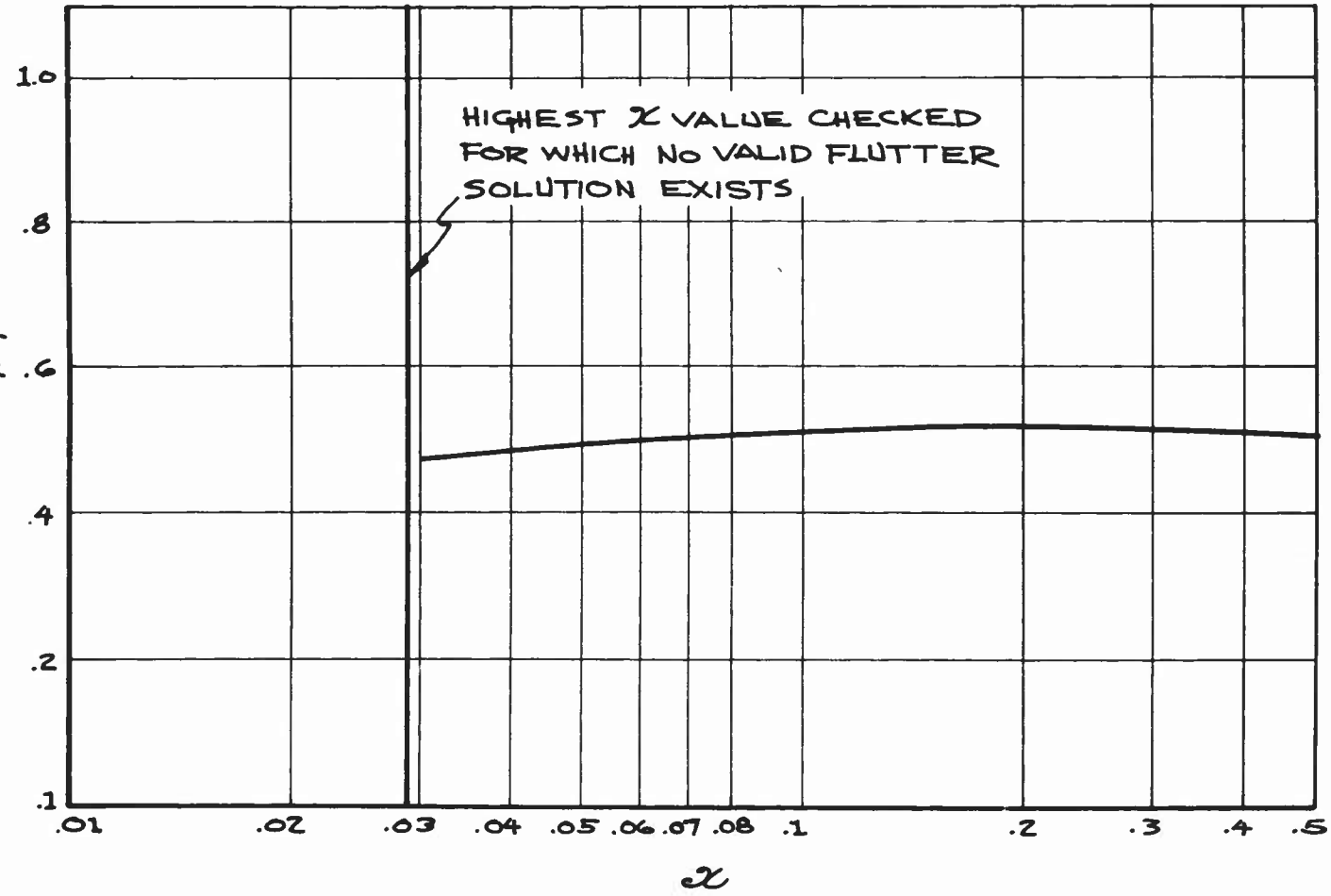


FIGURE 32

A COMPARISON OF THE FLUTTER BOUNDARIES PREDICTED BY THE "EXACT" AND THE APPROXIMATE QUASI-STEADY THEORIES

MODEL – BAIRD #2 UNSWEPT

PARAMETERS – $r_c^2 = .26$ $\pi^2 = .011$ $\alpha = 0$ $x_m = .166$ $a = .38$

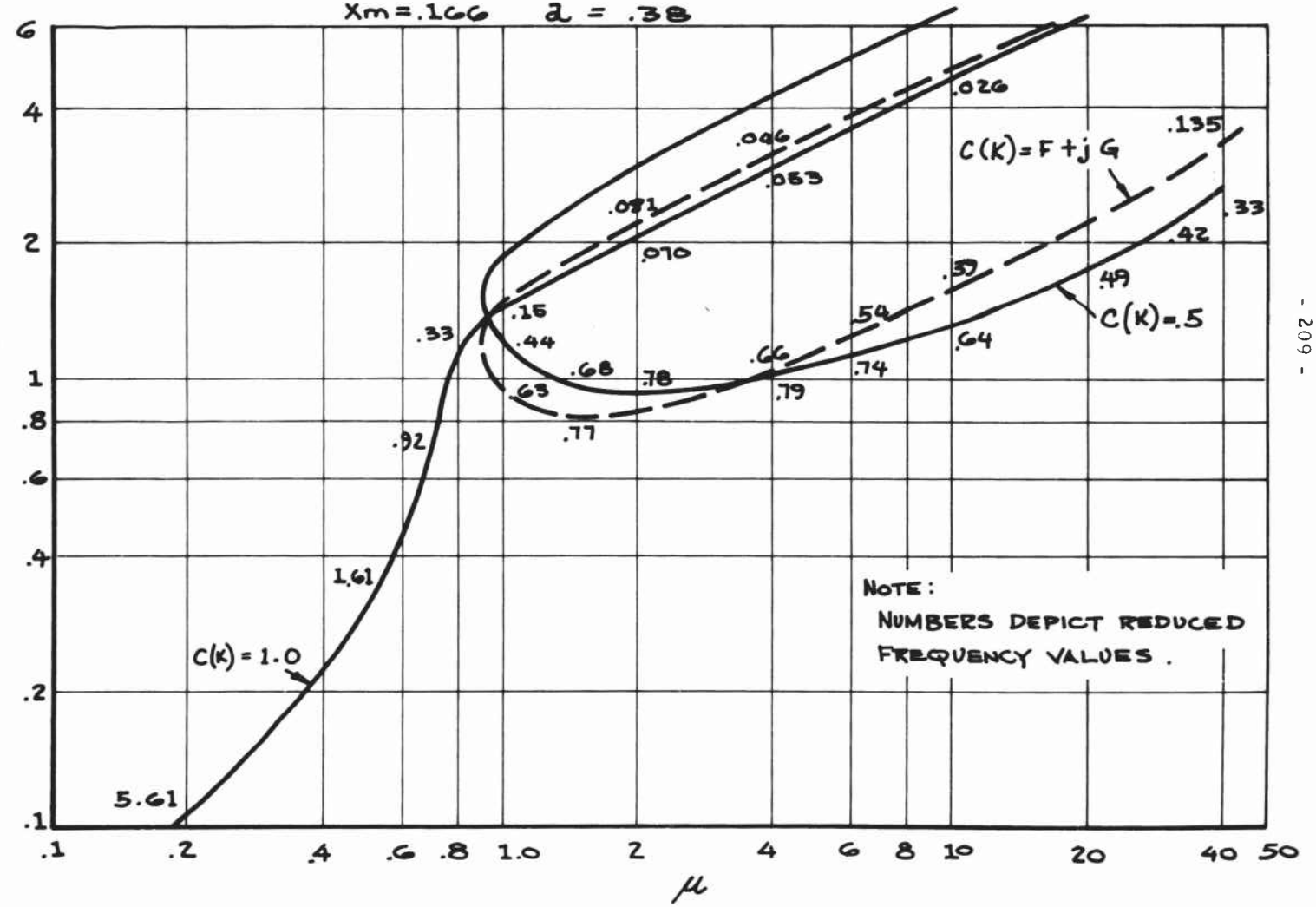


FIGURE 33

A COMPARISON OF THE FLUTTER FREQUENCY COEFFICIENTS PREDICTED BY THE "EXACT" AND THE APPROXIMATE QUASI-STEADY THEORIES

MODEL – BAIRD #2 UNSWEPT

PARAMETERS – $r_c^2 = .26$ $\pi^2 = .011$ $\chi = 0$

$X_m = .166$ $a = .38$

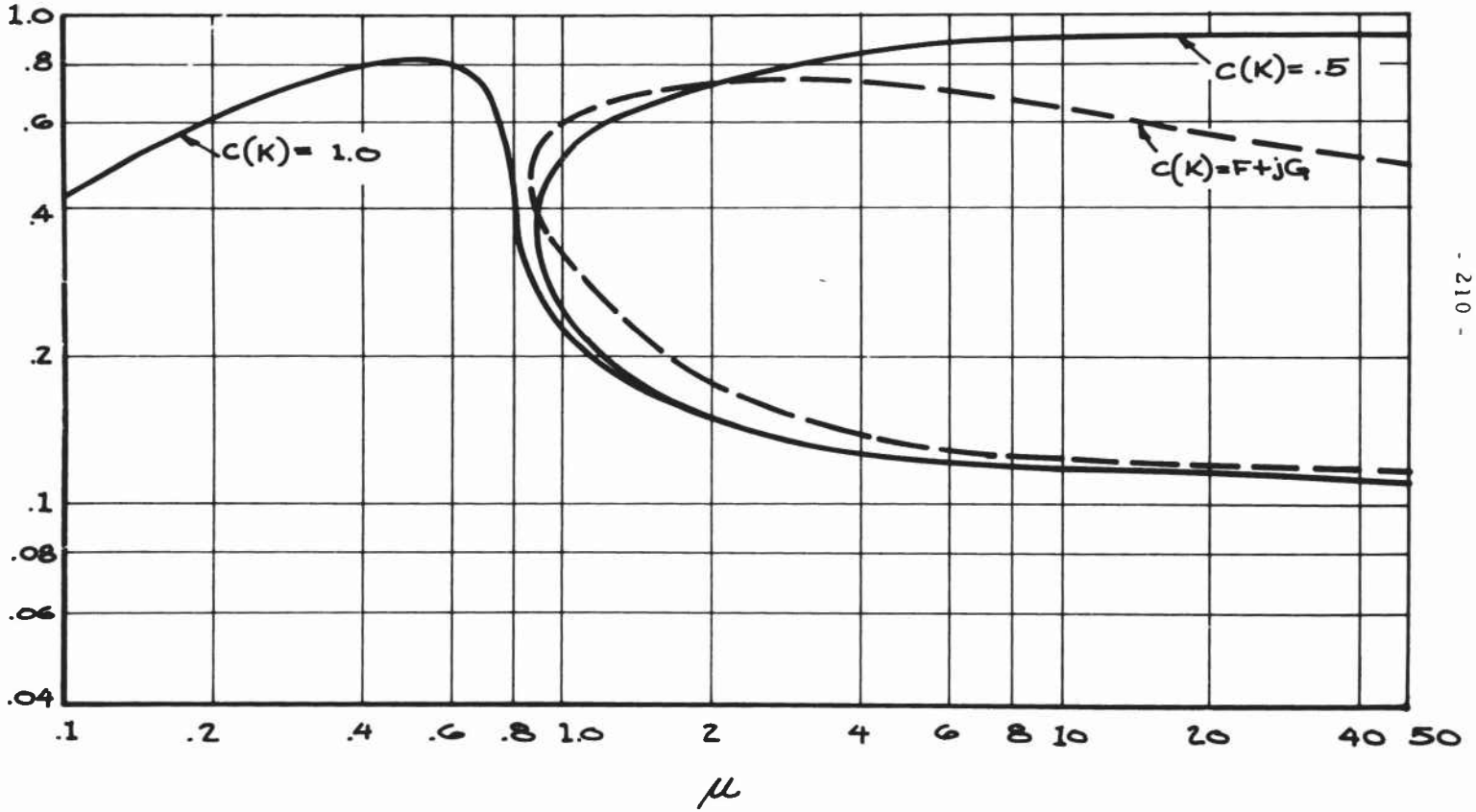


FIGURE 34

A COMPARISON OF THE FLUTTER BOUNDARIES BY THE "EXACT" AND THE APPROXIMATE QUASI-STEADY THEORIES

MODEL— BAIRD # 2 SWEPT

PARAMETERS— $r_c^2 = .26$ $\quad a = .38$

$X_m = .166$ $\quad \mu = 50$

$\pi^2 = .011$

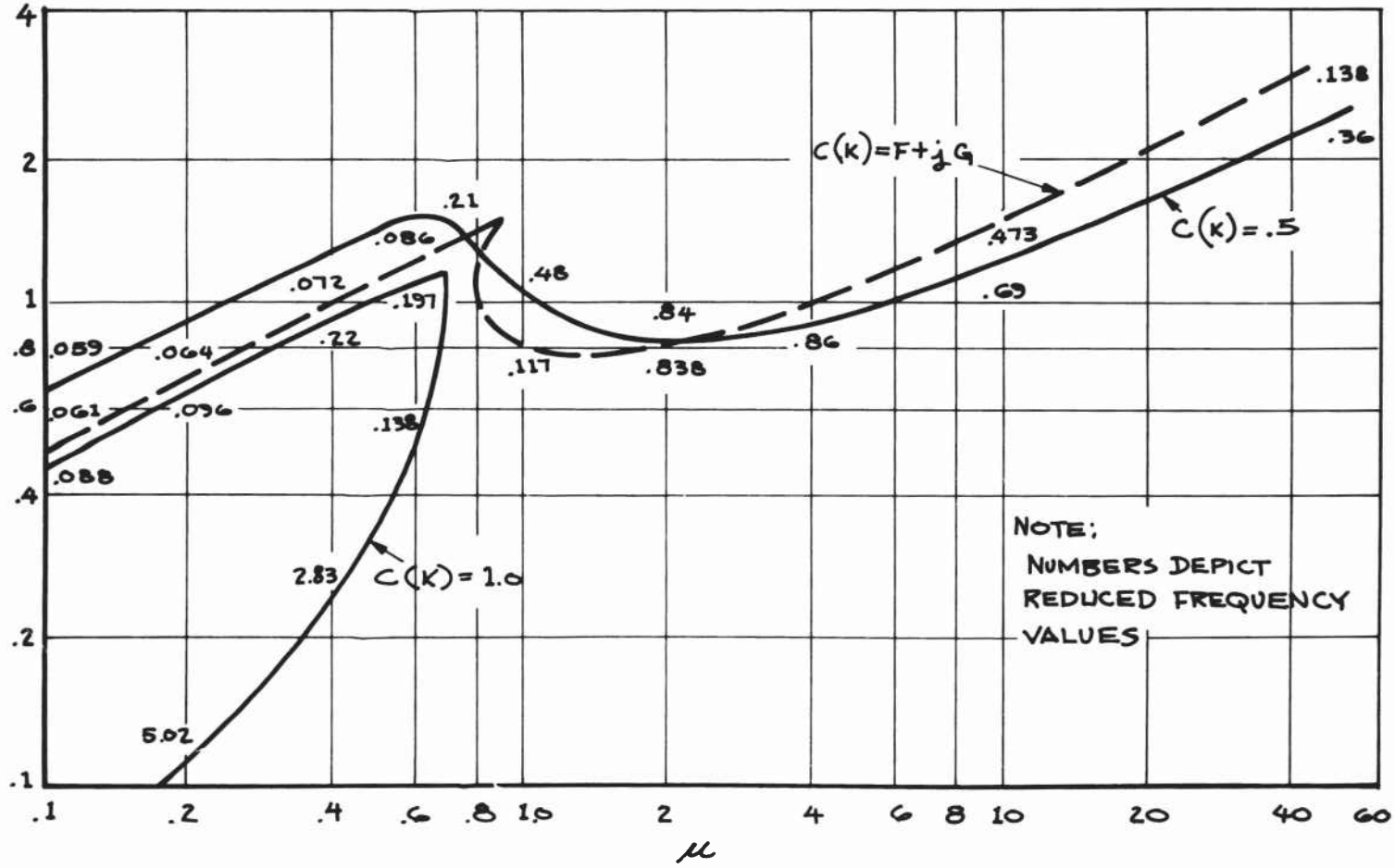


FIGURE 35

A COMPARISON OF THE FLUTTER FREQUENCY COEFFICIENTS PREDICTED BY THE "EXACT" AND THE APPROXIMATE QUASI-STEADY THEORIES.

MODEL — BAIRD #2 SWEPT

PARAMETERS — $r_c^2 = .26$ $T^2 = .011$ $\mathcal{K} = .05$

$X_m = .166$ $a = .38$

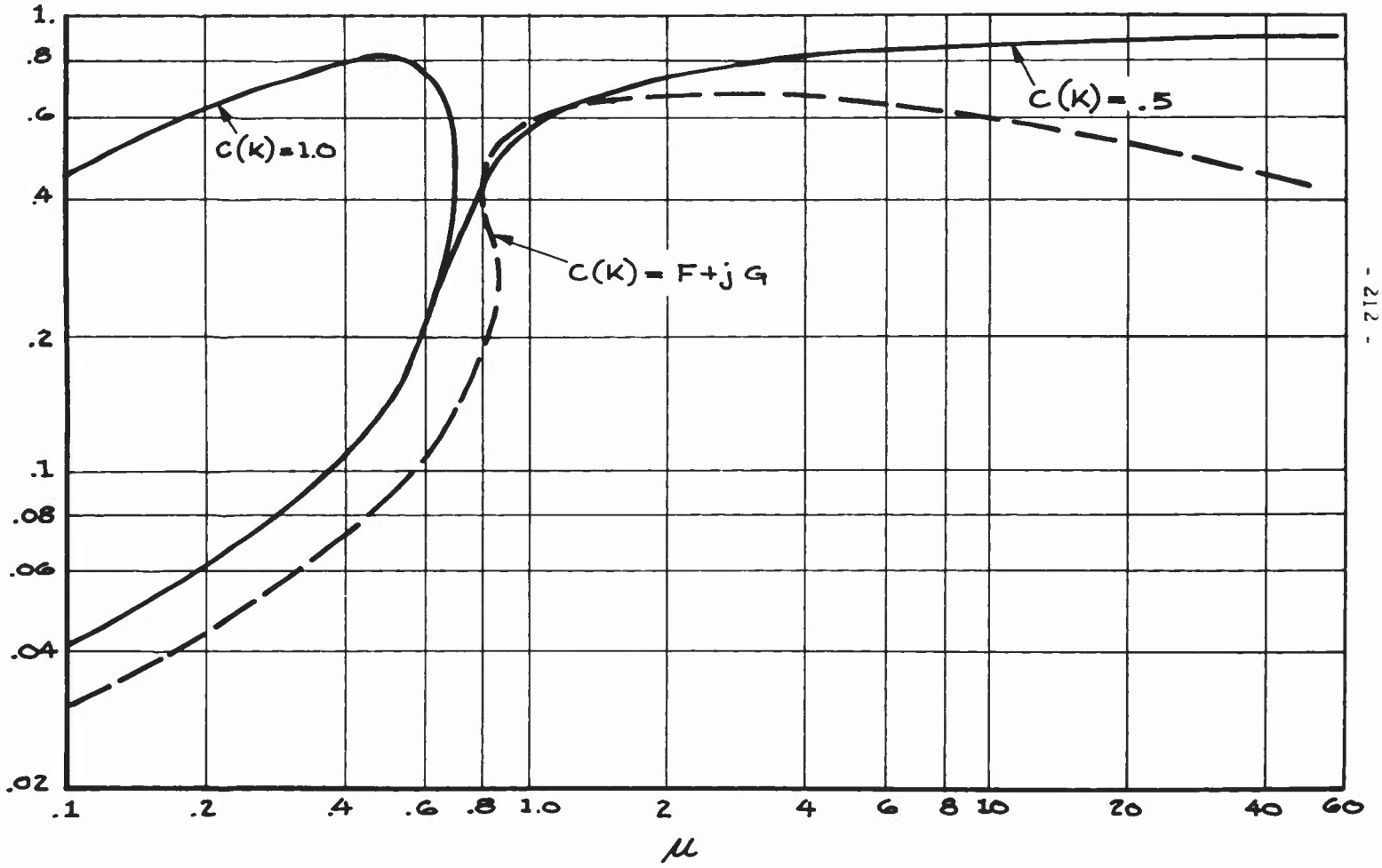


FIGURE 36

FLUTTER SPEED COEFFICIENT AS A FUNCTION OF THE MASS-DENSITY RATIO.

NOTE: PARAMETERS SAME AS BAIRD MODEL #2, BUT ANALYSIS PERFORMED WITH OFF-DIAGONAL COUPLING CONSTANT OF 1.0

PARAMETERS: — $r_c^2 = .26$ $\pi^2 = .011$ $X_m = .166$ $a = .38$

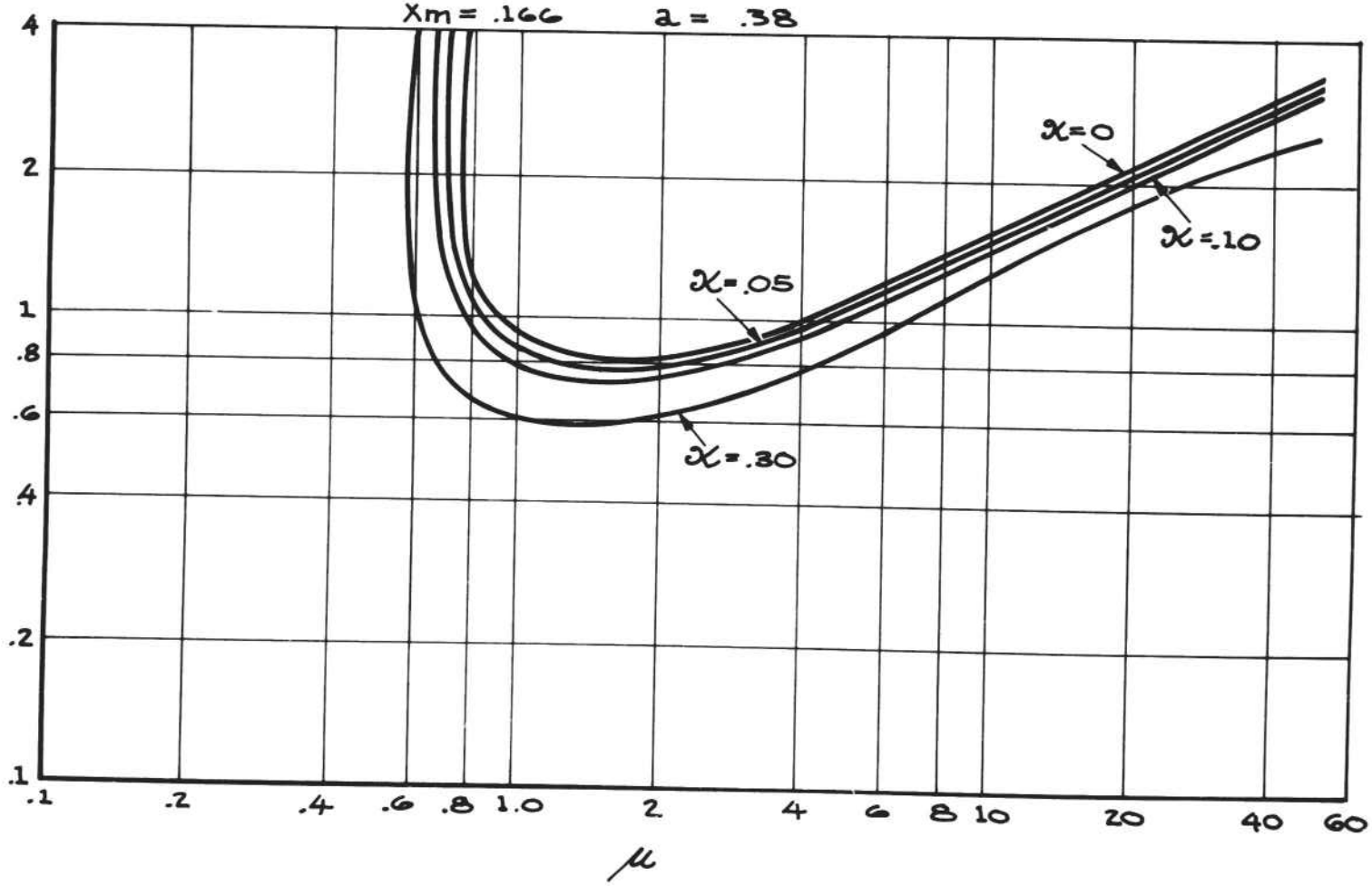


FIGURE 37

A PLOT OF THE FLUTTER SPEED COEFFICIENT VS. THE MASS-DENSITY RATIO FOR VARIOUS AMOUNTS OF OFF-DIAGONAL COUPLING.

PARAMETERS—USED ARE THOSE OF MODEL No 2 WITH 11.2° OF SWEEP.

$r_{\frac{3}{c}} = .26$ $\quad \pi^2 = .011$ $\quad \varkappa = .05$

$x_m = .166$ $\quad a = .38$

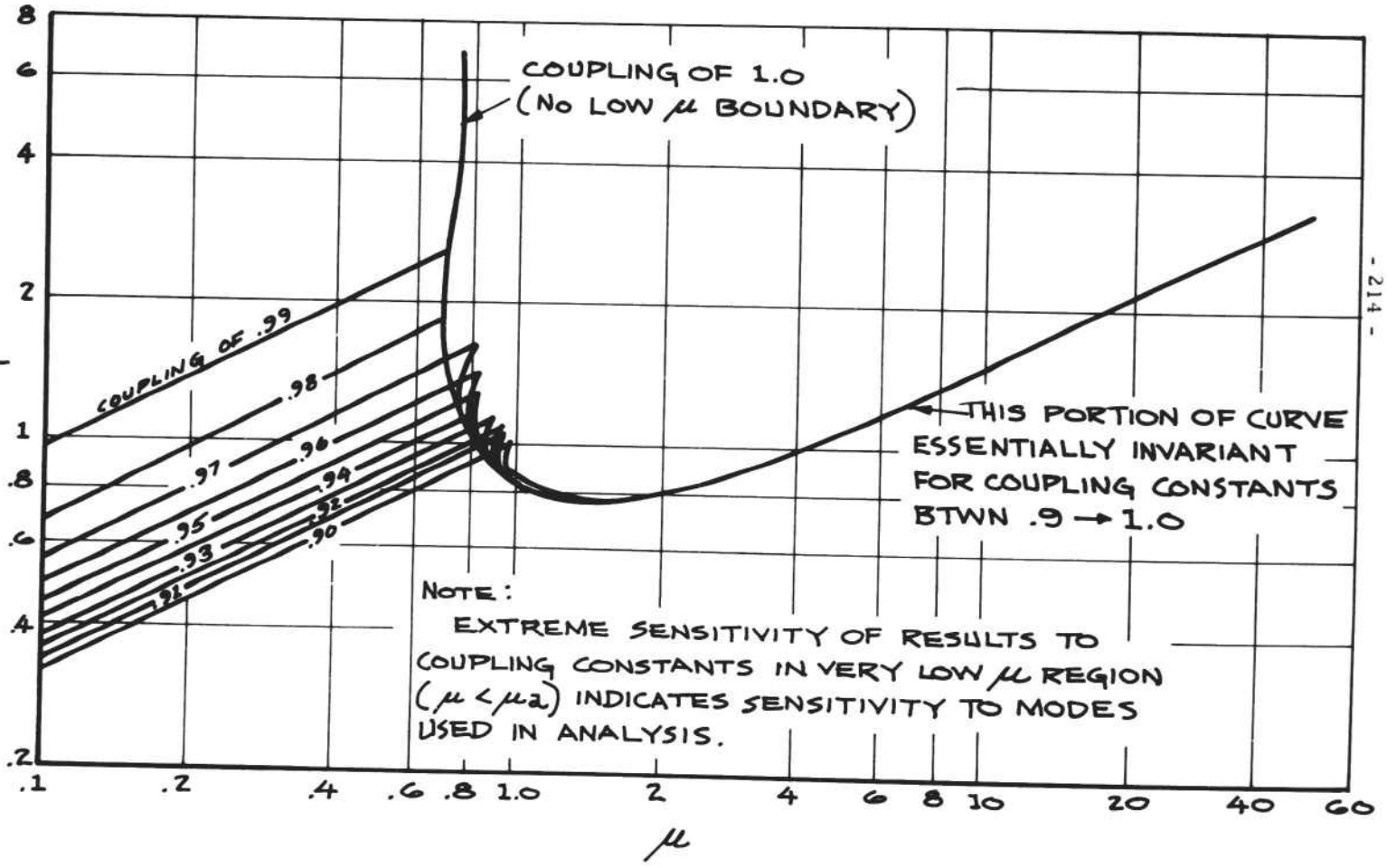


FIGURE 38

THE INVERSE OF THE FLUTTER FREQUENCY COEFFICIENT AS A FUNCTION OF THE SWEEP PARAMETER FOR A CONFIGURATION POSSESSING A $\mu=0$ SOLUTION.

PARAMETERS- $\pi_*^2 = .02$

$a = -.2$

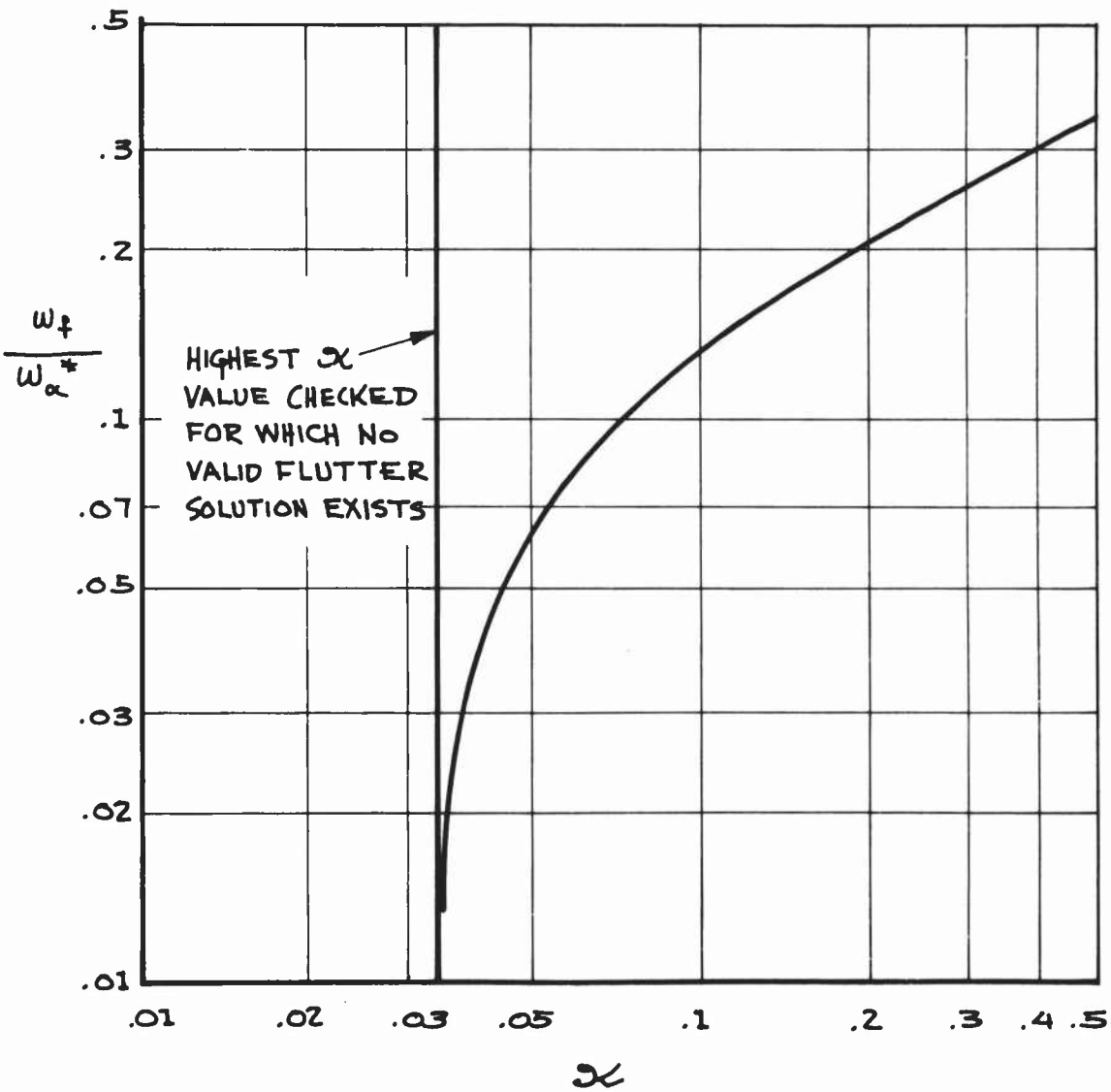


FIGURE 39

FLUTTER SPEED COEFFICIENT AS A FUNCTION OF THE SWEEP PARAMETER FOR A CONFIGURATION POSSESSING A $\mu = 0$ SOLUTION.

PARAMETERS — $\pi_4^2 = .02$

$a = -.2$

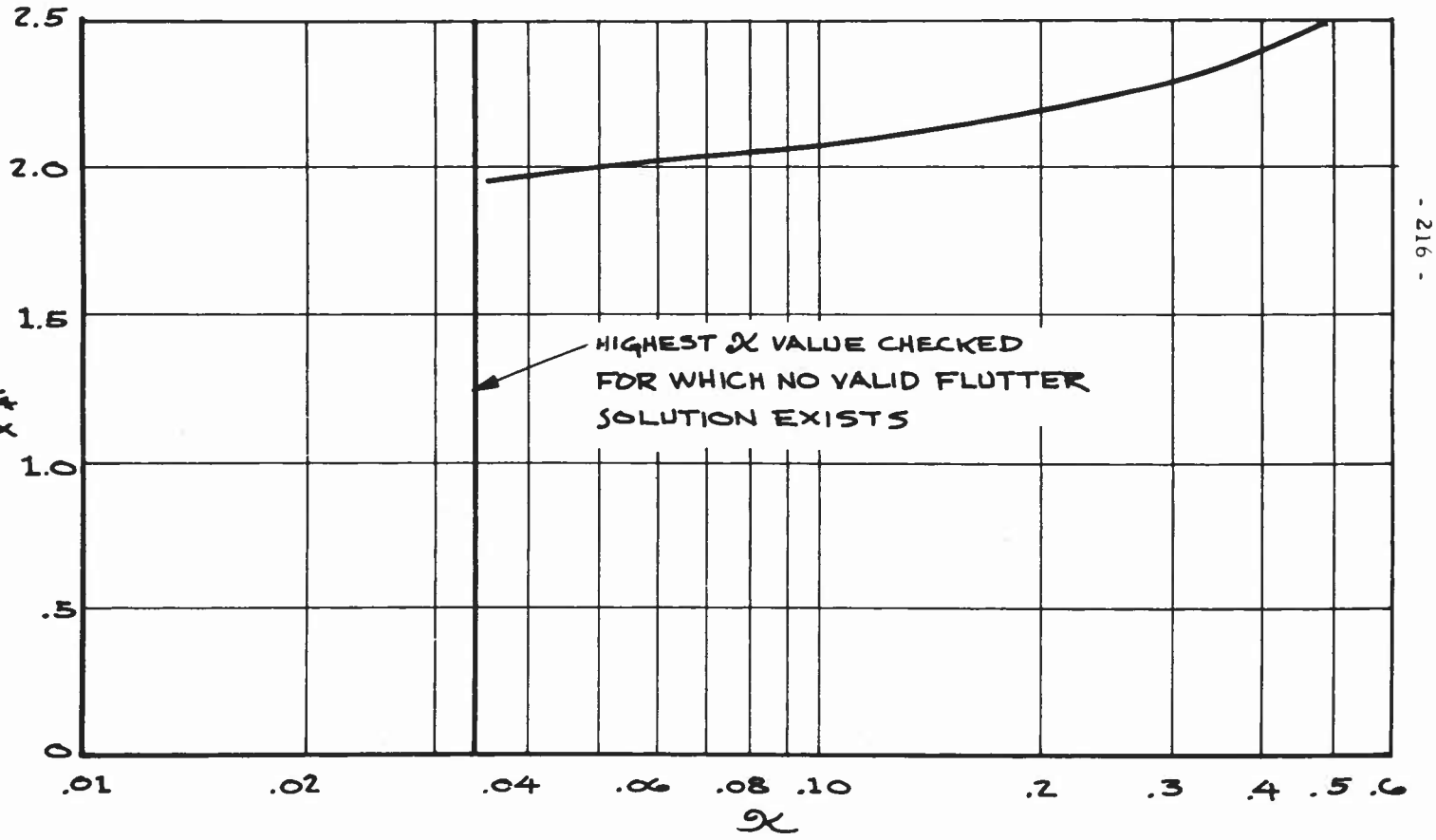


FIGURE 40

A PLOT SHOWING THE MINIMUM SWEEP PARAMETER VALUE REQUIRED FOR A UNIFORM CANTILEVERED FOIL TO POSSESS A VALID FLUTTER SOLUTION WITH A ZERO MASS-DENSITY RATIO.

NOTE:

THIS PLOT IS INDICATIVE OF WHETHER A VERY LOW MASS-DENSITY RATIO ($\mu < \mu_a$) FLUTTER BOUNDARY EXISTS FOR ANY GIVEN UNIFORM FULLY WETTED CANTILEVERED FOIL.

NOTE: $\pi_*^2 = \left[1/3 + a^2\right] \pi^2 / r_c^2 + \left[x_m - a\right]^2$

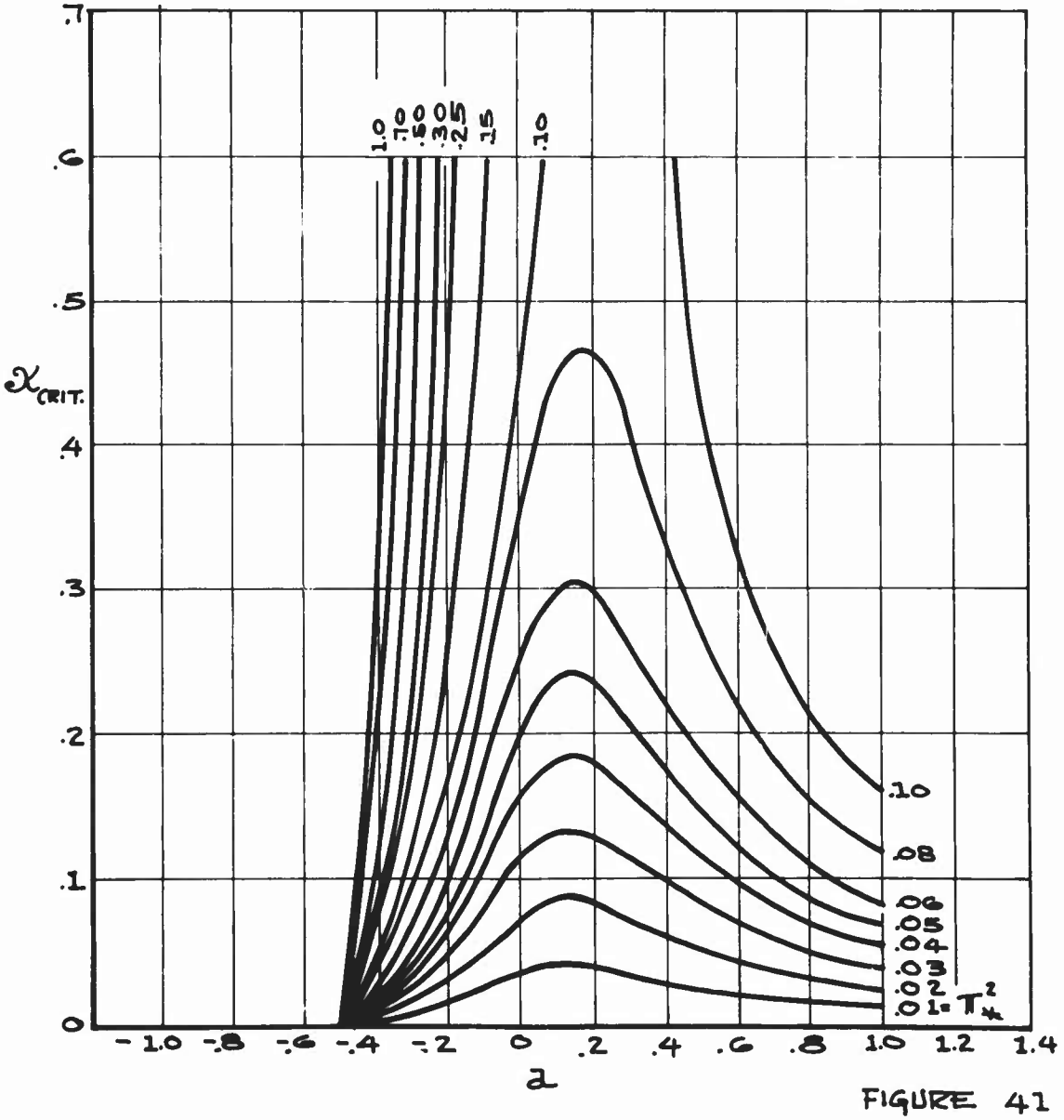


FIGURE 41

THE INVERSE OF THE FLUTTER FREQUENCY COEFFICIENT AS A FUNCTION OF THE SWEEP PARAMETER FOR A CONFIGURATION POSSESSING A LOW $\mu$ BOUNDARY.

PARAMETERS— $r_c^2 = .25$
$Xm = .1$
$\pi^2 = .0422$
$a = -.2$

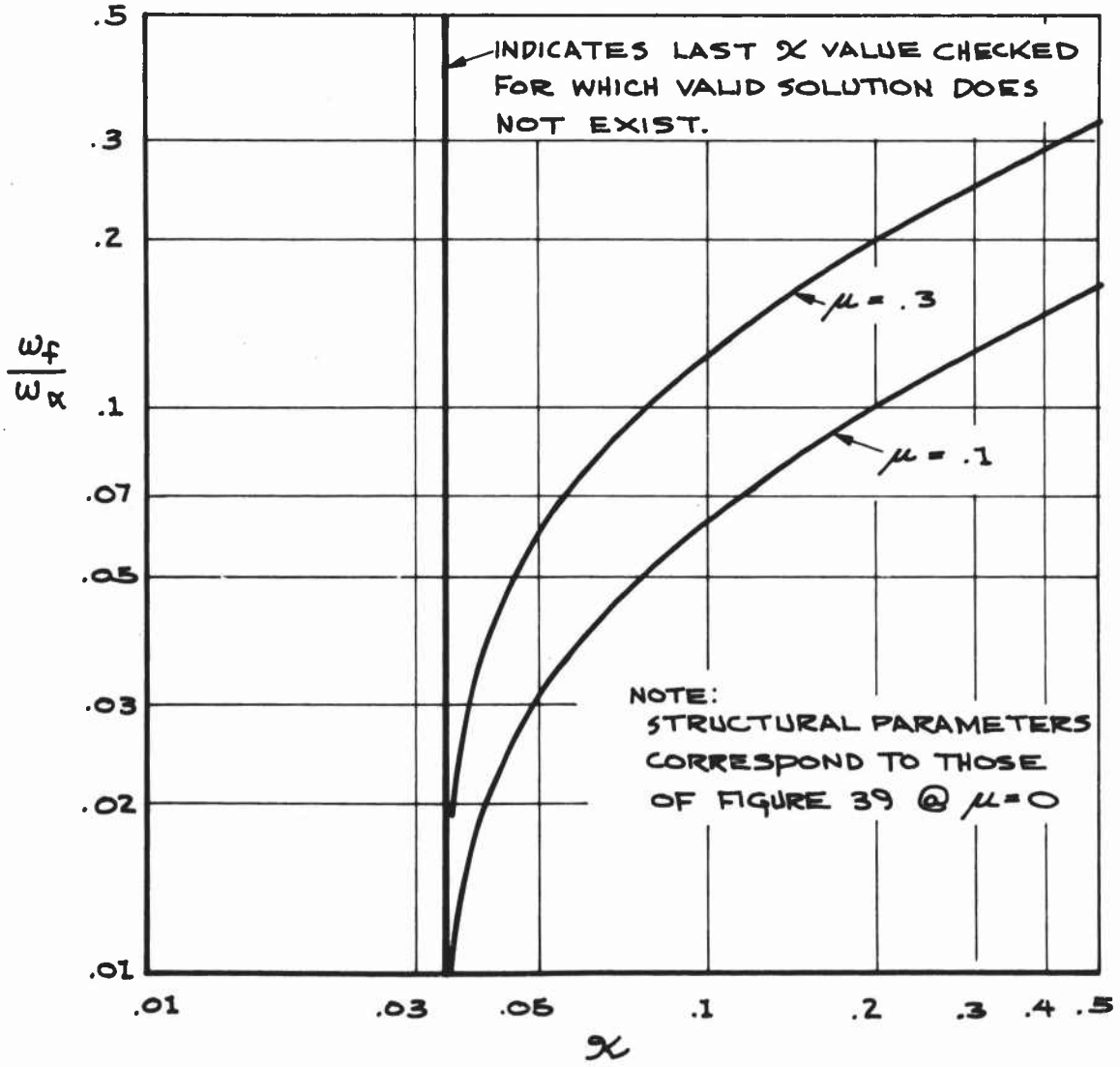


FIGURE 42

FLUTTER SPEED COEFFICIENT AS A FUNCTION OF THE SWEEP PARAMETER FOR A CONFIGURATION POSSESSING A LOW $\mu$ BOUNDARY.

PARAMETERS– $r_c^2 = .25$
$Xm = .1$
$\pi^2 = .0412$
$a = -.2$

NOTE: STRUCTURAL PARAMETERS CORRESPOND TO THOSE OF FIGURE 39 @ $\mu = 0$

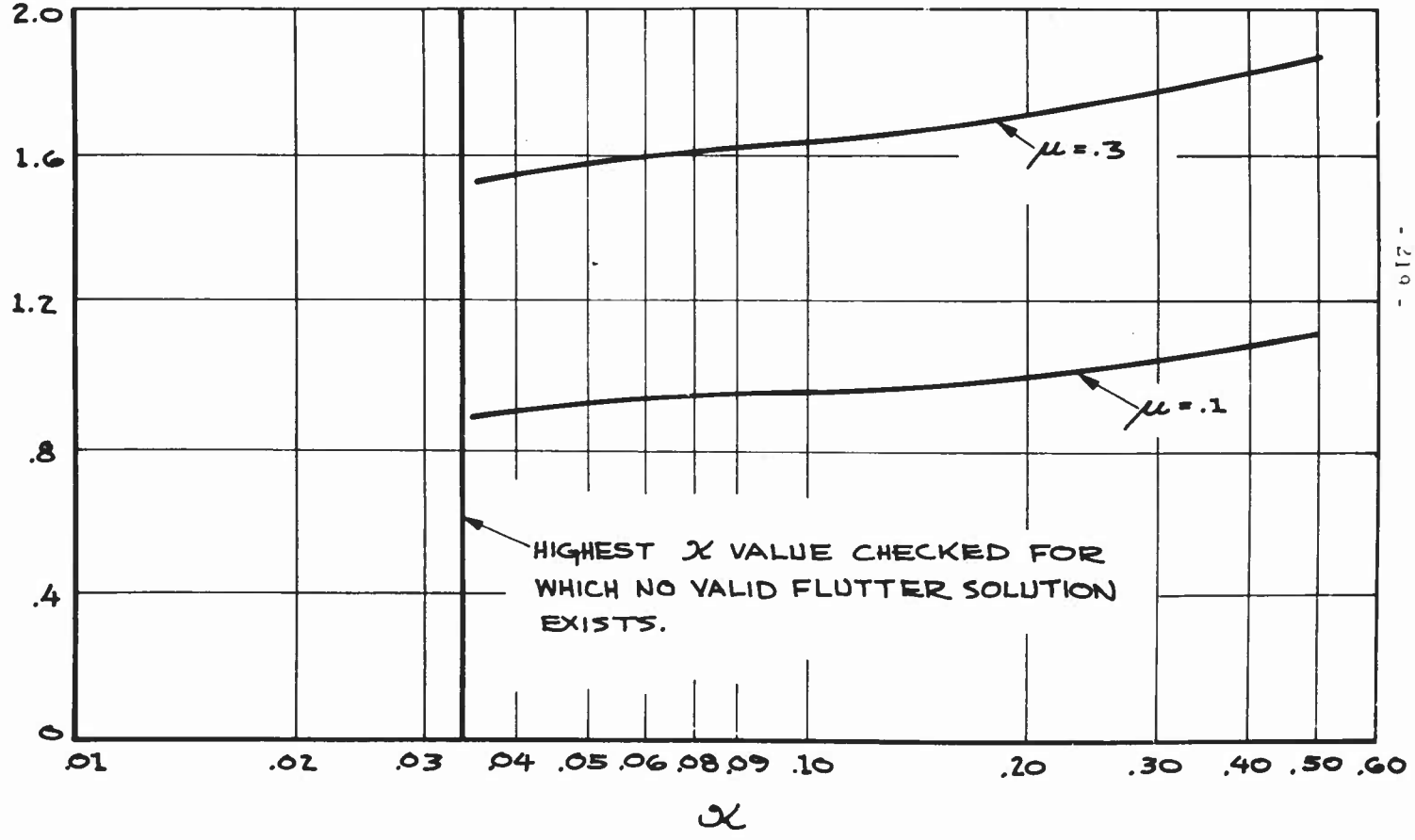


FIGURE 43

A PLOT OF THE IN-FLUID FLUTTER SPEED COEFFICIENT FOR THE MINIMUM SWEEP PARAMETER VALUE FOR WHICH A VALID ZERO MASS-DENSITY SOLUTION MAY BE FOUND.

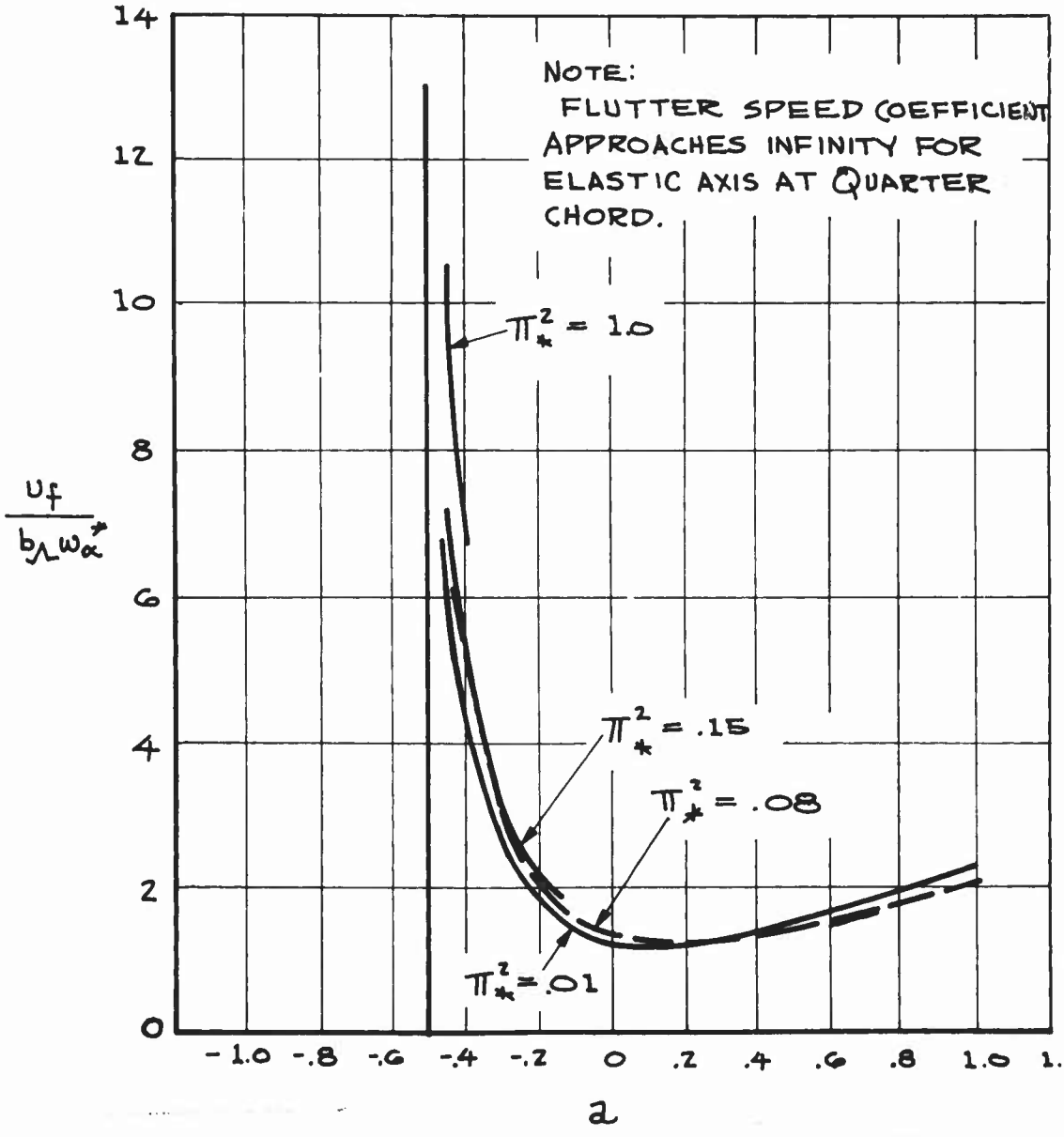


FIGURE 44

FLUTTER SPEED COEFFICIENT AS A FUNCTION OF THE LOCATION OF THE ELASTIC AXIS.

MODEL - MASS AND STIFFNESS OF BAIRD # 2

PARAMETERS - $r_c^2 = .26$

$X_m = .166$

$\pi^2 = .011$

$\mu = .1$

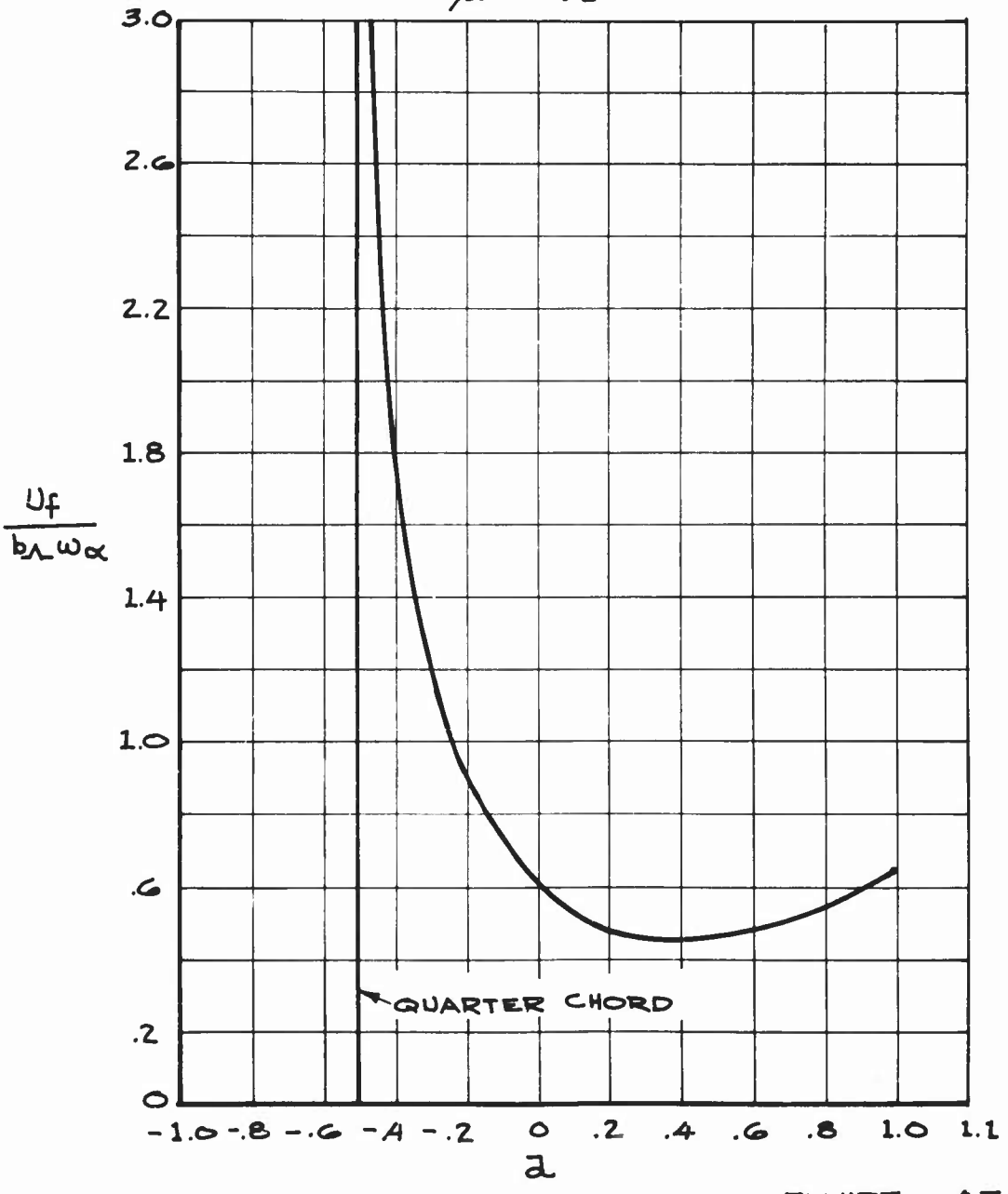


FIGURE 45

# A PLOT SHOWING THE CRITICAL SWEEP PARAMETER VALUE FOR VARIOUS $\pi_*^2$ AND $a$

NOTE:

THIS PLOT IS BASED UPON THE QUADRATIC APPROXIMATION DISCUSSED IN THE TEXT. HENCE THE VALIDITY DECREASES AS $\kappa_{CRIT.}$ INCREASES. SEE FIGURE 41 FOR QUARTIC RESULTS.

NOTE:

$$\pi_*^2 = \left[\tfrac{1}{8} + a^2\right] \pi^2/r^2 + \left[x_m - a\right]^2$$

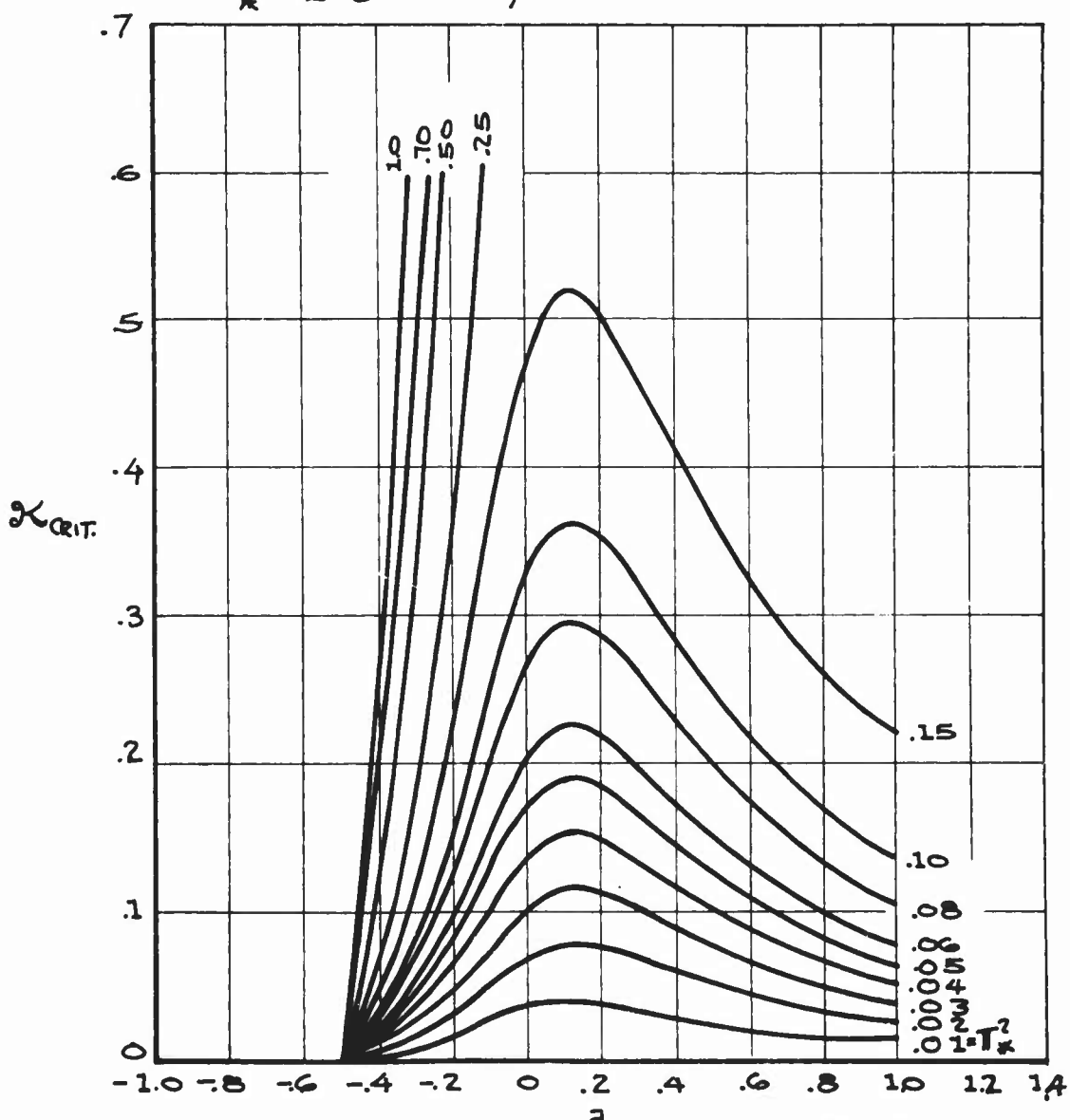


FIGURE 40

A PLOT OF THE FLUTTER SPEED AND FLUTTER FREQUENCY AS A FUNCTION OF THE ANGLE OF SWEEPBACK FOR SQUIRES MODEL.

PARAMETERS— $r_c^2 = .25$ $a = -.08$
$X_m = .194$ $\ell = 56$ IN.
$\pi^2 = .00652$

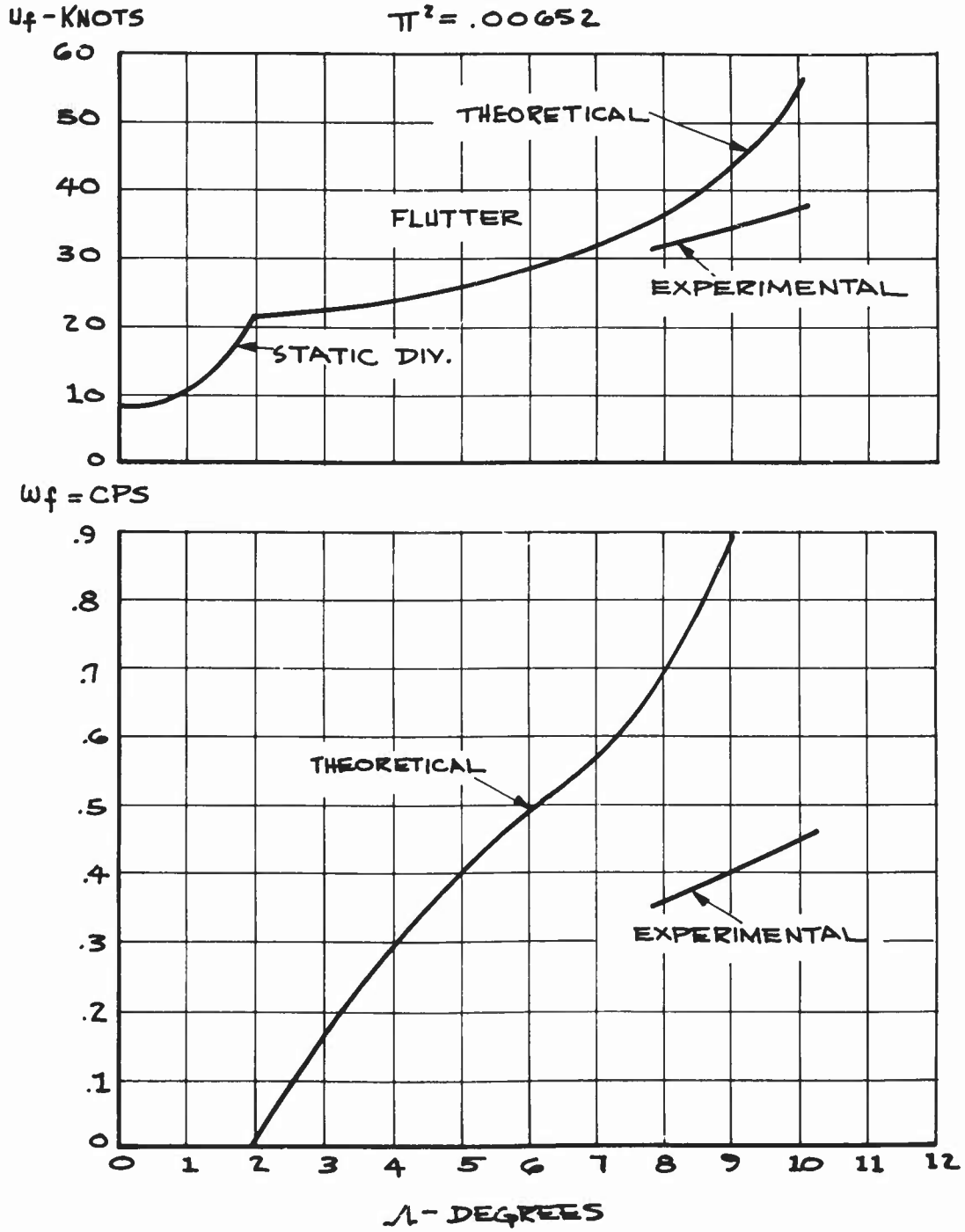


FIGURE 47